

Spring 5-15-2016

High-Valent Organometallic Palladium and Nickel Complexes and their Roles in Carbon-Carbon and Carbon-Heteroatom Bond Formation Reactions

Jason Wesley Schultz

Washington University in St. Louis

Follow this and additional works at: https://openscholarship.wustl.edu/art_sci_etds



Part of the [Inorganic Chemistry Commons](#), and the [Organic Chemistry Commons](#)

Recommended Citation

Schultz, Jason Wesley, "High-Valent Organometallic Palladium and Nickel Complexes and their Roles in Carbon-Carbon and Carbon-Heteroatom Bond Formation Reactions" (2016). *Arts & Sciences Electronic Theses and Dissertations*. 767.
https://openscholarship.wustl.edu/art_sci_etds/767

This Dissertation is brought to you for free and open access by the Arts & Sciences at Washington University Open Scholarship. It has been accepted for inclusion in Arts & Sciences Electronic Theses and Dissertations by an authorized administrator of Washington University Open Scholarship. For more information, please contact digital@wumail.wustl.edu.

WASHINGTON UNIVERSITY IN ST. LOUIS

Department of Chemistry

Dissertation Examination Committee:

Liviu M. Mirica, Chair

John R. Bleeke

Julio M. D'Arcy

Sophia E. Hayes

Nigam P. Rath

High-Valent Organometallic Palladium and Nickel Complexes and their Roles in Carbon-Carbon
and Carbon-Heteroatom Bond Formation Reactions

by

Jason W. Schultz

A dissertation presented to the
Graduate School of Arts & Sciences
of Washington University in
partial fulfillment of the
requirements for the degree
of Doctor of Philosophy

May 2016

St. Louis, Missouri

© 2016, Jason W. Schultz

Table of Contents

List of Figures.....	v
List of Schemes.....	ix
List of Tables.....	xi
Acknowledgements.....	xiv
Abstract.....	xvii

Chapter 1: Palladium and Nickel Complexes Relevant to Cross Coupling and Carbon-Heteroatom Bond Formation Reactions..... 1

1.1 Development of Palladium Catalysis.....	2
1.2 Transition to Nickel Catalysis.....	4
1.3 High-Valent Organometallic Palladium Complexes.....	5
1.4 High-Valent Organometallic Nickel Complexes.....	10

Chapter 2: Synthesis and Reactivity of Organometallic Palladium Complexes Supported by a Pseudo-Tridentate Ligand..... 20

2.1 Introduction.....	21
2.2 Experimental Section.....	22
2.2.1 Synthesis of Ligands and Complexes.....	22
2.2.2 Physical Measurements.....	28
2.2.3 Computational Studies.....	30
2.2.4 Reactivity Studies.....	30
2.3 Results and Discussion.....	32
2.3.1 Ligand Synthesis and Design.....	32
2.3.2 Destabilization of Pd ^{III} Complexes.....	33
2.3.3 Computational studies on Pd ^{III} Complexes.....	38
2.3.4 Aerobic reactivity of (T ^s MeN ₄)Pd ^{II} Me ₂	43
2.3.5 Proposed mechanism for the aerobic C–C bond formation reactivity.....	45
2.4 Conclusion.....	46
2.5 Acknowledgements.....	47
2.6 References.....	47

Chapter 3: Structural and Reactivity Comparison of *Ortho*-Substituted Organometallic Nickel(III) Complexes..... 50

3.1 Introduction.....	51
3.2 Experimental Section.....	52
3.2.1 Synthesis of Ligands and Complexes.....	52
3.2.2 Physical Measurements.....	54
3.2.3 Reactivity Studies.....	56

3.3	Results and Discussion	57
3.3.1	Synthesis and Structure of Ni ^{II} Complexes.....	57
3.3.2	Synthesis and Structure of Ni ^{III} Complexes.....	58
3.3.3	C-Halide Bond Formation Reactivity.....	60
3.4	Conclusion.....	62
3.5	Acknowledgements.....	62
3.6	References.....	63

Chapter 4: High-Valent Dimethyl Nickel Complexes Relevant to Cross-Coupling and C-C Bond Formation Reactions..... 66

4.1	Introduction.....	67
4.2	Experimental Section.....	68
4.2.1	Synthesis of Ligands and Complexes.....	68
4.2.2	Physical Measurements.....	72
4.2.3	Computational Studies.....	74
4.2.4	Reactivity Studies.....	74
4.3	Results and Discussion.....	77
4.3.1	Synthesis and Structure of Ni ^{II} Complexes.....	77
4.3.2	Synthesis and Structure of Ni ^{III} Complexes.....	79
4.3.3	C-C Bond Formation Reactivity.....	82
4.3.4	Catalytic Reactivity of Ni ^{II} /Ni ^{III} Complexes.....	87
4.3.5	Reaction of Alkyl and Aryl Halides with (^{Me} N ₄)Ni ^{II} Me ₂ Complex.....	89
4.4	Conclusion.....	92
4.5	Acknowledgements.....	92
4.6	References.....	93

Chapter 5: Synthesis and Isolation of High-Valent Organometallic Nickel Complexes Supported by Cycloneophyl Group..... 97

5.1	Introduction.....	98
5.2	Experimental Section.....	99
5.2.1	Synthesis of Ligands and Complexes.....	99
5.2.2	Physical Measurements.....	101
5.2.3	Characterization Studies	103
5.2.4	Reactivity Studies.....	103
5.3	Results and Discussion.....	104
5.3.1	Synthesis and Structure of Ni ^{II} Complex.....	104
5.3.2	Synthesis and Structure of Ni ^{III} Complex.....	106
5.3.3	Synthesis and Characterization of Ni ^{IV} Complex.....	107
5.3.4	C-C Bond Formation Reactivity.....	109
5.4	Conclusion.....	110

5.5	Acknowledgements.....	110
5.6	References.....	110
Chapter 6: Deprotonation of Pyridinophane Ligands Resulting in the Formation of Neutral Nickel(III) Complexes.....		
6.1	Introduction.....	113
6.2	Experimental Section.....	114
6.2.1	Synthesis of Ligands and Complexes.....	114
6.2.2	Physical Measurements.....	115
6.2.3	Deprotonation Comparison Studies.....	117
6.3	Results and Discussion.....	118
6.3.1	Synthesis and Structure of Deprotonated Ni ^{III} Complex.....	118
6.3.2	Comparison of Cationic and Deprotonated Ni ^{III} Complexes.....	120
6.3.3	Preliminary C-H Activation Studies.....	124
6.4	Conclusion.....	125
6.5	Acknowledgements.....	126
6.6	References.....	126
Chapter 7: Future Directions.....		
7.1	Reactivity of Organometallic Palladium Complexes	130
7.2	Characterization of Arene-Substituted Nickel Complexes	131
7.3	Reactivity of Dialkyl and Diaryl Nickel Complexes	132
7.4	Reactivity of Cycloneophyl Supported Ni ^{IV} Complexes	133
7.5	Deprotonation of Organometallic Nickel Complexes.....	135
7.6	References.....	136
Appendix A: Select NMR Spectra of Ligands and Metal Complexes.....		137
Appendix B: X-ray Crystal Structure Data of Metal Complexes.....		147
Appendix C: Supplemental Reactivity Data.....		191

List of Figures

- Figure 1.1: ORTEP representation of $[\text{Pd}^{\text{III}}(\text{ttcn})_2](\text{ClO}_4)_3$ (left) and $(\text{bpy})\text{Pd}^{\text{IV}}\text{Me}_3\text{I}$ (right). Selected bond distances (Å), $[\text{Pd}^{\text{III}}(\text{ttcn})_2](\text{ClO}_4)_3$: Pd1-S1, 2.545; Pd1-S2, 2.356; Pd1-S3, 2.369. $(\text{bpy})\text{Pd}^{\text{IV}}\text{Me}_3\text{I}$: Pd1-C1, 2.046; Pd1-C2, 2.034; Pd1-C3, 2.040; Pd1-N1, 2.188; Pd1-N2, 2.173; Pd1-I1, 2.834..... 6
- Figure 1.2: UV-Vis spectrum for $[(^{\text{tBu}}\text{N}_4)\text{Pd}^{\text{III}}\text{MeCl}](\text{ClO}_4)$ in MeCN (left) and EPR spectrum of $[(^{\text{tBu}}\text{N}_4)\text{Pd}^{\text{III}}\text{MeCl}](\text{ClO}_4)$ in 3:1 PrCN/MeCN (right) experimental (red line) and simulated spectrum (black line) using the following parameters: $g_x = 2.239$, $g_y = 2.134$, $g_z = 2.005$ ($A_N = 19.5$ G)..... 9
- Figure 1.3: ORTEP representation of $[\text{Ni}^{\text{III}}(\text{diars})_2\text{Cl}_2]\text{Cl}$ (left), $\text{Ni}[\text{C}_6\text{H}_3(\text{CH}_2\text{NMe}_2)_{2-o,o}]\text{I}_2$ (middle) and $[\text{Ni}_2(\eta\text{-C}_5\text{H}_5)_2(\text{C}_6\text{F}_5\text{C}\equiv\text{CC}_6\text{F}_5)]$ (right). Selected bond distances (Å), $[\text{Ni}^{\text{III}}(\text{diars})_2\text{Cl}_2]\text{Cl}$: Ni1-As1, 2.37; Ni1-As2, 2.34; Ni1-Cl1, 2.43. $\text{Ni}[\text{C}_6\text{H}_3(\text{CH}_2\text{NMe}_2)_{2-o,o}]\text{I}_2$: Ni1-I1, 2.613; Ni1-I2, 2.627; Ni1-N1, 2.050; Ni1-N2, 2.038; Ni1-C1, 1.898. $[\text{Ni}_2(\eta\text{-C}_5\text{H}_5)_2(\text{C}_6\text{F}_5\text{C}\equiv\text{CC}_6\text{F}_5)]$: Ni1-Ni2, 2.329; Ni1-Cp1, 2.096; Ni1-C7, 1.914; Ni1-C8, 1.899; Ni2-Cp2, 2.106; Ni2-C7, 1.904; Ni2-C8, 1.924; C7-C8, 1.362..... 11
- Figure 1.4: Prominent high-valent Ni^{IV} complexes: $\text{Ni}^{\text{IV}}[\text{C}_6\text{H}_4(\text{NH})_2]_2$, $[(\text{Cp}^*)\text{Ni}^{\text{IV}}]^{2+}$ and $\text{Ni}^{\text{IV}}\text{Me}(3\text{-tertbutyl-5-methyl-2-oxobenzoy})(\text{PMe}_3)_2\text{I}$ 12
- Figure 2.1: ORTEP representation (50% probability ellipsoids) of **1** (left), **2** (middle), and **3** (right). Selected bond distances (Å): **1**, Pd1-Cl1 2.279, Pd1-Cl2 2.307, Pd1-N1 2.057, Pd1-N2 2.062; **2**, Pd1-C1 2.027, Pd1-Cl1 2.307, Pd1-N1 2.044, Pd1-N2 2.172; **3**, Pd1-C1 2.053, Pd1-C2 2.053, Pd1-N1 2.151, Pd1-N2 2.151..... 34
- Figure 2.2: Cyclic voltammograms of **1** (left), **2** (middle), and **3** (right) in 0.1 M Bu_4NClO_4 in CH_2Cl_2 or THF, 100 mV/s scan rate..... 35
- Figure 2.3 UV-Vis spectra of a solution of $[\mathbf{1}^+]\text{ClO}_4$ (left) and $[\mathbf{2}^+]\text{ClO}_4$ (right) in MeCN..... 36
- Figure 2.4: EPR spectra of a solution of $[\mathbf{1}^+]\text{ClO}_4$ (left) and $[\mathbf{2}^+]\text{ClO}_4$ (right) in 3:1 PrCN/MeCN (red lines), and simulated EPR spectra (black lines) using the following parameters: $[\mathbf{1}^+]\text{ClO}_4$, $g_x = 2.163$, $g_y = 2.129$, $g_z = 2.001$ ($A_{\text{N},1} = 35.5$ G, $A_{\text{N},2} = 10.0$ G); $[\mathbf{2}^+]\text{ClO}_4$, $g_x = 2.222$, $g_y = 2.118$, $g_z = 2.011$ ($A_{\text{N},1} = 31.5$ G, $A_{\text{N},2} = 5.0$ G)..... 37
- Figure 2.5: Comparison of experimental (red line) and computational simulated (black line) UV-Vis spectra of complexes $[\mathbf{1}^+]\text{ClO}_4$ (left) and $[\mathbf{2}^+]\text{ClO}_4$ (right) in MeCN..... 40
- Figure 2.6: TD-DFT calculated UV-Vis spectra of complexes $[\mathbf{1}^+]$ (left) and $[\mathbf{2}^+]$ (right)..... 40
- Figure 2.7: DFT-calculated (UB3LYP/CEP-31G) molecular orbitals (β -LUMOs) of $[\mathbf{1}^+]$ (bottom-left) and $[\mathbf{2}^+]$ (bottom-right) compared to similar $^{\text{Me}}\text{N}_4$ supported complexes (top). The calculated atomic contributions, DFT-calculated (X-ray diffraction) axial Pd-N bond distances and the experimental EPR superhyperfine couplings are listed for each complex..... 42

Figure 2.8:	UV-vis spectrum of 2.14 mM solution of 3 in methanol under O ₂ at 20°C (t = 0-1560 min). The UV-Vis spectrum was recorded continuous at 10 minute intervals (left). To highlight the growth of the band at 440 nm, the spectrum at 2 hour intervals is also plotted (right).....	44
Figure 3.1:	Cyclic voltammograms of 1 in 0.1 M Bu ₄ NClO ₄ in tetrahydrofuran: (left) full range, (right) Ni ^{II} /Ni ^{III} couple. Scan rate: 100 mV/s.....	58
Figure 3.2:	ORTEP representation of the cation of 6 with 50% probability thermal ellipsoids. Selected bond distances (Å), Ni1-N1, 1.981; Ni1-N2, 1.956; Ni1-N3, 2.342; Ni1-N4, 2.345; Ni1-C23, 1.993; Ni1-Br1, 2.440.....	59
Figure 3.3:	EPR spectra (black lines) of 6 (left) and 7 (right) in 3:1 PrCN/THF at 77K, and the simulated EPR spectrum (red lines) using the following parameters: 6 , g _x = 2.260, g _y = 2.187 (A _{Br} = 12.0 G), g _z = 2.023 (A _{2N} = 13.0 G and A _{Br} = 12.7 G); 7 , g _x = 2.269, g _y = 2.181, g _z = 2.025 (A _{2N} = 13.8 G).....	60
Figure 4.1:	ORTEP representation of 1 (left) and 3 (right) with 50% prob. thermal ellipsoids. Selected bond lengths (Å), 1 : Ni1-C1, 1.913; Ni1-C2, 1.913; Ni1-N1, 1.973; Ni1-N2, 1.973; 3 : Ni-N1 2.005; Ni-N2 2.005; Ni-C1 1.930; Ni-C2 1.930.....	78
Figure 4.2:	Cyclic voltammograms of 1 (left) and 3 (right) in 0.1 M Bu ₄ NPF ₆ in MeCN. Scan rate: 100 mV/s.....	79
Figure 4.3:	ORTEP representation of the cations 2 (left) and 4 (right) with 50% probability thermal ellipsoids. Selected bond lengths (Å), 2 : Ni1-C1, 1.987; Ni1-C2, 1.978; Ni1-N1, 1.979; Ni1-N2, 1.996; Ni1-N3, 2.252; Ni1-N4, 2.240; 4 : Ni-N1 1.966; Ni-N2 1.956; Ni-N3 2.400; Ni-N4 2.372; Ni-C23 1.968; Ni-C24 1.957.....	80
Figure 4.4:	(Left) EPR spectrum (black line) of 2 in PrCN at 77K, and the simulated EPR spectrum (red line) using the following parameters: g _x = 2.228, g _y = 2.210, g _z = 2.014 (A _{2N} = 14.3 G). (Right) DFT calculated Mulliken spin density for 2 (shown as a 0.005 isodensity contour plot), and the relevant atomic and Ni orbital contributions to the spin density.....	81
Figure 4.5:	(Left) EPR spectrum (black line) of 4 in PrCN at 77K, and the simulated EPR spectrum (red line) using the following parameters: g _x = 2.314, g _y = 2.264, g _z = 2.009 (A _{2N} = 11.0 G). (Right) DFT calculated Mulliken spin density for 4 (shown as a 0.005 isodensity contour plot), and the relevant atomic and Ni orbital contributions to the spin density.....	81
Figure 5.1:	ORTEP representation of 1 (left) and the cation of 2 (right) with 50% probability thermal ellipsoids. Selected bond distances (Å), 1 : Ni1-C1, 1.879; Ni1-C8, 1.954; Ni1-N1, 1.936; Ni1-N2, 1.997. 2 : Ni1-C17, 1.973; Ni1-C18, 1.920; Ni1-N1, 2.001; Ni1-N2, 1.997; Ni1-N3, 2.241; Ni1-N4, 2.266.....	105
Figure 5.2:	Cyclic voltammograms of 1 (left) and 2 (right) in 0.1 M Bu ₄ NPF ₆ in MeCN with a scan rate of 100 mV/s.....	105

Figure 5.3:	EPR spectrum (black line) of 2 in PrCN at 77K, and the simulated EPR spectrum (red line) using the following parameters: $g_x= 2.223$, $g_y= 2.201$, $g_z= 2.012$ ($A_{2N} = 14.5$ G).....	106
Figure 5.4:	X-ray photoelectron spectra of the nickel region for complexes 2 (black line) and 3 (red line). Selected bonding energies (eV), 2 : $2p_{3/2}$, 854.43; $2p_{1/2}$, 871.79. 3 : $2p_{3/2}$, 854.97; $2p_{1/2}$, 872.46.....	108
Figure 5.5:	XPS spectrum of 2 (left) and 3 (right), Bonding energies: 2 , $2p_{3/2}$, 854.43 eV and $2p_{1/2}$, 871.79 eV; 3 , $2p_{3/2}$, 854.97 eV and $2p_{1/2}$, 872.46 eV.....	108
Figure 6.1:	ORTEP representation of the cations 3 (left) and 5 (right) with 50% probability thermal ellipsoids. Selected bond lengths (Å), 3 : Ni1-C1, 1.987; Ni1-C2, 1.978; Ni1-N1, 1.979; Ni1-N2, 1.996; Ni1-N3, 2.252; Ni1-N4, 2.240; 5 : Ni1-C18, 1.959; Ni1-C17, 1.965; Ni1-N1, 1.945; Ni1-N2, 1.974; Ni1-N3, 2.233; Ni1-N4, 2.251, N4-C14, 1.455; C1-C14, 1.358; C14-H14, 0.970. Selected bond angles, 5 : C1-C14-H14, 122.8°.....	120
Figure 6.2:	Comparison of EPR spectra of $[(^{Me}N4)Ni^{III}Me_2]PF_6$ (right) and $(^{Me}N4^*)Ni^{III}Me_2$ (left) in 3:1 THF-Toluene at 77 K. The simulated EPR spectra (red lines) were obtained using the following parameters: $[(^{Me}N4)Ni^{III}Me_2]PF_6$; $g_x= 2.225$, $g_y= 2.208$, $g_z= 2.013$ ($A_{2N} = 14.0$ G) and $(^{Me}N4^*)Ni^{III}Me_2$; $g_x= 2.231$, $g_y= 2.208$, $g_z= 2.012$ ($A_{2N} = 14.0$ G).....	121
Figure 6.3:	Comparison of EPR spectra of $[(^{tBu}N4)Ni^{III}Me_2]PF_6$ (right) and $(^{tBu}N4^*)Ni^{III}Me_2$ (left) in 3:1 THF-Toluene at 77 K. The simulated EPR spectra (red lines) were obtained using the following parameters: $[(^{tBu}N4)Ni^{III}Me_2]PF_6$; $g_x= 2.314$, $g_y= 2.264$, $g_z= 2.009$ ($A_{2N} = 11.0$ G) and $(^{tBu}N4^*)Ni^{III}Me_2$; $g_x= 2.323$ ($A_N = 8.0$), $g_y= 2.269$ ($A_N = 8.0$), $g_z= 2.009$ ($A_{2N} = 10.75$ G).....	121
Figure 6.4:	Comparison of UV-Vis spectra of $[(^{Me}N4)Ni^{III}Me_2]PF_6$ (right) and $(^{Me}N4^*)Ni^{III}Me_2$ (left) in THF (1.25×10^{-4} M).....	122
Figure 6.5:	Comparison of UV-Vis spectra of $[(^{tBu}N4)Ni^{III}Me_2]PF_6$ (right) and $(^{tBu}N4^*)Ni^{III}Me_2$ (left) in THF (1.25×10^{-4} M).....	123
Figure 6.6:	Interconversion between $[(^{Me}N4)Ni^{III}Me_2]PF_6$ (black & blue lines) and $(^{Me}N4^*)Ni^{III}Me_2$ (red line) monitored by EPR (right) and UV-visible (left). LiHMDS (base) and TfOH (acid) were added as stock solutions.....	123
Figure 6.7:	Interconversion between $[(^{tBu}N4)Ni^{III}Me_2]PF_6$ (black & blue lines) and $(^{tBu}N4^*)Ni^{III}Me_2$ (red line) monitored by EPR (right) and UV-visible (left). LiHMDS (base) and TfOH (acid) were added as stock solutions.....	124
Figure A1:	1H NMR spectrum of $^{TsH}N4$ in $CDCl_3$	138
Figure A2:	1H NMR spectrum of $^{TsMe}N4$ in $CDCl_3$	138
Figure A3:	1H NMR spectrum of $(^{TsMe}N4)Pd^{II}Cl_2$ in DMSO.....	139
Figure A4:	1H NMR spectrum of $(^{TsMe}N4)Pd^{II}MeCl$ in $CDCl_3$. Peaks marked with an asterisk correspond to a trace amount of solvent (ether and pentane) in the sample.....	139

Figure A5:	^1H NMR spectrum of ($^{13}\text{C}_6\text{H}_5$) $\text{Pd}^{\text{II}}\text{Me}_2$ in Benzene. Peaks marked with an asterisk correspond to a trace amount of solvent (tetrahydrofuran) in the sample.....	140
Figure A6:	^1H NMR spectrum of ($^{13}\text{C}_6\text{H}_5$) $\text{Ni}^{\text{II}}\text{Me}_2$ in Tetrahydrofuran.....	140
Figure A7:	^1H NMR spectrum of ($^{13}\text{C}_6\text{H}_5$) $\text{Ni}^{\text{II}}(\text{cycloneophyl})$ in MeCN. Peaks marked with an asterisk correspond to a trace amount of solvent (tetrahydrofuran and pentane) in the sample.....	141
Figure A8:	^1H NMR spectrum of ($^{13}\text{C}_6\text{H}_5$) $\text{Ni}^{\text{II}}\text{Me}_2$ in Tetrahydrofuran.....	141
Figure A9:	Proton (left) and carbon (right) structural assignments from NMR expts.....	142
Figure A10:	^1H NMR spectrum of [$(^{13}\text{C}_6\text{H}_5)_2\text{Ni}^{\text{IV}}(\text{cycloneophyl})$](PF_6) $_2$ in MeCN at -15°C	143
Figure A11:	^{13}C NMR spectrum of [$(^{13}\text{C}_6\text{H}_5)_2\text{Ni}^{\text{IV}}(\text{cycloneophyl})$](PF_6) $_2$ in MeCN at -15°C	143
Figure A12:	^1H - ^1H COSY spectrum of [$(^{13}\text{C}_6\text{H}_5)_2\text{Ni}^{\text{IV}}(\text{cycloneophyl})$](PF_6) $_2$ in MeCN.....	144
Figure A13:	^1H - ^{13}C HMBC spectrum of [$(^{13}\text{C}_6\text{H}_5)_2\text{Ni}^{\text{IV}}(\text{cycloneophyl})$](PF_6) $_2$ in MeCN.....	145
Figure A14:	^1H - ^{13}C HSQC spectrum of [$(^{13}\text{C}_6\text{H}_5)_2\text{Ni}^{\text{IV}}(\text{cycloneophyl})$](PF_6) $_2$ in MeCN.....	146
Figure C1:	UV-Vis spectra of 0.50 mM solution of $^{13}\text{C}_6\text{H}_5\text{Ni}(\text{II})\text{Me}_2$ in MeCN reacted with 2 equivalents of $^{13}\text{C}_6\text{H}_5\text{BF}_4$ at -35°C . The spectra are shown at different time points: A) Full reaction, B) Individual species, C) Oxidation Reaction, and D) Warming to RT.....	198
Figure C2:	UV-Vis spectra of 0.50 mM solution of $^{13}\text{C}_6\text{H}_5\text{Ni}(\text{II})\text{Me}_2$ in MeCN reacted with 2 equivalents of H_2O_2 at -35°C . The spectra are shown at different time points: A) Full reaction, B) Individual species, C) Oxidation Reaction, and D) Warming to RT.....	199
Figure C3:	A) EPR monitoring of ($^{13}\text{C}_6\text{H}_5$) NiMe_2 reacting with 1 equivalent of CD_3I at RT over 24 hours. B) EPR spectrum and simulation of reaction species at the 4 hour time point. The ratio of species A to species B at 4 hours is 9:1. Simulation used the following parameters: Species A) $g_x=2.2283$, $g_y=2.2100$, $g_z=2.0137$ ($A_N=14.30$ G), Species B) $g_x=2.2960$, $g_y=2.2398$, $g_z=2.0100$ ($A_N=12.00$ G).....	200
Figure C4:	A) EPR monitoring of ($^{13}\text{C}_6\text{H}_5$) NiMe_2 reacting with 1 equivalent of Iodotoluene at RT over 24 hours. B) EPR spectrum and simulation of reactions species at 4 hour time point. Simulation used the following parameters: $g_x=2.2283$, $g_y=2.2100$, $g_z=2.0137$ ($A_N=14.30$ G).....	200

List of Schemes

Scheme 1.1:	Notable cross-coupling reactions.....	2
Scheme 1.2:	General Pd ^{0/II} catalytic cycle for palladium-catalyzed cross-coupling reaction.....	3
Scheme 1.3:	General Ni ^{I/III} catalytic cycle for nickel-catalyzed cross-coupling reaction.....	4
Scheme 1.4:	Organometallic Ni ^{III} species capable of C-heteroatom bond formation reported by our group.	5
Scheme 1.5:	Select organometallic Pd ^{IV} complexes stabilized by multidentate ligand systems: (TMEDA)Pd ^{IV} Me ₂ (O ₂ CAr), [(Tp)Pd ^{IV} (cycloneophyl)(L)] ⁺ , [(pz ₃ CH)Pd ^{IV} Me ₃] ⁺ and (bpy)Pd ^{IV} I ₂ Me(Tol).....	7
Scheme 1.6:	A stable organometallic Pd ^{III} -Pd ^{III} paddlewheel complexes (left) and the carbon-heteroatom bond formation facilitated by a bimetallic Pd ^{III} complex (right).....	7
Scheme 1.7:	Reactivity of mononuclear organometallic (^t BuN ₄)Pd ^{III} complexes.....	8
Scheme 1.8:	Direct structural and reactivity comparison of [(^{Me} N ₄)Pd ^{III} Me ₂] ⁺ and [(^{Me} N)Pd ^{IV} Me ₂] ²⁺ complexes.....	10
Scheme 1.9:	Aromatic methoxylation by organometallic high-valent nickel complexes.....	12
Scheme 2.1:	Synthetic route for the pseudo-tridentate ^{TsMe} N ₄	32
Scheme 2.5:	Aerobic Reactivity of (^{TsMe} N ₄)Pd ^{II} Me ₂ (3).....	43
Scheme 2.6:	Proposed Mechanism for Aerobic Oxidation of (^{TsMe} N ₄)Pd ^{II} Me ₂ (3) and Subsequent Ethane Elimination.....	46
Scheme 3.1:	C-Halide bond formation reactivity of [(^t BuN ₄)Ni ^{III} (<i>p</i> -aryl)halide] ⁺ complexes...	51
Scheme 3.2:	Synthesis of Ni ^{II} complexes 1-5 and the resulting ligand exchange in organic solvents.....	57
Scheme 3.3:	C-Halide Bond Formation Reactivity of [(^t BuN ₄)Ni ^{III} (<i>ortho</i> -aryl)halide] ⁺ complexes.....	61
Scheme 4.1:	Synthesis of (^R N ₄)Ni ^{II} Me ₂ and [(^R N ₄)Ni ^{III} Me ₂] ⁺ Complexes (R = ^t Bu or Me).....	77
Scheme 4.2:	C-C bond formation reactivity of the complexes 1 and 2	83
Scheme 4.3:	C-C bond formation reactivity of the complexes 3 and 4	83
Scheme 4.4:	C-C bond formation reactivity of crossover experiments using a 1:1 mixture of complexes 1 , 3 and 4	84
Scheme 4.5:	C-C bond formation reactivity of the complexes 1 and 4 in the presence of radical trap TEMPO	84
Scheme 4.6:	Proposed pathway for reactivity of complexes 1 and 2 resulting in C-C bond formation.....	86
Scheme 4.7:	Proposed pathway for the reactivity of complexes 1 , 2 and 4 resulting in C-C bond formation.....	86
Scheme 4.8:	Proposed pathway for the reactivity of complexes 3 and 4 resulting in C-C bond formation.....	87
Scheme 4.9:	Proposed catalytic cycle for the Kumada cross-coupling reactions catalyzed by (^{Me} N ₄)Ni ^{II} Me ₂	89

Scheme 4.10: C-C bond formation reactivity from the oxidation of $(^{\text{Me}}\text{N4})\text{Ni}^{\text{II}}\text{Me}_2$ complex using alkyl and aryl halides.....	90
Scheme 4.11: C-C bond formation reactivity from the reaction of $[(^{\text{Me}}\text{N4})\text{Ni}^{\text{III}}\text{Me}_2]$ BPh ₄ complex with alkyl and aryl halides.....	91
Scheme 4.12: Proposed reaction pathway for the oxidation of $(^{\text{Me}}\text{N4})\text{Ni}^{\text{II}}\text{Me}_2$ by alkyl and aryl halides and the corresponding C-C bond formation reactivity.....	91
Scheme 5.1: Synthesis of $[(\text{Py}_3\text{CH})\text{Ni}^{\text{IV}}(\text{cycloneophyl})(\text{CF}_3)]\text{OTf}$	98
Scheme 5.2: Synthesis of complexes 1-3	104
Scheme 5.3: C-C Bond Formation Reactivity of the $(^{\text{Me}}\text{N4})\text{Ni}^{\text{II}}(\text{cycloneophyl})$ Complex.....	109
Scheme 6.1: Synthesis of $(^{\text{R}}\text{N4}^*)\text{Ni}^{\text{III}}\text{Me}_2$ Complex (R = ^t Bu or Me).....	119
Scheme 6.2: Proposed mechanism for C-H activation by pyridinophane supported Ni complexes.....	125
Scheme 6.3: C-H activation reactivity of pyridinophane supported nickel complexes.....	125
Scheme 7.1: Possible modifications to the N4 ligand system.....	130
Scheme 7.2: Proposed aerobically induced C-C bond formation reactivity of the $(^{\text{Ts}}\text{N4})\text{Pd}^{\text{II}}\text{Me}_2$ complex.....	131
Scheme 7.3: Proposed synthesis and reactivity of <i>meta</i> -substituted nickel complex.....	132
Scheme 7.4: Proposed reactivity of the $[(^{\text{TsMe}}\text{N4})\text{Ni}^{\text{III}}\text{Me}_2]^+$ complex.....	133
Scheme 7.5: Proposed reactivity of Ni^{IV} complex via nucleophilic attack.....	134
Scheme 7.6: Proposed reactivity of Ni^{II} complexes with various oxidants.....	134
Scheme 7.7: Proposed C-H activation studies on deprotonated (N4)Ni complexes.....	135

List of Tables

Table 2.1:	Redox potentials obtained from the CV of complexes 1 , 2 and 3	35
Table 2.2:	DFT-calculated (UB3LYP/CEP-31G) bond lengths (Å) for complexes [1 ⁺] and [2 ⁺] compared to experimentally determined parameters of similar ^{Me} N4 supported complexes.....	39
Table 2.3:	DFT-calculated (UB3LYP/CEP-31G) bond angles (degrees) for complexes [1 ⁺] and [2 ⁺] compared to experimentally determined parameters of similar ^{Me} N4 supported complexes.....	39
Table 2.4:	TD-DFT calculated absorption bands and the corresponding orbital compositions for [1 ⁺]. Only the transitions with oscillator strengths larger than 0.007 are listed; similarly only contributing transitions with greater than 35% contribution to the absorption band are included.....	41
Table 2.5:	TD-DFT calculated absorption bands and the corresponding orbital compositions for [2 ⁺]. Only the transitions with oscillator strengths larger than 0.007 are listed; similarly only contributing transitions with greater than 35% contribution to the absorption band are included.....	41
Table 4.1:	Substrates used in the Kumada cross-coupling reactions catalyzed by 5 mol % (^{Me} N4)Ni ^{II} Me ₂ or [(^{Me} N4)Ni ^{III} Me ₂]BPh ₄ with 1 equivalent R'MgX and 1 equivalent aryl halide at room temperature in THF.....	88
Table 4.2:	Substrates used in the Kumada cross-coupling reactions catalyzed by 5 mol % (^{Me} N4)Ni ^{II} Me ₂ or [(^{Me} N4)Ni ^{III} Me ₂]BPh ₄ with 1 equivalent R'MgX and 1 equivalent alkyl halide at room temperature in THF.....	88
Table B1:	Crystal data and structure refinement for (^{TsMe} N4)Pd ^{II} Cl ₂	148
Table B2:	Bond lengths [Å] and angles [°] for (^{TsMe} N4)Pd ^{II} Cl ₂	149
Table B3:	Crystal data and structure refinement for (^{TsMe} N4)Pd ^{II} MeCl.....	151
Table B4:	Bond lengths [Å] and angles [°] for (^{TsMe} N4)Pd ^{II} MeCl.....	152
Table B5:	Crystal data and structure refinement for (^{TsMe} N4)Pd ^{II} Me ₂	154
Table B6:	Bond lengths [Å] and angles [°] for (^{TsMe} N4)Pd ^{II} Me ₂	155
Table B7:	Crystal data and structure refinement for [(^{tBu} N4)Ni ^{III} (<i>o</i> -PhF)Br]PF ₆	157
Table B8:	Bond lengths [Å] and angles [°] for [(^{tBu} N4)Ni ^{III} (<i>o</i> -PhF)Br]PF ₆	158
Table B9:	Crystal data and structure refinement for (^{Me} N4)Ni ^{II} Me ₂	162
Table B10:	Bond lengths [Å] and angles [°] for (^{Me} N4)Ni ^{II} Me ₂	163
Table B11:	Crystal data and structure refinement for [(^{Me} N4)Ni ^{III} Me ₂]BPh ₄	165
Table B12:	Bond lengths [Å] and angles [°] for [(^{Me} N4)Ni ^{III} Me ₂]BPh ₄	166
Table B13:	Crystal data and structure refinement for (^{Me} N4)Ni ^{II} (cycloneophyl).....	170
Table B14:	Bond lengths [Å] and angles [°] for (^{Me} N4)Ni ^{II} (cycloneophyl).....	171
Table B15:	Crystal data and structure refinement for [(^{Me} N4)Ni ^{III} (cycloneophyl)]BPh ₄	176
Table B16:	Bond lengths [Å] and angles [°] for [(^{Me} N4)Ni ^{III} (cycloneophyl)]BPh ₄	177
Table B17:	Crystal data and structure refinement for (^{tBu} N4)Ni ^{II} Me ₂	182

Table B18:	Bond lengths [Å] and angles [°] for (^t BuN4)Ni ^{II} Me ₂	183
Table B19:	Crystal data and structure refinement for [(^t BuN4)Ni ^{III} Me ₂](BPh ₄).....	184
Table B20:	Bond lengths [Å] and angles [°] for [(^t BuN4)Ni ^{III} Me ₂](BPh ₄).....	185
Table B21:	Crystal data and structure refinement for (^{Me} N4*)Ni ^{III} Me ₂	188
Table B22:	Bond lengths [Å] and angles [°] for (^{Me} N4*)Ni ^{III} Me ₂	189
Table C1:	Yields of the products of elimination from (^{TsMe} N4)Pd ^{II} Me ₂ in saturated CD ₃ OD with O ₂ at 20°C (average of 2 runs).....	192
Table C2:	Yields of the products of elimination from (^{TsMe} N4)Pd ^{II} Me ₂ in saturated CD ₃ OD with O ₂ in the presence of TEMPO at 20°C.....	192
Table C3:	Yields of the products of elimination from (^{TsMe} N4)Pd ^{II} Me ₂ in d ₆ -actone with 1 equivalent of MeI at 20°C (average of 2 runs).....	192
Table C4:	Yields of the products of elimination from (^{TsMe} N4)Pd ^{II} Me ₂ in d ₆ -actone with 20 equivalents MeI at 20°C.....	192
Table C5:	Yields of the products of elimination from (^{TsMe} N4)Pd ^{II} Me ₂ in d ₆ -actone with CD ₃ I at 20°C (average of 2 runs).....	193
Table C6:	Yields of the products from the reaction of (^t BuN4)Ni ^{II} (<i>o</i> -PhF)Br with 1 equivalent of FcPF ₆ in d ₃ -MeCN at RT.....	193
Table C7:	Yields of the products from the reaction of [(^t BuN4)Ni ^{III} (<i>o</i> -PhF)Br]PF ₆ in MeCN at RT.....	193
Table C8:	Yields of the products of elimination from (^{Me} N4)NiMe ₂ in d ₃ -MeCN at RT.....	193
Table C9:	Yields of the products from the reaction of (^{Me} N4)NiMe ₂ with 1 equivalent of FcPF ₆ in d ₃ -MeCN at RT.....	194
Table C10:	Yields of the products from the reaction of (^{Me} N4)NiMe ₂ with 1 equivalent of ^{Ac} FcBF ₄ in d ₃ -MeCN at RT.....	194
Table C11:	Yields of the products from the reaction of (^{Me} N4)NiMe ₂ with 1 equivalent of ^{Ac} FcBF ₄ and 2 equivalents of TEMPO in d ₃ -MeCN at RT.....	194
Table C12:	Yields of the products from the crossover of (^{Me} N4)NiMe ₂ and (^{Me} N4)Ni(CD ₃) ₂ with 1 equivalent of ^{Ac} FcBF ₄ in d ₃ -MeCN at RT.....	194
Table C13:	Yields of the products from the crossover of (^{Me} N4)NiMe ₂ and (^{Me} N4)Ni(CD ₃) ₂ with 1 equivalent of ^{Ac} FcBF ₄ and 2 equivalents of TEMPO in at RT.....	195
Table C14:	Yields of the products from the reaction of (^{Me} N4)NiMe ₂ with 2 equivalents of ^{Ac} FcBF ₄ in d ₃ -MeCN at RT.....	195
Table C15:	Yields of the products from the reaction of (^{Me} N4)NiMe ₂ with 2 equivalents of ^{Ac} FcBF ₄ and 2 equivalents of TEMPO in d ₃ -MeCN at RT.....	195
Table C16:	Yields of the products from the crossover of (^{Me} N4)NiMe ₂ and (^{Me} N4)Ni(CD ₃) ₂ with 2 equivalents of ^{Ac} FcBF ₄ in d ₃ -MeCN at RT.....	195
Table C17:	Yields of the products from the crossover of (^{Me} N4)NiMe ₂ and (^{Me} N4)Ni(CD ₃) ₂ with 2 equivalents of ^{Ac} FcBF ₄ and 2 equivalents of TEMPO in at RT.....	196
Table C18:	Yields of the products from the reaction of (^{Me} N4)NiMe ₂ with 1 equivalent of CD ₃ I in d ₃ -MeCN at RT.....	196

Table C19:	Yields of the products from the reaction of (^{Me} N4)NiMe ₂ with 1 equivalent of CD ₃ I and 2 equivalents of TEMPO in d ₃ -MeCN at RT.....	196
Table C20:	Yields of the products from the reaction of (^{Me} N4)NiMe ₂ with 2 equivalents CD ₃ I in d ₃ -MeCN at RT.....	196
Table C21:	Yields of the products from the reaction of (^{Me} N4)NiMe ₂ with 1 equivalent of FcPF ₆ and 1 equivalent of CD ₃ I in d ₃ -MeCN at RT.....	197
Table C22:	Yields of the products from the reaction of (^{Me} N4)NiMe ₂ with 1 equivalents of CD ₃ I and 2 equivalents of TEMPO in d ₃ -MeCN at RT.....	197
Table C23:	Yields of the products from the reaction of [(^{Me} N4)Ni ^{III} Me ₂]BPh ₄ in d ₃ -MeCN at RT.....	197
Table C24:	Yields of the products from the reaction of [(^{Me} N4)Ni ^{III} Me ₂]BPh ₄ with 1 equivalent of ^{Ac} FcBF ₄ in d ₃ -MeCN at RT.....	197
Table C25:	Products and yields from the Kumada cross-coupling reactions of Iodotoluene and PhMgBr catalyzed by 5 mol % (^{Me} N4)NiMe ₂ or [(^{Me} N4)Ni ^{III} Me ₂]BPh ₄	201
Table C26:	Products and yields from the Kumada cross-coupling reactions of Iodotoluene and MeMgCl catalyzed by 5 mol % (^{Me} N4)NiMe ₂ or [(^{Me} N4)Ni ^{III} Me ₂]BPh ₄	201
Table C27:	Products and yields from the Kumada cross-coupling reactions of Chlorotoluene and PhMgBr catalyzed by 5 mol % (^{Me} N4)NiMe ₂ or [(^{Me} N4)Ni ^{III} Me ₂]BPh ₄	202
Table C28:	Products and yields from the Kumada cross-coupling reactions of Chlorotoluene and MeMgCl catalyzed by 5 mol % (^{Me} N4)NiMe ₂ or [(^{Me} N4)Ni ^{III} Me ₂]BPh ₄	202
Table C29:	Products and yields from the Kumada cross-coupling reactions of Iodooctane and PhMgBr catalyzed by 5 mol % (^{Me} N4)NiMe ₂ or [(^{Me} N4)Ni ^{III} Me ₂]BPh ₄	203
Table C30:	Products and yields from the Kumada cross-coupling reactions of Iodooctane and MeMgCl catalyzed by 5 mol % (^{Me} N4)NiMe ₂ or [(^{Me} N4)Ni ^{III} Me ₂]BPh ₄	203
Table C31:	Products and yields from the Kumada cross-coupling reactions of PhMgBr and (Bromomethyl)cyclopropane catalyzed by 5 mol % (^{Me} N4)NiMe ₂	204
Table C32:	Yields of the products from the reaction of (^{tBu} N4)NiMe ₂ PF ₆ at 50°C.....	204
Table C33:	Yields of the products from the reaction of (^{tBu} N4)NiMe ₂ PF ₆ and (^{tBu} N4)Ni(CD ₃) ₂ PF ₆ in d ₃ -MeCN at 50°C.....	205
Table C34:	Yields of the products from the reaction of (^{tBu} N4)NiMe ₂ PF ₆ with 2 eq TEMPO in d ₃ -MeCN at 50°C.....	205
Table C35:	Yields of the products from the reaction of (^{tBu} N4)NiMe ₂ with O ₂ in d ₃ -MeCN at 50°C.....	205
Table C36:	Yields of the products from the reaction of (^{tBu} N4)NiMe ₂ PF ₆ with 1 eq ThBF ₄ d ₃ -MeCN at 50°C.....	205
Table C37:	Yields of the products from the reaction of (^{tBu} N4)NiMe ₂ with 1 eq FcPF ₆ d ₃ -MeCN at 50°C.....	206
Table C38:	Yields of the products from the reaction of (^{tBu} N4)NiMe ₂ and (^{tBu} N4)Ni(CD ₃) ₂ with 1 eq FcPF ₆ in d ₃ -MeCN at 50°C.....	206

Acknowledgements

At this time I would like to thank several people for their support and guidance throughout my graduate studies. First, I would like to thank my advisor, Professor Liviu M. Mirica, for all of his help, support, and guidance. He was truly a wonderful mentor. The chemist I am today is directly related to his support and guidance. I greatly appreciate everything he has done for me throughout my graduate studies.

I would also like to thank Professors Sophia E. Hayes and Kevin D. Moeller for being members of my annual committee. Your insights and support have been extraordinarily beneficial. Additionally, I would like to thank Professors John R. Bleeke, Julio M. D'Arcy and Nigam P. Rath for being members of my defense committee. Furthermore, I would like to acknowledge Professor Nigam P. Rath for his help and advice in the analysis of all the X-ray structures reported in this work and obtained throughout my graduate studies.

This work would not have been possible without the support and guidance of numerous people. I would like to thank all the current and former members of the Mirica Group for their constant support, advice and friendship. You guys were always there when I needed a helping hand or a good laugh. I wish you all the best in your future endeavors. In addition, I would like to thank the entire chemistry department research and administrative staff for their great guidance throughout the past few years.

I would like to thank the following organizations for the financial support during my graduate studies: the Department of Chemistry at Washington University in St. Louis, the American Chemical Society Petroleum Research Fund (52988-ND3), the Department of Energy (DE-FG02-11ER16254), the National Science Foundation (CHE-1255424 and CHE-1429711),

the Homeyer Fellowship, and the Washington University in St. Louis Dean's Dissertation Fellowship.

Lastly, I would like to thank my family, to whom I dedicate this work, for all they have done for me. To my mother, your unyielding love and support has made this work possible. The person I am today is a testament to your patience and caring nature. To my father, you are my best friend and my hero. You are a constant reminder of the importance of family. I am exceedingly grateful for every additional day we have had together. To my wife and son, you bring purpose to my life. You are the driving force behind everything I do in my life, putting joy and happiness into every day. Your love and support is truly a gift.

Jason W. Schultz

Washington University in St. Louis

May 2016

This work is dedicated to my family.

ABSTRACT OF THE DISSERTATION

High-Valent Organometallic Palladium and Nickel Complexes and their Roles in Carbon-Carbon
and Carbon-Heteroatom Bond Formation Reactions

by

Jason W. Schultz

Doctor of Philosophy in Chemistry

Washington University in St. Louis, 2016

Professor Liviu M. Mirica, Chair

The development of palladium catalysis has been influential in a wide range of organic transformations, in particular C-C coupling, C-Heteroatom coupling and C-H functionalization reactions. These catalytic transformations normally proceed through the Pd^{0/II} catalytic cycle. These reactions are remarkably useful, however, they suffer from two major problems: β -hydride elimination and palladium black deposition. To circumvent these problems, recent reports have been focused on developing novel organic transformations proceeding through high-valent palladium and nickel catalytic cycles.

To this point, we recently reported the isolation and characterization of various mononuclear Pd^{III} complexes using the tetradentate ligands, *N,N'*-di-*alkyl*-2,11-diaza[3.3](2,6)pyridinophane (^RN₄, R = ^tBu, ⁱPr, Me). As a result, the ligand effects on the stability and reactivity of the corresponding high-valent palladium complexes were studied. Herein, we report our continued effects to improve our overall understanding of these high-valent complexes and the roles they may play in catalytic transformations.

First, we investigated the synthesis and utilization of an asymmetric N4 ligand, resulting in the destabilization of the ensuing Pd^{III} complexes. Then we synthesized a series of arene-substituted nickel complexes to study the effect of altering the electronics and sterics of the ligand on the nickel complexes' stability and reactivity. The synthesis and reactivity of the first reported dialkyl Ni^{III} complexes was investigated next. These studies along with additional synthesis and characterization of a Ni^{IV} complex provided strong evidence for the involvement of Ni^{IV} intermediates during nickel catalyzed cross-coupling reactions. Lastly, we investigated the deprotonation of the N4 ligand system in hopes of facilitating various C-H activation reactions. All told, these studies gave us valuable insights into high-valent palladium and nickel complexes relevant to C-C coupling, C-Heteroatom coupling and C-H functionalization reactions. By continuing to improve our understanding of these valuable organic transformations, we can continue to develop more effective catalytic systems.

Chapter 1

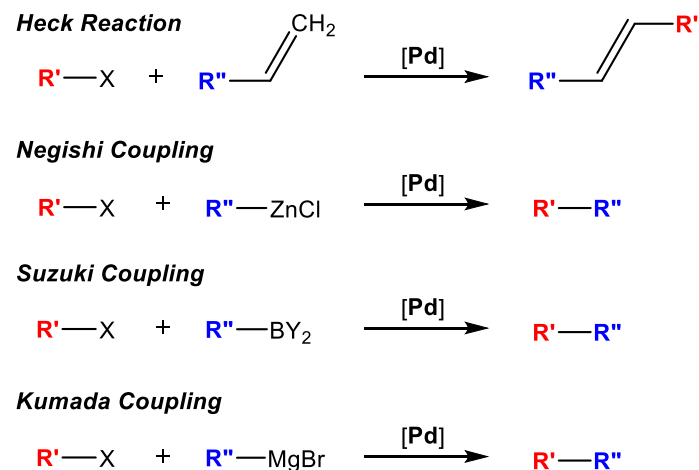
Palladium and Nickel Complexes Relevant to Cross-Coupling and Carbon-Heteroatom Bond Formation Reactions

1.1 Developments in Palladium Catalysis

The development of palladium catalysis has been influential in a wide range of organic transformations, in particular C-C coupling, C-Heteroatom coupling and C-H functionalization reactions. These catalytic transformations normally proceed with high versatility and selectivity. The majority of the reported transformations involve a Pd^{0/II} catalytic cycle, which correlates nicely to palladium's strong affinity for the Pd⁰ and Pd^{II} oxidation states.¹⁻³

Of the numerous palladium catalyzed reactions, cross-coupling reactions are of particular importance. The ability to control and understand the formation of new carbon-carbon bonds plays a critical role in the synthesis of new organic molecules. Over the past few decades many cross-coupling reactions have been developed, thus affording new pathways to previously unattainable organic molecules (Scheme 1.1).⁴⁻¹⁰

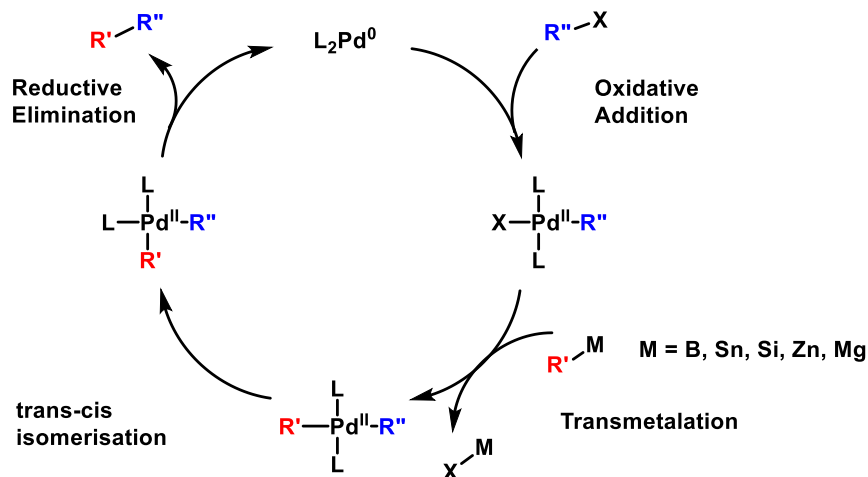
Scheme 1.1 Notable cross-coupling reactions.



Through the years, palladium catalyzed cross-coupling reactions have played significant roles in the development of numerous pharmaceuticals, natural products, and polymers. The majority of these cross-coupling reactions involve the conventional Pd^{0/II} catalytic cycle, which

contains three fundamental steps: oxidative addition, transmetalation, and reductive elimination (Scheme 1.2).^{1,4-15} These reactions are remarkably useful, however, they suffer from two major problems: β -hydride elimination and Pd^0 deposition. To circumvent these problems, novel catalytic systems employing high-valent Pd^{III} and/or Pd^{IV} active intermediates have recently been reported as alternatives for the well-established Pd^0 and Pd^{II} catalysts. For instance, a number of organic transformations have been developed utilizing the advantageous Pd^{III} or Pd^{IV} catalytic cycles.¹⁶⁻³⁴ These high-valent reactions generally proceed under mild reaction conditions with exceptional site selectivity due to the increased reactivity of the Pd^{III} and Pd^{IV} intermediates.³⁵ Further development of these high-valent palladium-catalyzed transformations is vital to developing improved catalytic systems.

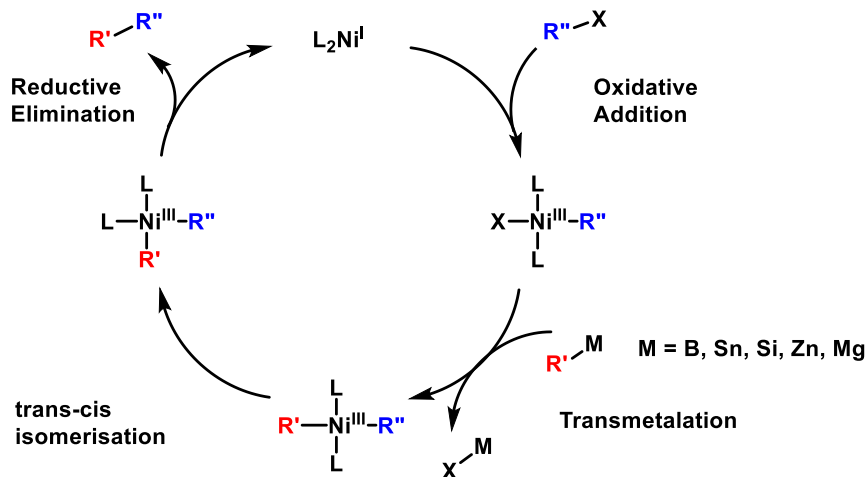
Scheme 1.2 General $\text{Pd}^{0/\text{II}}$ catalytic cycle for palladium-catalyzed cross-coupling reaction.



1.2 Transition to Nickel Catalysis

Nickel complexes similar to palladium complexes have been employed in a wide range of organic transformations, most notably in cross-coupling and C-heteroatom bond formation reactions.³⁶⁻⁴¹ Nickel and palladium are both group 10 metals and have significant similarities. Therefore utilizing nickel catalysts instead of palladium catalysts could provide major cost and toxicity benefits. Additionally, nickel can more easily undergo both one- and two-electron redox reactions, thus enabling the Ni^{III} and/or Ni^I oxidation states to be more commonly proposed as catalytic intermediates in cross-coupling reactions⁴²⁻⁶⁶ and oxidatively induced C-heteroatom bond formation reactions (Scheme 1.3).⁶⁷⁻⁷¹

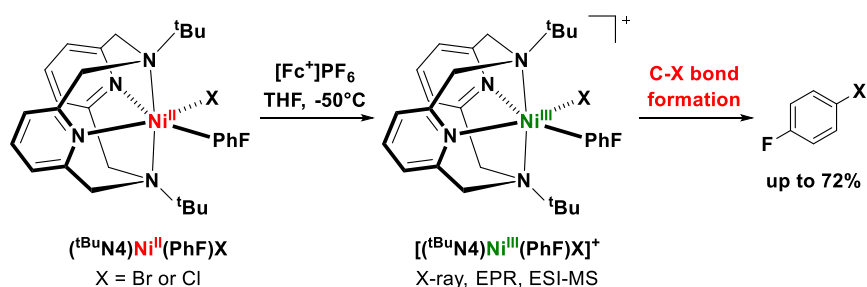
Scheme 1.3 General Ni^{I/III} catalytic cycle for nickel-catalyzed cross-coupling reaction.



The mechanism for nickel-catalyzed cross-coupling is not fully understood, unlike its thoroughly-studied palladium-catalyzed counterpart. The presence of highly reactive paramagnetic species generally makes reactivity studies more difficult. To this point, no organometallic Ni^{III} species capable of undergoing C-C or C-heteroatom bond formation had been isolated or characterized until our group reported the synthesis of a series of Ni^{III}(aryl)halide

complexes in 2014 (Scheme 1.4).⁷² Overcoming the limitations associated with nickel catalysis is essential to gaining a better understanding of these reactions and the role they may play in the future development of new organic molecules.

Scheme 1.4 Organometallic Ni^{III} species capable of C-heteroatom bond formation reported by our group.



1.3 High-Valent Organometallic Palladium Complexes

The investigation of high-valent Pd^{III} and Pd^{IV} complexes is relatively new compared to the heavily investigated Pd⁰ and Pd^{II} complexes. The first reported structural characterization of an organometallic Pd^{IV} complex, (bpy)Pd^{IV}Me₃I, was in 1986 by Canty *et al* (Figure 1.1).⁷³⁻⁷⁵ A year later the first reported structural characterization of a mononuclear Pd^{III} complex, [Pd^{III}(ttcn)₂]³⁺ (ttcn = 1,4,7-trithiacyclononane), was reported by Schroder *et al* (Figure 1.1).⁷⁶ The reported structures revealed the Pd^{III} and Pd^{IV} oxidation states preferred an octahedral geometry. Additionally, the X-ray structures of [Pd^{III}(ttcn)₂]³⁺ revealed a strong Jahn-Teller distortion to the octahedral geometry as expected for a Pd^{III} d⁷ metal center.

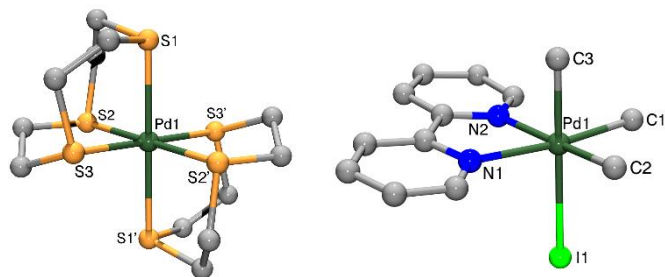
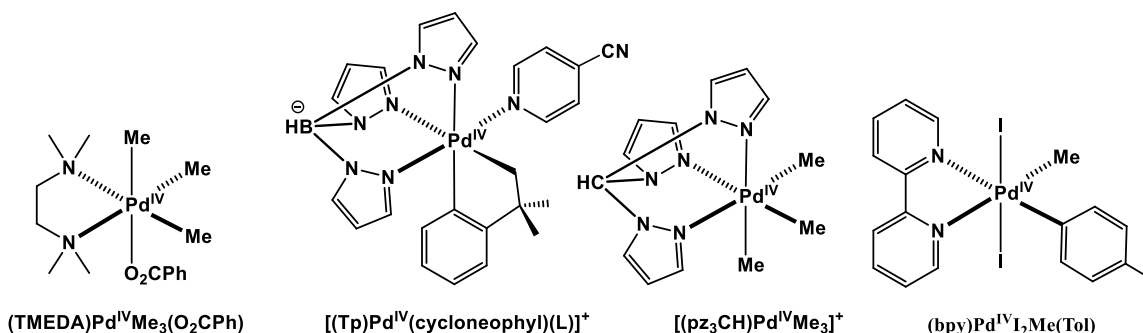


Figure 1.1 ORTEP⁷⁷ representation of $[\text{Pd}^{\text{III}}(\text{ttcn})_2](\text{ClO}_4)_3$ (left) and $(\text{bpy})\text{Pd}^{\text{IV}}\text{Me}_3\text{I}$ (right). Selected bond distances (\AA), $[\text{Pd}^{\text{III}}(\text{ttcn})_2](\text{ClO}_4)_3$: Pd1-S1, 2.545; Pd1-S2, 2.356; Pd1-S3, 2.369. $(\text{bpy})\text{Pd}^{\text{IV}}\text{Me}_3\text{I}$: Pd1-C1, 2.046; Pd1-C2, 2.034; Pd1-C3, 2.040; Pd1-N1, 2.188; Pd1-N2, 2.173; Pd1-I1, 2.834.

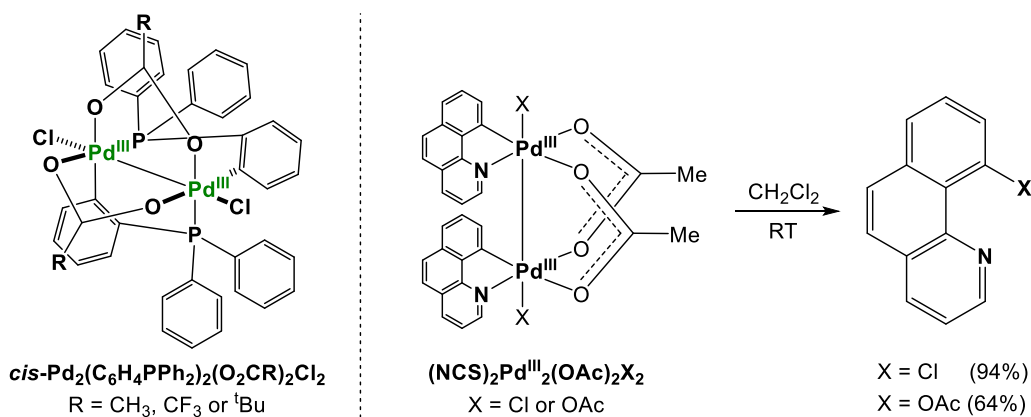
Over the past three decades, organometallic Pd^{IV} complexes have been heavily investigated. As a result, a wide range of organometallic Pd^{IV} complexes have been isolated and characterized. Multidentate ligand systems, including Tetramethylethylenediamine [TMEDA], 1,4,7-Triazacyclononane [TACN], hydrotris(pyrazolyl)borate [Tp], tris(pyrazol-1-yl)methane [(pz)₃CH] and bipyridine derivatives have been utilized to stabilize and support these reactive Pd^{IV} complexes (Scheme 1.5).⁷⁸⁻⁸⁴ A majority of the reported Pd^{IV} complexes were synthesized from commercially available Pd^{II} precursors using a wide range of chemical and electrochemical oxidation methods.^{1,85} These enhanced Pd^{IV} systems have resulted in a significant number of new organic transformations vital in the development of improved pharmaceuticals, natural products and polymers.

Scheme 1.5 Select organometallic Pd^{IV} complexes stabilized by multidentate ligand systems: (TMEDA)Pd^{IV}Me₂(O₂CAr)⁸⁶, [(Tp)Pd^{IV}(cycloneophyl)(L)]⁺⁸⁷, [(pz₃CH)Pd^{IV}Me₃]⁺⁸⁸ and (bpy)Pd^{IV}I₂Me(Tol)⁸⁶.



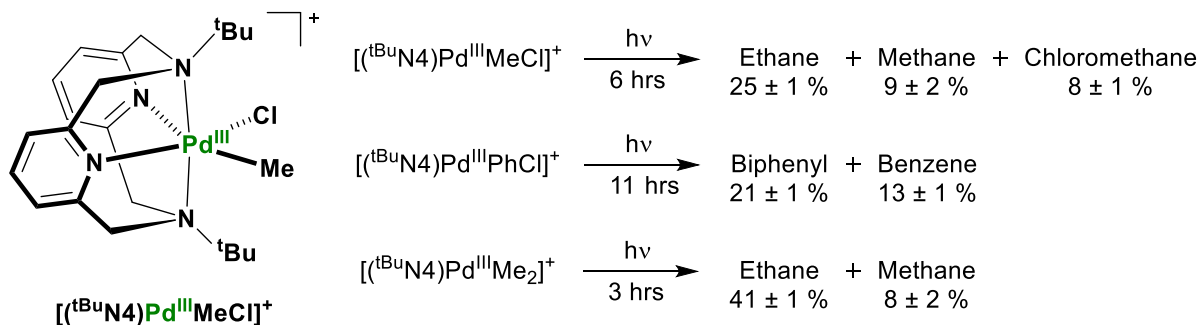
In contrast to the extensive investigation of organometallic Pd^{IV} complexes, the investigation of Pd^{III} complexes was relatively dormant until the late 2000s. At this time, several organometallic Pd^{III} complexes were reported, starting with Cotton *et al* reporting the synthesis of a stable Pd^{III}-Pd^{III} paddlewheel complex in 2006 (Scheme 1.6).⁸⁹ Followed shortly thereafter by Ritter *et al* reporting the first organometallic reaction facilitated by a bimetallic Pd^{III} complex in 2009 (Scheme 1.6).^{90,91} Likewise in 2010, our group reported the first isolation and structural characterization of a series of mononuclear organometallic Pd^{III} complexes (Scheme 1.7).⁹²

Scheme 1.6 A stable organometallic Pd^{III}-Pd^{III} paddlewheel complexes (left) and the carbon-heteroatom bond formation facilitated by a bimetallic Pd^{III} complex (right).



Our group's work utilized a special tetradentate ligand, N,N'-di-tert-butyl-2,11-diaza[3.3](2,6)pyridinophane (^tBuN4), to stabilize the Pd^{III} complexes by allowing them to adopt the preferred distorted octahedral geometry. This unprecedented stability provided a unique platform to study the properties and reactivity of organometallic Pd^{III} complexes. Our isolated Pd^{III} complexes were brightly colored with strong LMCT bands observable via UV-Vis spectroscopy. The characteristic Pd^{III} electron paramagnetic resonance (EPR) spectra confirmed the unpaired electron was localized in the *d*_{z²} ground state for most of our Pd^{III} complexes (Figure 1.2). The reactivity of these Pd^{III} complexes showed the formation of various organic products (ethane, methane, chloromethane, biphenyl and benzene) upon irradiation via a radical mechanism initiated by the homolytic cleavage of the Pd-Carbon bond (Scheme 1.7).⁹²

Scheme 1.7 Reactivity of mononuclear organometallic (^tBuN4)Pd^{III} complexes.



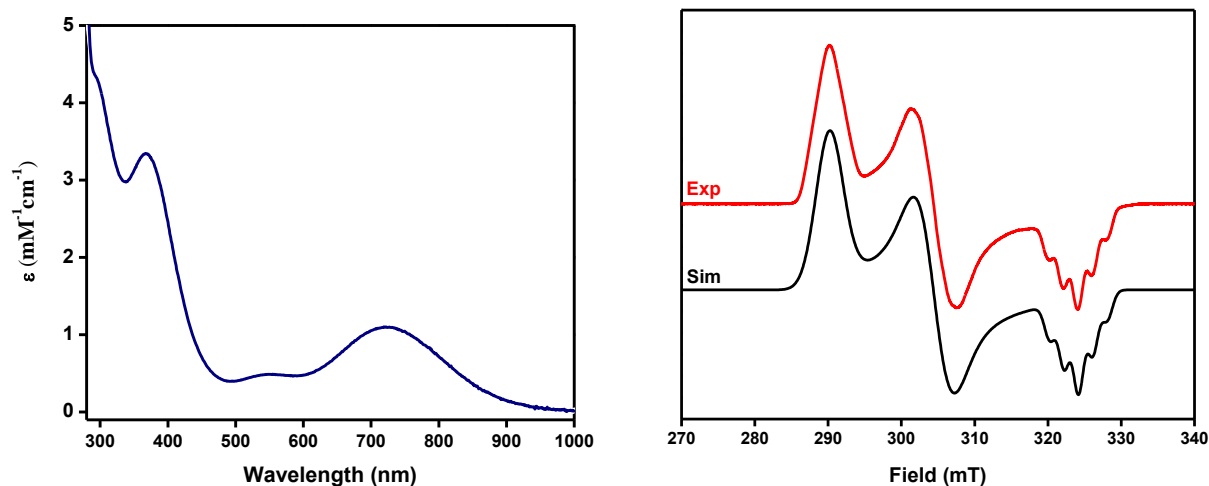
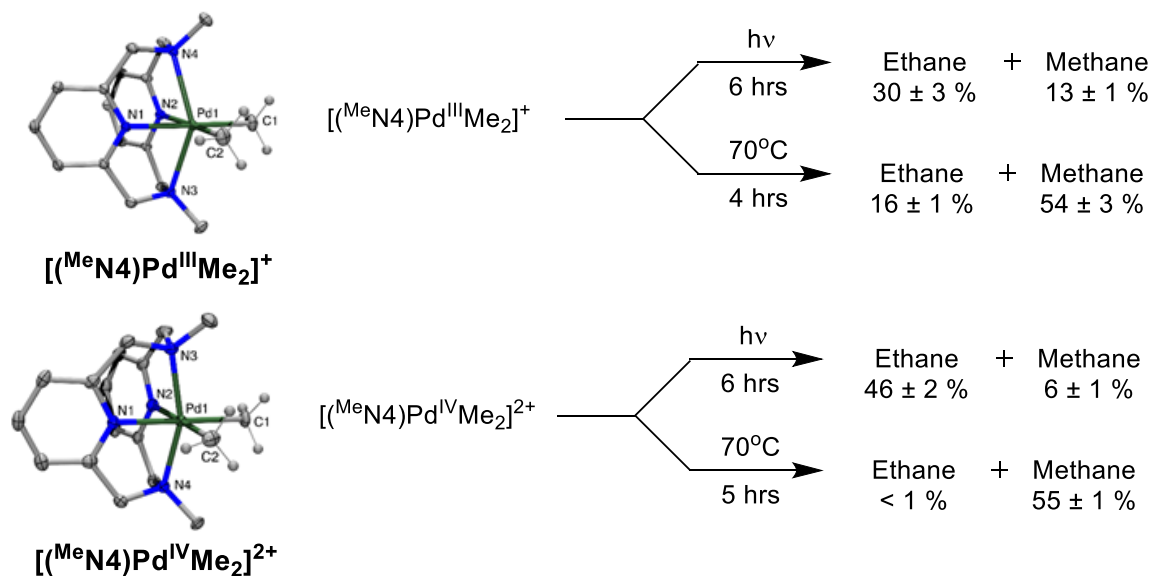


Figure 1.2 UV-Vis spectrum for $[(^t\text{BuN}4)\text{Pd}^{\text{III}}\text{MeCl}](\text{ClO}_4)$ in MeCN (left) and EPR spectrum of $[(^t\text{BuN}4)\text{Pd}^{\text{III}}\text{MeCl}](\text{ClO}_4)$ in 3:1 PrCN/MeCN (right) experimental (red line) and simulated spectrum (black line) using the following parameters: $g_x = 2.239$, $g_y = 2.134$, $g_z = 2.005$ ($A_N = 19.5$ G).

Over the past few years, our group has continued to show the unique opportunities offered by these pyridinophane (N4) supported complexes. In 2012, we reported the first aerobic oxidation of a dimethyl Pd^{II} complex capable of oxidatively-induced C-C bond formation involving Pd^{III} and Pd^{IV} intermediates.⁹³ Shortly thereafter, the conformational flexibility associated with the N4 ligand system was found to be quintessential to the stabilization of these rare Pd^{III} complexes.⁹⁴ To this end, the N4 ligand system has been modified to study the electronic and steric effect associated with this unique stabilization.⁹⁵⁻¹⁰⁰ In particular, the N,N'-di-methyl-2,11-diaza[3.3](2,6)pyridinophane ($^{\text{Me}}\text{N}4$) ligand has been shown to not only stabilize the Pd^{III} oxidation state, but the Pd^{IV} oxidation state as well. This unprecedented stability allowed the first direct comparison of two palladium oxidations in an identical ligand environment (Scheme 1.8).^{95,96}

Scheme 1.8 Direct structural and reactivity comparison of $[(^{\text{Me}}\text{N}_4)\text{Pd}^{\text{III}}\text{Me}_2]^+$ and $[(^{\text{Me}}\text{N})\text{Pd}^{\text{IV}}\text{Me}_2]^{2+}$ complexes. Selected bond distances (Å), $[(^{\text{Me}}\text{N}_4)\text{Pd}^{\text{III}}\text{Me}_2]^+$: Pd1-C1, 2.043; Pd1-C2, 2.043; Pd1-N1, 2.139; Pd1-N2, 2.139; Pd1-N3, 2.401; Pd1-N4, 2.351. $[(^{\text{Me}}\text{N})\text{Pd}^{\text{IV}}\text{Me}_2]^{2+}$: Pd1-C1, 2.042; Pd1-C2, 2.039; Pd1-N1, 2.054; Pd1-N2, 2.058; Pd1-N3, 2.129; Pd1-N4, 2.116.



Over the past few decades, great progress has been made in the isolation and characterization of reactive high-valent palladium complexes. These fundamental studies on Pd^{III} and Pd^{IV} have strongly reinforced the potential high-valent catalysis may play in the future. Continued exploration of Pd^{III} and Pd^{IV} complexes will generally aid our overall understanding of palladium catalysis and improve our ability to develop novel organic transformations.

1.4 High-Valent Organometallic Nickel Complexes

In recent years, the investigation of high-valent nickel complexes has greatly progressed. However, a number of Ni^{III} complexes were reported as early as 1936.¹⁰¹ Even though many of the early reported Ni^{III} complexes were later found to be Ni^{II} -stabilized ligand cation radicals by using electron paramagnetic resonance (EPR) studies,¹⁰² the first reported X-ray structure of a

stable Ni^{III} was reported back in 1968 by Gray *et al* (Figure 1.3).¹⁰³ Nearly two decades later, the first stable mononuclear organometallic Ni^{III} was reported by Welch *et al* in 1983 (Figure 1.3).¹⁰⁴ Additionally, numerous binuclear organometallic Ni^{III} complexes have been reported over the past four decades utilizing a cyclopentadienyl ring moiety (Figure 1.3).¹⁰⁵⁻¹⁰⁷

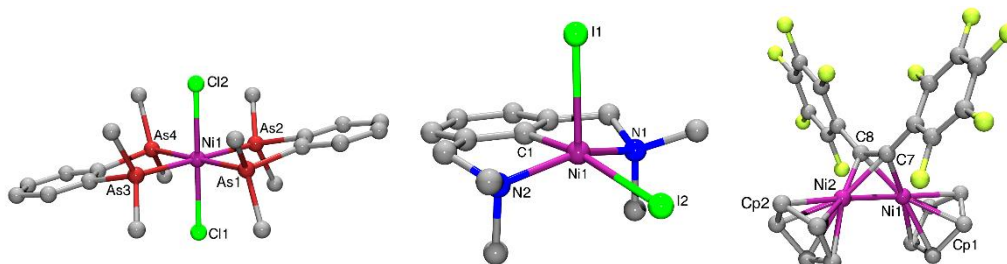


Figure 1.3 ORTEP⁷⁷ representation of [Ni^{III}(diars)₂Cl₂]Cl (left), Ni[C₆H₃(CH₂NMe₂)_{2-o,o'}]I₂ (middle) and [Ni₂(η-C₅H₅)₂(C₆F₅C≡CC₆F₅)] (right). Selected bond distances (Å), [Ni^{III}(diars)₂Cl₂]Cl: Ni1-As1, 2.37; Ni1-As2, 2.34; Ni1-Cl1, 2.43. Ni[C₆H₃(CH₂NMe₂)_{2-o,o'}]I₂: Ni1-I1, 2.613; Ni1-I2, 2.627; Ni1-N1, 2.050; Ni1-N2, 2.038; Ni1-C1, 1.898. [Ni₂(η-C₅H₅)₂(C₆F₅C≡CC₆F₅)]: Ni1-Ni2, 2.329; Ni1-Cp1, 2.096; Ni1-C7, 1.914; Ni1-C8, 1.899; Ni2-Cp2, 2.106; Ni2-C7, 1.904; Ni2-C8, 1.924; C7-C8, 1.362.

Similar to Ni^{III} complexes, Ni^{IV} complexes have likewise become a subject of increased focus. Most notably, Sanford *et al* has reported the reactivity and isolation of Ni^{IV} intermediates which are implicated in various organic transformations (i.e. nickel catalyzed C-C cross-coupling and C-heteroatom bond formation).¹⁰⁸⁻¹¹¹ Although these recent reports have garnered excitement, the first Ni^{IV} complex was reported over a century ago. A series of alkali nickel molybdate complexes were first reported by Hall *et al* in 1907.¹¹² Sixty years later, the first reported X-ray structure of a stable Ni^{IV} complex was reported in 1968 by Soderberg *et al* (Figure 1.4).¹¹³ Furthermore, the first organometallic Ni^{IV} complex was reported in 1982 and the first organometallic Ni^{IV} X-ray structures were reported in 1994 (Figure 1.4).^{114,115}

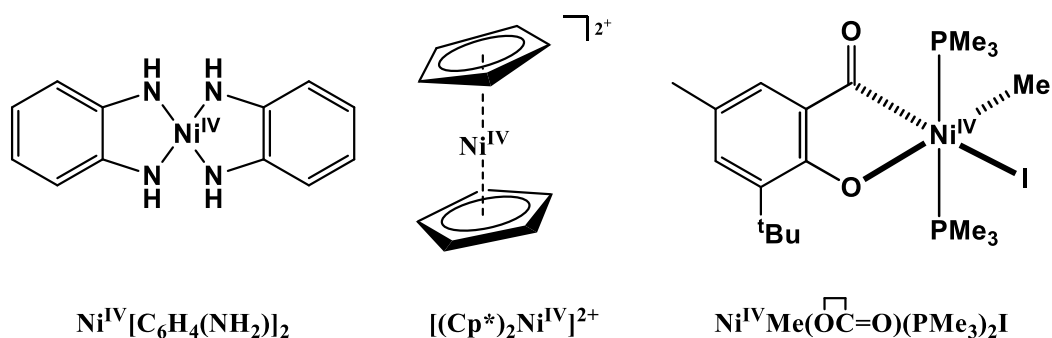
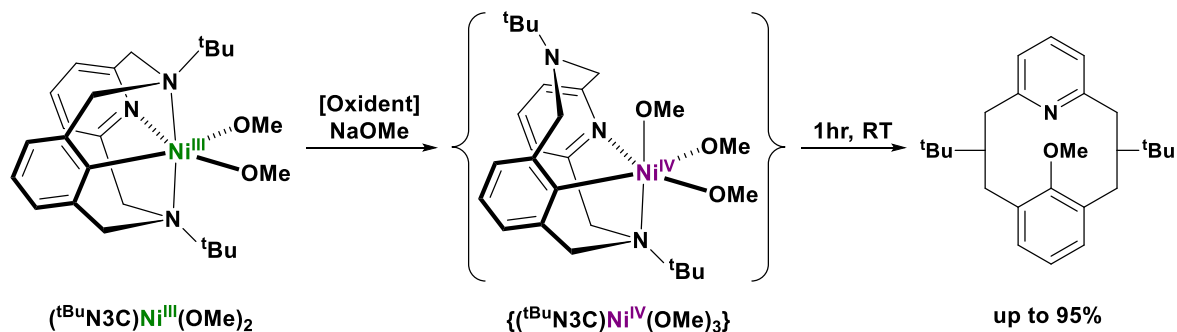


Figure 1.4 Prominent high-valent Ni^{IV} complexes: $\text{Ni}^{\text{IV}}[\text{C}_6\text{H}_4(\text{NH}_2)_2]_2$ ¹¹³, $[(\text{Cp}^*)_2\text{Ni}^{\text{IV}}]^{2+}$ ¹¹⁴ and $\text{Ni}^{\text{IV}}\text{Me}(3\text{-tertbutyl-5-methyl-2-oxobenzoyl})(\text{PMe}_3)_2\text{I}$ ¹¹⁵.

Inspired by these previous reports and our group's aforementioned experience investigating high-valent palladium complexes, in 2014 we reported the first isolation and characterization of a series of organometallic Ni^{III} species capable of undergoing C-C or C-heteroatom bond formation (Scheme 1.4).⁷² Additionally, in 2015 we reported the isolation and characterization of a pair of extraordinarily stable $(\text{N}_4)\text{Ni}^{\text{III}}(\text{CF}_3)_2$ complexes.¹¹⁶ Lastly, we recently reported an aromatic methoxylation and hydroxylation proposed to proceed through a highly-reactive Ni^{IV} intermediate (Scheme 1.9).¹¹⁷

Scheme 1.9 Aromatic methoxylation by organometallic high-valent nickel complexes.



Over the past century, high-valent nickel chemistry has developed into a growing area of investigation. Similar to its counterpart palladium, these fundamental studies on Ni^{III} and Ni^{IV} have revealed the ample possibilities high-valent catalysis may offer in the future. Continued exploration into Ni^{III} and Ni^{IV} complexes will further our overall understanding of nickel chemistry, subsequently improving our ability to develop novel catalytic systems.

1.5 References

1. Negishi, E. *Handbook of Organopalladium Chemistry for Organic Synthesis*; John Wiley & Sons: Hoboken, NJ, 2002.
2. Henry, P. M. *Palladium Catalyzed Oxidation of Hydrocarbons*; D. Reidel: Boston, 1980.
3. Hartwig, J. F. *Organotransition Metal Chemistry: From Bonding to Catalysis*; University Science Books: Sausalito, 2010.
4. Mizoroki, T.; Mori, K.; Ozaki, A. *Bull. Chem. Soc. Jpn.* **1971**, *44*, 581.
5. Tamao, K.; Sumitani, K.; Kumada, M. *J. Am. Chem. Soc.* **1972**, *94*, 4374.
6. Sonogashira, K.; Tohda, Y.; Hagihara, N. *Tetrahedron Lett.* **1975**, *16*, 4467.
7. King, A. O.; Okukado, N.; Negishi, E.-i. *J. Chem. Soc., Chem. Commun.* **1977**, 683.
8. Milstein, D.; Stille, J. K. *J. Am. Chem. Soc.* **1978**, *100*, 3636.
9. Miyaura, N.; Suzuki, A. *J. Chem. Soc., Chem. Commun.* **1979**, 866.
10. Hatanaka, Y.; Hiyama, T. *Synlett* **1991**, *1991*, 845.
11. Beccalli, E. M.; Brogini, G.; Martinelli, M.; Sottocornola, S. *Chem. Rev.* **2007**, *107*, 5318.
12. Buchwald, S. L.; Mauger, C.; Mignani, G.; Scholz, U. *Adv. Synth. Catal.* **2006**, *348*, 23.
13. Muzart, J. *Tetrahedron* **2005**, *61*, 5955.

14. Stahl, S. S. *Angew. Chem. Int. Ed.* **2004**, *43*, 3400.
15. Guilarte, V.; Fernández-Rodríguez, M. A.; García-García, P.; Hernando, E.; Sanz, R. *Org. Lett.* **2011**, *13*, 5100.
16. Muniz, K. *Angew. Chem. Int. Ed.* **2009**, *48*, 9412.
17. Sehnal, P.; Taylor, R. J. K.; Fairlamb, I. J. S. *Chem. Rev.* **2010**, *110*, 824.
18. Hull, K. L.; Lanni, E. L.; Sanford, M. S. *J. Am. Chem. Soc.* **2006**, *128*, 14047.
19. Kalyani, D.; Deprez, N. R.; Desai, L. V.; Sanford, M. S. *J. Am. Chem. Soc.* **2005**, *127*, 7330.
20. Dick, A. R.; Hull, K. L.; Sanford, M. S. *J. Am. Chem. Soc.* **2004**, *126*, 2300.
21. Desai, L. V.; Malik, H. A.; Sanford, M. S. *Org. Lett.* **2006**, *8*, 1141.
22. Wang, G.-W.; Yuan, T.-T.; Wu, X.-L. *The Journal of Organic Chemistry* **2008**, *73*, 4717.
23. Jordan-Hore, J. A.; Johansson, C. C. C.; Gulias, M.; Beck, E. M.; Gaunt, M. J. *J. Am. Chem. Soc.* **2008**, *130*, 16184.
24. Kalyani, D.; Sanford, M. S. *Org. Lett.* **2005**, *7*, 4149.
25. Hull, K. L.; Anani, W. Q.; Sanford, M. S. *J. Am. Chem. Soc.* **2006**, *128*, 7134.
26. Hull, K. L.; Sanford, M. S. *J. Am. Chem. Soc.* **2009**, *131*, 9651.
27. Ye, Y.; Ball, N. D.; Kampf, J. W.; Sanford, M. S. *J. Am. Chem. Soc.* **2010**, *132*, 14682.
28. Wang, X.; Truesdale, L.; Yu, J.-Q. *J. Am. Chem. Soc.* **2010**, *132*, 3648.
29. Zhang, J.; Khaskin, E.; Anderson, N. P.; Zavalij, P. Y.; Vedernikov, A. N. *Chem. Commun.* **2008**, 3625.
30. Zhang, Y.-H.; Yu, J.-Q. *J. Am. Chem. Soc.* **2009**, *131*, 14654.
31. Wang, A.; Jiang, H.; Chen, H. *J. Am. Chem. Soc.* **2009**, *131*, 3846.

32. Boisvert, L.; Denney, M. C.; Kloek, H. S.; Goldberg, K. I. *J. Am. Chem. Soc.* **2009**, *131*, 15802.
33. Zhu, M.-K.; Zhao, J.-F.; Loh, T.-P. *J. Am. Chem. Soc.* **2010**, *132*, 6284.
34. Vedernikov, A. N. *Acc. Chem. Res.* **2012**, *45*, 803.
35. Lyons, T. W.; Sanford, M. S. *Chem. Rev.* **2010**, *110*, 1147.
36. Meijere, A. d.; Diederich, F. *Metal-Catalyzed Cross-Coupling Reactions*; Wiley-VCH: Weinheim, New York, 2004.
37. Netherton, M. R.; Fu, G. C. *Adv. Synth. Catal.* **2004**, *346*, 1525.
38. Frisch, A. C.; Beller, M. *Angew. Chem. Int. Ed.* **2005**, *44*, 674.
39. Phapale, V. B.; Cardenas, D. J. *Chem. Soc. Rev.* **2009**, *38*, 1598.
40. Rudolph, A.; Lautens, M. *Angew. Chem. Int. Ed.* **2009**, *48*, 2656.
41. Knochel, P.; Thaler, T.; Diene, C. *Isr. J. Chem.* **2012**, *50*, 547.
42. Tsou, T. T.; Kochi, J. K. *J. Am. Chem. Soc.* **1978**, *100*, 1634.
43. Tsou, T. T.; Kochi, J. K. *J. Am. Chem. Soc.* **1979**, *101*, 7547.
44. Amatore, C.; Jutand, A. *Organometallics* **1988**, *7*, 2203.
45. Zhou, J.; Fu, G. C. *J. Am. Chem. Soc.* **2004**, *126*, 1340.
46. Powell, D. A.; Fu, G. C. *J. Am. Chem. Soc.* **2004**, *126*, 7788.
47. Owston, N. A.; Fu, G. C. *J. Am. Chem. Soc.* **2010**, *132*, 11908.
48. Zultanski, S. L.; Fu, G. C. *J. Am. Chem. Soc.* **2011**, *133*, 15362.
49. Dudnik, A. S.; Fu, G. C. *J. Am. Chem. Soc.* **2012**, *134*, 10693.
50. Zultanski, S. L.; Fu, G. C. *J. Am. Chem. Soc.* **2013**, *135*, 624.
51. Jones, G. D.; McFarland, C.; Anderson, T. J.; Vicic, D. A. *Chem. Commun.* **2005**, 4211.

52. Jones, G. D.; Martin, J. L.; McFarland, C.; Allen, O. R.; Hall, R. E.; Haley, A. D.; Brandon, R. J.; Konovalova, T.; Desrochers, P. J.; Pulay, P.; Vicic, D. A. *J. Am. Chem. Soc.* **2006**, *128*, 13175.
53. Klein, A.; Budnikova, Y. H.; Sinyashin, O. G. *J. Organomet. Chem.* **2007**, *692*, 3156.
54. Phapale, V. B.; Bunuel, E.; Garcia-Iglesias, M.; Cardenas, D. J. *Angew. Chem. Int. Ed.* **2007**, *46*, 8790.
55. Phapale, V. B.; Guisan-Ceinos, M.; Bunuel, E.; Cardenas, D. J. *Chem. Eur. J.* **2009**, *15*, 12681.
56. Gong, H. G.; Gagné, M. R. *J. Am. Chem. Soc.* **2008**, *130*, 12177.
57. Gong, H. G.; Andrews, R. S.; Zuccarello, J. L.; Lee, S. J.; Gagné, M. R. *Org. Lett.* **2009**, *11*, 879.
58. Vechorkin, O.; Hu, X. *Angew. Chem. Int. Ed.* **2009**, *48*, 2937.
59. Vechorkin, O.; Proust, V. r.; Hu, X. *J. Am. Chem. Soc.* **2009**, *131*, 9756.
60. Hu, X. *Chem. Sci.* **2011**, *2*, 1867.
61. Everson, D. A.; Shrestha, R.; Weix, D. J. *J. Am. Chem. Soc.* **2010**, *132*, 920.
62. Biswas, S.; Weix, D. J. *J. Am. Chem. Soc.* **2013**, *135*, 16192.
63. Joshi-Pangu, A.; Wang, C. Y.; Biscoe, M. R. *J. Am. Chem. Soc.* **2011**, *133*, 8478.
64. Yu, X. L.; Yang, T.; Wang, S. L.; Xu, H. L.; Gong, H. G. *Org. Lett.* **2011**, *13*, 2138.
65. Dai, Y. J.; Wu, F.; Zang, Z. H.; You, H. Z.; Gong, H. G. *Chem. Eur. J.* **2012**, *18*, 808.
66. Xu, H.; Zhao, C.; Qian, Q.; Deng, W.; Gong, H. *Chem. Sci.* **2013**, *4*, 4022.
67. Matsunaga, P. T.; Hillhouse, G. L.; Rheingold, A. L. *J. Am. Chem. Soc.* **1993**, *115*, 2075.
68. Koo, K. M.; Hillhouse, G. L.; Rheingold, A. L. *Organometallics* **1995**, *14*, 456.
69. Han, R. Y.; Hillhouse, G. L. *J. Am. Chem. Soc.* **1997**, *119*, 8135.

70. Koo, K.; Hillhouse, G. L. *Organometallics* **1995**, *14*, 4421.
71. Lin, B. L.; Clough, C. R.; Hillhouse, G. L. *J. Am. Chem. Soc.* **2002**, *124*, 2890.
72. Zheng, B.; Tang, F.; Luo, J.; Schultz, J. W.; Rath, N. P.; Mirica, L. M. *J. Am. Chem. Soc.* **2014**, *136*, 6499.
73. Byers, P. K.; Canty, A. J.; Skelton, B. W.; White, A. H. *J. Chem. Soc., Chem. Commun.* **1986**, 1722.
74. Byers, P. K.; Canty, A. J.; Skelton, B. W.; White, A. H. *Organometallics* **1990**, *9*, 826.
75. Duecker-Benfer, C.; van Eldik, R.; Canty, A. J. *Organometallics* **1994**, *13*, 2412.
76. Blake, A. J.; Holder, A. J.; Hyde, T. I.; Schröder, M. *J. Chem. Soc., Chem. Commun.* **1987**, 987.
77. Burnett, M. N.; Johnson, C. K. *ORTEP-III: Oak Ridge Thermal Ellipsoid Plot Program for Crystal Structure Illustrations, Oak Ridge National Laboratory Report ORNL-6895* **1996**.
78. Canty, A. J. *Acc. Chem. Res.* **1992**, *25*, 83.
79. Alsters, P. L.; Engel, P. F.; Hogerheide, M. P.; Copijn, M.; Spek, A. L.; van Koten, G. *Organometallics* **1993**, *12*, 1831.
80. van Asselt, R.; Rijnberg, E.; Elsevier, C. J. *Organometallics* **1994**, *13*, 706.
81. van Belzen, R.; Hoffmann, H.; Elsevier, C. J. *Angew. Chem. Int. Ed.* **1997**, *36*, 1743.
82. de Graaf, W.; Boersma, J.; Smeets, W. J. J.; Spek, A. L.; van Koten, G. *Organometallics* **1989**, *8*, 2907.
83. de Graaf, W.; Boersma, J.; van Koten, G. *Organometallics* **1990**, *9*, 1479.
84. Trofimenko, S. *Chem. Rev.* **1993**, *93*, 943.
85. Hamburg, A.; Ho, C.; Getek, T. A. *Inorg. Chem.* **1985**, *24*, 2593.
86. Canty, A. J.; Denney, M. C.; Skelton, B. W.; White, A. H. *Organometallics* **2004**, *23*, 1122.

87. Campora, J.; Palma, P.; del Rio, D.; Lopez, J. A.; Alvarez, E.; Connelly, N. G. *Organometallics* **2005**, *24*, 3624.
88. Byers, P. K.; Canty, A. J.; Skelton, B. W.; White, A. H. *J. Chem. Soc., Chem. Commun.* **1987**, 1093.
89. Cotton, F. A.; Koshevoy, I. O.; Lahuerta, P.; Murillo, C. A.; Sanau, M.; Ubeda, M. A.; Zhao, Q. *J. Am. Chem. Soc.* **2006**, *128*, 13674.
90. Powers, D. C.; Ritter, T. *Nature Chem.* **2009**, *1*, 302.
91. Powers, D. C.; Geibel, M. A. L.; Klein, J.; Ritter, T. *J. Am. Chem. Soc.* **2009**, *131*, 17050.
92. Khusnutdinova, J. R.; Rath, N. P.; Mirica, L. M. *J. Am. Chem. Soc.* **2010**, *132*, 7303.
93. Khusnutdinova, J. R.; Rath, N. P.; Mirica, L. M. *J. Am. Chem. Soc.* **2012**, *134*, 2414.
94. Khusnutdinova, J. R.; Rath, N. P.; Mirica, L. M. *Inorg. Chem.* **2014**, *53*, 13112.
95. Tang, F.; Qu, F.; Khusnutdinova, J. R.; Rath, N. P.; Mirica, L. M. *Dalton Trans.* **2012**, *41*, 14046.
96. Tang, F.; Zhang, Y.; Rath, N. P.; Mirica, L. M. *Organometallics* **2012**, *31*, 6690.
97. Luo, J.; Khusnutdinova, J. R.; Rath, N. P.; Mirica, L. M. *Chem. Commun.* **2012**, *48*, 1532.
98. Mirica, L. M.; Khusnutdinova, J. R. *Coord. Chem. Rev.* **2013**, *257*, 299.
99. Khusnutdinova, J. R.; Luo, J.; Rath, N. P.; Mirica, L. M. *Inorg. Chem.* **2013**, *52*, 3920.
100. Luo, J.; Rath, N. P.; Mirica, L. M. *Organometallics* **2013**, *31*, 3343.
101. Jensen, K. A. *Zeitschrift fuer Anorganische und Allgemeine Chemie* **1936**, *229*, 265.
102. Nag, K.; Chakravorty, A. *Coord. Chem. Rev.* **1980**, *33*, 87.
103. Kreisman, P.; Marsh, R. E.; Preer, J. R.; Gray, H. B. *J. Am. Chem. Soc.* **1968**, *90*, 1067.
104. Grove, D. M.; Van Koten, G.; Zoet, R.; Murrall, N. W.; Welch, A. J. *J. Am. Chem. Soc.* **1983**, *105*, 1379.

105. Forbes, E. J.; Goodhand, N.; Hamor, T. A.; Iranpoor, N. *J. Fluorine Chem.* **1980**, *16*, 339.
106. Forbes, E. J.; Iranpoor, N. *J. Organomet. Chem.* **1982**, *236*, 403.
107. Sappa, E.; Tiripicchio, A.; Camellini, M. T. *J. Organomet. Chem.* **1980**, *199*, 243.
108. Camasso, N. M.; Sanford, M. S. *Science* **2015**, *347*, 1218.
109. Bour, J. R.; Camasso, N. M.; Sanford, M. S. *J. Am. Chem. Soc.* **2015**, *137*, 8034.
110. Higgs, A. T.; Zinn, P. J.; Sanford, M. S. *Organometallics* **2010**, *29*, 5446.
111. Higgs, A. T.; Zinn, P. J.; Simmons, S. J.; Sanford, M. S. *Organometallics* **2009**, *28*, 6142.
112. Hall, R. D. *J. Am. Chem. Soc.* **1907**, *29*, 692.
113. Hall, G. S.; Soderberg, R. H. *Inorg. Chem.* **1968**, *7*, 2300.
114. Robbins, J. L.; Edelstein, N.; Spencer, B.; Smart, J. C. *J. Am. Chem. Soc.* **1982**, *104*, 1882.
115. Klein, H.-F.; Bickelhaupt, A.; Jung, T.; Cordier, G. *Organometallics* **1994**, *13*, 2557.
116. Tang, F. Z.; Rath, N. P.; Mirica, L. M. *Chem. Commun.* **2015**, *51*, 3113.
117. Zhou, W.; Schultz, J. W.; Rath, N. P.; Mirica, L. M. *J. Am. Chem. Soc.* **2015**, *137*, 7604.

Chapter 2

Synthesis and Reactivity of Organometallic Palladium Complexes Supported by a Pseudo-Tridentate Ligand

2.1 Introduction

Recent developments in aerobic transformations catalyzed by palladium complexes are a vastly growing synthetic method that provides a practical use of dioxygen as an environmentally benign and inexpensive oxidant for a range of oxidative organic transformations.¹⁻⁸ The majority of the reported transformations involve a Pd⁰/Pd^{II} catalytic cycle in which dioxygen regenerates the Pd^{II} species.¹⁻⁸ However, recently an increasing number of high-valent Pd^{IV} and/or Pd^{III} active intermediates have been reported in several catalytic and stoichiometric aerobic transformations.⁹⁻¹⁴

We have recently reported several Pd^{II}Me₂ complexes supported by tetradentate ligands that are capable of undergoing facile oxidation by O₂ or peroxides to produce Pd^{III} and Pd^{IV} intermediates, which undergo elimination of ethane under ambient conditions.^{15,16} Similarly, we have reported the aerobic oxidation of (Me₃tacn)Pd^{II}Me₂ (Me₃tacn = N,N',N''-trimethyl-1,4,7-triazacyclononane) to produce a stable high-valent Pd^{IV} complex [(Me₃tacn)Pd^{IV}Me₃]⁺, which can undergo reductive elimination of ethane at elevated temperatures.¹⁷ From both of these studies the stability of the high-valent Pd species was shown to be essential in controlling the subsequent C-C bond formation reactivity. Therefore, one could imagine increasing the rate of reactivity by destabilizing the resulting high-valent Pd intermediates.

Herein, we report the synthesis and reactivity of Pd^{II} complexes supported by the ligand, *N*-methyl-*N'*-tosyl-2,11-diaza[3.3](2,6)pyridinophane (^{TsMe}N4), where an amine has a tosyl substituent. Given the limited donating ability of a tosylated amine, we proposed ^{TsMe}N4 could act as a “pseudo-tridentate” ligand. Indeed, the pseudo-tridentate nature of the ^{TsMe}N4 was experimentally confirmed using electron paramagnetic resonance (EPR). Yet, this ligand was still able to stabilize the high-valent Pd species, albeit to a lesser extent. As a result, the aerobic

oxidation of the Pd^{II}Me₂ complex was improved and progresses directly to the key Pd^{IV}Me₃ intermediate, with only trace quantities of the previously observed Pd^{III}Me₂ intermediate. However, the rate of ethane formation was narrowly affected, suggesting the reductive elimination step from the high-valent Pd^{IV}Me₃ intermediate is rate-determining.

2.2 Experimental Section

2.2.1 Synthesis of Ligands and Complexes

Reagents and Materials. All manipulations were carried out under a nitrogen atmosphere using standard Schlenk and glove box techniques if not indicated otherwise. All reagents for which synthesis is not given were commercially available from Sigma-Aldrich, Fisher Scientific, VWR, Acros, STREM or Pressure Chemical and were used as received without further purification. Solvents were purified prior to use by passing through a column of activated alumina using an MBRAUN Solvent Purification System. 2,11-diaza[3.3](2,6)pyridinophane (N₄H₂)¹⁸, (COD)Pd^{II}Cl₂¹⁹, (COD)Pd^{II}MeCl²⁰ and (COD)Pd^{II}Me₂¹⁵ were prepared according to the literature procedures.

***N*-tosyl-2,11-diaza[3.3](2,6)pyridinophane (T^{SH}N₄).** Solid N₄H₂ (1.67g, 6.95mmol) was placed in a 1000 mL round bottom flask equipped with a magnetic stirring bar and dissolved in 200 mL dry CH₂Cl₂. Then triethylamine (970μL, 6.95mmol) was added. The resulting solution was cooled down to 0°C under nitrogen atmosphere. And a solution of *p*-toluenesulfonyl chloride (1.325g, 6.95mmol) in 400 mL dry CH₂Cl₂ was added dropwise. After the addition was complete, the reaction was stirred at 0 °C for an additional three hours. After the reaction was complete the reaction mixture was washed with a solution of saturated sodium bicarbonate (3 x 200 mL). The

organic layer was then dried over potassium carbonate for 30 minutes and concentrated to dryness to isolate a product mixture of $\text{T}^{\text{SH}}\text{N}_4$ and N_4Ts_2 . The product mixture was then suspended in 600 mL of isopropanol. The suspension was stirred overnight and then vacuum filtered. The solid and filtrate were dried separately resulting in N_4Ts_2 (1.14g, 2.08mmol) and $\text{T}^{\text{SH}}\text{N}_4$ (1.28g, 3.24mmol, 47%) respectively. $^1\text{H-NMR}$ (300 MHz, CDCl_3), δ (ppm): 7.83 (d, 2H, Ts-H), 7.41 (d, 2H, Ts-H), 7.22 (t, 2H, Py-H), 7.10 (d, 2H, Py-H), 6.64 (d, 2H, Py-H), 4.52 (s, 4H, $-\text{CH}_2-$), 3.96 (s, 4H, $-\text{CH}_2-$), and 2.46 (s, 3H, $-\text{CH}_3$). $^{13}\text{C-NMR}$ (600 MHz, CDCl_3), δ (ppm): 158.60, 155.31, 143.60, 136.37, 129.94, 126.91, 122.06, 120.88, 57.16, 55.75, 21.54. ESI-MS of $\text{T}^{\text{SH}}\text{N}_4$ in Acetonitrile: m/z 395.1535; Calculated: m/z 395.1463.

***N*-methyl-*N'*-tosyl-2,11-diaza[3.3](2,6)pyridinophane ($\text{T}^{\text{Me}}\text{N}_4$).** Solid $\text{T}^{\text{SH}}\text{N}_4$ (1.28g, 3.24mmol) was placed in a 500 mL round bottom flask equipped with a magnetic stirring bar and dissolved in 200 mL concentrated formic acid and 20 mL 40% formaldehyde solution. The solution was stirred and refluxed at 110 °C for 24 hours under nitrogen atmosphere. The solution was then treated with 20 mL of concentrated hydrochloric acid. After several minutes the solution was concentrated to dryness. The residue was basified with 1M sodium hydroxide solution and extracted with CH_2Cl_2 (4x200mL). The combined organic portions were dried over anhydrous potassium carbonate, and filtered. The filtrate was concentrated to dryness resulting in a yellow-white solid, $\text{T}^{\text{Me}}\text{N}_4$ (1.145g, 2.82mmol, 87%). $^1\text{H-NMR}$ (300 MHz, CDCl_3), δ (ppm): 7.78 (d, 2H, Ts-H), 7.40 (d, 2H, Ts-H), 7.23 (t, 2H, Py-H), 7.10 (d, 2H, Py-H), 6.86 (d, 2H, Py-H), 4.52 (s, 4H, $-\text{CH}_2-$), 3.80 (s, 4H, $-\text{CH}_2-$), 2.72 (s, 3H, $-\text{CH}_3$), 2.49 (s, 3H, $-\text{CH}_3$). $^{13}\text{C-NMR}$ (600 MHz, CDCl_3), δ (ppm): 157.16, 154.55, 143.56, 136.33, 135.99, 129.91, 126.86, 123.20, 122.53, 65.73, 56.56, 49.04, 21.49. ESI-MS in Acetonitrile: m/z 409.1695; Calculated: m/z 409.1620.

Synthesis of $^{TsMe}N_4PdCl_2$ (1). Solid samples of (COD) $PdCl_2$ (71.1 mg, 2.50mmol) and $^{TsMe}N_4$ (102.3mg, 2.50mmol) were placed into a 100 mL round bottom flask equipped with a magnetic stirring bar and a septum. The flask was evacuated and refilled with nitrogen three times. Then 60 mL anhydrous CH_2Cl_2 was added with a syringe and the reaction mixture was stirred vigorously under nitrogen for 2 days in the dark. Using an ice-bath the CH_2Cl_2 was rotary evaporated, leaving an orange precipitate. The precipitate was re-dissolved in the minimal amount of dichloromethane and precipitated with the addition of excess diethyl ether. The precipitate was filtered off, washed with ether, pentane, and dried under vacuum. The resulting precipitation was a pale orange-brown solid (0.1250g, 2.13mmol, 86%). 1H -NMR (600 MHz, DMSO), δ (ppm) for *Major Isomer I'* ($N_{py}N_{am}Pd^II Cl_2$): 8.00 (d, 2H, Ts-H), 7.96 (t, 2H, Py-H), 7.56 (m, 6H, Ts-H & Py-H), 6.25 (dd, 4H, -CH₂-), 5.50 (d, 2H, -CH₂-), 4.53 (d, 2H, -CH₂-), 2.47 (s, 3H, -CH₃), 2.22 (s, 3H, -CH₃). 1H -NMR (600 MHz, DMSO), δ (ppm) for *Minor Isomer I''* ($N_{py}N_{py}Pd^II Cl_2$): 7.90 (d, 2H, Ts-H), 7.66 (t, 2H, Py-H), 7.55 (d, 2H, Ts-H), 7.26 (d, 2H, Py-H), 7.14 (d, 2H, Py-H), 5.22 (d, 2H, -CH₂-), 5.15 (d, 2H, -CH₂-) 4.66 (d, 2H, -CH₂-), 3.96 (d, 2H, -CH₂-), 3.03 (s, 3H, -CH₃), 2.47 (s, 3H, -CH₃). ESI-MS: m/z 549.0; Calculated for [$^{TsMe}N_4PdCl$]⁺: m/z 549.0. Anal. Found: C, 42.57; H, 3.52; N, 8.59. Calcd for $C_{22}H_{24}Cl_2N_4O_2Pd_2S$ (1/2 CH_2Cl_2): C, 43.01; H, 4.01; N, 8.92.

Synthesis of $^{TsMe}N_4PdMeCl$ (2). Solid samples of (COD) $PdMeCl$ (63.7mg, 2.40mmol) and $^{TsMe}N_4$ (98.2mg, 2.40mmol) were placed into a 100 mL round bottom flask equipped with a magnetic stirring bar and a septum. The flask was evacuated and refilled with nitrogen three times. Then 40 mL anhydrous ether was added with a syringe and the reaction mixture was stirred vigorously under nitrogen for 2 days in the dark. Pale grey precipitate was filtered off, washed with ether, pentane, and dried under vacuum. The solid was dissolved in a minimal amount of

dichloromethane and precipitated with the addition of excess pentane. The precipitate was a pale grey solid (114.2mg, 2.02mmol, 84%). ¹H-NMR (300 MHz, CDCl₃), δ (ppm): 7.84 (d, 2H, Ts-H), 7.52 (m, 4H, Py-H), 7.44 (d, 2H, Ts-H), 7.06 (dd, 2H, Py-H), 6.15 (m, 4H, -CH₂-), 5.18 (dd, 2H, -CH₂-), 4.24 (dd, 2H, -CH₂-), 2.53 (s, 3H, -CH₃), 2.34 (s, 3H, -CH₃), 1.62 (s, 3H, Pd-CH₃). ¹³C-NMR (600 MHz, CDCl₃), δ (ppm): 158.30, 157.00, 144.41, 138.19, 136.39, 130.33, 126.79, 125.34, 125.01, 66.02, 63.43, 59.66, 57.41, 39.52, 21.59, -6.92. ESI-MS: m/z 529.1; Calculated for [(^{TsMe}N₄)PdMe]⁺: m/z 529.1. Anal. Found: C, 44.31; H, 3.90; N, 8.47. Calcd for C₂₃H₂₇ClN₄O₂Pd₂S (CH₂Cl₂): C, 44.32; H, 4.49; N, 8.61.

Synthesis of ^{TsMe}N₄PdMe₂ (3). Solid samples of (COD)PdMe₂ (0.3740grams, 1.52mmol) and ^{TsMe}N₄ (0.6227grams, 1.52mmol) was cooled down to 0°C in an ice bath, then the flask was evacuated/refilled with nitrogen three times. Then under nitrogen 30 mL of anhydrous ether was added. The reaction mixture was stirred vigorously at 0°C for 3 hours, and then the solvents were removed by evaporation on a high vacuum line at 0°C. The resulting pale yellow-white solid was transported under nitrogen into the glove box. The solid was washed with pentane, and then dissolved in a minimal amount of tetrahydrofuran. The resulting orange colored solution was precipitated with pentane. The cloudy solution was then decanted and the solid dried under vacuum, resulting in a pale yellow-orange solid (0.4889 grams, 0.90mmol, 59%). ¹H-NMR (300 MHz, Benzene), δ (ppm) for *Major Isomer I'* (*N_{py}N_{py}Pd^{II}Me₂*): 7.65 (d, 2H, Ts-H), 7.34 (d, 2H, Ts-H), 6.81 (d, 2H, Py-H), 6.66 (t, 2H, Py-H), 6.37 (m, 4H, -CH₂-), 6.22 (d, 2H, Py-H), 4.83 (d, 2H, -CH₂-), 3.68 (d, 2H, -CH₂-), 1.97 (s, 3H, -CH₃), 1.95 (s, 3H, -CH₃), 0.84 (s, 6H, Pd-CH₃). ¹H-NMR (300 MHz, Benzene), δ (ppm) for *Minor Isomer I''* (*N_{py}N_{am}Pd^{II}Me₂*): 7.57 (d, 2H, Ts-H), 7.39 (d, 2H, Ts-H), 7.25 (m, 2H, Py-H), 6.55 (t, 2H, Py-H), 6.04 (m, 2H, Py), 5.28 (d, 1H, -

CH₂-), 4.74 (dd, 2H, -CH₂-), 3.86 (d, 1H, -CH₂-), 1.97 (s, 3H, -CH₃), 1.95 (s, 3H, -CH₃), 0.70 (d, 6H, Pd-CH₃). ¹³C-NMR (600 MHz, Benzene), δ (ppm): 157.86, 157.45, 143.27, 138.10, 136.61, 130.11, 128.30, 127.05, 124.47, 63.66, 57.46, 39.57, 21.21, and -9.45. ESI-MS: m/z 529.1; Calculated for [(^{TsMe}N₄)PdMe]⁺: m/z 529.1. The elemental analysis of this complex could not be obtained due to its high aerobic sensitivity.

Synthesis of [(^{TsMe}N₄)Pd^{III}Cl₂]ClO₄ [1⁺]. Low temperature controlled potential electrolysis was performed in a stirred solution of **1** (17.6 mg, 30 μmol) in 10 mL of 0.1 M Bu₄NClO₄ solution in MeCN at a potential of 1.3 V in a sealed H-shaped electrolysis cell using a reticulated vitreous carbon working electrode and a non-aqueous silver wire reference electrode. The controlled potential electrolysis was conducted at -40 °C. The electrolysis was stopped after the charge corresponding to one electron oxidation was transferred, resulting in the formation of a dark teal green solution. The solution was then stored at -20 °C and used for all further characterization. UV-Vis, λ, nm (ε, M⁻¹·cm⁻¹), MeCN: 380 (1480), 635 (450).

Synthesis of [(^{TsMe}N₄)Pd^{III}MeCl]ClO₄ [2⁺]. Controlled potential electrolysis was performed in a stirred solution of **2** (5.7 mg, 10 μmol) in 10 mL of 0.1 M Bu₄NClO₄ solution in MeCN at a potential of 0.50 V in a H-shaped electrolysis cell using a reticulated vitreous carbon working electrode and a non-aqueous Ag/0.01M AgNO₃ reference electrode. The electrolysis was stopped after the charge corresponding to one electron oxidation was transferred, resulting in the formation of a purple solution. The solution was then stored at -20 °C and used for all further characterization. UV-Vis, λ, nm (ε, M⁻¹·cm⁻¹), MeCN: 350 (sh, 1220), 545 (203), 665 (120).

Synthesis of $[(^{\text{TSMc}}\text{N}_4)\text{Pd}^{\text{II}}\text{Me}(\text{MeCN})](\text{OTf})$. The complex $[(^{\text{TSMc}}\text{N}_4)\text{Pd}^{\text{II}}\text{Me}(\text{MeCN})](\text{OTf})$ was prepared according to the modified literature procedure for preparation of $[(\text{N}_4)\text{Pd}^{\text{II}}\text{Me}(\text{MeCN})](\text{OTf})$.²¹ A solution of AgOTf (11.8 mg, 0.045 mmol) in 2 mL of MeCN was added dropwise to a stirred solution of $(^{\text{TSMc}}\text{N}_4)\text{Pd}^{\text{II}}\text{MeCl}$ (25 mg, 0.045 mmol) in 4 mL of MeCN. The resulting suspension was stirred at RT for 5 hours in the dark. The white precipitate of AgCl was removed by filtration through 0.2 μm syringe filter and the resulting clear yellow solution was concentrated to dryness at RT. The solid residue was triturated with dry ether causing precipitation of a yellow solid which was filtered, washed with ether, pentane, and dried under vacuum. Yield: 14.1 mg, 0.027 mmol, 60.0%.

Synthesis of $(^{\text{TSMc}}\text{N}_4)\text{Pd}^{\text{II}}\text{Me}(\text{OH})$ (5). $[(^{\text{TSMc}}\text{N}_4)\text{Pd}^{\text{II}}\text{Me}(\text{MeCN})](\text{OTf})$ (14.1 mg, 0.027 mmol) was dissolved in 0.6 mL of MeOD. Then 1 equivalent of 40% NaOD in D₂O (2.47 μL) was added to give a clear yellow solution of $(^{\text{TSMc}}\text{N}_4)\text{Pd}^{\text{II}}\text{Me}(\text{OH})$. In ¹H NMR spectrum of the resulting solution there were two overlapping complexes $(^{\text{TSMc}}\text{N}_4)\text{Pd}^{\text{II}}\text{Me}(\text{OH})$ and $(^{\text{TSMc}}\text{N}_4)\text{Pd}^{\text{II}}\text{Me}(\text{OMe})$. Several attempts to isolate this complex were unsuccessful, likely due to decomposition and sensitivity to water. UV-Vis, λ , nm (ϵ , M⁻¹·cm⁻¹), MeOH: 390 (sh, 92). ¹H-NMR (300 MHz, MeOD), δ (ppm): 7.93 (dd, 2H, Ts-H), 7.73 (m, 4H, Py-H), 7.50 (dd, 2H, Ts-H), 7.33 (m, 2H, Py-H), 6.03 (dd, 2H, -CH₂-), 5.79 (dd, 2H, -CH₂-), 5.34 (m, 2H, -CH₂-), 4.37 (m, 2H, -CH₂-), 2.51 (s, 3H, -CH₃), 2.40 (s, 3H, -CH₃), 0.48 (s, 3H/2, Pd-Me), 0.45 (s, 3H/2, Pd-Me).

2.2.2 Physical Measurements

^1H NMR spectra were recorded on a Varian Mercury-300 spectrometer (300.121 MHz) or a Varian Unity Inova-600 spectrometer (599.746 MHz). ^{13}C NMR spectra were recorded on a Varian Unity Inova-600 spectrometer (599.746 MHz). Chemical shifts are reported in parts per million (ppm) with residual solvent resonance peaks as internal reference.²² Abbreviations for the multiplicity of NMR signals are singlet (s), doublet (d), triplet (t), quartet (q), multiplet (m), and broad (br). UV-visible spectra were recorded on a Varian Cary 50 Bio spectrophotometer and are reported as λ_{max} , nm (ϵ , $\text{M}^{-1}\cdot\text{cm}^{-1}$). EPR spectra were recorded on a JEOL JES-FA X-band (9.2 GHz) EPR spectrometer in frozen solution at 77 K. ESI-MS experiments were performed using a Thermo FT or Bruker Maxis Q-TOF mass spectrometer with an electrospray ionization source. ESI mass-spectrometry was provided by the Washington University Mass Spectrometry Resource. Elemental analyses were carried out by the Columbia Analytical Services Tucson Laboratory.

Cyclic voltammetry (CV) experiments were performed using a BASi EC Epsilon electrochemical workstation or a CHI 660D Electrochemical Analyzer. Electrochemical-grade supporting electrolytes were purchased from Fluka. The electrochemical measurements were performed under a blanket of nitrogen, and the analyzed solutions were deaerated by purging with nitrogen. A glassy carbon disk electrode was used as the working electrode, and the auxiliary electrode was a Pt wire. A non-aqueous Ag/0.01M AgNO_3 electrode in MeCN was used as a reference electrode. The reference electrode was calibrated against ferrocene (Fc) at the conclusion of each CV experiment.

Electrochemical oxidations were performed using controlled potential electrolysis (CPE) in a two compartment H-shaped electrolysis cell separated by a fine-frit glass junction. A reticulated vitreous carbon working electrode and a non-aqueous Ag/0.01M AgNO_3 or silver wire

reference electrode were used in the anodic chamber. Similarly, platinum gauze (25 mm x 10 mm) was used as the auxiliary electrode in the cathodic chamber. The anodic chamber was equipped with a magnetic stirring bar and was under a blanket of nitrogen. Prior to all CPE experiments, a CV was obtained to determine the proper potential for electrolysis. Solvents were purified prior to use by passing through a column of activated alumina using an MBRAUN Solvent Purification System, and electrochemical-grade supporting electrolytes were purchased from Fluka.

X-ray diffraction quality crystals of **1** and **2** were obtained by slow ether vapor diffusion into acetonitrile or CH₂Cl₂ solutions. Similarly, quality crystals of **3** were obtained by slow pentane vapor diffusion into a tetrahydrofuran solution. Suitable crystals of appropriate dimensions were mounted and preliminary examination and data collection were performed using a Bruker Kappa Apex-II Charge Coupled Device (CCD) Detector system single crystal X-Ray diffractometer equipped with an Oxford Cryostream LT device. Data were collected using graphite monochromated Mo K α radiation ($\lambda = 0.71073 \text{ \AA}$) from a fine focus sealed tube X-Ray source. Apex II and SAINT software packages²³ were used for data collection and data integration. Final cell constants were determined by global refinement of reflections from the complete data set. Data were corrected for systematic errors using SADABS²³ based on the Laue symmetry using equivalent reflections. Structure solutions and refinement were carried out using the SHELXTL-PLUS software package²⁴. The structures were refined with full matrix least-squares refinement by minimizing $\sum w(F_o^2 - F_c^2)^2$. All non-hydrogen atoms were refined anisotropically to convergence. Typically, H atoms are added at the calculated positions in the final refinement cycles. The complete listings of x-ray diffraction parameters are included in Appendix B.

2.2.3 Computational Studies

The density functional theory (DFT) and time-dependent density functional theory (TD-DFT) calculations were performed with the program package Gaussian 09.²⁵ The UB3LYP hybrid functional^{26,27} along with Stevens (CEP-31G)^{28,29} valence basis sets and effective core potentials were employed for single point and geometry optimization calculations. This combination of hybrid functional and basis sets have been previously shown to work well for reproducing experimental parameters of complexes containing palladium.^{30,31} The ground state wave function was investigated by analyzing the frontier MOs, and the atomic contributions to MOs were calculated using the program Chemissian.³² TD-DFT calculations were employed to obtain the predicted absorption bands and their major contributing transitions. The calculated UV-Vis spectra were generated using GaussSum³³, with a full width at half maximum (FWHM) values of 3000 to 3500 cm⁻¹.

2.2.4 Reactivity Studies

¹H NMR reactivity studies for aerobic oxidation. A 3-4 mM solution of **3** with an equimolar amount of 1,3,5-trimethoxybenzene (used as internal standard) was dissolved in O₂-saturated CD₃OD solution, and an NMR tube was filled to the top (to avoid the escape of volatiles into the headspace) and sealed with a septum. The reaction mixture was kept in the dark and periodically analyzed by ¹H NMR. The yields of Pd intermediates and organic/Pd products were determined by integration versus the internal standard, calculated as [moles of product]/[moles of **3**]*100% and given as an average of two runs.

¹H NMR reactivity studies with methyl iodide. A 3-4 mM solution of **3** with 1,3,5-trimethoxybenzene (used as internal standard) was dissolved in d₆-acetone. To which, a methyl iodide solution was added. The NMR tube was then filled to the top with additional d₆-acetone (so that no headspace is left to avoid the escape of volatiles) and sealed with a septum. The reaction mixture was kept in the dark and periodically analyzed by ¹H NMR. The yields of Pd intermediates and organic/Pd products were determined by integration versus the internal standard, calculated as [moles of product]/[moles of **3**]*100% and given as an average of two runs.

UV-Vis reactivity studies for aerobic oxidation. A 2.14 mM solution of **3** in CD₃OD was placed into a quartz cuvette (1 cm pathlength) equipped with a septum-sealed cap and a magnetic stirring bar. Dry O₂ was bubbled through the solution for 2 minutes and the reaction mixture was stirred at 20°C in the dark. The reactivity reaction was then monitored using a Varian Cary 50 Bio spectrophotometer.

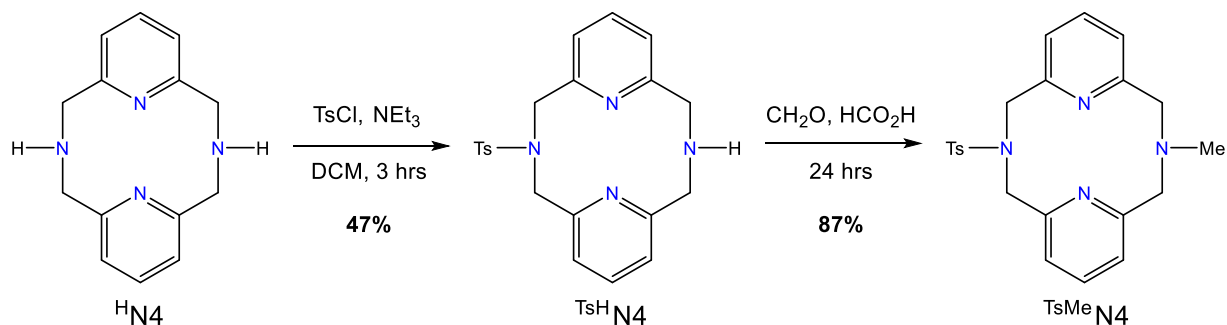
ESI-MS reactivity studies for aerobic oxidation. A solution of 0.1 mg of **3** in methanol was prepared in the absence of O₂. To which, an O₂-saturated methanol solution was added immediately prior to ESI-MS analysis. Then approximately 50 μL of the resulting solution was injected into the instrument at various time points to detect any intermediates formed during the aerobic oxidation. The ESI-MS experiments were performed using a Bruker Maxis Q-TOF mass spectrometer with an electrospray ionization source.

2.3 Results and Discussion

2.3.1 Ligand Synthesis and Design

The *N*-methyl-*N'*-tosyl-2,11-diaza[3.3](2,6)pyridinophane (^{TsMe}N4) ligand is a variant of the previously studied tetradentate ligands, *N,N'*-di-*tert*-butyl-2,11-diaza[3.3](2,6)pyridinophane (^{tBu}N4)³⁴ and *N,N'*-di-methyl-2,11-diaza[3.3](2,6)pyridinophane (^{Me}N4)¹⁶. ^{TsMe}N4 was designed to behave like a “pseudo-tridentate” ligand by attaching a bulky electron-withdrawing protecting group to one of the axial amines in order to alter the metal-binding ability of this N donor. The ^{TsMe}N4 variant was successfully synthesized by a new synthetic route (Scheme 2.1). The synthesis began with the preparation of the new intermediate, ^{TsH}N4, which was prepared in 47% yield via selective tosylation of the ^HN4 precursor¹⁸ using 4-toluenesulfonyl chloride. The ^{TsH}N4 intermediate was then methylated using Eschweiler-Clarke conditions to produce the desired ligand, ^{TsMe}N4, in 87% yield.

Scheme 2.1 Synthetic route for the pseudo-tridentate ^{TsMe}N4.



2.3.2 Destabilization of Pd^{III} Complexes

A series of Pd complexes supported by the newly designed ^{TsMe}N4 ligand were synthesized to determine if the proposed pseudo-tridentate nature of the ligand resulted in destabilization of the high-valent Pd^{III} metal center. The Pd^{II} complexes (^{TsMe}N4)PdCl₂ (**1**), (^{TsMe}N4)PdMeCl (**2**), and (^{TsMe}N4)PdMe₂ (**3**) were obtained in a manner similar to the previously synthesized N4 analogues.^{15,16,35} Complex **1**, was prepared in 86% yield from the precursor (COD)Pd^{II}Cl₂¹⁹ via ligand exchange with ^{TsMe}N4. Similarly, complexes **2** and **3** were prepared in 84% and 59% yields from precursors (COD)Pd^{II}MeCl²⁰ and (COD)Pd^{II}Me₂¹⁵ respectively.

The X-ray structure of **1** revealed a unique square planer geometry around the Pd^{II} metal center with two chloride ligands, one amine donor and one pyridine N atom of the ^{TsMe}N4 ligand binding equatorially (Figure 2.1). This unique bonding geometry is different from the previously synthesized N4 supported complexes, since a square planar geometry involving the two exogenous ligands and the two pyridine N atoms is most commonly observed. However, the metrical parameters of complex **1** are generally comparable to those of previously synthesized complexes (^{tBu}N4)PdCl₂ and (^{Me}N4)PdCl₂.

The X-ray structures of complexes **2** and **3** revealed both complexes adopted the more commonly observed bonding geometry featuring both the pyridine N atoms bound to the Pd metal center (Figure 2.1). Additionally, the metrical parameters of complexes **2** and **3** are again generally comparable to those of the corresponding previously synthesized complexes.

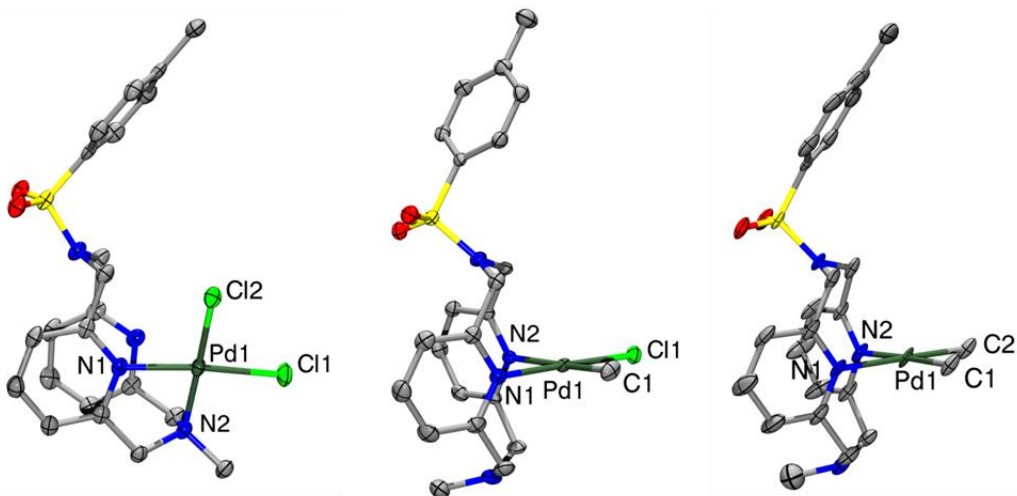


Figure 2.1 ORTEP³⁶ representation (50% probability ellipsoids) of **1** (left), **2** (middle), and **3** (right). Selected bond distances (Å): **1**, Pd1-Cl1 2.279, Pd1-Cl2 2.307, Pd1-N1 2.057, Pd1-N2 2.062; **2**, Pd1-C1 2.027, Pd1-Cl1 2.307, Pd1-N1 2.044, Pd1-N2 2.172; **3**, Pd1-C1 2.053, Pd1-C2 2.053, Pd1-N1 2.151, Pd1-N2 2.151. A complete listings of structural parameters are included in Appendix B.

Cyclic voltammetry of all three compounds in 0.1 M Bu₄NClO₄ in CH₂Cl₂ or THF revealed a series of oxidation waves covering a wide range of potentials (Figure 2.2, Table 2.1). The cyclic voltammogram (CV) of **1** revealed oxidation peaks at 715 and 950 mV and a reversible wave at 1100 mV vs Fc⁺/Fc. Similarly, the cyclic voltammogram of **3** exhibited two oxidation peaks and a reversible wave at -440, -130 and 73.4 mV vs Fc⁺/Fc, respectively. The cyclic voltammograms of **2**, however, revealed a single oxidation wave at 100 mV and a reversible wave at 605 mV vs Fc⁺/Fc. Since the ^{TsMe}N4 ligand is not redox active within this potential range, the irreversible oxidation peaks are assigned to the κ³ and κ⁴ Pd^{II/III} oxidations and the reversible oxidation was assigned to the Pd^{III/IV} oxidation. These assignments are consistent with our reported electrochemical analysis of the previously synthesized complexes supported by the tetradentate N4 analogues.^{35,37} The observed oxidation potentials of **1-3** are slightly higher than the previously synthesized complexes^{15,16,35} due to the inability of the protected amine to support the high valent

Pd metal center. This is contributed to the large steric and electronic effects introduced to the ligand by the protected amine.

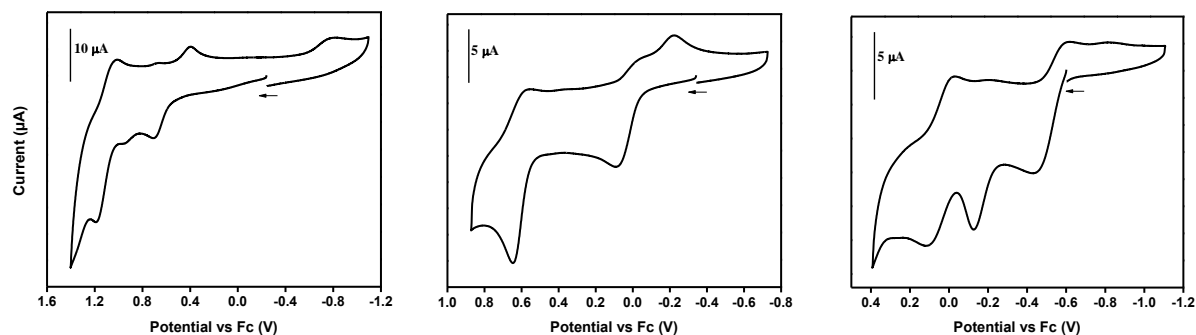


Figure 2.2 Cyclic voltammograms of **1** (left), **2** (middle), and **3** (right) in 0.1 M Bu₄NClO₄ in CH₂Cl₂ or THF, 100 mV/s scan rate.

Table 2.1 Redox potentials obtained from the CV of complexes **1**, **2** and **3**.

Complex	E _{pa} Pd ^{II/III} [mV]	E _{pc} Pd ^{III/II} [mV]	E _{1/2} Pd ^{III/IV} [mV]
(^{TsMe} N ₄)Pd ^{II} Cl ₂ (1)	715, 950	670, 396	1100
(^{TsMe} N ₄)Pd ^{II} MeCl (2)	100	-45, -220	605
(^{TsMe} N ₄)Pd ^{II} Me ₂ (3)	-440, -130	-615	74

* CV measurements were obtained in 0.1 M Bu₄NClO₄ at a 100 mV/s scan rate. The reported potentials are adjusted versus Fc⁺/Fc.

Controlled potential electrolysis (CPE) of **1** and **2** at potentials above the first anodic wave were performed to generate deeply colored solutions of complexes [(^{TsMe}N₄)Pd^{III}Cl₂]⁺ (**1**⁺, forest green) and [(^{TsMe}N₄)Pd^{III}MeCl]⁺ (**2**⁺, purple). Neither electrochemical nor chemical oxidations were capable of producing detectable amounts of the corresponding Pd^{III} product (**3**⁺) of complex **3**, due to the instability of the Pd^{III} product. The UV-Vis spectra of [**1**⁺] and [**2**⁺] in MeCN (Figure 2.3) show strong absorption bands at 545-665 and 350-380 nm. Additionally, the reduced stability

of the Pd^{III} complexes was also monitored via UV-Vis spectroscopy. The characteristic Pd^{III} absorption bands for complexes [1⁺] and [2⁺] decay at room temperature within 30 minutes and 2 hours, respectively.

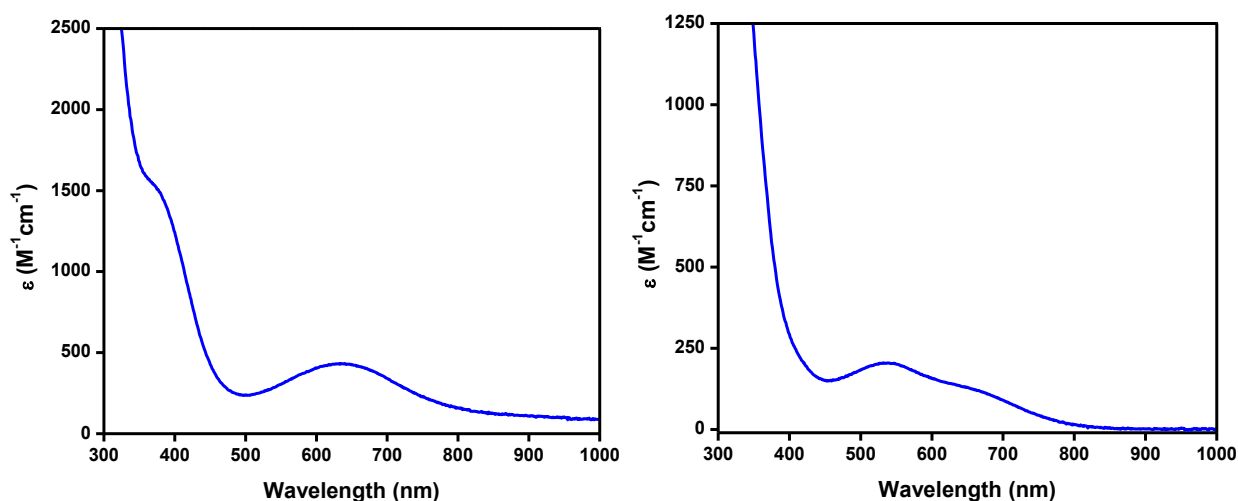


Figure 2.3 UV-Vis spectra of a solution of [1⁺]ClO4 (left) and [2⁺]ClO4 (right) in MeCN.

Complexes [1⁺] and [2⁺] are both paramagnetic, allowing the bonding interactions with the Pd metal center to be probed using electron paramagnetic resonance spectroscopy (EPR). The EPR spectra of [1⁺] and [2⁺] (Figure 2.4) [77 K, 3:1 PrCN/MeCN glass] revealed the bonding coordination of these complexes differs from the previously reported complexes supported by tetradentate ligands.^{3,4,12} The EPR spectra confirm the N atoms of the two axial amines couple differently with the Pd metal center.

In complex [1⁺] the Pd metal center strongly couples to the N atom of the methylated amine [$A_{\text{N1}} = 35.5$ G] and weakly couples to the N atom of the protected amine [$A_{\text{N2}} = 10.0$ G]. This variance in the N atom hyperfine coupling constants produces the distinctive superhyperfine coupling pattern observed in the experimental EPR spectrum. The weakly coupled N atom of the

protected amine causes a broadening effect on the superhyperfine coupling pattern of the N atom of the methylated amine, resulting in the observed broadened triplet of triplets. Additionally, in complex $[2^+]$ the coupling between the Pd metal center and the N atom of the protected amine is even less [$A_{N2} = 5.0$ G]. As a result the broadening of the observed superhyperfine coupling is reduced.

These distinctly different coupling values for the different N atoms strongly support the proposed pseudo-tridentate nature of the $TsMe_cN_4$ supported complexes. Furthermore, the extent to which the N atom of the protected amine couples with the Pd metal center appears to be dependent on the exogenous ligands bonded to the Pd metal center. The more electronegative the exogenous ligands, the greater interaction the Pd metal center requires from the protected amine, resulting in greater coupling. From this general trend, the binding coordination of complex $[3^+]$ was proposed to be almost completely tridentate, corresponding to its instability.

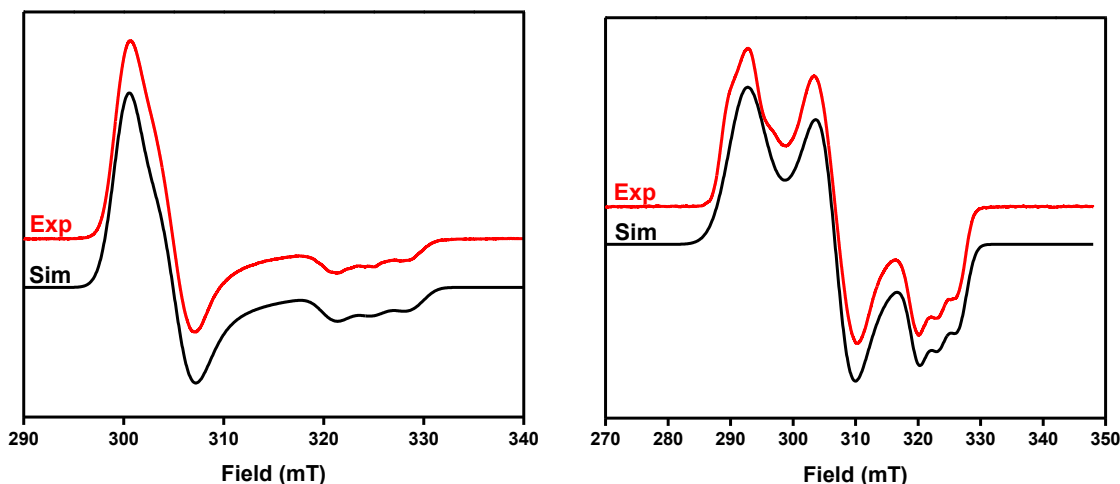


Figure 2.4 EPR spectra of a solution of $[1^+]ClO_4$ (left) and $[2^+]ClO_4$ (right) in 3:1 PrCN/MeCN (red lines), and simulated EPR spectra (black lines) using the following parameters: $[1^+]ClO_4$, $g_x = 2.163$, $g_y = 2.129$, $g_z = 2.001$ ($A_{N,1} = 35.5$ G, $A_{N,2} = 10.0$ G); $[2^+]ClO_4$, $g_x = 2.222$, $g_y = 2.118$, $g_z = 2.011$ ($A_{N,1} = 31.5$ G, $A_{N,2} = 5.0$ G).

2.3.3 Computational studies on Pd^{III} Complexes

Due to the low stability of complexes [1⁺] and [2⁺] x-ray quality crystals of these complexes were not able to be isolated and characterized. However, it is shown in the above spectroscopic experiments that complexes [1⁺] and [2⁺] are clearly formed. Furthermore, the resulting EPR results suggest the bonding geometry around the Pd^{III} metal center adopts a pseudo-tridentate nature (Figure 2.4). To support the proposed structures, density functional theory (DFT) and time-dependent density functional theory (TD-DFT) calculations were performed to support the proposed pseudo-tridentate structures.

The resulting metrical parameters for the optimized geometries of complexes [1⁺] and [2⁺] (Table 2.2 and 2.3) were compared to the previously characterized tetradentate Me₄N supported complexes [(Me₄N)Pd^{III}Cl₂]⁺ (4⁺) and [(Me₄N)Pd^{III}MeCl]⁺ (5⁺). The bond length of the axial nitrogen atoms in [4⁺] and [5⁺] were determined to be nearly symmetric, whereas, in complexes [1⁺] and [2⁺] the bond lengths of the two axial nitrogen atoms differ. The electron-deficient protected amine is unable to form a strong bond with the high-valent Pd^{III} metal center, resulting in an elongated bond length. Thus, confirming the proposed pseudo-tridentate assignments for complexes [1⁺] and [2⁺].

Additionally, the comparison of complexes [1⁺] and [2⁺] correlates perfectly with the experimental EPR results. The bond length between the protected amine and the high-valent Pd^{III} metal center is dependent on the electronegativity of the exogenous ligands. As seen in the EPR spectra for complexes [1⁺] and [2⁺] the more electronegative the exogenous ligands, the greater coupling observed between the protected amine and the Pd metal center. The calculated metrical parameters summarized in Tables 2.2 and 2.3 clearly follow the proposed trend.

Table 2.2 DFT-calculated (UB3LYP/CEP-31G) bond lengths (Å) for complexes [1⁺] and [2⁺] compared to experimentally determined parameters of similar ^{Me}N4 supported complexes.

Metrical Parameters	[1⁺] (calc.)	[4⁺] (expt.)	[2⁺] (calc.)	[5⁺] (expt.)
Pd-N1(Ts/Me)	2.498	2.310	2.529	2.302
Pd-N2 (Me)	2.318	2.311	2.313	2.338
Pd-N3 (Py)	2.063	2.002	2.111	2.085
Pd-N4 (Py)	2.067	2.029	2.181	2.085
Pd-Cl1	2.416	2.303	2.466	2.344
Pd-Cl2/C1	2.417	2.322	2.073	2.021

Table 2.3 DFT-calculated (UB3LYP/CEP-31G) bond angles (degrees) for complexes [1⁺] and [2⁺] compared to experimentally determined parameters of similar ^{Me}N4 supported complexes.

Metrical Parameters	[1⁺] (calc.)	[4⁺] (expt.)	[2⁺] (calc.)	[5⁺] (expt.)
N1-Pd-N2	150.6	153.5	146.5	149.1
N3-Pd-N4	82.8	82.3	80.9	81.4

Furthermore, TD-DFT calculations were employed to simulate the UV/Vis spectra for complexes [1⁺] and [2⁺] (Figure 2.5 and 2.6). The calculated absorption bands for both complexes and their resulting compositions were summarized in Table 2.3 and 2.4. The β-LUMO's for both complexes were likewise generated and the corresponding atomic contributions were computed. The resulting β-LUMO, atomic contributions, axial Pd-N bond distances and the experimental EPR superhyperfine couplings were once again compared to the ^{Me}N4 supported complexes (Figure 2.7).

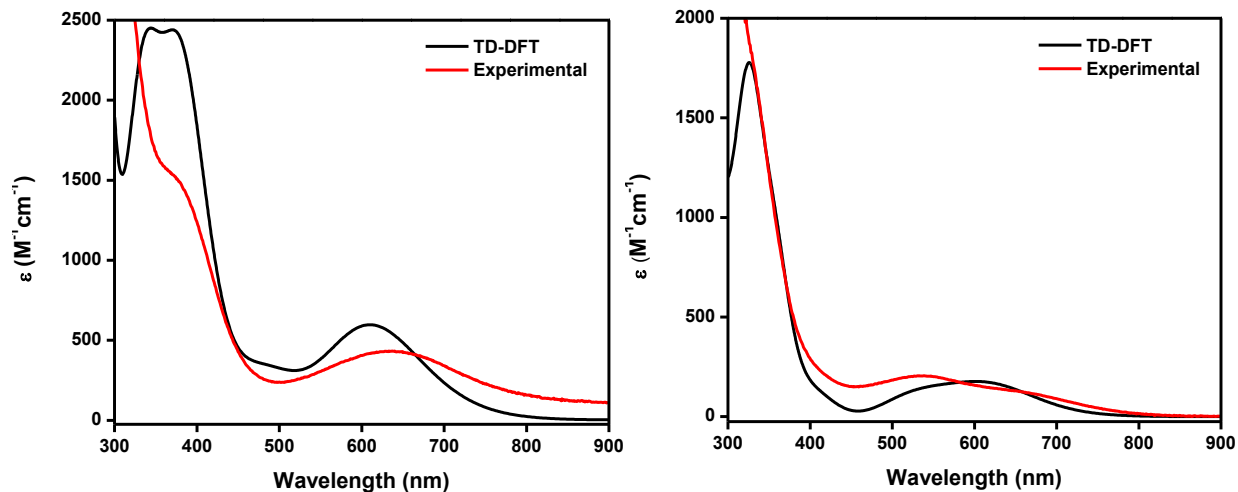


Figure 2.5 Comparison of experimental (red line) and computational simulated (black line) UV-Vis spectra of complexes $[1^+]\text{ClO}_4$ (left) and $[2^+]\text{ClO}_4$ (right) in MeCN.

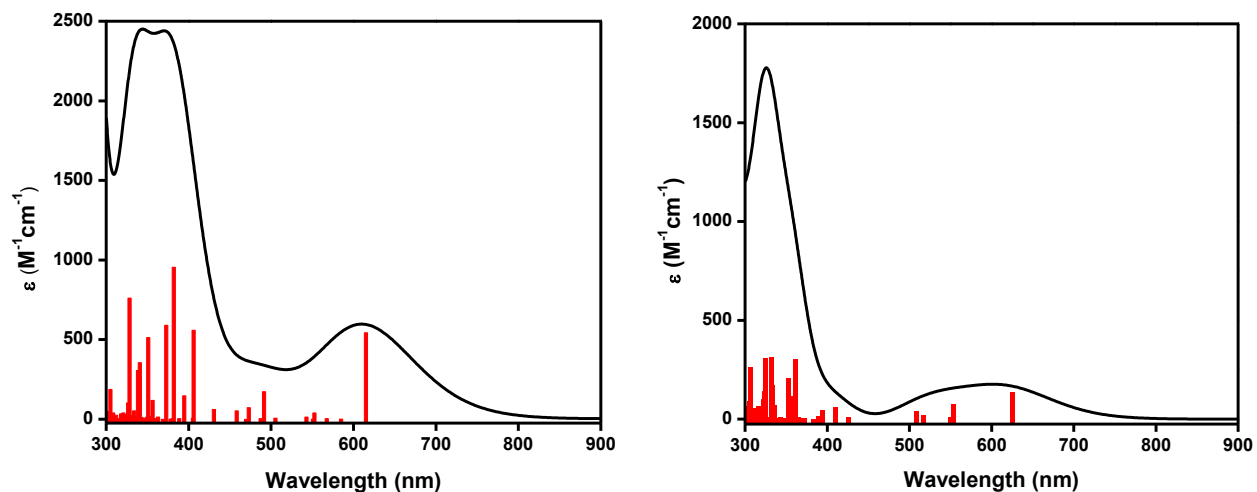


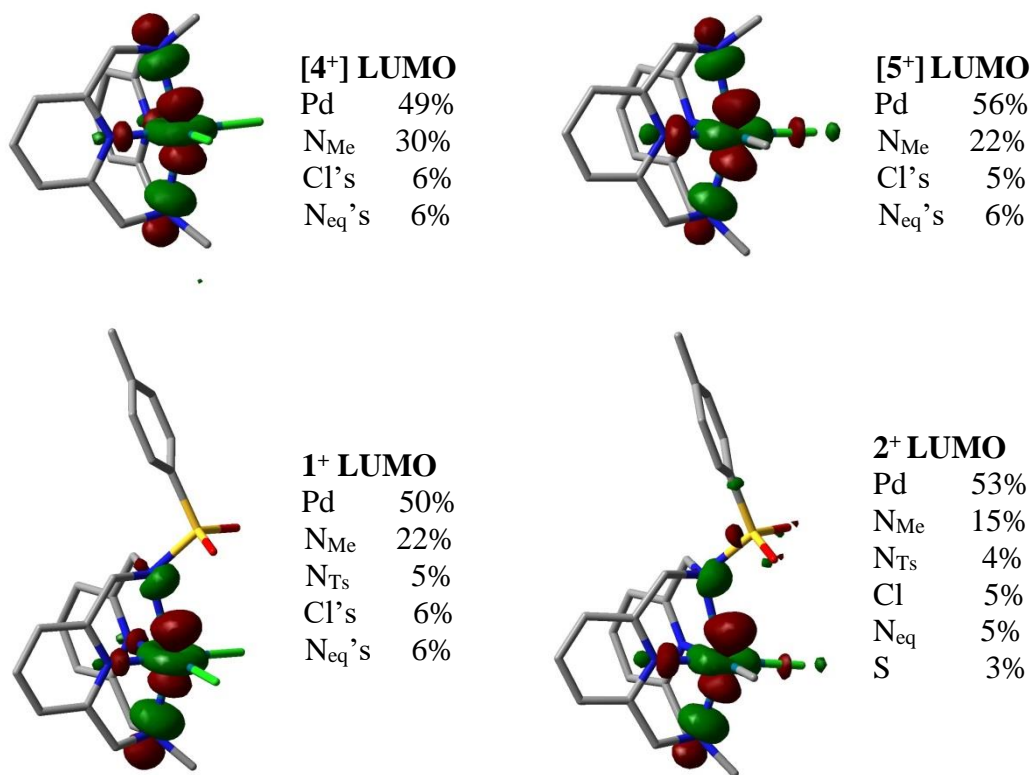
Figure 2.6 TD-DFT calculated UV-Vis spectra of complexes $[1^+]$ (left) and $[2^+]$ (right).

Table 2.3 TD-DFT calculated absorption bands and the corresponding orbital compositions for [1⁺]. Only the transitions with oscillator strengths larger than 0.007 are listed; similarly only contributing transitions with greater than 35% contribution to the absorption band are included.

Wavelength (nm)	Oscillator Strength	Major Contributing Transitions
614.81	0.036	β -HOMO \rightarrow β -LUMO (75%)
491.26	0.012	α -HOMO \rightarrow α -LUMO+1 (76%)
405.88	0.037	β -HOMO-3 \rightarrow β -LUMO (70%)
372.74	0.039	β -HOMO-7 \rightarrow β -LUMO (50%)
356.06	0.008	β -HOMO-6 \rightarrow β -LUMO+1 (77%)
305.05	0.013	α -HOMO-10 \rightarrow α -LUMO (46%)

Table 2.4 TD-DFT calculated absorption bands and the corresponding orbital compositions for [2⁺]. Only the transitions with oscillator strengths larger than 0.007 are listed; similarly only contributing transitions with greater than 35% contribution to the absorption band are included.

Wavelength (nm)	Oscillator Strength	Major Contributing Transitions
625.04	0.016	β -HOMO \rightarrow β -LUMO (40%)
553.60	0.009	α -HOMO \rightarrow α -LUMO (81%)
361.98	0.036	β -HOMO-1 \rightarrow β -LUMO+1 (35%)
355.98	0.014	β -HOMO-3 \rightarrow β -LUMO (46%)
354.76	0.011	β -HOMO-3 \rightarrow β -LUMO (37%)
320.33	0.008	α -HOMO \rightarrow α -LUMO+5 (75%)



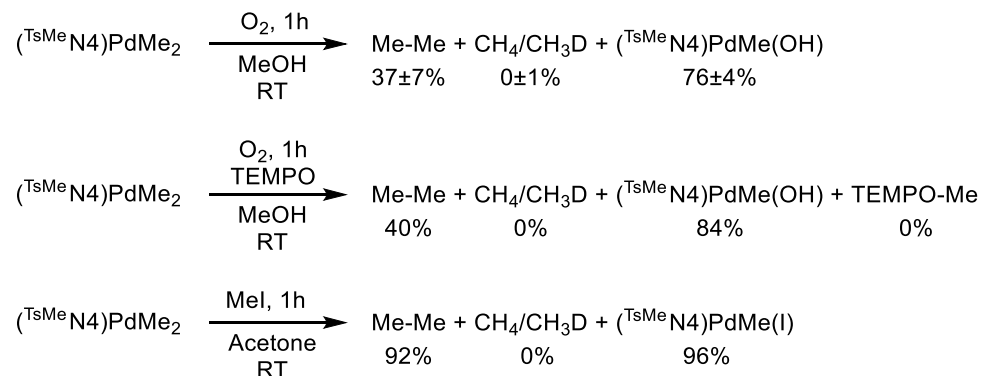
	[1 ⁺]	[2 ⁺]	[4 ⁺]	[5 ⁺]
Axial Bond Lengths [Å]	N _{Ts} -Pd 2.498 N _{Me} -Pd 2.318	N _{Ts} -Pd 2.529 N _{Me} -Pd 2.313	N ₁ -Pd 2.365 (2.310) N ₂ -Pd 2.368 (2.311)	N ₁ -Pd 2.379 (2.302) N ₂ -Pd 2.377 (2.338)
EPR Coupling Parameters [G]	A _{N, Ts} 10.0 A _{N, Me} 35.5	A _{N, Ts} 5.0 A _{N, Me} 31.5	A _{N, Me} 25.5	A _{N, Me} 23.0

Figure 2.7 DFT-calculated (UB3LYP/CEP-31G) molecular orbitals (β -LUMOs) of [1⁺] (bottom-left) and [2⁺] (bottom-right) compared to similar ^{Me}N₄ supported complexes (top). The calculated atomic contributions, DFT-calculated or experimentally determined axial Pd-N bond distances and the experimental EPR superhyperfine couplings are listed for each complex.

2.3.4 Aerobic reactivity of $(^{\text{TsMe}}\text{N4})\text{Pd}^{\text{II}}\text{Me}_2$

On account of the low oxidation potential observed for complex **3**, as well as the previously observed aerobic oxidation of $(^{\text{tBu}}\text{N4})\text{Pd}^{\text{II}}\text{Me}_2$ and $(^{\text{Me}}\text{N4})\text{Pd}^{\text{II}}\text{Me}_2$, we proposed that **3** could be similarly oxidized using mild oxidants to form reactive high-valent Pd species. Therefore, a solution of **3** in methanol was reacted with O_2 and the reaction was monitored by NMR to reveal the formation of ethane in up to 49% yield (Scheme 2.5). This yield is similar to results previously reported for similar complexes.^{15,16} Furthermore, the observed C-C bond formation reactivity was not affected by the presence of the alkyl radical trap TEMPO, suggesting a non-radical mechanism (Scheme 2.5).

Scheme 2.5 Aerobic Reactivity of $(^{\text{TsMe}}\text{N4})\text{Pd}^{\text{II}}\text{Me}_2$ (**3**).



In the previously reported cases, the formation of high-valent Pd^{III} species formed via the aerobic oxidation was monitored by UV-Vis spectroscopy. Similarly, the formation of the Pd^{III} species was confirmed using EPR and ESI-MS.^{15,16} The utilization of these techniques to verify the presence of the Pd^{III} intermediates was possible due to the inherent stability of these complexes. In the case of our newly synthesized pseudo-tridentate supported complex, $[\mathbf{3}^+]$, the ligand cannot stabilize the Pd^{III} metal center, therefore, the Pd^{III} intermediate was not observed during the aerobic

oxidation of complex $[3^+]$ using UV-Vis spectroscopy (Figure 2.8). The reaction was observed directly progressing from the starting material to the final product.

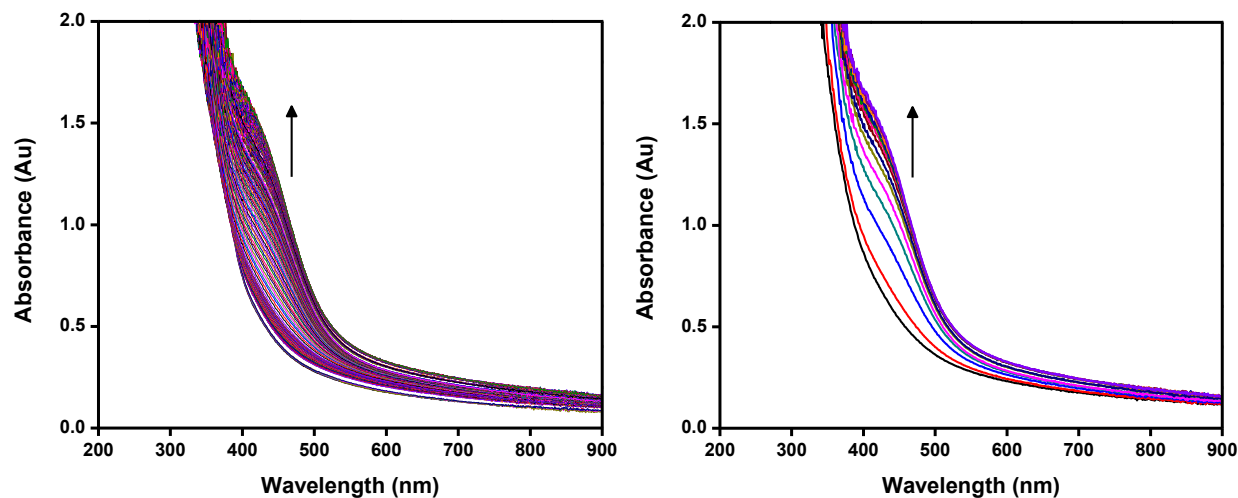


Figure 2.8 UV-vis spectrum of 2.14 mM solution of **3** in methanol under O_2 at $20^\circ C$ ($t = 0-1560$ min). The UV-Vis spectrum was recorded continuous at 10 minute intervals (left). To highlight the growth of the band at 440 nm, the spectrum at 2 hour intervals is also plotted (right).

Similarly, the formation of the Pd^{III} intermediate was not observed using EPR spectroscopy. However, a trace amount of the short lived Pd^{III} intermediate was observed using ESI-MS, which reveals a peak at m/z 545.1131 (calculated for 3^+ : 544.1124). The Pd^{III} species $[3^+]$ is initially present right after aerobic oxidation. However, it fades rather quickly, with complete transformation to the key intermediate $[(^{TsMe}N_4)Pd^{IV}Me_3]^+$, **4**, within 10 minutes. The life-time of **4** conversely is much longer; the ESI-MS results confirm the presence of **4** until completion of the reaction. These results suggest a rapid formation of the key Pd^{IV} intermediate and only a very transient formation of the Pd^{III} intermediate.

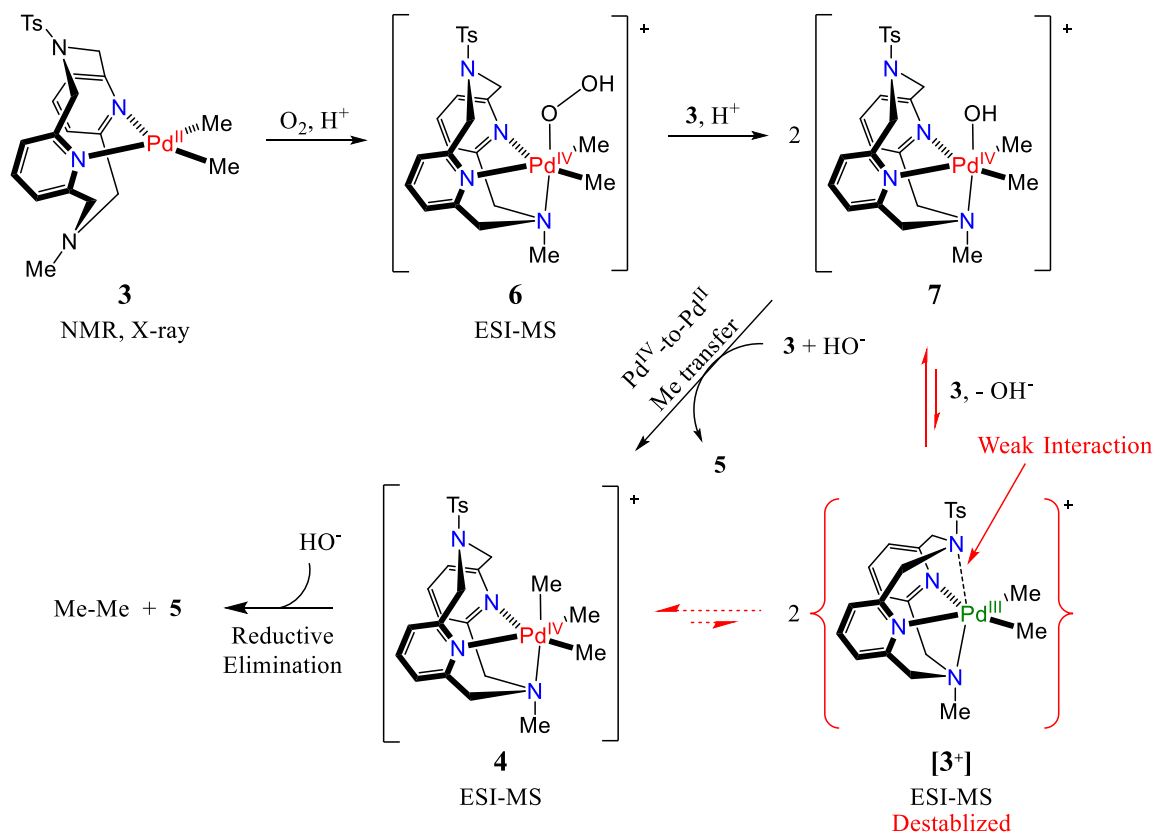
Additionally, the observed rate of reactivity is comparable to the previously reported tetradentate supported complexes, suggesting that the formation of the high-valent $Pd^{IV}Me_3$

intermediate is not rate-determining. Overall, these results suggest the rate determining step is the subsequent reductive elimination from the Pd^{IV}Me₃ intermediate, and thus the destabilization of the Pd^{III} intermediate had a minimal effect on the rate of the C-C bond formation.

2.3.5 Proposed mechanism for the aerobic C–C bond formation reactivity

Based on the experimental results described above, and by analogy with the aerobic oxidation of previously reported Pt^{II} and Pd^{II} dimethyl complexes,³⁸⁻⁴⁰ we proposed the mechanism for the aerobically induced C-C bond formation from **3** is altered from the previously reported mechanisms for (^{*t*}BuN4)Pd^{II}Me₂ and (^{*Me*}N4)Pd^{II}Me₂.^{15,16} We proposed a mechanism that proceeds directly to the key intermediate **4** without generating the [**3**⁺] intermediate (Scheme 2.6). Oxidation of **3** by O₂ through an inner sphere mechanism is expected to generate a transient Pd^{III}-superoxide intermediate, [(κ³-^{*TsMe*}N4)Pd^{III}Me₂(O₂)].¹⁸ Upon protonation, this would yield the Pd^{IV}hydroperoxo species **6**, which was shortly detected via ESI-MS during the aerobic oxidation. Then complex **6** can further oxidize another molecule of **3** to give two molecules of the Pd^{IV}-hydroxo species **7**. Complex **7** can then undergo a Pd^{IV}-to-Pd^{II} methyl group transfer along with complex **3** to produce the key reactive intermediate **4** and the observed by-product **5**. From intermediate **4** the rate-determining reductive elimination of ethane can occur to produce additional by-product **5**. The reductive elimination of ethane from intermediate **4** was independently confirmed via the observed reactivity of methyl iodide with complex **3**. The reaction was monitored by NMR to reveal the formation of ethane in up to 92% yield in 1 hour (Scheme 2.5).

Scheme 2.6 Proposed Mechanism for Aerobic Oxidation of (^{TsMe}N₄)Pd^{II}Me₂ (**3**) and Subsequent Ethane Elimination.



2.4 Conclusion

In summary, reported herein is the synthesis and reactivity of an organometallic Pd^{II}Me₂ complex supported by a newly synthesized “pseudo-tridentate” N₄ ligand. The pseudo-tridentate ligand was shown via spectroscopic methods to destabilize the high-valent Pd^{III} metal center. As a result, the corresponding aerobic transformation of the organometallic Pd^{II}Me₂ complex was improved by favoring the direct formation of the key intermediate Pd^{IV}Me₃. Subsequently, the selective C-C bond formation reaction was minimally affected by the destabilization of the Pd^{III} intermediate. Consequently, these studies provided experimental evidence that the rate determining step controlling the aerobically induced C-C bond formation is in fact the reductive elimination of ethane from the key intermediate Pd^{IV}Me₃, as previously proposed.

2.5 Acknowledgements

I appreciate my colleague Ying Zhang for her help and advice in performing the in situ ESI-MS experiments. Similarly, I appreciate Professor Nigam P. Rath of the Department of Chemistry and Biochemistry at the University of Missouri-St. Louis for his help and advice in solving all the reported crystal structures.

2.6 References

1. Stoltz, B. M. *Chem. Lett.* **2004**, *33*, 362.
2. Stahl, S. S. *Angew. Chem. Int. Ed.* **2004**, *43*, 3400.
3. Stahl, S. S. *Science* **2005**, *309*, 1824.
4. Beck, E. M.; Grimster, N. P.; Hatley, R.; Gaunt, M. J. *J. Am. Chem. Soc.* **2006**, *128*, 2528.
5. Sigman, M. S.; Jensen, D. R. *Acc. Chem. Res.* **2006**, *39*, 221.
6. Gligorich, K. M.; Sigman, M. S. *Chem. Commun.* **2009**, 3854.
7. Campbell, A. N.; Stahl, S. S. *Acc. Chem. Res.* **2012**, *45*, 851.
8. Shi, Z.; Zhang, C.; Tang, C.; Jiao, N. *Chem. Soc. Rev.* **2012**, *41*, 3381.
9. Zhang, J.; Khaskin, E.; Anderson, N. P.; Zavalij, P. Y.; Vedernikov, A. N. *Chem. Commun.* **2008**, 3625.
10. Zhang, Y.-H.; Yu, J.-Q. *J. Am. Chem. Soc.* **2009**, *131*, 14654.
11. Wang, A.; Jiang, H.; Chen, H. *J. Am. Chem. Soc.* **2009**, *131*, 3846.
12. Boisvert, L.; Denney, M. C.; Kloek, H. S.; Goldberg, K. I. *J. Am. Chem. Soc.* **2009**, *131*, 15802.
13. Zhu, M.-K.; Zhao, J.-F.; Loh, T.-P. *J. Am. Chem. Soc.* **2010**, *132*, 6284.

14. Vedernikov, A. N. *Acc. Chem. Res.* **2012**, *45*, 803.
15. Khusnutdinova, J. R.; Rath, N. P.; Mirica, L. M. *J. Am. Chem. Soc.* **2012**, *134*, 2414.
16. Tang, F.; Zhang, Y.; Rath, N. P.; Mirica, L. M. *Organometallics* **2012**, *31*, 6690.
17. Khusnutdinova, J. R.; Qu, F.; Zhang, Y.; Rath, N. P.; Mirica, L. M. *Organometallics* **2012**, *31*, 4627.
18. Bottino, F.; Di Grazia, M.; Finocchiaro, P.; Fronczek, F. R.; Mamo, A.; Pappalardo, S. *J. Org. Chem.* **1988**, *53*, 3521.
19. Drew, D.; Doyle, J. R. *Inorg. Synth.* **1990**, *28*, 346.
20. Rulke, R. E.; Ernsting, J. M.; Spek, A. L.; Elsevier, C. J.; Leeuwen, P. W. N. M. v.; Vrieze, K. *Inorg. Chem.* **1993**, *32*, 5769.
21. Meneghetti, S. P.; Lutz, P. J.; Kress, J. *Organometallics* **2001**, *20*, 5050.
22. Fulmer, G. R.; Miller, A. J. M.; Sherden, N. H.; Gottlieb, H. E.; Nudelman, A.; Stoltz, B. M.; Bercaw, J. E.; Goldberg, K. I. *Organometallics* **2010**, *29*, 2176.
23. Bruker Analytical X-Ray, Madison, WI, 2008
24. Sheldrick, G. *Acta Crystallogr. Sect. A: Found. Crystallogr.* **2008**, *64*, 112.
25. M. J. Frisch, G. W. T., H. B. Schlegel, G. E. Scuseria, M. A. Robb, J. R. Cheeseman, G. Scalmani, V. Barone, B. Mennucci, G. A. Petersson, H. Nakatsuji, M. Caricato, X. Li, H. P. Hratchian, A. F. Izmaylov, J. Bloino, G. Zheng, J. L. Sonnenberg, M. Hada, M. Ehara, K. Toyota, R. Fukuda, J. Hasegawa, M. Ishida, T. Nakajima, Y. Honda, O. Kitao, H. Nakai, T. Vreven, J. A. Montgomery, Jr., J. E. Peralta, F. Ogliaro, M. Bearpark, J. J. Heyd, E. Brothers, K. N. Kudin, V. N. Staroverov, R. Kobayashi, J. Normand, K. Raghavachari, A. Rendell, J. C. Burant, S. S. Iyengar, J. Tomasi, M. Cossi, N. Rega, J. M. Millam, M. Klene, J. E. Knox, J. B. Cross, V. Bakken, C. Adamo, J. Jaramillo, R. Gomperts, R. E. Stratmann, O. Yazyev, A. J. Austin, R. Cammi, C. Pomelli, J. W. Ochterski, R. L. Martin, K. Morokuma, V. G. Zakrzewski, G. A. Voth, P. Salvador, J. J. Dannenberg, S. Dapprich, A. D. Daniels, O. Farkas, J. B. Foresman, J. V. Ortiz, J. Cioslowski, D. J. Fox, Gaussian, Inc.
26. Becke, A. D. *J. Chem. Phys.* **1993**, *98*, 1372.
27. Lee, C. T.; Yang, W. T.; Parr, R. G. *Phys. Rev. B* **1988**, *37*, 785.

28. Stevens, W. J.; Basch, H.; Krauss, M. *J. Chem. Phys.* **1984**, *81*, 6026.
29. Stevens, W. J.; Krauss, M.; Basch, H.; Jasien, P. G. *Can. J. Chem.* **1992**, *70*, 612.
30. Foley, N. A.; Lail, M.; Lee, J. P.; Gunnoe, T. B.; Cundari, T. R.; Petersen, J. L. *J. Am. Chem. Soc.* **2007**, *129*, 6765.
31. Veige, A. S.; Slaughter, L. M.; Wolczanski, P. T.; Matsunaga, N.; Decker, S. A.; Cundari, T. R. *J. Am. Chem. Soc.* **2001**, *123*, 6419.
32. Skripnikov, L. www.chemissian.com, accessed June 2011
33. O'Boyle, N. M.; Tenderholt, A. L.; Langner, K. M. *J. Comput. Chem.* **2008**, *29*, 839.
34. Khusnutdinova, J. R.; Rath, N. P.; Mirica, L. M. *J. Am. Chem. Soc.* **2010**, *132*, 7303.
35. Tang, F.; Qu, F.; Khusnutdinova, J. R.; Rath, N. P.; Mirica, L. M. *Dalton Trans.* **2012**, *41*, 14046.
36. Burnett, M. N.; Johnson, C. K. *ORTEP-III: Oak Ridge Thermal Ellipsoid Plot Program for Crystal Structure Illustrations, Oak Ridge National Laboratory Report ORNL-6895* **1996**.
37. Khusnutdinova, J. R.; Rath, N. P.; Mirica, L. M. *Inorg. Chem.* **2014**, *53*, 13112.
38. Rostovtsev, V. V.; Henling, L. M.; Labinger, J. A.; Bercaw, J. E. *Inorg. Chem.* **2002**, *41*, 3608.
39. Prokopchuk, E. M.; Puddephatt, R. J. *Can. J. Chem.* **2003**, *81*, 476.
40. Prokopchuk, E. M.; Jenkins, H. A.; Puddephatt, R. J. *Organometallics* **1999**, *18*, 2861.

Chapter 3

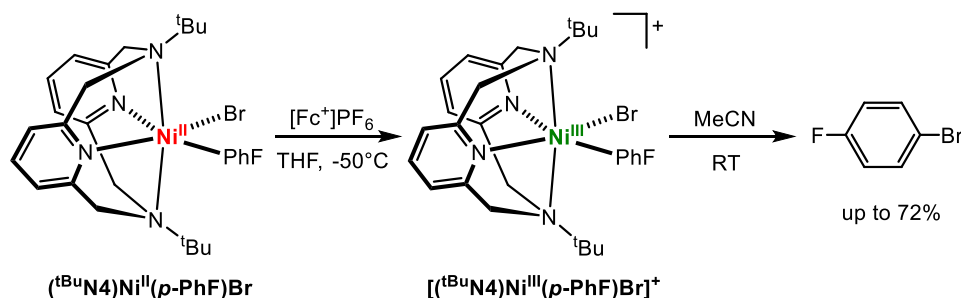
Structural and Reactivity Comparison of *Ortho*-Substituted Organometallic Nickel(III) Complexes

3.1 Introduction

The use of ligand modification has been frequently studied to gain a greater understanding of the role electronic and steric properties play in ligand design. Various ligand modifications have thus been used to improve numerous catalytic systems for a range of organometallic transformations.¹⁻⁵ Furthermore, several of these organometallic transformations propose the involvement of high-valent Ni^{III} intermediates, in particular during various cross coupling⁶⁻³⁰ and carbon-heteroatom bond formation reactions³¹⁻³⁵. Therefore, studying the effects of ligand modifications on these Ni^{III} intermediates would improve the development of catalytic systems for these important organic transformations.

To this point, we have reported the isolation and characterization of a series of Ni^{III}(*para*-aryl)halide complexes stabilized by utilizing the tetradentate ligand system, N,N'-di-tert-butyl-2,11-diaza[3.3](2,6)pyridinophane (^tBuN4).³⁶ These Ni^{III} complexes were found to be stable at low temperatures, but would undergo C-halide bond formation upon warming to room temperature (Scheme 3.1). Herein, we report the isolation and characterization of a series of Ni^{III}(*ortho*-aryl)halide complexes stabilized utilizing the tetradentate ligand (^tBuN4). These complexes were then directly compared to the previously synthesized *para*-substituted complexes to gain a greater insight into the effect of the electronics and sterics of the aryl ligand.

Scheme 3.1 C-Halide bond formation reactivity of [(^tBuN4)Ni^{III}(*para*-aryl)halide]⁺ complexes.³⁶



3.2 Experimental Section

3.2.1 Synthesis of Ligands and Complexes

Reagents and Materials. All manipulations were carried out under a nitrogen atmosphere using standard Schlenk and glove box techniques if not indicated otherwise. All reagents for which synthesis is not given were commercially available from Sigma-Aldrich, Fisher Scientific, VWR, Acros, STREM or Pressure Chemical and were used as received without further purification. Solvents were purified prior to use by passing through a column of activated alumina using a MBRAUN Solvent Purification System. N,N' -di-tert-butyl-2,11-diaza[3.3](2,6)pyridinophane (${}^t\text{BuN4}$)³⁷, $({}^t\text{BuN4})\text{Ni}^{\text{II}}(p\text{-FPh})\text{Br}$ ³⁶, and FcPF_6 ³⁸ were prepared according to the literature procedures.

$({}^t\text{BuN4})\text{Ni}^{\text{II}}(o\text{-PhF})\text{Br}$ (1). A suspension of ${}^t\text{BuN4}$ (100.0 mg, 0.26 mmol) in 1-bromo-2-fluorobenzene (3 mL) was added to $[\text{Ni}(\text{COD})_2]$ (70.2 mg, 0.26 mmol) and the mixture was stirred at room temperature for 3 hours. Pentane (10 mL) was added and the olive green precipitate was separated by filtration, washed with pentane (2 x 3 mL), and dried under vacuum. Yield: 119.0 mg, 0.20 mmol, 77%.

$({}^t\text{BuN4})\text{Ni}^{\text{II}}(o\text{-PhF})\text{Cl}$ (2). A suspension of ${}^t\text{BuN4}$ (50.0 mg, 0.13 mmol) in 1-chloro-2-fluorobenzene (2 mL) was added to $[\text{Ni}(\text{COD})_2]$ (35.1 mg, 0.13 mmol) and the mixture was stirred at room temperature for 2 hours. Pentane (10 mL) was added and the grey precipitate was separated by filtration, washed with pentane (2 x 3 mL), and dried under vacuum. Yield: 43.1 mg, 0.08 mmol, 62%.

(^tBuN4)Ni^{II}(*o*-PhMe)Br (3). A suspension of ^tBuN4 (100.0 mg, 0.26 mmol) in 2-bromotoluene (3 mL) was added to [Ni(COD)₂] (70.2 mg, 0.26 mmol) and the mixture was stirred at room temperature for 3 hours. Pentane (10 mL) was added and the tan precipitate was separated by filtration, washed with pentane (2 x 3 mL), and dried under vacuum. Yield: 109.0 mg, 0.19 mmol, 73%.

(^tBuN4)Ni^{II}(*o*-PhMe)Cl (4). A suspension of ^tBuN4 (100.0 mg, 0.26 mmol) in 2-chlorotoluene (3 mL) was added to [Ni(COD)₂] (70.2 mg, 0.26 mmol) and the mixture was stirred at room temperature for 1.5 hours. Pentane (10 mL) was added and the grey precipitate was separated by filtration, washed with pentane (2 x 3 mL), and dried under vacuum. Yield: 67.4 mg, 0.13 mmol, 49%.

(^tBuN4)Ni^{II}(*o*-PhOMe)Br (5). A suspension of ^tBuN4 (50.0 mg, 0.13 mmol) in 2-bromoanisole (3 mL) was added to [Ni(COD)₂] (35.1 mg, 0.13 mmol) and the mixture was stirred at room temperature for 3 hours. Pentane (10 mL) was added and the grey precipitate was separated by filtration, washed with pentane (2 x 3 mL), and dried under vacuum. Yield: 41.2 mg, 0.07 mmol, 54%.

[(^tBuN4)Ni(*o*-PhF)Br]PF₆ (6). A THF solution of **1** (34.3 mg, 0.058 mmol) and FcPF₆ (19.4 mg, 0.058 mmol) was stirred at -50 °C for 5 hours. The resulting solution was then filtered at -50 °C and pentane was diffused into the filtrate at -35 °C. After 3 days, the product was obtained as X-ray quality yellow-brown crystals. Yield: 8.7 mg, 0.012 mmol, 21%.

$[(^t\text{Bu}_4\text{N})\text{Ni}(o\text{-PhF})\text{Cl}]\text{PF}_6$ (**7**). A THF solution of **2** (10.0 mg, 0.018 mmol) and FcPF_6 (6.1 mg, 0.018 mmol) was stirred at $-50\text{ }^\circ\text{C}$ for 2 hours. At which time, 100 μL aliquot of the resulting dark green solution was mixed with 300 μL pre-cooled PrCN in an EPR tube. The EPR sample was thoroughly mixed, frozen at 77 K and analyzed confirming the formation of the desired Ni^{III} complex, however all attempts to isolate X-ray quality crystals of complex **2** have been unsuccessful.

3.2.2 Physical Measurements

^1H NMR and ^{19}F NMR spectra were recorded on a Varian Mercury-300 spectrometer (300.121 MHz). Chemical shifts are reported in parts per million (ppm) with residual solvent resonance peaks as internal reference.³⁹ Abbreviations for the multiplicity of NMR signals are singlet (s), doublet (d), triplet (t), quartet (q), multiplet (m), and broad (br). EPR spectra were recorded on a JEOL JES-FA X-band (9.2 GHz) EPR spectrometer in frozen solution at 77 K.

Cyclic voltammetry (CV) experiments were performed using a BASi EC Epsilon electrochemical workstation or a CHI 660D Electrochemical Analyzer. Electrochemical-grade supporting electrolytes were purchased from Fluka. The electrochemical measurements were performed under a blanket of nitrogen, and the analyzed solutions were deaerated by purging with nitrogen. A glassy carbon disk electrode and auxiliary Pt wire were used as the working electrode for cyclic voltammetry. Two different non-aqueous reference electrodes were used: Ag/filled with 0.01M AgNO_3 /0.1M Bu_4NClO_4 /MeCN solution or silver wire. The reference electrodes were calibrated against ferrocene (Fc) at the conclusion of each CV experiment.

X-ray diffraction quality crystals of $[(^t\text{Bu}_4\text{N})\text{Ni}(o\text{-PhF})\text{Br}]\text{PF}_6$ were obtained by slow pentane vapor diffusion into a tetrahydrofuran solution. Suitable crystals of appropriate

dimensions were mounted and preliminary examination and data collection were performed using a Bruker Kappa Apex-II Charge Coupled Device (CCD) Detector system single crystal X-Ray diffractometer equipped with an Oxford Cryostream LT device. Data were collected using graphite monochromated Mo K α radiation ($\lambda = 0.71073 \text{ \AA}$) from a fine focus sealed tube X-Ray source. Apex II and SAINT software packages⁴⁰ were used for data collection and data integration. Final cell constants were determined by global refinement of reflections from the complete data set. Data were corrected for systematic errors using SADABS⁴⁰ based on the Laue symmetry using equivalent reflections. Structure solutions and refinement were carried out using the SHELXTL-PLUS software package⁴¹. The structures were refined with full matrix least-squares refinement by minimizing $\sum w(F_o^2 - F_c^2)^2$. All non-hydrogen atoms were refined anisotropically to convergence. Typically, H atoms are added at the calculated positions in the final refinement cycles. The complete listings of x-ray diffraction parameters are included in Appendix B.

3.2.3 Reactivity Studies

¹H NMR reactivity studies. A 3-4 mM solution of **1** or **2** in d₃-MeCN was added into a NMR tube containing 1,3,5-trimethoxybenzene as an internal standard. Then a solution of FcPF₆ in MeCN-d₃ was added to the NMR tube. The reaction mixture was kept in the dark and periodically analyzed by ¹H NMR. The yield of the products were determined by integration versus the internal standard, calculated as [moles of product]/[moles of **1** or **2**]*100%.

¹⁹F NMR reactivity studies. Periodically following the ¹H NMR analysis the same solution was monitored via ¹⁹F NMR. For these studies the counterion PF₆ from the FcPF₆ was used as the internal standard. Similar to the ¹H NMR studies, the yield of the products were determined by integration versus the internal standard, calculated as [moles of product]/[moles of **1** or **2**]*100%.

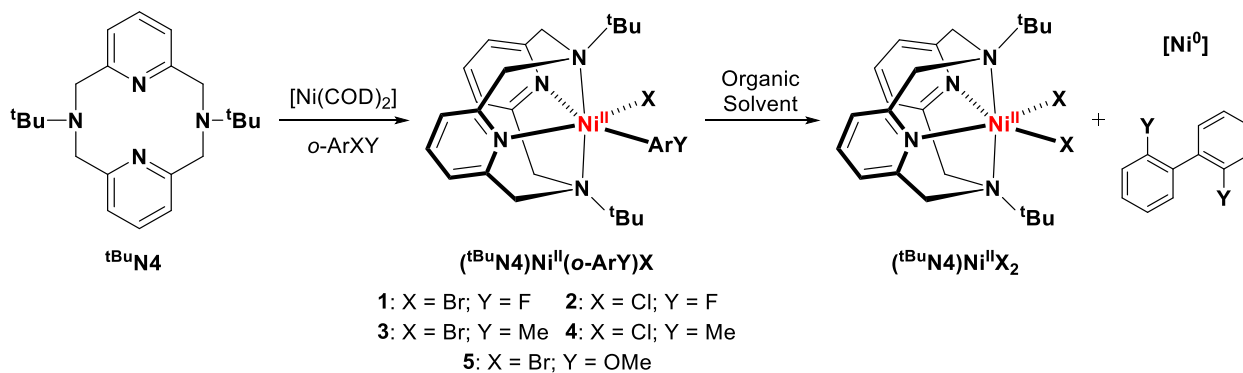
GC reactivity studies. At -50°C 20-21 mM solution of **1** or **2** in MeCN was added to a 20 mL vial containing hexamethylbenzene as an internal standard. Then a solution of FcPF₆ in MeCN was added and the reaction mixture was warmed up to room temperature and stirred in the dark. After the reaction was complete, the reaction was quenched with 1 mL concentrated ammonium chloride. The resulting solution was stirred for 15 minutes, then extracted with diethyl ether. The organic layer was separated and dried using magnesium sulfate prior to GC analysis. The yield of the products were determined by integration versus the internal standard, calculated as [moles of product]/[moles of **1** or **2**]*100%. The identity of the organic products were confirmed by GC-MS.

3.3 Results and Discussion

3.3.1 Synthesis and Structure of Ni^{II} Complexes.

A series of Ni^{II} complexes (**1-5**) were effectively prepared using the previously reported method for the synthesis of (t^{Bu}N4)Ni^{II}(*p*-PhF)Br (Scheme 3.2).³⁶ The characterization of the resulting complexes, however, was problematic due to the complexes having low solubility in common organic solvents. Furthermore, even if the complexes were soluble in select organic solvents they would rapidly undergo ligand exchange forming the stable (t^{Bu}N4)Ni^{II}X₂ and the highly reactive di-aryl Ni^{II} species, which subsequently, reductive eliminated to produce the *ortho*-substituted biphenyl and [Ni⁰] (Scheme 3.2).

Scheme 3.2 Synthesis of Ni^{II} complexes **1-5** and the resulting ligand exchange in organic solvents.



Complex **1** showed the slowest decomposition in tetrahydrofuran, thus allowing limited cyclic voltammetry (CV) experiments to be conducted. The CV of complex **1** shows two oxidation processes at -0.27 and 0.30 V vs Fc⁺/Fc (Figure 3.1). The low oxidative process is assigned to the Ni^{II}/Ni^{III} couple, while the higher oxidative wave is tentatively assigned to a

Ni^{III}/Ni^{IV} couple. These potentials are extremely low and indicate the Ni^{III} oxidation state should be readily attainable.

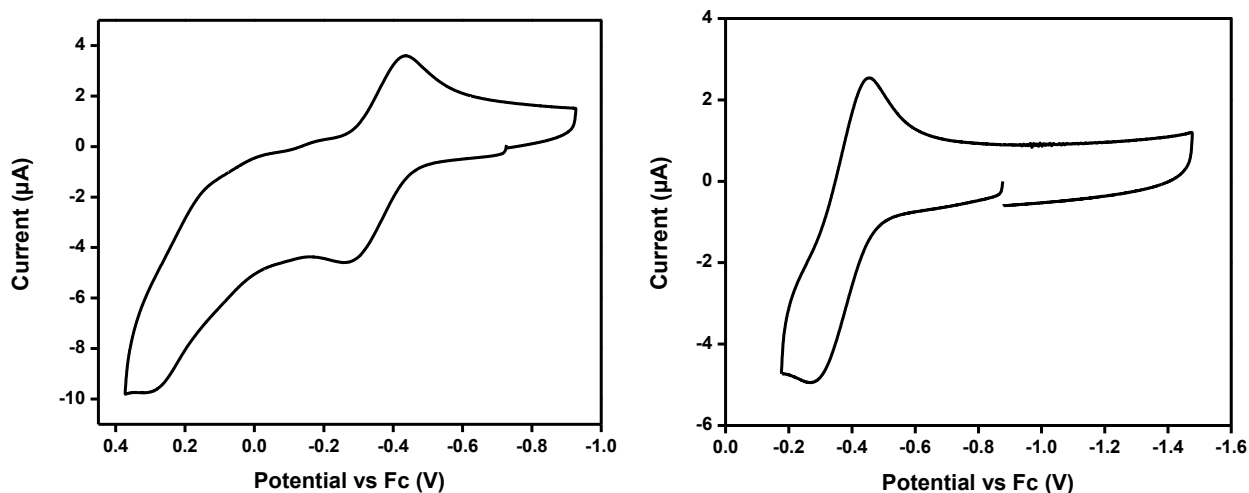


Figure 3.1 Cyclic voltammograms of **1** in 0.1 M Bu₄NClO₄ in tetrahydrofuran: (left) full range, (right) Ni^{II}/Ni^{III} couple. Scan rate: 100 mV/s.

3.3.2 Synthesis and Structure of Ni^{III} Complexes.

The Ni^{II}/Ni^{III} oxidation potential for complex **1** was extremely low, therefore the analogous complex **2** was proposed to have a similarly low Ni^{II}/Ni^{III} oxidation potential. Complexes **1** and **2** were both oxidized with 1 equivalent [Fc⁺]PF₆ in THF at -50°C to yield [(^tBuN₄)Ni^{III}(*o*-PhF)Br]PF₆, **6**, as a yellow-brown solution, and [(^tBuN₄)Ni^{III}(*o*-PhF)Cl]PF₆, **7**, as a dark green solution, respectively. The oxidation of complex **3-5** failed to produce detectable quantities of the corresponding Ni^{III} complexes, therefore the ensuing studies focused on complexes **1** and **2** and their Ni^{III} counterparts **6** and **7**.

X-ray quality crystals of **6** were obtained from THF/pentane (Figure 3.2). Complex **6** adopts a distorted octahedral geometry with an average axial Ni-N_{amine} bond length of 2.344 Å, a shorter average equatorial Ni-N_{pyridyl} bond length of 1.969 Å, a Ni-C bond length of 1.993 Å and

Ni-Br bond length of 2.440 Å. These values are consistent with the previously reported $[(^t\text{BuN}4)\text{Ni}^{\text{II}}(p\text{-PhF})\text{Br}]^+$ and $[(^t\text{BuN}4)\text{Ni}^{\text{II}}(p\text{-PhF})\text{Cl}]^+$ complexes (Ni- N_{amine} bond lengths of 2.305-2.323 Å, Ni- $\text{N}_{\text{pyridyl}}$ bond length of 1.903 and 1.965 Å, Ni-C bond length of 1.980-2.018 Å and Ni-Halide bond length of 2.273-2.395 Å)³⁷, and the only other reported six-coordinate Ni^{III} complexes.⁴⁴⁻⁴⁶

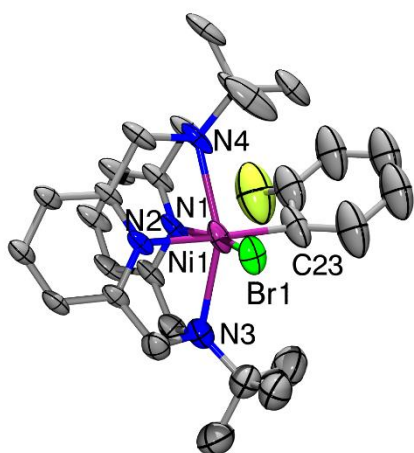


Figure 3.2 ORTEP⁴² representation of the cation of **6** with 50% probability thermal ellipsoids. Selected bond distances (Å), Ni1-N1, 1.981; Ni1-N2, 1.956; Ni1-N3, 2.342; Ni1-N4, 2.345; Ni1-C23, 1.993; Ni1-Br1, 2.440. A complete listings of structural parameters are included in Appendix B.

The EPR spectra of complexes **6** and **7** exhibited rhombic signals with a g_{avg} of 2.157 and 2.158, respectively. Superhyperfine coupling was observed in the g_z direction (**6**: $A_{2\text{N}} = 13.0$ G; **7**: $A_{2\text{N}} = 13.8$ G) due to the two axial N donors ($I = 1$) coupling to the Ni^{III} center (Figure 3.3). Additionally, the EPR spectrum of complex **6** contained superhyperfine coupling in the g_y and g_z direction (g_y : $A_{\text{Br}} = 12.0$ G; g_z : $A_{\text{Br}} = 12.7$ G) due to the equatorial Br donor ($I = 3/2$) coupling to the Ni^{III} center. These results are consistent with a distorted octahedral Ni^{III} metal center in a d_z^2

ground state.⁴³⁻⁴⁷ As a whole, these values are consistent with the previously reported $[(^t\text{Bu}_4\text{N})\text{Ni}^{\text{II}}(p\text{-PhF})\text{Br}]^+$ and $[(^t\text{Bu}_4\text{N})\text{Ni}^{\text{II}}(p\text{-PhF})\text{Cl}]^+$ complexes.³⁶

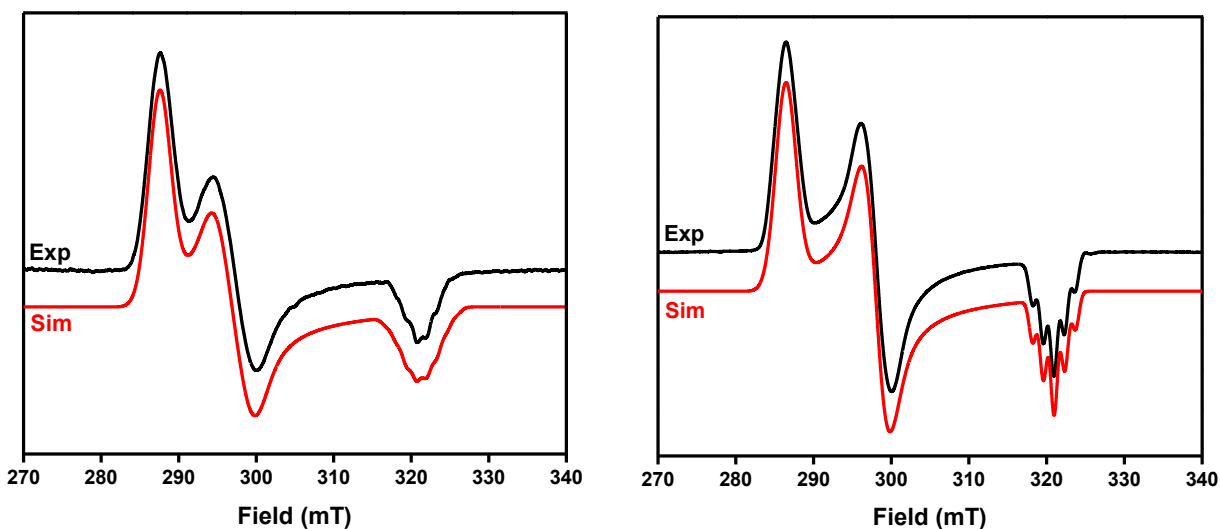
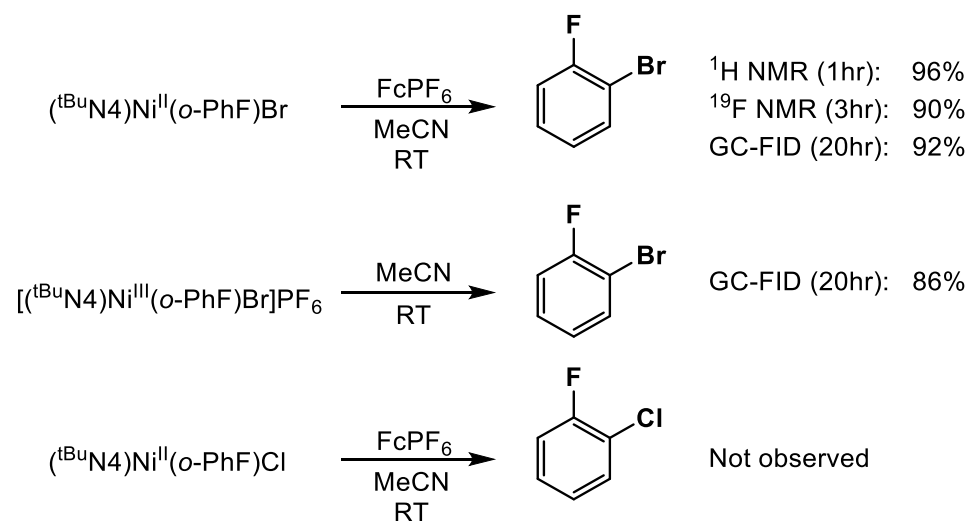


Figure 3.3 EPR spectra (black lines) of **6** (left) and **7** (right) in 3:1 PrCN/THF at 77K, and the simulated EPR spectrum (red lines) using the following parameters: **6**, $g_x = 2.260$, $g_y = 2.187$ ($A_{\text{Br}} = 12.0$ G), $g_z = 2.023$ ($A_{2\text{N}} = 13.0$ G and $A_{\text{Br}} = 12.7$ G); **7**, $g_x = 2.269$, $g_y = 2.181$, $g_z = 2.025$ ($A_{2\text{N}} = 13.8$ G).

3.3.3 C-Halide Bond Formation Reactivity.

In addition to the characterization of complexes **6** and **7**, the C-Halide bond formation reactivity of these complexes was investigated. Oxidation of complex **1** in MeCN at room temperature generated observable quantities of 1-bromo-2-fluorobenzene via ^1H NMR, ^{19}F NMR and GC-FID. Conversely, the oxidation of complex **2** exhibited limited reactivity with no observable quantities of 1-chloro-2-fluorobenzene. Additionally, isolated complex **6** generated observable quantities of 1-bromo-2-fluorobenzene upon warming to room temperature (Scheme 3.3).

Scheme 3.3 C-Halide Bond Formation Reactivity of $[(^t\text{BuN4})\text{Ni}^{\text{III}}(\textit{ortho}\text{-aryl})\text{halide}]^+$ complexes.



Reactivity of complex **1** resulted in formation of a similar product to the previously reported $(^t\text{BuN4})\text{Ni}^{\text{II}}(\textit{p}\text{-PhF})\text{Br}$, however complex **1** was significantly more reactive. The reaction with complex **1** had reached completion within 1 hour, whereas $(^t\text{BuN4})\text{Ni}^{\text{II}}(\textit{p}\text{-PhF})\text{Br}$ took nearly 6 hours.³⁶ We propose the increased reactivity of complex **1** is due to the increased steric effects caused by the *ortho*-fluoride definitively observed in the X-ray crystal structure (Figure 3.2). The complex's limited stabilization is most likely due to the electronic effects of the *ortho*-fluoride similar to the para-substituted analog. The non-reactivity of complex **2** is not fully understood, but we propose the high instability of complex **7** leads to limited reductive elimination of the desired product. Overall, the steric effects introduced by the *ortho*-fluoride outweigh the stabilizing electronic effects, thus causing the Ni^{III} intermediates to be highly destabilized. These studies have shown controlling a ligand's electronics and steric effect is vital to regulating the stability of these high-valent nickel intermediates.

3.4 Conclusion

In summary, the studies reported herein provide the synthesis and reactivity of a series of *ortho*-substituted organometallic Ni^{III} complexes. These complexes were directly compared to the previously synthesized *para*-substituted counterparts to study the impact of altering the electronic and steric effects of these ligands. The steric and electronic effects introduced by the *ortho*-substituent were found to destabilize the resulting Ni^{III} intermediates. The decreased stability had varying results ranging from greatly improving the rate of reactivity to preventing the formation of the desired product. Overall, these studies have confirmed the importance ligand electronics and sterics play in controlling the stability of high-valent nickel intermediates. This combination of *ortho*- and *para*-substituted Ni^{III} complexes has provided a rare opportunity to directly investigate intermediates fundamentally important to various catalytic reactions.

3.5 Acknowledgements

I appreciate my colleagues from the Mirica group for the collaboration on the *para*-substituted counterparts to these studies.³⁶ Similarly, I appreciate Professor Nigam P. Rath of the Department of Chemistry and Biochemistry at the University of Missouri-St. Louis for his help and advice in solving all the reported crystal structures.

3.6 References

1. Tang, F.; Qu, F.; Khusnutdinova, J. R.; Rath, N. P.; Mirica, L. M. *Dalton Trans.* **2012**, 41, 14046.
2. Roodt, A.; Otto, S.; Steyl, G. *Coord. Chem. Rev.* **2003**, 245, 121.
3. Akita, M.; Hikichi, S. *Bull. Chem. Soc. Jpn.* **2002**, 75, 1657.
4. Piers, W. E.; Emslie, D. J. H. *Coord. Chem. Rev.* **2002**, 233–234, 131.
5. Flanagan, S. P.; Guiry, P. J. *J. Organomet. Chem.* **2006**, 691, 2125.
6. Tsou, T. T.; Kochi, J. K. *J. Am. Chem. Soc.* **1978**, 100, 1634.
7. Tsou, T. T.; Kochi, J. K. *J. Am. Chem. Soc.* **1979**, 101, 7547.
8. Amatore, C.; Jutand, A. *Organometallics* **1988**, 7, 2203.
9. Zhou, J.; Fu, G. C. *J. Am. Chem. Soc.* **2004**, 126, 1340.
10. Powell, D. A.; Fu, G. C. *J. Am. Chem. Soc.* **2004**, 126, 7788.
11. Owston, N. A.; Fu, G. C. *J. Am. Chem. Soc.* **2010**, 132, 11908.
12. Zultanski, S. L.; Fu, G. C. *J. Am. Chem. Soc.* **2011**, 133, 15362.
13. Dudnik, A. S.; Fu, G. C. *J. Am. Chem. Soc.* **2012**, 134, 10693.
14. Zultanski, S. L.; Fu, G. C. *J. Am. Chem. Soc.* **2013**, 135, 624.
15. Jones, G. D.; McFarland, C.; Anderson, T. J.; Vicic, D. A. *Chem. Commun.* **2005**, 4211.
16. Jones, G. D.; Martin, J. L.; McFarland, C.; Allen, O. R.; Hall, R. E.; Haley, A. D.; Brandon, R. J.; Konovalova, T.; Desrochers, P. J.; Pulay, P.; Vicic, D. A. *J. Am. Chem. Soc.* **2006**, 128, 13175.
17. Klein, A.; Budnikova, Y. H.; Sinyashin, O. G. *J. Organomet. Chem.* **2007**, 692, 3156.

18. Phapale, V. B.; Bunuel, E.; Garcia-Iglesias, M.; Cardenas, D. J. *Angew. Chem. Int. Ed.* **2007**, *46*, 8790.
19. Phapale, V. B.; Guisan-Ceinos, M.; Bunuel, E.; Cardenas, D. J. *Chem. Eur. J.* **2009**, *15*, 12681.
20. Gong, H. G.; Gagné, M. R. *J. Am. Chem. Soc.* **2008**, *130*, 12177.
21. Gong, H. G.; Andrews, R. S.; Zuccarello, J. L.; Lee, S. J.; Gagné, M. R. *Org. Lett.* **2009**, *11*, 879.
22. Vechorkin, O.; Hu, X. *Angew. Chem. Int. Ed.* **2009**, *48*, 2937.
23. Vechorkin, O.; Proust, V. r.; Hu, X. *J. Am. Chem. Soc.* **2009**, *131*, 9756.
24. Hu, X. *Chem. Sci.* **2011**, *2*, 1867.
25. Everson, D. A.; Shrestha, R.; Weix, D. J. *J. Am. Chem. Soc.* **2010**, *132*, 920.
26. Biswas, S.; Weix, D. J. *J. Am. Chem. Soc.* **2013**, *135*, 16192.
27. Joshi-Pangu, A.; Wang, C. Y.; Biscoe, M. R. *J. Am. Chem. Soc.* **2011**, *133*, 8478.
28. Yu, X. L.; Yang, T.; Wang, S. L.; Xu, H. L.; Gong, H. G. *Org. Lett.* **2011**, *13*, 2138.
29. Dai, Y. J.; Wu, F.; Zang, Z. H.; You, H. Z.; Gong, H. G. *Chem. Eur. J.* **2012**, *18*, 808.
30. Xu, H.; Zhao, C.; Qian, Q.; Deng, W.; Gong, H. *Chem. Sci.* **2013**, *4*, 4022.
31. Matsunaga, P. T.; Hillhouse, G. L.; Rheingold, A. L. *J. Am. Chem. Soc.* **1993**, *115*, 2075.
32. Koo, K. M.; Hillhouse, G. L.; Rheingold, A. L. *Organometallics* **1995**, *14*, 456.
33. Han, R. Y.; Hillhouse, G. L. *J. Am. Chem. Soc.* **1997**, *119*, 8135.
34. Koo, K.; Hillhouse, G. L. *Organometallics* **1995**, *14*, 4421.
35. Lin, B. L.; Clough, C. R.; Hillhouse, G. L. *J. Am. Chem. Soc.* **2002**, *124*, 2890.
36. Zheng, B.; Tang, F.; Luo, J.; Schultz, J. W.; Rath, N. P.; Mirica, L. M. *J. Am. Chem. Soc.* **2014**, *136*, 6499.

37. Che, C. M.; Li, Z. Y.; Wong, K. Y.; Poon, C. K.; Mak, T. C. W.; Peng, S. M. *Polyhedron* **1994**, *13*, 771.
38. Connelly, N. G.; Geiger, W. E. *Chem. Rev.* **1996**, *96*, 877.
39. Fulmer, G. R.; Miller, A. J. M.; Sherden, N. H.; Gottlieb, H. E.; Nudelman, A.; Stoltz, B. M.; Bercaw, J. E.; Goldberg, K. I. *Organometallics* **2010**, *29*, 2176.
40. Bruker Analytical X-Ray, Madison, WI, 2008
41. Sheldrick, G. *Acta Crystallogr. Sect. A: Found. Crystallogr.* **2008**, *64*, 112.
42. Burnett, M. N.; Johnson, C. K. *ORTEP-III: Oak Ridge Thermal Ellipsoid Plot Program for Crystal Structure Illustrations, Oak Ridge National Laboratory Report ORNL-6895* **1996**.
43. Grove, D. M.; Vankoten, G.; Mul, W. P.; Vanderzeijden, A. A. H.; Terheijden, J.; Zoutberg, M. C.; Stam, C. H. *Organometallics* **1986**, *5*, 322.
44. van de Kuil, L. A.; Veldhuizen, Y. S. J.; Grove, D. M.; Zwikker, J. W.; Jenneskens, L. W.; Drenth, W.; Smeets, W. J. J.; Spek, A. L.; van Koten, G. J. *Organomet. Chem.* **1995**, *488*, 191.
45. Grove, D. M.; van Koten, G.; Zoet, R.; Murrall, N. W.; Welch, A. J. *J. Am. Chem. Soc.* **1983**, *105*, 1379.
46. Grove, D. M.; van Koten, G.; Mul, P.; Zoet, R.; van der Linden, J. G. M.; Legters, J.; Schmitz, J. E. J.; Murrall, N. W.; Welch, A. J. *Inorg. Chem.* **1988**, *27*, 2466.
47. Iluc, V. M.; Miller, A. J. M.; Anderson, J. S.; Monreal, M. J.; Mehn, M. P.; Hillhouse, G. L. *J. Am. Chem. Soc.* **2011**, *133*, 13055.

Chapter 4

High-Valent Dimethyl Nickel Complexes Relevant to Cross-Coupling and C-C Bond Formation Reactions

4.1 Introduction

Nickel complexes have been employed in a wide range of catalytic organometallic transformations, most notably Negishi, Kumada, and Suzuki cross-coupling reactions.¹⁻⁶ Nickel-catalyzed cross-coupling reactions in contrast to the Palladium-catalyzed reactions can more easily undergo both one- and two-electron redox reactions. Therefore, the Ni^{III} and/or Ni^I oxidation states are more commonly proposed as catalytic intermediates of cross-coupling reactions⁷⁻³¹ and oxidatively induced C-heteroatom bond formation reactions.³²⁻³⁶ To this point, we recently published the first isolated Ni^{III} species that could undergo C-heteroatom bond formation reactions.³⁷ Nevertheless, the Ni^{III} intermediates being proposed for cross-coupling and oxidatively induced C-C bond formation reactions are dialkyl Ni^{III} intermediates. To date, no reported dialkyl Ni^{III} complex has been isolated or characterized. Previously, however, we have reported a series of rare mononuclear organometallic Pd^{III} and Pd^{IV} complexes capable of C-C and C-heteroatom bond formations.³⁸⁻⁴² These complexes were stabilized using a series of unique tetradentate ligands, most notably N,N'-di-tert-butyl-2,11-diaza[3.3](2,6)pyridinophane (^tBuN4) and N,N'-di-methyl-2,11-diaza[3.3](2,6)pyridinophane (^{Me}N4), which allowed for the isolation of these rare high-valent metal complexes. Consequently, using these same pyridinophane ligands we report herein the isolation, structural and spectroscopic characterization, and resulting C-C bond formation reactivity of the first reported stable dialkyl Ni^{III} complexes relevant to cross coupling reactions. Notably, the aforementioned C-C bond formation was shown to proceed slowly from the Ni^{III} intermediate. However, upon further oxidation to a proposed Ni^{IV} intermediate the observed C-C bond formation greatly improved. Moreover, both the Ni^{II} and Ni^{III} complexes were shown to be active catalysts for Kumada cross-coupling reactions. As a whole, these studies provide for the first time structural and spectroscopic evidence for existence of

dialkyl Ni^{III} complexes directly involved in C-C bond formation and most notably provide strong evidence the reactive species involved in nickel catalyzed cross-coupling reactions are in fact Ni^{IV} intermediates rather than the previously proposed Ni^{III} intermediates.

4.2 Experimental Section

4.2.1 Synthesis of Ligands and Complexes

Reagents and Materials. All manipulations were carried out under a nitrogen atmosphere using standard Schlenk and glove box techniques if not indicated otherwise. All reagents for which synthesis is not given were commercially available from Sigma-Aldrich, Fisher Scientific, VWR, Acros, STREM or Pressure Chemical and were used as received without further purification. Solvents were purified prior to use by passing through a column of activated alumina using a MBRAUN Solvent Purification System. N,N'-ditertbutyl-2,11-diaza[3,3](2,6)pyridinophane (^tBuN4)⁴³, N,N'-methyl-2,11-diaza[3,3](2,6)pyridinophane (^{Me}N4)⁴⁴, Mg(CD₃)I³⁹, (^tBuN4)Ni^{II}Br₂⁴⁵ and FcPF₆⁴⁶ were prepared according to the literature procedures.

Preparation of (^{Me}N4)Ni^{II}Br₂. (DME)NiBr₂ (0.345 g, 1.12 mmol) and ^{Me}N4 (0.300 grams, 1.12 mmol) were dissolved in 60 ml of CH₂Cl₂ at RT under N₂. The solution turned from orange to green. After 24 hours, the solvent was evaporated under vacuum and the solid residue was recrystallized from CH₂Cl₂ with slow ether diffusion to afford green paramagnetic crystals (0.341 grams, 0.70 mmol, 63%). UV-Vis, λ, nm (ε, M⁻¹·cm⁻¹), DCM: 259 (2305), 315 (sh, 680), 405 (281), 623 (22), 980 (33). Evans method (CD₃CN): μ_{eff} = 3.05μ_B. ¹H-NMR (300 MHz, CDCl₃), δ (ppm): 68.45 (br), 56.41 (br), 13.23 (br), 1.58 (br). Anal. Found: C, 37.18; H, 4.03; N, 10.41. Calculated for C₁₆H₂₀Br₂N₄Ni·(1/2 CH₂Cl₂): C, 37.44; H, 4.00; N, 10.58.

Synthesis of $(^{\text{Me}}\text{N}_4)\text{Ni}^{\text{II}}\text{Me}_2$ (1). To a stirred suspension of $(^{\text{Me}}\text{N}_4)\text{NiBr}_2$ (177 mg, 0.364 mmol) in THF (5 mL), cooled at -50°C , was added 0.56 mL of a ca. 1.94 M solution of MeMgCl in THF solution. The mixture was stirred at this temperature for 30 minutes, and then slowly warmed up to -5°C overnight. Next dioxane (5 mL) was added to the deep red solution. The resulting suspension was let stand for 1 hour in the -35°C freezer. The suspension was then filtered and the solvent was completely removed under vacuum at -50°C and the residue was extracted with precooled diethyl ether (100 mL). The deep red solution was filtered and dried under vacuum. A red solid was obtained (84.1 mg, 0.235 mmol, 65%). X-ray quality crystals were obtained by slow pentane diffusion into a diethyl ether solution at -35°C . Several attempts to obtain elemental analysis data proved unsuccessful, likely due to its decomposition during transportation and handling. UV-Vis, λ , nm (ϵ , $\text{M}^{-1}\cdot\text{cm}^{-1}$), THF: 400 (3100). $^1\text{H-NMR}$ (300 MHz, $\text{d}_3\text{-MeCN}$), δ (ppm): 7.42 (t, 2H, Py-H), 7.00 (d, 4H, Py-H), 6.77 (d, 2H, $-\text{CH}_2-$), 4.22 (d, 2H, $-\text{CH}_2-$), 2.25 (s, 18H, $-\text{CH}_3$), -0.91 (s, 6H, Ni- CH_3). $^{13}\text{C-NMR}$ (600 MHz, $\text{d}_8\text{-THF}$), δ (ppm): 159.22, 134.46, 124.58, 63.94, 63.94, 38.48, -9.65.

Preparation of $[(^{\text{Me}}\text{N}_4)\text{Ni}^{\text{III}}\text{Me}_2]\text{PF}_6$ (2). A solution of **1** (32.8 mg, 0.092 mmol) and FcPF_6 (30.4 mg, 0.092 mmol) in pre-cooled THF was stirred at -50°C for 3 hours and the resulting solution was then filtered at -50°C . To the filtrate was added pre-cooled pentane producing a precipitate immediately. After filtration, an orange-red solid was isolated and dried under vacuum (17.6 mg, 0.035 mmol, 38%). X-ray quality crystals were obtained by slow pentane diffusion into a tetrahydrofuran solution at -35°C in the presence of NaBPh_4 . Elemental analysis sample was obtained using similar X-ray quality crystals obtained under the same conditions.

Evans method (CD₃CN): $\mu_{\text{eff}} = 1.70\mu_{\text{B}}$. UV-Vis, λ , nm (ϵ , M⁻¹·cm⁻¹), MeCN: 240 (10800), 465 (470). ESI-MS (HR) in Acetonitrile: m/z 356.1501; Calculated for [(^{Me}N₄)Ni^{III}Me₂]⁺: m/z 356.1511. Anal. Found: C, 71.31; H, 6.89; N, 7.55. Calculated for C₄₂H₄₆BN₄Ni·C₄H₈O, based on the composition of the unit cell obtained from X-ray analysis: C, 73.82; H, 7.27; N, 7.49.

Synthesis of (^{Me}N₄)Ni^{II}(CD₃)₂ (1-d₆). To a stirred suspension of (^{Me}N₄)NiBr₂ (220 mg, 0.452 mmol) in THF (6 mL), cooled at -50°C, was added 1.35 mL of the CD₃MgI solution. The mixture was stirred at this temperature for 30 minutes, and then slowly warmed up to -5°C overnight. Next dioxane (6 mL) was added to the deep red solution. The resulting suspension was let stand for 1 hour in the -35°C freezer. The suspension was then filtered and the solvent was completely removed under vacuum and the residue was extracted with precooled diethyl ether (150 mL). The deep red solution was filtered and dried under vacuum. A red solid was obtained (150 mg, 0.413 mmol, 91%). The ¹H NMR spectrum of the product is identical to that of (^{Me}N₄)Ni^{II}Me₂ except for the missing singlet for the Ni-Me group.

Synthesis of (^{tBu}N₄)Ni^{II}Me₂ (3). To a stirred suspension of (^{tBu}N₄)Ni^{II}Br₂ (120 mg, 0.210 mmol) in THF (5 mL), cooled at -50°C, was added 0.28 mL of a ca. 1.94 M solution of MeMgCl in THF solution. The mixture was stirred at this temperature for 30 minutes, and then slowly warmed up to -5°C overnight. Next dioxane (5 mL) was added to the deep red solution. The resulting suspension was let stand for 1 hour in the -35°C freezer. The suspension was then filtered and the solvent was completely removed under vacuum and the residue was extracted with precooled diethyl ether (100 mL). The deep red solution was filtered and dried under vacuum. A red solid was obtained (59.1 mg, 0.124 mmol, 64%). X-ray quality crystals were obtained by slow

evaporation of a diethyl ether solution at -35°C . Several attempts to obtain elemental analysis data proved unsuccessful, likely due to its decomposition during transportation and handling. UV-Vis, λ , nm (ϵ , $\text{M}^{-1}\cdot\text{cm}^{-1}$), THF: 397 (1500). $^1\text{H-NMR}$ (300 MHz, MeCN-d_3), δ (ppm): 7.42 (t, 2H, Py-H), 7.01 (d, 4H, Py-H), 6.57 (d, 2H, $-\text{CH}_2-$), 4.67 (d, 2H, $-\text{CH}_2-$), 1.35 (s, 18H, tBu), -1.07 (s, 6H, Ni- CH_3).

Synthesis of $[(^t\text{BuN}_4)\text{Ni}^{\text{III}}\text{Me}_2]\text{PF}_6$ (4). A solution of **3** (56.2 mg, 0.127 mmol) and FcPF_6 (42.2 mg, 0.127 mmol) in pre-cooled THF was stirred at -50°C for 3 hours and the resulting solution was then filtered at -50°C . To the filtrate was added pre-cooled pentane producing a precipitate immediately. After filtration a bright yellow solid was isolated and dried under vacuum (46.8 mg, 0.080 mmol, 63%). X-ray quality crystals were obtained by slow pentane diffusion into a tetrahydrofuran solution at -35°C . Evans method (CD_3CN): $\mu_{\text{eff}} = 1.85\mu_{\text{B}}$. UV-Vis, λ , nm (ϵ , $\text{M}^{-1}\cdot\text{cm}^{-1}$), MeCN : 260 (9900), 310 (sh, 1350), 448 (300). ESI-MS (HR) in Acetonitrile: m/z 440.2458; Calculated for $[(^t\text{BuN}_4)\text{Ni}^{\text{III}}\text{Me}_2]^+$: m/z 440.2450.

Synthesis of $(^t\text{BuN}_4)\text{Ni}^{\text{II}}(\text{CD}_3)_2$ (3-d₆). To a stirred suspension of $(^t\text{BuN}_4)\text{NiBr}_2$ (102 mg, 0.179 mmol) in THF (6 mL), cooled at -50°C , was added 0.5 mL of the CD_3MgI solution. The mixture was stirred at this temperature for 30 minutes, and then slowly warmed up to -5°C overnight. Next dioxane (6 mL) was added to the deep red solution. The resulting suspension was let stand for 1 hour in the -35°C freezer. The suspension was then filtered and the solvent was completely removed under vacuum and the residue was extracted with precooled diethyl ether (150 mL). The deep red solution was filtered and dried under vacuum. A red solid was obtained (66.1 mg, 0.148

mmol, 83%). The ^1H NMR spectrum of the product is identical to that of $(^t\text{BuN4})\text{Ni}^{\text{II}}\text{Me}_2$ except for the missing singlet for the Ni-Me group.

Synthesis of $[(^t\text{BuN4})\text{Ni}^{\text{III}}(\text{CD}_3)_2]\text{PF}_6$ (4-d6**).** A solution of **3-d6** (37.1 mg, 0.083 mmol) and FcPF_6 (27.5 mg, 0.083 mmol) in pre-cooled THF was stirred at $-50\text{ }^\circ\text{C}$ for 3 hours and the resulting solution was then filtered at $-50\text{ }^\circ\text{C}$. To the filtrate was added pre-cooled pentane producing a precipitate immediately. After filtration, an orange-red solid was isolated and dried under vacuum (43.0 mg, 0.073 mmol, 88%). The EPR spectrum of the product is identical to that of $[(^t\text{BuN4})\text{Ni}^{\text{III}}\text{Me}_2]\text{PF}_6$.

4.2.2 Physical Measurements

^1H NMR spectra were recorded on a Varian Mercury-300 spectrometer (300.121 MHz), Agilent DD2-500 spectrometer (499.885 MHz) or Agilent DD2-600 spectrometer (599.736 MHz). ^{13}C NMR spectra were recorded on an Agilent DD2-600 spectrometer (599.736 MHz). Chemical shifts are reported in ppm and referenced to residual solvent resonance peaks.⁴⁷ Abbreviations for the multiplicity of NMR signals are s (singlet), d (doublet), t (triplet), q (quartet), m (multiplet), br (broad). UV-visible spectra were recorded on a Varian Cary 50 Bio spectrophotometer and are reported as λ_{max} , nm (ϵ , $\text{M}^{-1}\cdot\text{cm}^{-1}$). EPR spectra were recorded on a JEOL JES-FA X-band (9.2 GHz) EPR spectrometer in frozen solution at 77 K. ESI-MS experiments were performed using a Thermo FT or Bruker Maxis Q-TOF mass spectrometer with an electrospray ionization source. ESI mass-spectrometry was provided by the Washington University Mass Spectrometry Resource, an NIH Research Resource (Grant No. P41RR0954). Elemental analyses were carried out by the Intertek Pharmaceutical Services.

Electrochemical-grade electrolytes from Fluka were used as the supporting electrolyte for electrochemical measurements. Cyclic voltammetry and controlled potential electrolysis experiments were performed with a BASi EC Epsilon electrochemical workstation or a CHI 660D Electrochemical Analyzer. The electrochemical measurements were performed under a blanket of nitrogen, and the analyzed solutions were deaerated by purging with nitrogen. A glassy carbon disk electrode ($d = 1.6$ mm) was used as the working electrode for cyclic voltammetry. The auxiliary electrode was a Pt wire for cyclic voltammetry measurements. Two different non-aqueous reference electrodes were used: Ag/filled with 0.01M AgNO₃/0.1M Bu₄NClO₄/MeCN solution or silver wire. The reference electrode was calibrated against ferrocene (Fc) at the conclusion of each CV experiment.

X-ray quality crystals of (^{Me}N4)Ni^{II}Me₂ were obtained by slow pentane diffusion into a diethyl ether solution at -35°C. Similarly, quality crystals of (^{tBu}N4)Ni^{II}Me₂ were obtained by slow evaporation of a diethyl ether solution. X-ray quality crystals of [(^{Me}N4)Ni^{III}Me₂]BPh₄ and [(^{tBu}N4)Ni^{III}Me₂]BPh₄ were obtained by slow pentane vapor diffusion into a tetrahydrofuran solution at -35°C. Suitable crystals of appropriate dimensions were mounted and preliminary examination and data collection were performed using a Bruker Kappa Apex-II Charge Coupled Device (CCD) Detector system single crystal X-Ray diffractometer equipped with an Oxford Cryostream LT device. Data were collected using graphite monochromated Mo K α radiation ($\lambda = 0.71073$ Å) from a fine focus sealed tube X-Ray source. Apex II and SAINT software packages⁴⁸ were used for data collection and data integration. Final cell constants were determined by global refinement of reflections from the complete data set. Data were corrected for systematic errors using SADABS⁴⁸ based on the Laue symmetry using equivalent reflections. Structure solutions and refinement were carried out using the SHELXTL- PLUS software package.⁴⁹ The structures

were refined with full matrix least-squares refinement by minimizing $\Sigma w(F_o^2 - F_c^2)^2$. All non-hydrogen atoms were refined anisotropically to convergence. Typically, H atoms are added at the calculated positions in the final refinement cycles. The complete listings of x-ray diffraction parameters are included in Appendix B.

4.2.3 Computational Studies

The density functional theory (DFT) and time-dependent density functional theory (TD-DFT) calculations were performed with the program package Gaussian 09.⁵⁰ The UB3LYP hybrid functional with the 6-31G* basis set for C, N, H and the modified m6-31G* basis set for Ni were employed. This combination of hybrid functional and basis sets have been previously shown to work well for reproducing experimental parameters of Ni complexes.^{51,52} Geometry optimization calculations were performed using the X-ray coordinates as the starting geometry. The ground state wave function was investigated by analyzing the frontier MOs, and the atomic contributions to MOs were calculated using the program Chemissian.⁵³

4.2.4 Reactivity Studies

¹H NMR reactivity studies of (MeN4)Ni^{II}Me₂ or (tBuN4)Ni^{II}Me₂. A solution of 5-7 mg **1** or **3** in d₃-MeCN was added into a NMR tube containing 1,3,5-trimethoxybenzene as an internal standard. To this solution were added the additional reagents in d₃-MeCN. For crossover experiments, equimolar amounts of **1** and **1-d₆** or **3** and **3-d₆** in d₃-MeCN were added to the NMR as individual solutions. For all experiments the NMR tube was then filled to the top with additional d₃-MeCN (so that no headspace was left to avoid the escape of volatiles) and sealed with a septum. The reaction mixtures were mixed carefully to form homogeneous solutions. The reaction mixtures

were then kept in the dark and periodically analyzed by ^1H NMR. The yield of the products were determined by integration versus the internal standard, calculated as $[\text{moles of product}]/[\text{moles of } \mathbf{1} \text{ or } \mathbf{3}] * 100\%$.

^1H NMR reactivity studies of $[(^{\text{Me}}\text{N}_4)\text{Ni}^{\text{III}}\text{Me}_2]\text{BPh}_4$ and $[(^{\text{tBu}}\text{N}_4)\text{Ni}^{\text{III}}\text{Me}_2]\text{PF}_6$. A solution of 5-7 mg $\mathbf{2}$ or $\mathbf{4}$ in $\text{d}_3\text{-MeCN}$ was added into a NMR tube containing 1,3,5-trimethoxybenzene as an internal standard. For some experiments, to this solution was added additional reagents in $\text{d}_3\text{-MeCN}$. For all experiments the NMR tube was then filled to the top with additional $\text{d}_3\text{-MeCN}$ (so that no headspace was left to avoid the escape of volatiles) and sealed with a septum. The reaction mixtures were mixed carefully to form homogeneous solutions. The reaction mixtures were then kept in the dark and periodically analyzed by ^1H NMR. The yield of the products were determined by integration versus the internal standard, calculated as $[\text{moles of product}]/[\text{moles of } \mathbf{2} \text{ or } \mathbf{4}] * 100\%$ and given as an average of two runs. For each experiment the moles of $\mathbf{2}$ and $\mathbf{4}$ were determined using EPR spin quantitation versus a standard $[(^{\text{Me}}\text{N}_4)\text{Ni}^{\text{III}}(\text{Cycle})]\text{PF}_6$ solution.

GC Product Analysis for the reactivity of $(^{\text{Me}}\text{N}_4)\text{Ni}^{\text{II}}\text{Me}_2$. The NMR samples were quenched with 100 μL of 1.0 M HCl and 5 mL H_2O , and extracted with ethyl ether (6 mL). The organic layer was then separated and dried over MgSO_4 . The yield of product(s) was obtained by GC/FID using 1,3,5-trimethoxybenzene as the internal standard. The identity of the products were confirmed by GC/MSD.

UV-Vis Monitoring of the oxidation of $(^{\text{Me}}\text{N}_4)\text{Ni}^{\text{II}}\text{Me}_2$. A 1.0 mL aliquot of a 0.5 mM solution of $\mathbf{1}$ or $\mathbf{3}$ in MeCN was placed into a quartz cuvette (pathlength 1 cm) equipped with a septum-sealed cap and a magnetic stirring bar. A pre-oxidized sample was collected. The sample was then

oxidized and mixed thoroughly, then the reaction mixture was let stand at 20 °C in the dark. The reaction progress was monitored using a Varian Cary 50 Bio spectrophotometer.

EPR Monitoring of the oxidation of $(\text{Me}_4\text{N})\text{Ni}^{\text{II}}\text{Me}_2$. A solution of **1** or **3** in degassed butyronitrile was prepared immediately before the experiment. Oxidant was then added and the solution mixed for 1 minute at 20°C. The solution was transferred to a quartz EPR tube and the samples were then frozen (77 K) and analyzed using a JEOL JES-FA X-band (9.2 GHz) EPR spectrometer. The EPR spectrum was monitored over 24 hours at RT in the dark.

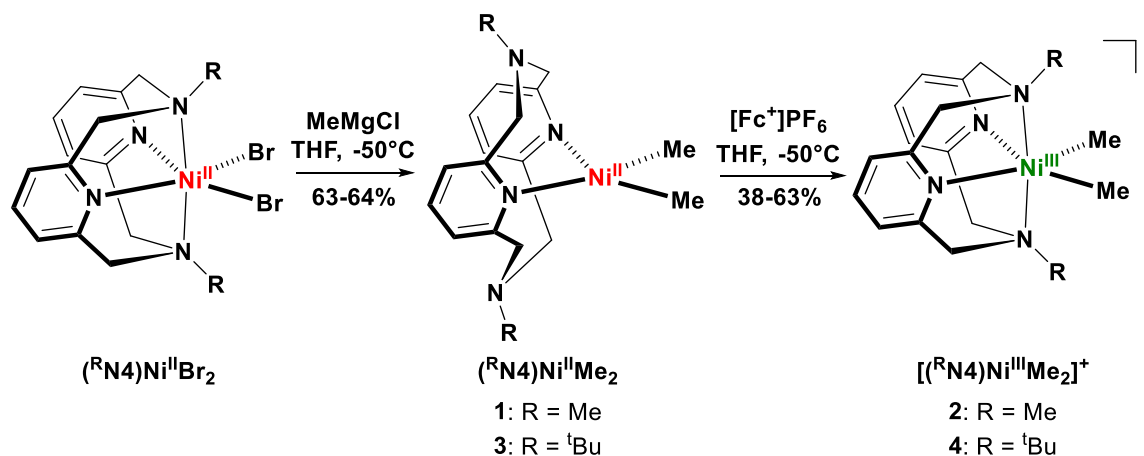
Kumada cross-coupling with $(\text{Me}_4\text{N})\text{Ni}^{\text{II}}\text{Me}_2$ and $[(\text{Me}_4\text{N})\text{Ni}^{\text{III}}\text{Me}_2]\text{BPh}_4$. Inside a nitrogen filled glove box, a small vial equipped with a magnetic stir bar was charged with the corresponding alkyl halide or aryl halide substrate (0.1 mmol), internal standard (hexamethylbenzene or dodecane), and **1** (2.0 mg, 0.05 equivalents) or **2** (3.4 mg, 0.05 equivalents) in THF (3.0 mL). To the stirring solution, the Grignard reagent (1.2 equivalents) was added via syringe and the resulting solution was allowed to stir at room temperature. After the allotted reaction time, the reaction mixture was worked up by quenching with 100 μL of 1.0 M HCl and 5 mL H_2O , and extracting the mixture with diethyl ether (6 mL). The organic layer was separated and dried over MgSO_4 . The yield of product(s) was obtained by GC/FID using the internal standard for calibration, while the identity of the products was supported by GC/MSD.

4.3 Results and Discussion

4.3.1 Synthesis and Structure of Ni^{II} Complexes.

The Ni^{II} complexes (^{Me}N₄)Ni^{II}Me₂, **1**, and (^{tBu}N₄)Ni^{II}Me₂, **3**, were prepared in 63-64% yield from the (^{Me}N₄)Ni^{II}Br₂ and (^{tBu}N₄)Ni^{II}Br₂ precursors, respectively, via transmetalation with methylmagnesium chloride (Scheme 4.1). The resulting red complexes were determined to be diamagnetic, suggesting a square planar geometry comprised of two pyridyl nitrogen atoms from the N₄ ligands and two exogenous methyl groups. The strong σ -donating behavior of the exogenous methyl groups greatly favors the low-spin square planar geometry. The X-ray structures of **1** and **3** confirmed the square planar geometry, with an average equatorial Ni-N_{pyridyl} bond length of 1.973 and 2.005 Å and an average Ni-C_{Me} bond length of 1.913 and 1.930 Å, respectively (Figure 4.1).

Scheme 4.1 Synthesis of (^RN₄)Ni^{II}Me₂ and [(^RN₄)Ni^{III}Me₂]⁺ Complexes (R = ^tBu or Me).



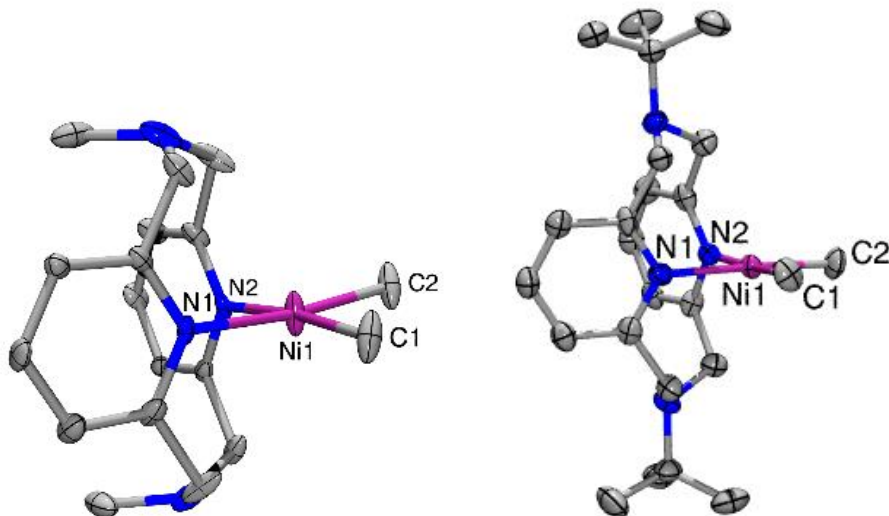


Figure 4.1 ORTEP⁵⁴ representation of **1** (left) and **3** (right) with 50% probability thermal ellipsoids. Selected bond lengths (Å), **1**: Ni1-C1, 1.913; Ni1-C2, 1.913; Ni1-N1, 1.973; Ni1-N2, 1.973; **3**: Ni-N1 2.005; Ni-N2 2.005; Ni-C1 1.930; Ni-C2 1.930. A complete listings of structural parameters are included in Appendix B.

The cyclic voltammetry (CV) of complex **1** shows two oxidation processes at -1.44 and -0.42 V vs Fc⁺/Fc, as well as a reversible oxidation wave at 0.08 V vs Fc⁺/Fc (Figure 4.2). Similarly, the CV of complex **3** shows two oxidation processes at -1.35 and -0.53 V vs Fc⁺/Fc, as well as a reversible oxidation wave at 0.49 V vs Fc⁺/Fc (Figure 4.2). The lower two oxidative processes for both complexes are assigned to the κ^3 and κ^4 Ni^{II}/Ni^{III} couples, while the higher oxidative wave is tentatively assigned to a Ni^{III}/Ni^{IV} couple. These potentials are extremely low and indicate the Ni^{III} and Ni^{IV} oxidation states for both complexes should be readily attainable.

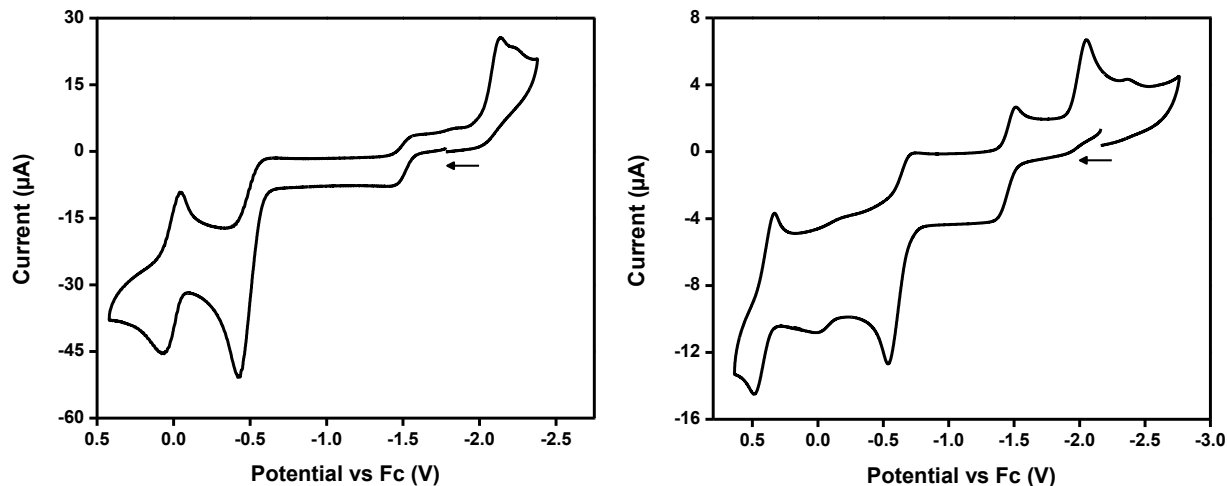


Figure 4.2 Cyclic voltammograms of **1** (left) and **3** (right) in 0.1 M Bu₄NPF₆ in MeCN. Scan rate: 100 mV/s.

4.3.2 Synthesis and Structure of Ni^{III} Complexes.

Complex **1** was oxidized with 1 equivalent [Fc⁺]PF₆ in THF at -50°C to yield [(^{Me}N4)Ni^{III}Me₂]PF₆, **2**, as an orange-red solid in 38% yield. Similarly, complex **3** was oxidized to yield [(^{tBu}N4)Ni^{III}Me₂]PF₆, **4**, as a yellow solid in 63% yield (Scheme 4.1). Quality crystals of both complexes for single crystal X-ray diffraction analysis were obtained (Figure 4.3). Both complexes **2** and **4** adopt a distorted octahedral geometry with an average axial Ni-N_{amine} bond length of 2.246 and 2.386 Å and a shorter average equatorial Ni-N_{pyridyl} bond length of 1.988 and 1.961 Å, respectively. These values are consistent with our previously reported organometallic Ni^{III} complexes (Ni-N_{amine} bond lengths of 2.314 and 2.315 Å, Ni-N_{pyridyl} bond length of 1.947 and 1.929 Å)³⁷, and the only other reported six-coordinate Ni^{III} complexes.⁴⁴⁻⁴⁶ Similarly, the average Ni-C_{Me} bond lengths of 1.983 and 1.963 Å are consistent with the only other structurally characterized Ni^{III}-alkyl complexes reported (1.923, 1.994, and 2.015 Å).^{51,55,56}

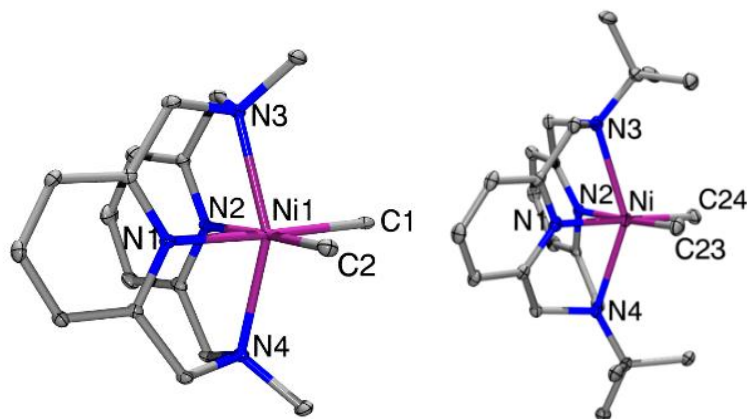


Figure 4.3 ORTEP⁵⁴ representation of the cations **2** (left) and **4** (right) with 50% probability thermal ellipsoids. Selected bond lengths (Å), **2**: Ni1-C1, 1.987; Ni1-C2, 1.978; Ni1-N1, 1.979; Ni1-N2, 1.996; Ni1-N3, 2.252; Ni1-N4, 2.240; **4**: Ni-N1 1.966; Ni-N2 1.956; Ni-N3 2.400; Ni-N4 2.372; Ni-C23 1.968; Ni-C24 1.957. A complete listings of structural parameters are included in Appendix B.

The EPR spectrum of complex **2** exhibited a pseudo axial signal with a g_x , g_y , and g_z of 2.228, 2.210, and 2.014, respectively, whereas, the EPR spectrum of complex **4** exhibited a rhombic signal with a g_x , g_y , and g_z of 2.314, 2.264, and 2.009, respectively. Additionally, superhyperfine coupling was observed in both complexes in the g_z direction (**2**: $A_{2N} = 14.3$ G; **4**: $A_{2N} = 11.0$ G) due to the two axial N donors ($I=1$) coupling to the Ni^{III} center (Figure 4.4 and 4.5). These results are consistent with a distorted octahedral Ni^{III} metal center in a d_z^2 ground state.⁵⁷⁻⁶¹ Furthermore, density functional theory (DFT) calculations proposed a metal-based radical description for both complexes and the calculated spin density revealed the unpaired electron resides mostly on the nickel center (Figure 4.4 and 4.5). Overall, complexes **2** and **4** are the first reported stable dialkyl Ni^{III} complexes to be isolated with full structural and spectroscopic characterization. Since such organometallic Ni^{III} species are proposed as key intermediates in cross coupling reactions, these studies provide the first evidence for existence of a dialkyl Ni^{III} intermediate.

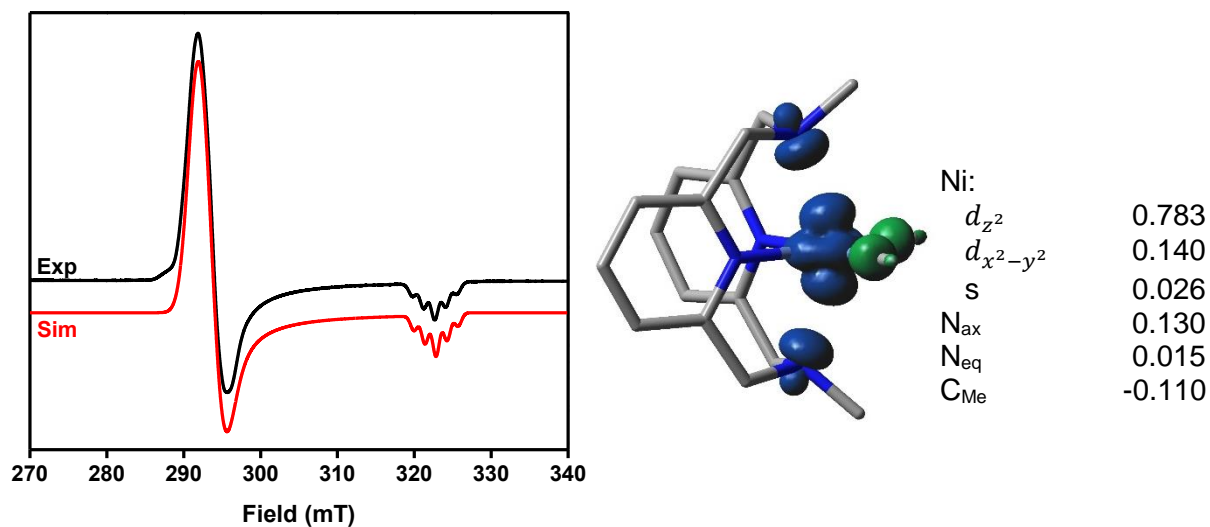


Figure 4.4 (Left) EPR spectrum (black line) of **2** in PrCN at 77K, and the simulated EPR spectrum (red line) using the following parameters: $g_x = 2.228$, $g_y = 2.210$, $g_z = 2.014$ ($A_{2N} = 14.3$ G). (Right) DFT calculated Mulliken spin density for **2** (shown as a 0.005 isodensity contour plot), and the relevant atomic and Ni orbital contributions to the spin density.

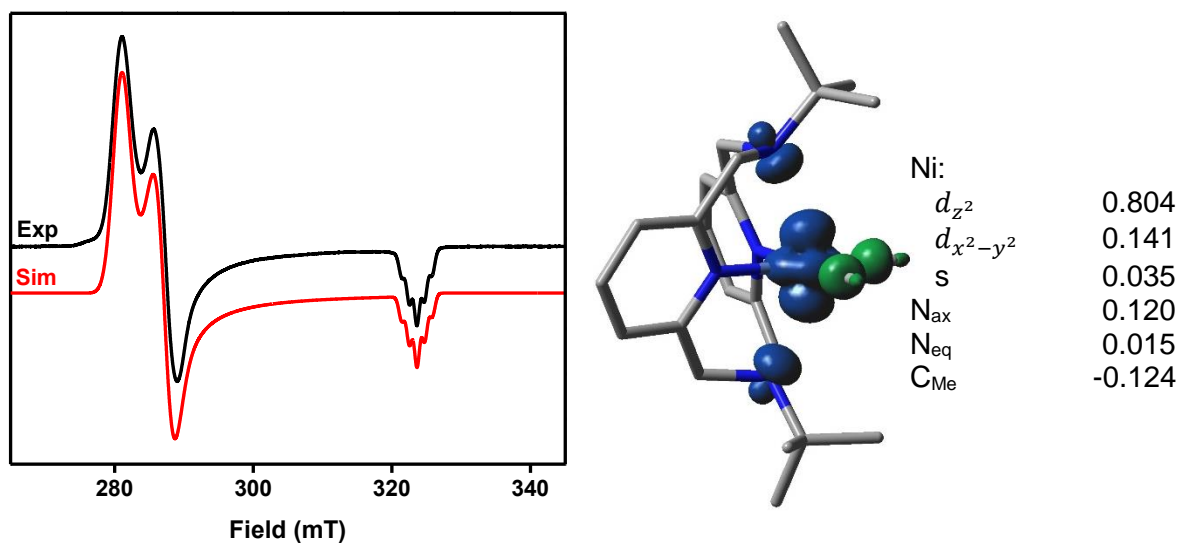
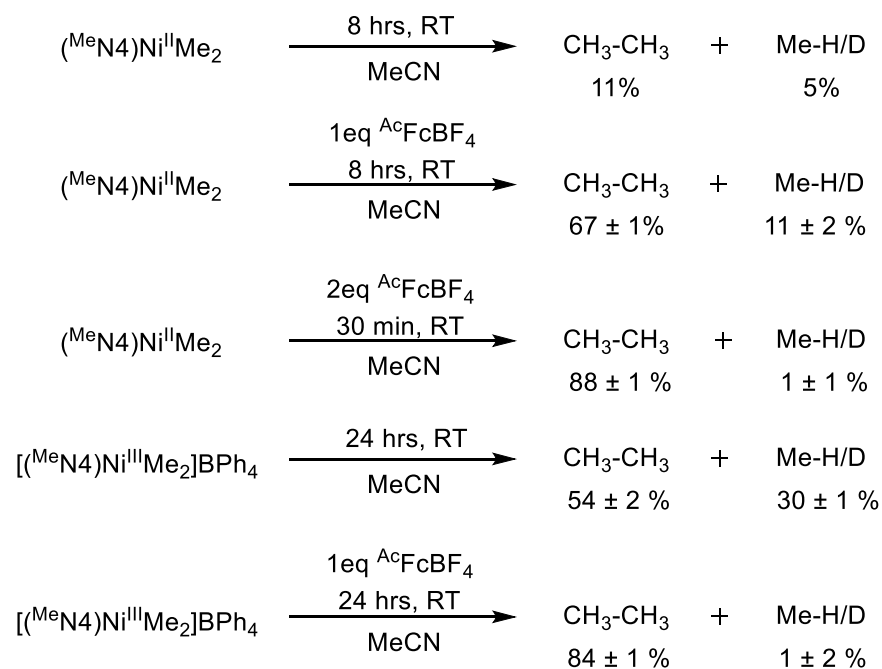


Figure 4.5 (Left) EPR spectrum (black line) of **4** in PrCN at 77K, and the simulated EPR spectrum (red line) using the following parameters: $g_x = 2.314$, $g_y = 2.264$, $g_z = 2.009$ ($A_{2N} = 11.0$ G). (Right) DFT calculated Mulliken spin density for **4** (shown as a 0.005 isodensity contour plot), and the relevant atomic and Ni orbital contributions to the spin density.

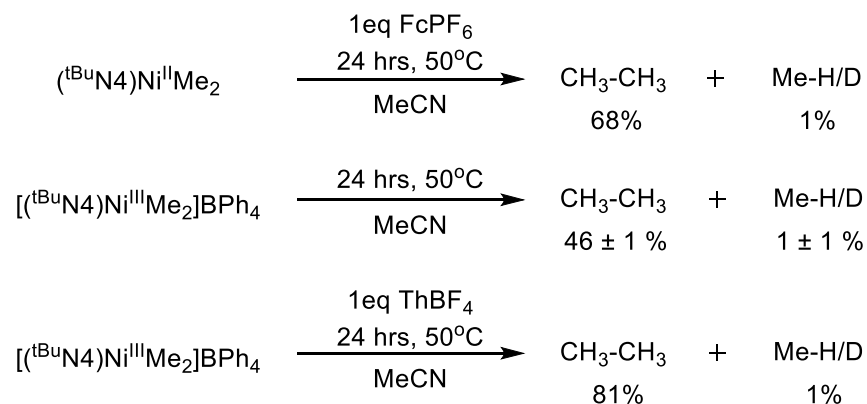
4.3.3 C-C Bond Formation Reactivity.

In addition to the isolation and characterization of complexes **2** and **4**, the C-C bond formation reactivity was investigated for complexes **1-4** using different oxidative conditions. Both one- and two- electron oxidations of complex **1** in MeCN at room temperature generated observable quantities of ethane via NMR (Scheme 4.2). Similarly, the reactivity of isolated complex **2** both with and without one-electron oxidation generated observable quantities of ethane at room temperature. Complex **4** was stable at room temperature, therefore all the reactivity for complexes **2** and **4** were conducted at 50°C. The one-electron oxidation of complex **2** generated observable quantities of ethane via NMR (Scheme 4.3). Additionally, complex **4** with and without one-electron oxidation also generated observable quantities of ethane. All reactions were monitored until no additional changes were observed. Surprisingly, complexes **2** and **4** both exhibited limited reactivity without further oxidation. However, promoted by further oxidations the reactivity of these complexes proceeded more rapidly, suggesting the involvement of a potential Ni^{IV} intermediate.

Scheme 4.2 C-C bond formation reactivity of the complexes **1** and **2**.



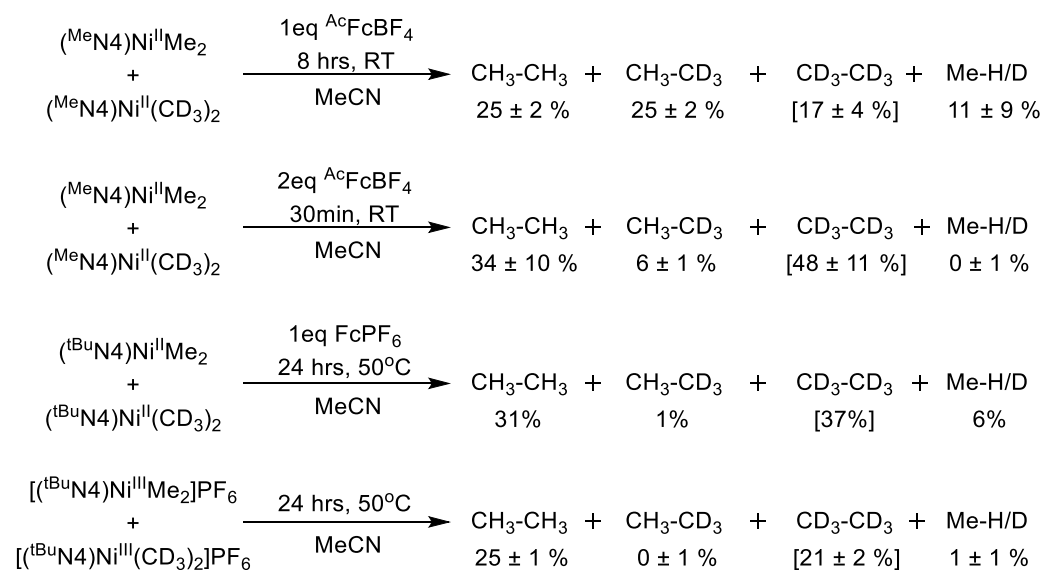
Scheme 4.3 C-C bond formation reactivity of the complexes **3** and **4**.



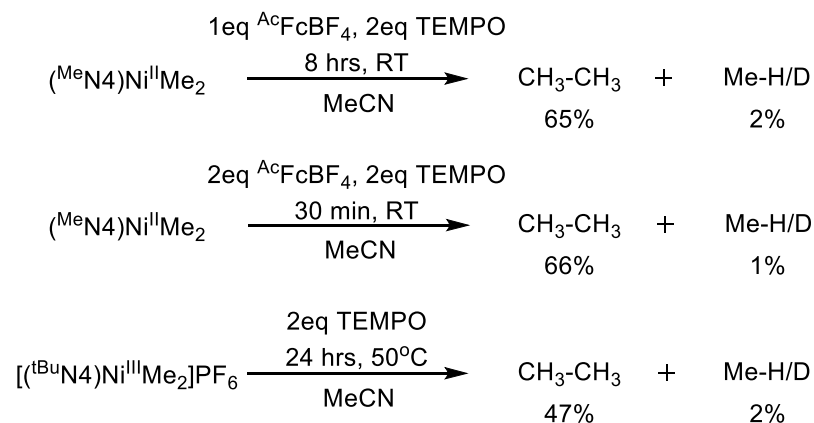
To investigate the different oxidative pathways several mechanistic studies were performed. Crossover experiments using a 1:1 mixtures of **1** and $(^{\text{Me}}\text{N4})\text{Ni}^{\text{II}}(\text{CD}_3)_2$, **1-d6**, **3** and $(^{\text{tBu}}\text{N4})\text{Ni}^{\text{II}}(\text{CD}_3)_2$, **3-d6**, or **4** and $[(^{\text{tBu}}\text{N4})\text{Ni}^{\text{III}}(\text{CD}_3)_2]\text{PF}_6$, **4-d6**, resulted in a similar difference between the one- and two-electron oxidation reactions (Scheme 4.4). The one-electron oxidation of complexes **1** resulted in significant crossover. Whereas, the one-electron oxidation of complex

3, the two-electron oxidation of complex **1** and the one-electron/non-oxidation of complex **4** all showed only trace amounts of crossover products. Furthermore, all reactions were unaffected in the presence of the radical trap (2,2,6,6-tetramethylpiperidin-1-yl)oxidanyl, TEMPO, suggesting the absence of radical mediated pathways (Scheme 4.5).

Scheme 4.4 C-C bond formation reactivity of crossover experiments using a 1:1 mixture of complexes **1**, **3** and **4**.



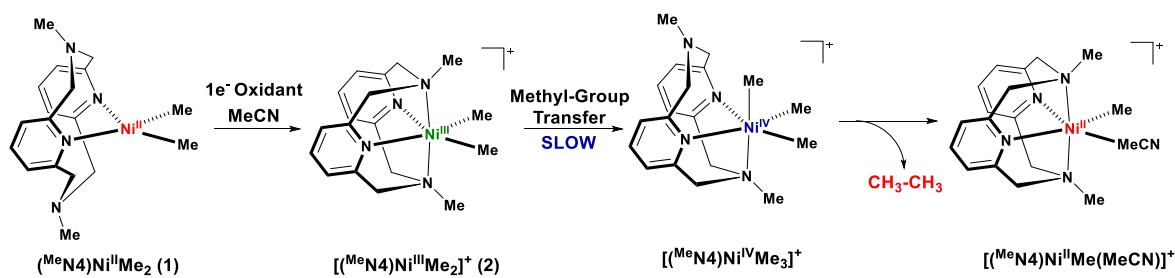
Scheme 4.5 C-C bond formation reactivity of the complexes **1** and **4** in the presence of radical trap TEMPO.



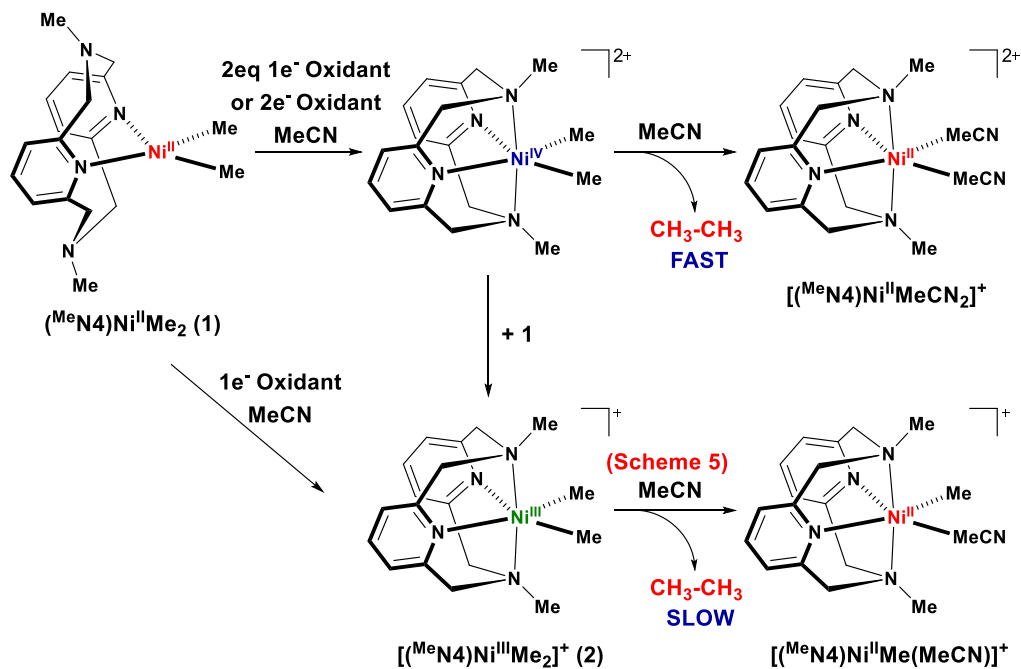
From the various reactivity studies three distinctive reaction pathways were proposed for the oxidatively induced C-C bond formation. The first pathway (Scheme 4.6) is slower and consistent with a slow non-radical methyl group transfer between two $\text{Ni}^{\text{III}}\text{Me}_2$ intermediates to form a reactive $\text{Ni}^{\text{IV}}\text{Me}_3$ intermediate, which undergoes rapid reductive elimination. The formation and corresponding slow decay of the Ni^{III} intermediate was confirmed via EPR and UV-Vis experiments. Additionally, the presence of crossover products further suggests the stability of the Ni^{III} intermediate allowing for methyl group transfer prior to reductive elimination. The reactivity of the one-electron oxidation of complex **1** and the non-oxidation of complex **2** are constant with this proposed pathway. The second pathway (Scheme 4.7), is proposed to involve a highly-reactive $\text{Ni}^{\text{IV}}\text{Me}_2$ intermediate which rapidly undergoes concerted reductive elimination resulting in rapid ethane formation. The presence of only trace crossover products and the rapid rate of reductive elimination suggest a more reactive intermediate was formed. The instability of the resulting high-valent intermediate hindered any possible detection using UV-Vis, NMR and ESI-MS experiments. Additionally, EPR and UV-Vis experiments showed the formation of trace Ni^{III} intermediate which accounts for the trace amounts of crossover products observed. The reactivity of the two-electron oxidation of complex **1** and the one-electron oxidation of complexes **2** and **4** are constant with this second pathway. The third and final pathway (Scheme 4.8), is proposed to involve a $\text{Ni}^{\text{III}}\text{Me}_2$ intermediate which undergoes concerted reductive elimination forming ethane and a reactive Ni^{I} intermediate. The Ni^{I} intermediate then rapidly undergoes comproportionation with an additional $\text{Ni}^{\text{III}}\text{Me}_2$ intermediate forming two stable $[(^{\text{tBu}}\text{N}_4)\text{Ni}^{\text{II}}\text{Me}(\text{MeCN})]^+$ species. The presence of only trace crossover products and the limited yields are constant with this proposed pathway. The reactivity of the one-electron oxidation of complex **3** and the non-oxidation of complex **4** are best describe by this third pathway. Overall,

we proposed three distinctive pathways, all involving high-valent Ni^{III} and Ni^{IV} intermediates which undergo reductive elimination resulting in C-C bond formation.

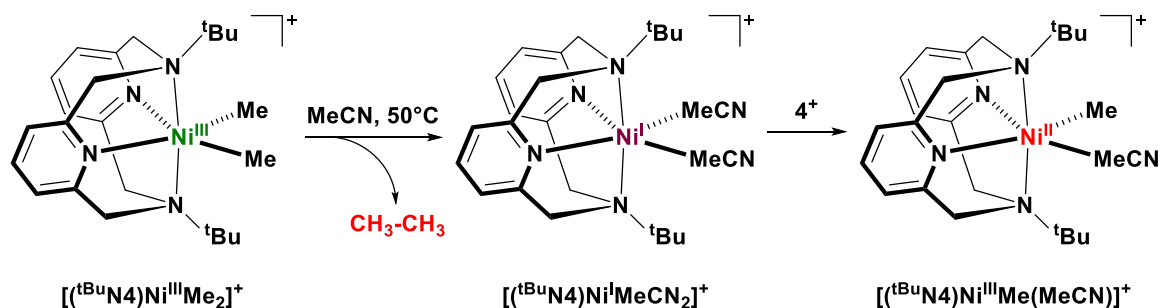
Scheme 4.6 Proposed pathway for reactivity of complexes **1** and **2** resulting in C-C bond formation.



Scheme 4.7 Proposed pathway for the reactivity of complexes **1**, **2** and **4** resulting in C-C bond formation.



Scheme 4.8 Proposed pathway for the reactivity of complexes **3** and **4** resulting in C-C bond formation.



4.3.4 Catalytic Reactivity of Ni^{II}/Ni^{III} Complexes.

In addition to the reactivity studies, complexes **1** and **2** were shown to be a capable catalyst for Kumada cross-coupling using both alkyl- and aryl-halides at moderate temperatures and reaction times. The unoptimized reactions of iodotoluene with PhMgBr and MeMgCl were achieved with yields of 52% and 44% respectively. Remarkably, chlorotoluene was also shown to react with PhMgBr with yields of 71% (Table 4.1). Additionally, the coupling of unactivated 1-iodooctane with PhMgBr and MeMgCl resulted in poor yields of 4-7% (Table 4.2).

To investigate the nature of the cross-coupling mechanism the radical clock substrate (bromomethyl)cyclopropane was utilized. The cross-coupling of (bromomethyl)cyclopropane with PhMgBr resulted in both rearranged and unarranged products, suggesting the formation of radical intermediates during the catalytic cycle. The proposed catalytic cycle, Scheme 4.9, begins with the oxidation of the Ni^{II} catalyst by the alkyl or aryl halide. Complex **1** was shown to rapidly undergo oxidation in the presence of both alkyl and aryl halides (*vide infra*). Complex **2** then reductively eliminates to the reactive Ni^{II} intermediate (A) as proposed above for the oxidation of complex **1** with 1 equivalent of oxidant (Scheme 4.6). The alkyl or aryl halide can then undergo oxidative addition forming a Ni^{IV} intermediate (B). Notably, the reduced yields observed when

using alkyl halide is attributed to the disfavored oxidative addition of alkyl halides. The Ni^{IV} intermediate (B) can then rapidly undergo transmetalation with the Grignard reagent producing the key Ni^{IV} intermediate (C), which reductively eliminates to produce the desired cross-coupled product. The reductive elimination from intermediate C is proposed to follow a similar pathway to that reported above for the oxidation of complex **1** with 2 equivalents of oxidant (Scheme 4.7). Remarkably, these results suggest the cross-coupling reactions proceed through a reactive Ni^{IV} intermediate instead of the more stable Ni^{III} intermediate which is more commonly proposed.

Table 4.1 Substrates used in the Kumada cross-coupling reactions catalyzed by 5 mol % (^{Me}N4)Ni^{II}Me₂ or [(^{Me}N4)Ni^{III}Me₂]BPh₄ with 1 equivalent R'MgX and 1 equivalent aryl halide at room temperature in THF.

Aryl Halide	R'MgX	Reaction Time, h	Ni ^{II} (1) Yield, %	Ni ^{III} (2) Yield, %
4-iodotoluene	PhMgBr	1	52	51
4-iodotoluene	MeMgCl	1, 4	43	44
4-chlorotoluene	PhMgBr	24	42	71
4-chlorotoluene	MeMgCl	24	6	5

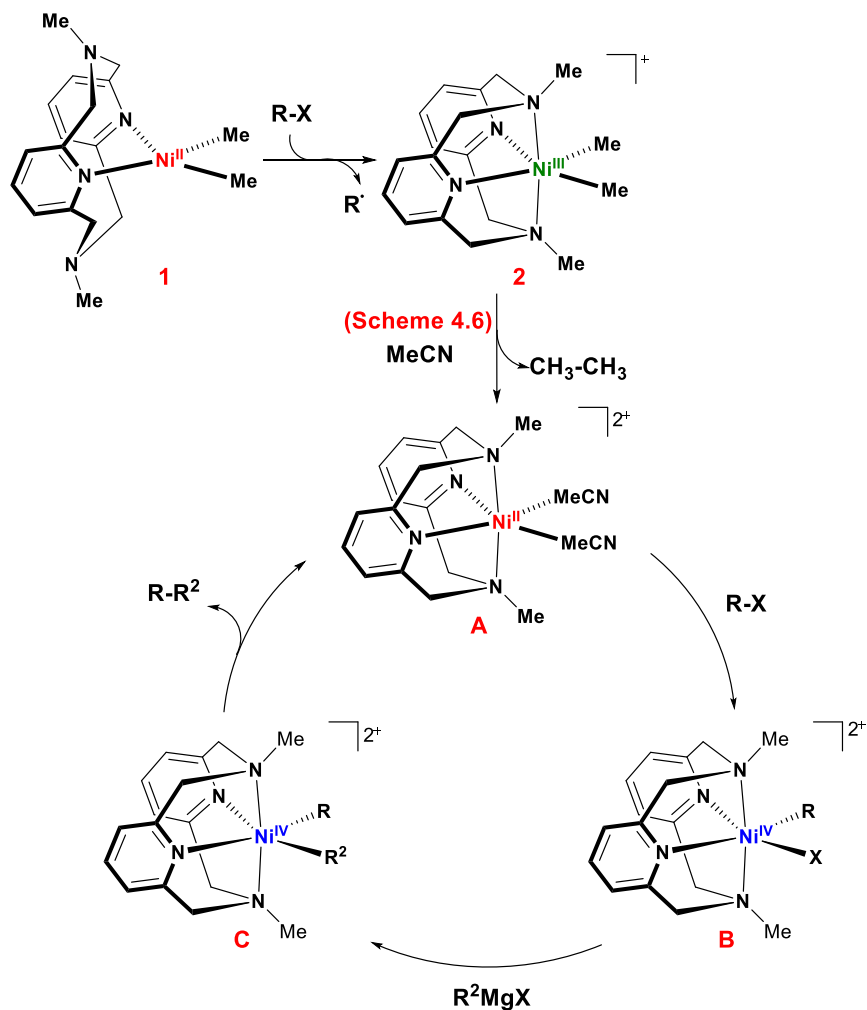
* Yield was determined using GC-FID with hexamethylbenzene as the internal standard.

Table 4.2 Substrates used in the Kumada cross-coupling reactions catalyzed by 5 mol % (^{Me}N4)Ni^{II}Me₂ or [(^{Me}N4)Ni^{III}Me₂]BPh₄ with 1 equivalent R'MgX and 1 equivalent alkyl halide at room temperature in THF.

Alkyl Halide	R'MgX	Reaction Time, h	Ni ^{II} (1) Yield, %	Ni ^{III} (2) Yield, %
1-iodooctane	PhMgBr	1	4	5
1-iodooctane	MeMgCl	1	7	6

* Yield was determined using GC-FID with dodecane as the internal standard.

Scheme 4.9 Proposed catalytic cycle for the Kumada cross-coupling reactions catalyzed by $(^{\text{Me}}\text{N}4)\text{Ni}^{\text{II}}\text{Me}_2$.

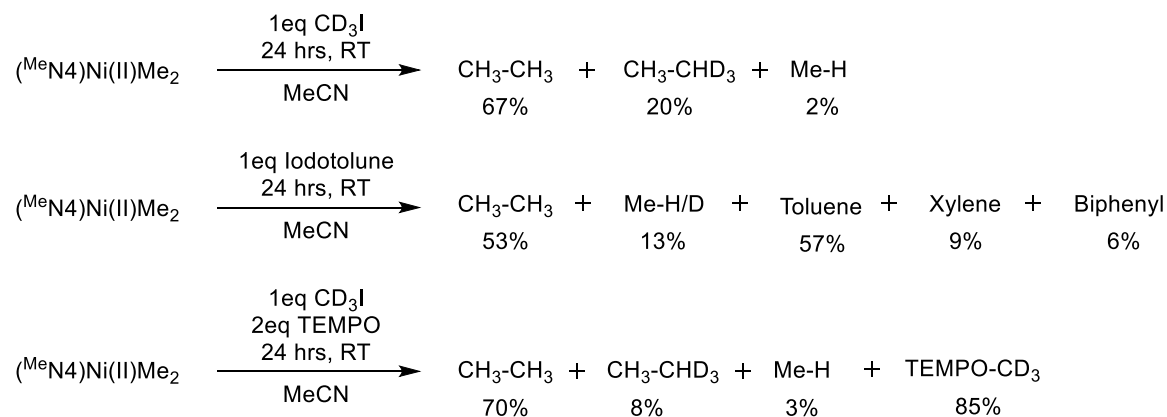


4.3.5 Reaction of Alkyl and Aryl Halides with $(^{\text{Me}}\text{N}4)\text{Ni}^{\text{II}}\text{Me}_2$ Complex.

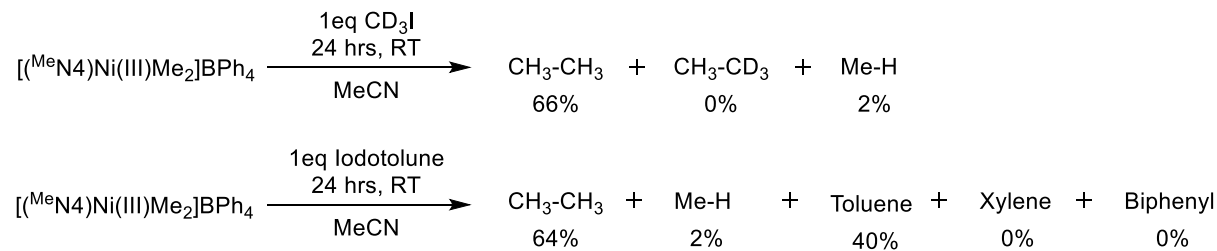
In order to assess whether Ni^{III} species could be formed under the catalytic cross-coupling conditions, we probed the reaction of the Ni^{II} precursor with alkyl and aryl halides. Complex **1** was shown to readily undergo oxidation in the presence of both alkyl and aryl halides. The formation of complex **2** was confirmed by EPR analysis. In addition, the reaction of complex **1** with CD_3I in the presence of the radical trap TEMPO was conducted and showed nearly quantitative formation of the TEMPO- CD_3 adduct determined by GC/FID analysis,

confirming the homolytic cleavage of the carbon halide bond. These results strongly suggest alkyl and aryl halides are acting as one-electron oxidants, instead of undergoing oxidation addition. Furthermore, the resulting complex **2** exhibited C-C bond formation reactivity and generated observable quantities of various organic products (Scheme 4.10 and 4.11). The major reaction pathway resulting in the formation of ethane is consistent with the proposed reactivity of complex **2** shown above (Scheme 4.6). However, the presence of both d₃-ethane and xylene provide evidence for a possible alternative pathway involving the interaction of the radical alkyl or aryl group with the Ni^{III} intermediate (Scheme 4.12). Overall, these studies provide strong evidence for the involvement of high-valent organometallic Ni species, both Ni^{III} and Ni^{IV}, in cross-coupling reactions.

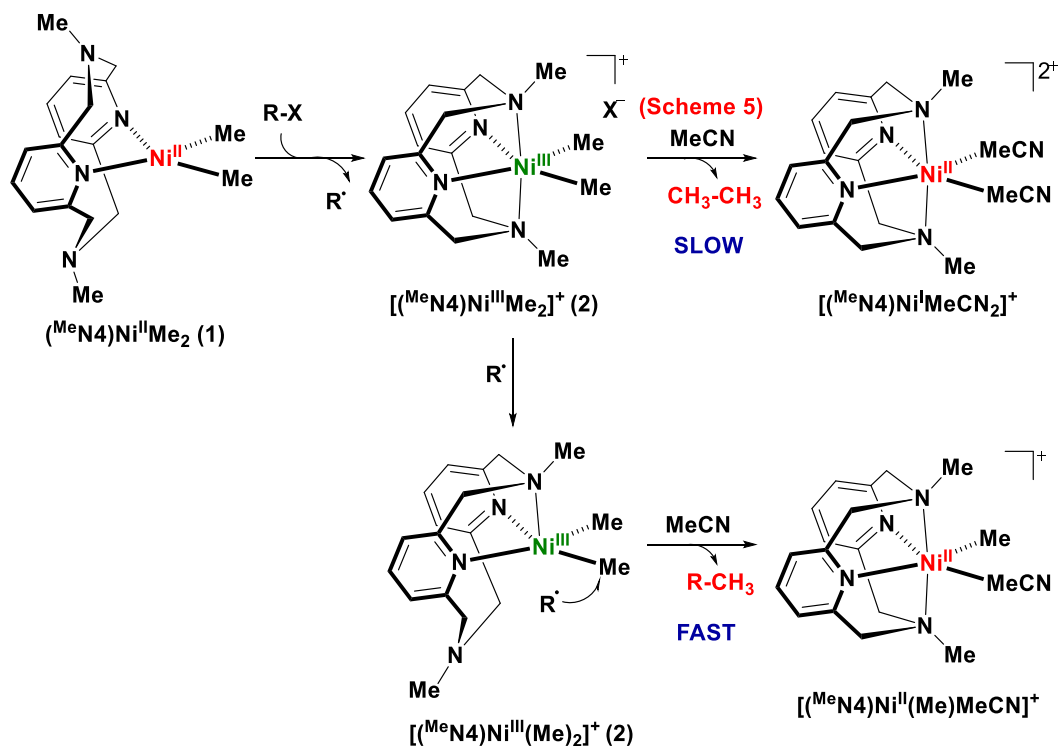
Scheme 4.10 C-C bond formation reactivity from the oxidation of (^{Me}N₄)Ni^{II}Me₂ complex using alkyl and aryl halides.



Scheme 4.11 C-C bond formation reactivity from the reaction of $[(^{\text{Me}}\text{N}4)\text{Ni}^{\text{III}}\text{Me}_2]\text{BPh}_4$ complex with alkyl and aryl halides.



Scheme 4.12 Proposed reaction pathway for the oxidation of $(^{\text{Me}}\text{N}4)\text{Ni}^{\text{II}}\text{Me}_2$ by alkyl and aryl halides and the corresponding C-C bond formation reactivity.



4.4 Conclusion

In summary, the studies reported herein provide the first stable Ni^{III} dialkyl complexes stabilized using the unique tetradentate pyridonophane ligands. The rare stability of these complexes allowed for the isolation and full structural and spectroscopic characterization of the Ni^{III} dimethyl complexes. Furthermore, both one- and two-electron oxidations were utilized to induce C-C bond formation reactivity. As a result, three distinctive high-valent pathways were observed providing strong support for various roles of Ni^{III} and Ni^{IV} dialkyl complexes in cross-coupling reactions. Additionally, the Ni^{II} and Ni^{III} dimethyl complexes were shown to be a capable catalyst for a variety of Kumada cross-coupling reactions. All told, these studies provided a rare opportunity to directly investigate high-valent Ni intermediates capable of undergoing C-C bond formation reactivity and provide for the first time viable evidence for their various roles in catalytic cross-coupling reactions.

4.5 Acknowledgements

I appreciate my colleagues Ying Zhang and Ming Cheng for their help and advice in performing the in situ ESI-MS experiments. Similarly, I appreciate Professor Nigam P. Rath of the Department of Chemistry and Biochemistry at the University of Missouri-St. Louis for his help and advice in solving all the reported crystal structures.

4.6 References

1. Meijere, A. d.; Diederich, F. *Metal-Catalyzed Cross-Coupling Reactions*; Wiley-VCH: Weinheim, New York, 2004.
2. Netherton, M. R.; Fu, G. C. *Adv. Synth. Catal.* **2004**, *346*, 1525.
3. Frisch, A. C.; Beller, M. *Angew. Chem. Int. Ed.* **2005**, *44*, 674.
4. Phapale, V. B.; Cardenas, D. J. *Chem. Soc. Rev.* **2009**, *38*, 1598.
5. Rudolph, A.; Lautens, M. *Angew. Chem. Int. Ed.* **2009**, *48*, 2656.
6. Knochel, P.; Thaler, T.; Diene, C. *Isr. J. Chem.* **2012**, *50*, 547.
7. Tsou, T. T.; Kochi, J. K. *J. Am. Chem. Soc.* **1978**, *100*, 1634.
8. Tsou, T. T.; Kochi, J. K. *J. Am. Chem. Soc.* **1979**, *101*, 7547.
9. Amatore, C.; Jutand, A. *Organometallics* **1988**, *7*, 2203.
10. Zhou, J.; Fu, G. C. *J. Am. Chem. Soc.* **2004**, *126*, 1340.
11. Powell, D. A.; Fu, G. C. *J. Am. Chem. Soc.* **2004**, *126*, 7788.
12. Owston, N. A.; Fu, G. C. *J. Am. Chem. Soc.* **2010**, *132*, 11908.
13. Zultanski, S. L.; Fu, G. C. *J. Am. Chem. Soc.* **2011**, *133*, 15362.
14. Dudnik, A. S.; Fu, G. C. *J. Am. Chem. Soc.* **2012**, *134*, 10693.
15. Zultanski, S. L.; Fu, G. C. *J. Am. Chem. Soc.* **2013**, *135*, 624.
16. Jones, G. D.; McFarland, C.; Anderson, T. J.; Vivic, D. A. *Chem. Commun.* **2005**, 4211.
17. Jones, G. D.; Martin, J. L.; McFarland, C.; Allen, O. R.; Hall, R. E.; Haley, A. D.; Brandon, R. J.; Konovalova, T.; Desrochers, P. J.; Pulay, P.; Vivic, D. A. *J. Am. Chem. Soc.* **2006**, *128*, 13175.
18. Klein, A.; Budnikova, Y. H.; Sinyashin, O. G. *J. Organomet. Chem.* **2007**, *692*, 3156.

19. Phapale, V. B.; Bunuel, E.; Garcia-Iglesias, M.; Cardenas, D. J. *Angew. Chem. Int. Ed.* **2007**, *46*, 8790.
20. Phapale, V. B.; Guisan-Ceinos, M.; Bunuel, E.; Cardenas, D. J. *Chem. Eur. J.* **2009**, *15*, 12681.
21. Gong, H. G.; Gagné, M. R. *J. Am. Chem. Soc.* **2008**, *130*, 12177.
22. Gong, H. G.; Andrews, R. S.; Zuccarello, J. L.; Lee, S. J.; Gagné, M. R. *Org. Lett.* **2009**, *11*, 879.
23. Vechorkin, O.; Hu, X. *Angew. Chem. Int. Ed.* **2009**, *48*, 2937.
24. Vechorkin, O.; Proust, V. r.; Hu, X. *J. Am. Chem. Soc.* **2009**, *131*, 9756.
25. Hu, X. *Chem. Sci.* **2011**, *2*, 1867.
26. Everson, D. A.; Shrestha, R.; Weix, D. J. *J. Am. Chem. Soc.* **2010**, *132*, 920.
27. Biswas, S.; Weix, D. J. *J. Am. Chem. Soc.* **2013**, *135*, 16192.
28. Joshi-Pangu, A.; Wang, C. Y.; Biscoe, M. R. *J. Am. Chem. Soc.* **2011**, *133*, 8478.
29. Yu, X. L.; Yang, T.; Wang, S. L.; Xu, H. L.; Gong, H. G. *Org. Lett.* **2011**, *13*, 2138.
30. Dai, Y. J.; Wu, F.; Zang, Z. H.; You, H. Z.; Gong, H. G. *Chem. Eur. J.* **2012**, *18*, 808.
31. Xu, H.; Zhao, C.; Qian, Q.; Deng, W.; Gong, H. *Chem. Sci.* **2013**, *4*, 4022.
32. Matsunaga, P. T.; Hillhouse, G. L.; Rheingold, A. L. *J. Am. Chem. Soc.* **1993**, *115*, 2075.
33. Koo, K. M.; Hillhouse, G. L.; Rheingold, A. L. *Organometallics* **1995**, *14*, 456.
34. Han, R. Y.; Hillhouse, G. L. *J. Am. Chem. Soc.* **1997**, *119*, 8135.
35. Koo, K.; Hillhouse, G. L. *Organometallics* **1995**, *14*, 4421.
36. Lin, B. L.; Clough, C. R.; Hillhouse, G. L. *J. Am. Chem. Soc.* **2002**, *124*, 2890.
37. Zheng, B.; Luo, J.; Tang, F.; Schultz, J. W.; Rath, N. P.; Mirica, L. M. *J. Am. Chem. Soc.* **2014**, *136*, DOI: 10.1021/ja5024749.

38. Khusnutdinova, J. R.; Rath, N. P.; Mirica, L. M. *J. Am. Chem. Soc.* **2010**, *132*, 7303.
39. Khusnutdinova, J. R.; Rath, N. P.; Mirica, L. M. *J. Am. Chem. Soc.* **2012**, *134*, 2414.
40. Tang, F.; Qu, F.; Khusnutdinova, J. R.; Rath, N. P.; Mirica, L. M. *Dalton Trans.* **2012**, *41*, 14046.
41. Mirica, L. M.; Khusnutdinova, J. R. *Coord. Chem. Rev.* **2013**, *257*, 299.
42. Tang, F.; Zhang, Y.; Rath, N. P.; Mirica, L. M. *Organometallics* **2012**, *31*, 6690.
43. Che, C. M.; Li, Z. Y.; Wong, K. Y.; Poon, C. K.; Mak, T. C. W.; Peng, S. M. *Polyhedron* **1994**, *13*, 771.
44. Bottino, F.; Di Grazia, M.; Finocchiaro, P.; Fronczek, F. R.; Mamo, A.; Pappalardo, S. *J. Org. Chem.* **1988**, *53*, 3521.
45. Meneghetti, S. P.; Lutz, P. J.; Fischer, J.; Kress, J. *Polyhedron* **2001**, *20*, 2705.
46. Connelly, N. G.; Geiger, W. E. *Chem. Rev.* **1996**, *96*, 877.
47. Gottlieb, H. E.; Kotlyar, V.; Nudelman, A. *J. Org. Chem.* **1997**, *62*, 7512.
48. Bruker Analytical X-Ray, Madison, WI, 2008
49. Sheldrick, G. *Acta Crystallogr. Sect. A: Found. Crystallogr.* **2008**, *64*, 112.
50. M. J. Frisch, G. W. T., H. B. Schlegel, G. E. Scuseria, M. A. Robb, J. R. Cheeseman, G. Scalmani, V. Barone, B. Mennucci, G. A. Petersson, H. Nakatsuji, M. Caricato, X. Li, H. P. Hratchian, A. F. Izmaylov, J. Bloino, G. Zheng, J. L. Sonnenberg, M. Hada, M. Ehara, K. Toyota, R. Fukuda, J. Hasegawa, M. Ishida, T. Nakajima, Y. Honda, O. Kitao, H. Nakai, T. Vreven, J. A. Montgomery, Jr., J. E. Peralta, F. Ogliaro, M. Bearpark, J. J. Heyd, E. Brothers, K. N. Kudin, V. N. Staroverov, R. Kobayashi, J. Normand, K. Raghavachari, A. Rendell, J. C. Burant, S. S. Iyengar, J. Tomasi, M. Cossi, N. Rega, J. M. Millam, M. Klene, J. E. Knox, J. B. Cross, V. Bakken, C. Adamo, J. Jaramillo, R. Gomperts, R. E. Stratmann, O. Yazyev, A. J. Austin, R. Cammi, C. Pomelli, J. W. Ochterski, R. L. Martin, K. Morokuma, V. G. Zakrzewski, G. A. Voth, P. Salvador, J. J. Dannenberg, S. Dapprich, A. D. Daniels, O. Farkas, J. B. Foresman, J. V. Ortiz, J. Cioslowski, D. J. Fox, Gaussian, Inc.
51. Lee, C. M.; Chen, C. H.; Liao, F. X.; Hu, C. H.; Lee, G. H. *J. Am. Chem. Soc.* **2010**, *132*, 9256.

52. Zhang, C. P.; Wang, H.; Klein, A.; Biewer, C.; Stimat, K.; Yarnaguchi, Y.; Xu, L.; Gomez-Benitez, V.; Vicic, D. A. *J. Am. Chem. Soc.* **2013**, *135*, 8141.
53. Skripnikov, L. www.chemissian.com, accessed June 2011
54. Burnett, M. N.; Johnson, C. K. *ORTEP-III: Oak Ridge Thermal Ellipsoid Plot Program for Crystal Structure Illustrations, Oak Ridge National Laboratory Report ORNL-6895* **1996**.
55. Lipschutz, M. I.; Yang, X.; Chatterjee, R.; Tilley, T. D. *J. Am. Chem. Soc.* **2013**, *135*, 15298.
56. Lipschutz, M. I.; Tilley, T. D. *Angew. Chem. Int. Ed.* **2014**, *53*, 7290.
57. Grove, D. M.; Vankoten, G.; Mul, W. P.; Vanderzeijden, A. A. H.; Terheijden, J.; Zoutberg, M. C.; Stam, C. H. *Organometallics* **1986**, *5*, 322.
58. van de Kuil, L. A.; Veldhuizen, Y. S. J.; Grove, D. M.; Zwikker, J. W.; Jenneskens, L. W.; Drenth, W.; Smeets, W. J. J.; Spek, A. L.; van Koten, G. *J. Organomet. Chem.* **1995**, *488*, 191.
59. Grove, D. M.; van Koten, G.; Zoet, R.; Murrall, N. W.; Welch, A. J. *J. Am. Chem. Soc.* **1983**, *105*, 1379.
60. Grove, D. M.; van Koten, G.; Mul, P.; Zoet, R.; van der Linden, J. G. M.; Legters, J.; Schmitz, J. E. J.; Murrall, N. W.; Welch, A. J. *Inorg. Chem.* **1988**, *27*, 2466.
61. Iluc, V. M.; Miller, A. J. M.; Anderson, J. S.; Monreal, M. J.; Mehn, M. P.; Hillhouse, G. L. *J. Am. Chem. Soc.* **2011**, *133*, 13055.

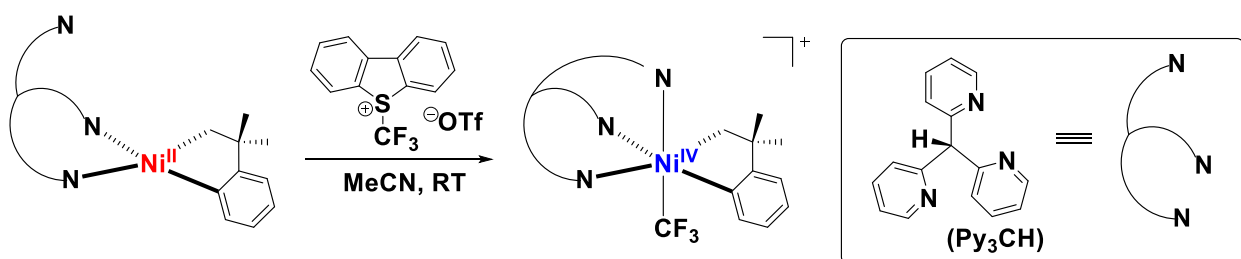
Chapter 5

Synthesis and Isolation of High-Valent Organometallic Nickel Complexes Supported by Cycloneophyl Group

5.1 Introduction

To better support the proposed reactive Ni^{IV} intermediates shown in Chapter 4 (Scheme 4.5 and 4.6) we aimed to synthesize a stable analogous Ni^{IV} complex supported by the same ^{Me}N₄ ligand system. We proposed modifying the exogenous ligands to disfavor reactive elimination, thus stabilizing the reactive Ni^{IV} complex. In recent reports, the utilization of the cycloneophyl group had been shown to minimize C-C bond formation from reactive Ni^{IV} and Pd^{IV} intermediates (Scheme 5.1).¹⁻⁸

Scheme 5.1 Synthesis of [(Py₃CH)Ni^{IV}(cycloneophyl)(CF₃)]OTf.³



Additionally, our group has utilized the stabilizing properties of the cycloneophyl group to stabilize various Pd^{IV} complexes.^{7,9} In particular, the [(Me₃tacn)Pd^{IV}(cycloneophyl)(OH)]⁺ complex was capable of being isolated and fully characterized, providing valuable insight into these high-valent Pd^{IV} complexes.⁷ Herein, we report the synthesis and characterization of the proposed Ni^{IV} complex stabilized by a cycloneophyl group and the ^{Me}N₄ ligand. As a result, these studies provide strong experimental evidence supporting the previously proposed Ni^{IV} intermediates.

5.2 Experimental Section

5.2.1 Synthesis of Ligands and Complexes

Reagents and Materials. All manipulations were carried out under a nitrogen atmosphere using standard Schlenk and glove box techniques if not indicated otherwise. All reagents for which synthesis is not given were commercially available from Sigma-Aldrich, Fisher Scientific, VWR, Acros, STREM or Pressure Chemical and were used as received without further purification. Solvents were purified prior to use by passing through a column of activated alumina using an MBRAUN Solvent Purification System. N,N' -di-methyl-2,11-diaza[3.3](2,6)pyridinophane ($^{\text{Me}}\text{N4}$)¹⁰, $(\text{PMe}_3)_2\text{Ni}^{\text{II}}(\text{cycloneophyl})$ ¹¹, FcPF_6 ¹² and FcBF_4 ¹² were prepared according to the literature procedures.

($^{\text{Me}}\text{N4}$)Ni^{II}(cycloneophyl) (1). A solution of $^{\text{Me}}\text{N4}$ (0.2300 grams, 0.86 mmol) and $(\text{PMe}_3)_2\text{Ni}^{\text{II}}(\text{cycloneophyl})$ (0.2940 grams, 0.86 mmol) in diethyl ether was stirred at room temperature overnight. The orange precipitate was then separated by filtration, washed with pentane (3 mL), and dried under vacuum. Yield: 0.2473 grams, 0.54 mmol, 63%. UV-vis (MeCN, RT), λ_{max} (ϵ , $\text{M}^{-1} \text{cm}^{-1}$): 247 (17500), 302 (5900), 367 (5530), 490 (350). ¹H-NMR (300 MHz, CDCl₃), δ (ppm): 7.54 (t, 1H, Py-H), 7.46 (t, 1H, Py-H), 7.11 (d, 2H, Py-H), 7.04 (d, 2H, Py-H), 6.66 (m, 6H, Cycle/-CH₂-), 6.38 (t, 1H, Cycle), 5.86 (d, 1H, Cycle), 4.22 (dd, 4H, -CH₂-), 2.24 (s, 6H, N-CH₃), 1.32 (s, 6H, CH₃), 1.24 (s, 2H, Ni-CH₂-Cycle). ¹³C-NMR (600 MHz, d₃-MeCN), δ (ppm): 159.21, 158.49, 136.35, 136.16, 136.05, 135.88, 125.59, 125.48, 123.89, 123.24, 122.95, 121.91, 66.70, 64.07, 63.95, 49.09, 38.87, 34.21. Anal. Found: C, 66.18; H, 6.74; N, 11.65. Calculated for $\text{C}_{26}\text{H}_{32}\text{N}_4\text{Ni} \cdot (1/3 \text{C}_4\text{H}_{10}\text{O})$: C, 67.83; H, 7.36; N, 11.58.

[(^{Me}N₄)Ni^{III}(cycloneophyl)]PF₆ (2). A THF solution of (^{Me}N₄)Ni^{II}(cycloneophyl) (0.1581 grams, 0.34 mmol) and FcPF₆ (0.1140 grams, 0.34 mmol) was stirred at -50 °C for 2 hours. The resulting solution was then precipitated with excess pentane. The red-orange precipitate was separated by filtration, washed with pentane (3 mL), and dried under vacuum. Yield: 0.1658 grams, 0.27 mmol, 79%. X-ray quality crystals were obtained by slow pentane diffusion into a tetrahydrofuran solution in the presence of NaBPh₄ at -35 °C. Evans method (CD₃CN): $\mu_{\text{eff}} = 1.894 \mu_{\text{B}}$. UV-vis (MeCN, RT), λ_{max} (ϵ , M⁻¹ cm⁻¹): 246 (18000), 473 (630), 964 (50). ESI-MS of [(^{Me}N₄)Ni^{III}(cycloneophyl)]PF₆, m/z 458.1969; calculated for [(^{Me}N₄)Ni^{III}(cycloneophyl)]⁺, 458.1980. Anal. Found: C, 52.32; H, 5.79; N, 7.96. Calculated for C₂₆H₃₂F₆N₄NiP•C₄H₈O, based on the composition of the unit cell obtained from X-ray analysis: C, 53.28; H, 5.96; N, 8.28.

[(^{Me}N₄)Ni^{IV}(cycloneophyl)](PF₆)₂ (3). A d₃-MeCN solution of [(^{Me}N₄)Ni^{III}(cycloneophyl)]PF₆ (20 mg, 0.03 mmol) and NOPF₆ (29 mg, 0.17 mmol) was stirred at -40 °C for 15 minutes. The resulting solution was then transferred to a pre-cooled NMR tube. NMR experiments were conducted at -15 °C. An X-ray structure was not obtained due to decomposition of X-ray quality crystals during data collection. X-ray quality crystals were however obtained by slow pentane diffusion into a tetrahydrofuran solution at -35 °C. Elemental analysis proved unsuccessful due to instability and decomposition of the complex. UV-vis (MeCN, RT), λ_{max} (ϵ , M⁻¹ cm⁻¹): 258 (8825), 305 (1400), 457 (525). ¹H-NMR (500 MHz, CDCl₃, -15 °C), δ (ppm): 8.05 (t, 1H, Py-H), 7.97 (t, 1H, Py-H), 7.51 (d, 2H, Py-H), 7.41 (d, 2H, Py-H), 7.25 (t, 1H, Cyc-H), 7.19 (d, 1H, Cyc-H), 6.92 (t, 1H, Cyc-H), 6.55 (d, 1H, Cyc-H), 5.33 (s, 2H, Ni-CH₂-Cyc), 5.01 (d, 2H, -CH₂-), 4.56 (d, 2H, -CH₂-), 4.22 (d, 2H, -CH₂-), 4.08 (d, 2H, -CH₂-), 2.38 (s, 6H, N-CH₃), 1.67 (s, 6H, -CH₃). ¹³C-

NMR (500 MHz, CDCl₃, -15°C), δ (ppm): 159.42, 158.44, 156.25, 154.50, 144.89, 133.85, 132.31, 131.31, 131.15, 125.82, 125.07, 79.77, 77.38, 57.31, 36.00.

5.2.2 Physical Measurements

¹H NMR spectra were recorded on a Varian Mercury-300 spectrometer (300.121 MHz) or Agilent DD2-600 spectrometer (599.736 MHz). ¹³C NMR spectra were recorded on an Agilent DD2-600 spectrometer (599.736 MHz). Chemical shifts are reported in parts per million (ppm) with residual solvent resonance peaks as internal reference.¹³ Abbreviations for the multiplicity of NMR signals are singlet (s), doublet (d), triplet (t), quartet (q), multiplet (m), and broad (br). UV-visible spectra were recorded on a Varian Cary 50 Bio spectrophotometer and are reported as λ_{\max} , nm (ϵ , M⁻¹*cm⁻¹). EPR spectra were recorded on a JEOL JES-FA X-band (9.2 GHz) EPR spectrometer in frozen solution at 77 K. ESI-MS experiments were performed using a Thermo FT or Bruker Maxis Q-TOF mass spectrometer with an electrospray ionization source. ESI mass-spectrometry was provided by the Washington University Mass Spectrometry Resource. Elemental analyses were carried out by the Columbia Analytical Services Tucson Laboratory.

Cyclic voltammetry (CV) experiments were performed using a BASi EC Epsilon electrochemical workstation or a CHI 660D Electrochemical Analyzer. Electrochemical-grade supporting electrolytes were purchased from Fluka. The electrochemical measurements were performed under a blanket of nitrogen, and the analyzed solutions were deaerated by purging with nitrogen. A glassy carbon disk electrode ($d = 1.6$ mm) was used as the working electrode for cyclic voltammetry. The auxiliary electrode was a Pt wire for cyclic voltammetry measurements. Two different non-aqueous references electrodes were used: Ag/filled with 0.01M AgNO₃/0.1M

Bu₄NClO₄/MeCN solution or silver wire. The reference electrode was calibrated against ferrocene (Fc) at the conclusion of each CV experiment.

X-ray photoelectron spectroscopy (XPS) spectra were recorded on a PHI 5000 Versa Probe II X-Ray Photoelectron Spectrometer. XPS was provided in conjunction with the Washington University Institute of Materials Science and Engineering. X-ray diffraction quality crystals of (^{Me}N₄)Ni^{II}(cycloneophyl) and [(^{Me}N₄)Ni^{III}(cycloneophyl)]BPh₄ were obtained by slow pentane vapor diffusion into tetrahydrofuran solutions. Suitable crystals of appropriate dimensions were mounted and preliminary examination and data collection were performed using a Bruker Kappa Apex-II Charge Coupled Device (CCD) Detector system single crystal X-Ray diffractometer equipped with an Oxford Cryostream LT device. Data were collected using graphite monochromated Mo K α radiation ($\lambda = 0.71073 \text{ \AA}$) from a fine focus sealed tube X-Ray source. Apex II and SAINT software packages¹⁴ were used for data collection and data integration. Final cell constants were determined by global refinement of reflections from the complete data set. Data were corrected for systematic errors using SADABS¹⁴ based on the Laue symmetry using equivalent reflections. Structure solutions and refinement were carried out using the SHELXTL-PLUS software package.¹⁵ The structures were refined with full matrix least-squares refinement by minimizing $\sum w(F_o^2 - F_c^2)^2$. All non-hydrogen atoms were refined anisotropically to convergence. Typically, H atoms are added at the calculated positions in the final refinement cycles. The complete listings of x-ray diffraction parameters are included in Appendix B.

5.2.3 Characterization Studies

NMR studies. A 65 mM solution of **2** in MeCN-d₃ was reacted with NOPF₆ (5 equivalents) at -40°C for 5 minutes. The resulting solution was then transferred to a pre-cooled NMR tube at -40°C. The NMR tube was sealed and quickly removed from the glove box and directly placed into the instrument. The temperature controls were set at -15°C for all NMR experiments.

XPS studies. In the glove box solid samples of **2** and **3** were prepared. The samples were then transported and stored on dry ice prior to XPS analysis. Immediately prior to analysis, the two samples were transferred at RT to a piece of tape pre-fixed to the XPS plate. The samples were compressed and quickly loaded into the instrument. A survey scan was first conducted, followed by high-resolution scans comprising the nickel and nitrogen regions.

UV-Vis studies. Solutions of complexes **1-3** in MeCN were placed into a quartz cuvettes (1 cm pathlength) equipped with a septum-sealed cap inside the nitrogen filled glove box at -50°C. The spectra were then recorded using a Varian Cary 50 Bio spectrophotometer.

5.2.4 Reactivity Studies

Gas Chromatography (GC) product analysis for the reactivity of (^{Me}N₄)Ni^{II}(cycloneophyl).

A solution of 5-7 mg **1** in MeCN was added into a 5 mL vial containing hexamethylbenzene as an internal standard. To this solution was added all additional reagents in MeCN. The reaction mixtures were mixed carefully to form homogeneous solutions and kept in the dark and periodically analyzed by GC. The reaction samples were quenched with 100 μL of 1.0 M HCl and 5 mL H₂O, and extracted with ethyl ether (6 mL). The organic layer was then separated and dried

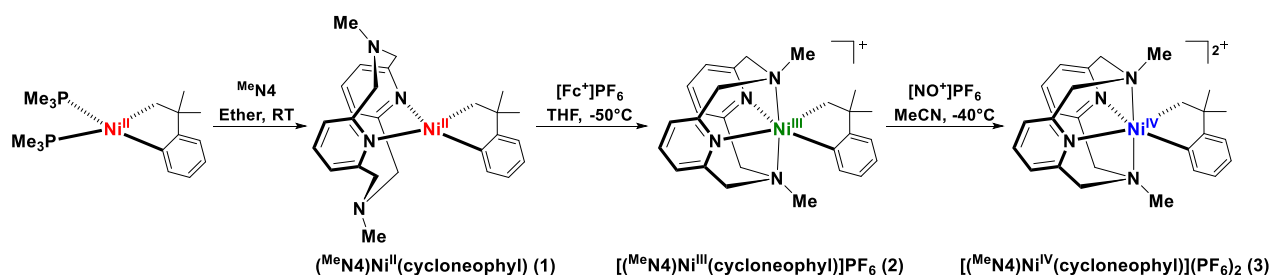
over MgSO₄. The yield of product(s) was obtained by GC/FID using hexamethylbenzene as the internal standard. The identity of the products were confirmed by GC/MSD.

5.3 Results and Discussion

5.3.1 Synthesis and Structure of Ni^{II} Complex.

The Ni^{II} complex (^{Me}N4)Ni^{II}(cycloneophyl), **1**, was prepared in 63% yield from the precursor (PMe₃)₂Ni^{II}(cycloneophyl) via ligand exchange with ^{Me}N4 (Scheme 5.2). The resulting orange-red complex was determined to be diamagnetic, suggesting a square planar geometry comprised of two pyridyl nitrogen atoms from the ^{Me}N4 ligand and two exogenous methyl groups. The strong σ-donating behavior of both the exogenous cycloneophyl group greatly favors the low-spin square planar geometry. The X-ray structure of **1** confirms the square planar geometry, with an average equatorial Ni-N_{pyridyl} bond length of 1.967 Å and an average Ni-C bond length of 1.917 Å (Figure 5.1).

Scheme 5.2 Synthesis of complexes **1-3**.



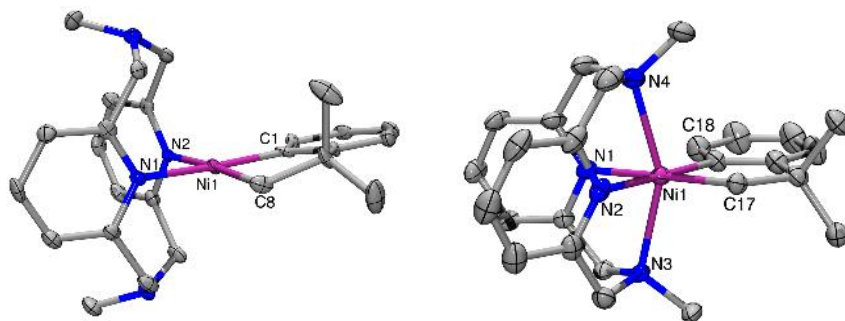


Figure 5.1 ORTEP¹⁶ representation of **1** (left) and the cation of **2** (right) with 50% probability thermal ellipsoids. Selected bond distances (Å), **1**: Ni1-C1, 1.879; Ni1-C8, 1.954; Ni1-N1, 1.936; Ni1-N2, 1.997. **2**: Ni1-C17, 1.973; Ni1-C18, 1.920; Ni1-N1, 2.001; Ni1-N2, 1.997; Ni1-N3, 2.241; Ni1-N4, 2.266. A complete listings of structural parameters are included in Appendix B.

The cyclic voltammetry (CV) of complex **1** shows an oxidation process at -1.17 V vs Fc⁺/Fc, as well as a reversible oxidation wave at 0.25 V vs Fc⁺/Fc (Figure 5.2). The lower oxidative process is assigned to the Ni^{II}/Ni^{III} couple, while the higher oxidative wave is tentatively assigned to a Ni^{III}/Ni^{IV} couple. These potentials are extremely low and indicate the Ni^{III} and Ni^{IV} oxidation states should be readily attainable.

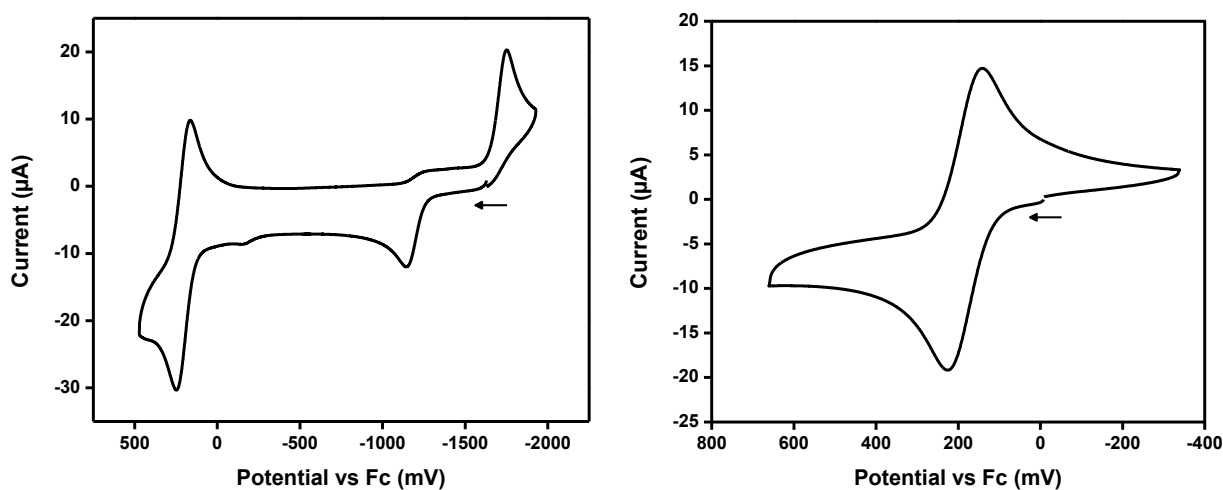


Figure 5.2 Cyclic voltammograms of **1** (left) and **2** (right) in 0.1 M Bu₄NPF₆ in MeCN with a scan rate of 100 mV/s.

5.3.2 Synthesis and Structure of Ni^{III} Complex.

Complex **1** was oxidized with 1 equivalent [Fc⁺]PF₆ in THF at -50°C to produce [(^{Me}N₄)Ni^{III}(cycloneophyl)]PF₆, **2**, as a red solid in 79% yield (Scheme 5.2). X-ray quality crystals of **2** were obtained from THF/pentane solutions (Figure 5.1). Complex **2** adopts a distorted octahedral geometry with an average axial Ni-N_{amine} bond length of 2.254 Å and a shorter average equatorial Ni-N_{pyridyl} bond length of 1.999 Å. As for the Ni-C bond lengths, the Ni-C_{sp3} was slightly longer than the Ni-C_{sp2} (1.973 Å vs 1.920 Å).

The EPR spectrum of complex **2** exhibited a pseudo-axial signal with a g_x , g_y , and g_z of 2.223, 2.201, and 2.012, respectively. Additionally, superhyperfine coupling was observed in the g_z direction ($A_{2N} = 14.5$ G) due to the two axial N donors ($I = 1$) coupling to the Ni^{III} center (Figure 5.3). These results are consistent with a distorted octahedral Ni^{III} metal center in a d_z^2 ground state.¹⁷⁻²¹ Overall, complex **2** provided a stable replacement for the previously synthesized [(^{Me}N₄)Ni^{III}Me₂]⁺ complex, providing an opportunity for the synthesis of a stable Ni^{IV} complex supported by the ^{Me}N₄ ligand system.

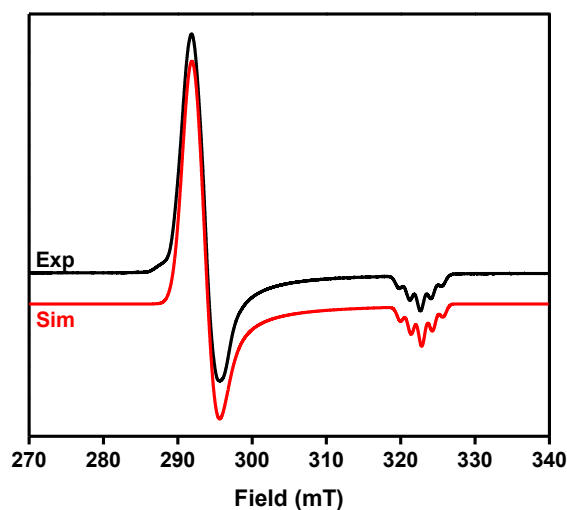


Figure 5.3 EPR spectrum (black line) of **2** in PrCN at 77K, and the simulated EPR spectrum (red line) using the following parameters: $g_x = 2.223$, $g_y = 2.201$, $g_z = 2.012$ ($A_{2N} = 14.5$ G).

5.3.3 Synthesis and Characterization of Ni^{IV} Complex.

Complex **2** was further oxidized using NOPF₆ in MeCN at -40°C to yield the desired [(^{Me}N4)Ni^{IV}(cycloneophyl)](PF₆)₂, **3** (Scheme 5.2). An X-ray structure of complex **3** was not obtained due to decomposition of X-ray quality crystals during data collection. However, the complex was confidently assigned via NMR and X-ray photoelectron spectroscopy (XPS). NMR experiments on complex **3** convincingly support the formation of a stabilized Ni^{IV} complex (Appendix A). The significant downfield shifts observed for complex **3** compared to complex **1** are characteristic of a highly oxidized species. The downfield shift was most notable for the aliphatic protons of the cycloneophyl group, which shift from 1.24 ppm in complex **1** to 5.33 ppm in complex **3**. The localized increase in electronegativity of a Ni^{IV} metal center is consistent with the significant deshielding we observed. Additionally, the observed XPS shift corresponding to binding energy between complexes **2** and **3** further supports a Ni^{IV} oxidation state (Figure 5.4 and 5.5). The observed increase in binding energy ($\Delta 2_{p_{3/2}}$, 0.54 eV and $\Delta 2_{p_{1/2}}$, 0.67 eV) for complex **3** is consistent with an oxidation of the nickel center. The difference in binding energy is minimal due to similarities in coordination geometry between complex **2** and **3**. As a whole, these experiments confidently confirmed the ^{Me}N4 ligand system is capable of supporting the Ni^{IV} oxidation state, providing viable evidence for our previously proposed reactivity pathways involving a Ni^{IV} intermediate (Chapter 4).

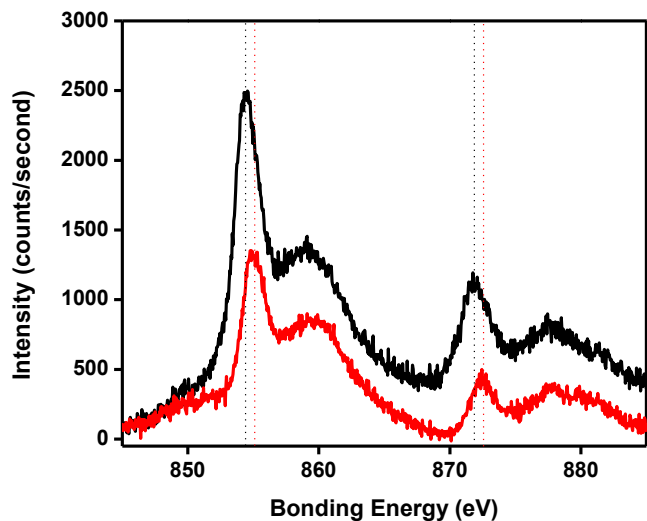


Figure 5.4 X-ray photoelectron spectra of the nickel region for complexes **2** (black line) and **3** (red line). Selected bonding energies (eV), **2**: $2p_{3/2}$, 854.43; $2p_{1/2}$, 871.79. **3**: $2p_{3/2}$, 854.97; $2p_{1/2}$, 872.46.

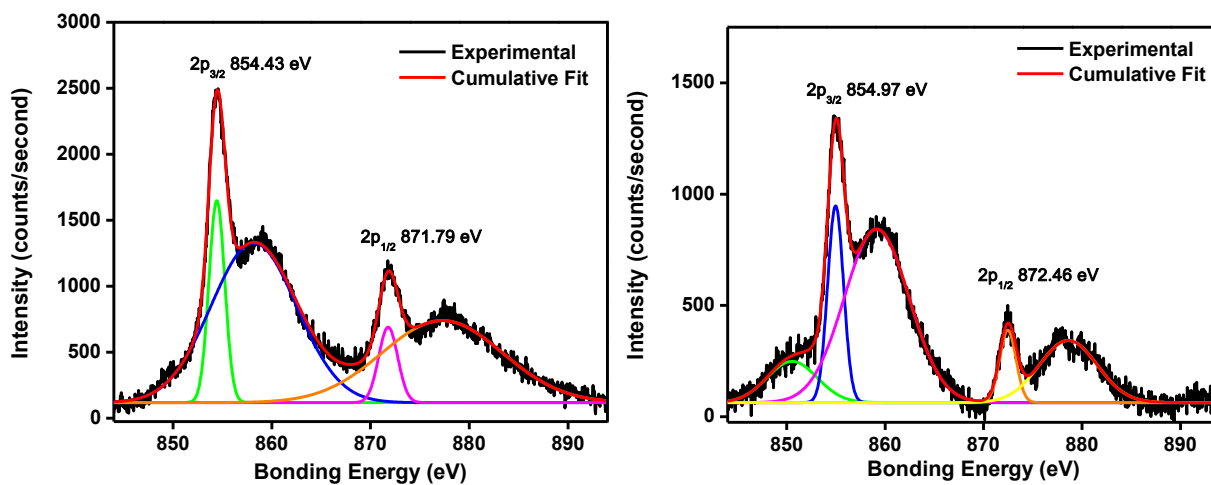
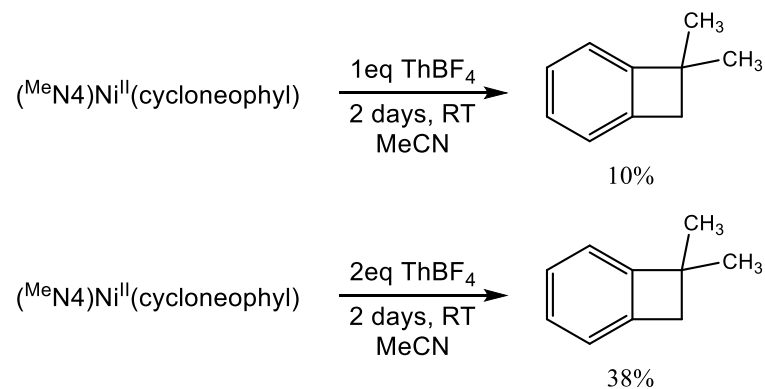


Figure 5.5 XPS spectrum of **2** (left) and **3** (right), Bonding energies: **2**, $2p_{3/2}$, 854.43 eV and $2p_{1/2}$, 871.79 eV; **3**, $2p_{3/2}$, 854.97 eV and $2p_{1/2}$, 872.46 eV.

5.3.4 C-C Bond Formation Reactivity.

In addition to the characterization of complex **3**, the reactivity of complex **1** was investigated using different oxidative conditions. Both one- and two- electron oxidations of complex **1** in MeCN at room temperature generated observable quantities of the C-C bond formation product via GC-FID (Scheme 5.3). Not surprisingly, complex **2** exhibited limited reactivity, however, the reactivity of **3** showed an increased amount of C-C bond formation product. These preliminary reactivity studies were successful in confirming the limited reductive elimination of complexes **2** and **3**. However, additional reactivity studies should be conducted to determine these complexes' affinity to nucleophilic attack, as well as their reactivity upon oxidation using a variety of different oxidants.

Scheme 5.3 C-C Bond Formation Reactivity of the $(^{\text{Me}}\text{N}_4)\text{Ni}^{\text{II}}(\text{cycloneophyl})$ Complex



5.4 Conclusion

In summary, the studies reported herein provide the synthesis of a stable Ni^{IV} complex using the cycloneophyl group and the ^{Me}N₄ ligand system. The identity of the Ni^{IV} complex was confirmed using comprehensive NMR and XPS studies. As a result, these studies provided validation to our previously proposed Ni^{IV} intermediates. Additionally, preliminary reactivity studies were successful in confirming the limited reductive elimination of the high-valent Ni^{III} and Ni^{IV} complexes due to the utilization of the cycloneophyl group. Overall, these studies provided a rare opportunity to directly investigate high-valent Ni complexes proposed as intermediates in C-C bond formation reactions.

5.5 Acknowledgements

I appreciate my colleagues Ying Zhang and Ming Cheng for their help and advice in performing the in situ ESI-MS experiments. Similarly, I appreciate Professor Nigam P. Rath of the Department of Chemistry and Biochemistry at the University of Missouri-St. Louis for his help and advice in solving all the reported crystal structures.

5.6 References

1. Koo, K. M.; Hillhouse, G. L.; Rheingold, A. L. *Organometallics* **1995**, *14*, 456.
2. Koo, K.; Hillhouse, G. L. *Organometallics* **1995**, *14*, 4421.
3. Camasso, N. M.; Sanford, M. S. *Science* **2015**, *347*, 1218.
4. Pérez-Temprano, M. H.; Racowski, J. M.; Kampf, J. W.; Sanford, M. S. *J. Am. Chem. Soc.* **2014**, *136*, 4097.

5. Camasso, N. M.; Pérez-Temprano, M. H.; Sanford, M. S. *J. Am. Chem. Soc.* **2014**, *136*, 12771.
6. Racowski, J. M.; Gary, J. B.; Sanford, M. S. *Angew. Chem. Int. Ed.* **2012**, *51*, 3414.
7. Qu, F.; Khusnutdinova, J. R.; Rath, N. P.; Mirica, L. M. *Chem. Commun.* **2014**, *50*, 3036.
8. Bour, J. R.; Camasso, N. M.; Sanford, M. S. *J. Am. Chem. Soc.* **2015**, *137*, 8034.
9. Unpublished results, Mirica Group.
10. Bottino, F.; Di Grazia, M.; Finocchiaro, P.; Fronczek, F. R.; Mamo, A.; Pappalardo, S. *J. Org. Chem.* **1988**, *53*, 3521.
11. Carmona, E.; Gutierrez-Puebla, E.; Marin, J. M.; Monge, A.; Paneque, M.; Poveda, M. L.; Ruiz, C. *J. Am. Chem. Soc.* **1989**, *111*, 2883.
12. Connelly, N. G.; Geiger, W. E. *Chem. Rev.* **1996**, *96*, 877.
13. Fulmer, G. R.; Miller, A. J. M.; Sherden, N. H.; Gottlieb, H. E.; Nudelman, A.; Stoltz, B. M.; Bercaw, J. E.; Goldberg, K. I. *Organometallics* **2010**, *29*, 2176.
14. Bruker Analytical X-Ray, Madison, WI, 2008
15. Sheldrick, G. *Acta Crystallogr. Sect. A: Found. Crystallogr.* **2008**, *64*, 112.
16. Burnett, M. N.; Johnson, C. K. *ORTEP-III: Oak Ridge Thermal Ellipsoid Plot Program for Crystal Structure Illustrations, Oak Ridge National Laboratory Report ORNL-6895* **1996**.
17. Grove, D. M.; Vankoten, G.; Mul, W. P.; Vanderzeijden, A. A. H.; Terheijden, J.; Zoutberg, M. C.; Stam, C. H. *Organometallics* **1986**, *5*, 322.
18. van de Kuil, L. A.; Veldhuizen, Y. S. J.; Grove, D. M.; Zwikker, J. W.; Jenneskens, L. W.; Drenth, W.; Smeets, W. J. J.; Spek, A. L.; van Koten, G. *J. Organomet. Chem.* **1995**, *488*, 191.
19. Grove, D. M.; van Koten, G.; Zoet, R.; Murrall, N. W.; Welch, A. J. *J. Am. Chem. Soc.* **1983**, *105*, 1379.
20. Grove, D. M.; van Koten, G.; Mul, P.; Zoet, R.; van der Linden, J. G. M.; Legters, J.; Schmitz, J. E. J.; Murrall, N. W.; Welch, A. J. *Inorg. Chem.* **1988**, *27*, 2466.
21. Iluc, V. M.; Miller, A. J. M.; Anderson, J. S.; Monreal, M. J.; Mehn, M. P.; Hillhouse, G. L. *J. Am. Chem. Soc.* **2011**, *133*, 13055.

Chapter 6

Deprotonation of Pyridinophane Ligands Resulting in the Formation of Neutral Nickel(III) Complexes

6.1 Introduction

Recently, there has been a growing interest in metal-ligand cooperation and the role it could play in homogenous catalysis.¹⁻¹⁰ In a short period of time, metal-ligand cooperation has already been shown to facilitate the activation of H-H,¹¹⁻¹⁵ C-H (sp² and sp³),^{11,16-19} O-H,^{20,21} S-H,²¹⁻²³ N-H,^{21,24-29} B-H,³⁰ and most recently O-O bonds.³¹ These typically thermodynamically uphill reactions normally have to be conducted using harsh energy intensive processes, however the development of metal-ligand cooperation has made more environmentally benign procedures feasible.³²

A notable usage of metal-ligand cooperation is the recent use of the PNP pincer ligand, 2,6-bis-(di-tert-butylphosphinomethyl)pyridine, by Milstein and co-workers.^{11,12,31} They showed the PNP pincer complex [(PNP)Ir^I(COE)]PF₆ could facilitate the C-H activation of benzene by utilizing the dearomatization and subsequent aromatization of the PNP ligand. The aforementioned dearomatization occurs under mild reaction conditions resulting in the formation of the dearomatized complex, (PNP*)Ir^I(COE). The dearomatized complex can then undergo quantitative C-H activation of benzene to form the neutral (PNP)Ir^I(C₆H₅) complex with no overall change in oxidation state.¹¹

Inspired by the work of Milstein, we noticed several similarities between the tetradentate ligands, N,N'-di-tert-butyl-2,11-diaza[3.3](2,6)pyridinophane (^{tBu}N4)³³ and N,N'-di-methyl-2,11-diaza[3.3](2,6)pyridinophane (^{Me}N4)³⁴, and the PNP pincer ligand. As a result, the neutral high-valent complexes (^{Me}N4*)Ni^{III}Me₂ and (^{tBu}N4*)Ni^{II}Me₂ were synthesized and characterized. Interestingly, the resulting high-valent complexes were stable providing a unique platform for the study of metal-ligand cooperation. Furthermore, investigating metal-ligand cooperation systems

which utilize naturally abundant and cheap metals like nickel would greatly improve the implementation of these environmentally friendly procedures on an industrial scale.

6.2 Experimental Section

6.2.1 Synthesis of Ligands and Complexes

Reagents and Materials. All manipulations were carried out under a nitrogen atmosphere using standard Schlenk and glove box techniques if not indicated otherwise. All reagents for which synthesis is not given were commercially available from Aldrich, Acros, STREM or Pressure Chemical and were used as received without further purification. Solvents were purified prior to use by passing through a column of activated alumina using an MBRAUN SPS. $(^{\text{Me}}\text{N4})\text{Ni}^{\text{II}}\text{Me}_2$ (**1**), $(^{\text{tBu}}\text{N4})\text{Ni}^{\text{II}}\text{Me}_2$ (**2**), $[(^{\text{Me}}\text{N4})\text{Ni}^{\text{III}}\text{Me}_2]\text{PF}_6$ (**3**) and $[(^{\text{tBu}}\text{N4})\text{Ni}^{\text{III}}\text{Me}_2]\text{PF}_6$ (**4**) were prepared according to the same procedures previously reported in Chapter 4.

Synthesis of $(^{\text{Me}}\text{N4}^*)\text{Ni}^{\text{III}}\text{Me}_2$ (5**).** A solution of **3** (55.8 mg, 0.111 mmol) and lithium bis(trimethylsilyl)amide (37.2 mg, 0.222 mmol) in THF was stirred at room temperature for 30 minutes. The solvent was then removed under vacuum and the residue was extracted with diethyl ether. The diethyl ether solution was dried, the red residue was then further extracted with pentane. A red solid was isolated after drying to completion under vacuum (26.4 mg, 0.074 mmol, 67%). X-ray quality crystals were obtained by slow evaporation of an ether solution of $(^{\text{Me}}\text{N4})\text{Ni}^{\text{II}}\text{Me}_2$ at -35°C . Evans method (THF- d_8): $\mu_{\text{eff}} = 1.49\mu_{\text{B}}$. UV-Vis, λ , nm (ϵ , $\text{M}^{-1}\cdot\text{cm}^{-1}$), THF: 313 (3750), 425 (830), 532 (420).

Synthesis of (tBuN4*)Ni^{III}Me₂ (6). A solution of **4** (57.5 mg, 0.127 mmol) and lithium bis(trimethylsilyl)amide (42.5 mg, 0.254 mmol) in THF was stirred at room temperature for 30 minutes. The solvent was then removed under vacuum and the residue was extracted with diethyl ether. The diethyl ether solution was dried, the red residue was then further extracted with pentane. A red solid was isolated after drying to completion under vacuum (39.9 mg, 0.091 mmol, 93%). Evans method (THF-d₈): $\mu_{\text{eff}} = 1.51 \mu\text{b}$. UV-Vis, λ , nm (ϵ , M⁻¹·cm⁻¹), THF: 261 (10725), 310 (4040), 451 (890).

6.2.2 Physical Measurements

¹H NMR spectra were recorded on a Varian Mercury-300 spectrometer (300.121 MHz), Agilent DD2-500 spectrometer (499.885 MHz) or Agilent DD2-600 spectrometer (599.736 MHz). ¹³C NMR spectra were recorded on an Agilent DD2-600 spectrometer (599.736 MHz). Chemical shifts are reported in parts per million (ppm) with residual solvent resonance peaks as internal reference.³⁵ Abbreviations for the multiplicity of NMR signals are singlet (s), doublet (d), triplet (t), quartet (q), multiplet (m), and broad (br). UV-visible spectra were recorded on a Varian Cary 50 Bio spectrophotometer and are reported as λ_{max} , nm (ϵ , M⁻¹·cm⁻¹). EPR spectra were recorded on a JEOL JES-FA X-band (9.2 GHz) EPR spectrometer in frozen solution at 77 K. ESI-MS experiments were performed using a Thermo FT or Bruker Maxis Q-TOF mass spectrometer with an electrospray ionization source. ESI mass-spectrometry was provided by the Washington University Mass Spectrometry Resource. Elemental analyses were carried out by the Columbia Analytical Services Tucson Laboratory.

Cyclic voltammetry (CV) experiments were performed using a BASi EC Epsilon electrochemical workstation or a CHI 660D Electrochemical Analyzer. Electrochemical-grade

supporting electrolytes were purchased from Fluka. The electrochemical measurements were performed under a blanket of nitrogen, and the analyzed solutions were deaerated by purging with nitrogen. A glassy carbon disk electrode ($d = 1.6$ mm) was used as the working electrode for cyclic voltammetry. The auxiliary electrode was a Pt wire for cyclic voltammetry measurements. Two different non-aqueous reference electrodes were used: Ag/filled with 0.01M $\text{AgNO}_3/0.1\text{M}$ $\text{Bu}_4\text{NClO}_4/\text{MeCN}$ solution or silver wire. The reference electrode was calibrated against ferrocene (Fc) at the conclusion of each CV experiment.

X-ray diffraction quality crystals of $(^{\text{Me}}\text{N4})\text{Ni}^{\text{II}}\text{Me}_2$ were obtained by slow pentane vapor diffusion into a diethyl ether solution. Similarly, quality crystals of $(^{\text{tBu}}\text{N4})\text{Ni}^{\text{II}}\text{Me}_2$ were obtained by slow evaporation of a diethyl ether solution. X-ray diffraction quality crystals of $[(^{\text{Me}}\text{N4})\text{Ni}^{\text{III}}\text{Me}_2]\text{BPh}_4$ and $[(^{\text{tBu}}\text{N4})\text{Ni}^{\text{III}}\text{Me}_2]\text{BPh}_4$ were obtained by slow pentane vapor diffusion into a tetrahydrofuran solutions. Remarkably, X-ray diffraction quality crystals of $(^{\text{Me}}\text{N4}^*)\text{Ni}^{\text{III}}\text{Me}_2$ were obtained serendipitously from a slow evaporation of complex **1** in a diethyl ether solution. Suitable crystals of appropriate dimensions were mounted and preliminary examination and data collection were performed using a Bruker Kappa Apex-II Charge Coupled Device (CCD) Detector system single crystal X-Ray diffractometer equipped with an Oxford Cryostream LT device. Data were collected using graphite monochromated Mo $\text{K}\alpha$ radiation ($\lambda = 0.71073$ Å) from a fine focus sealed tube X-Ray source. Apex II and SAINT software packages³⁶ were used for data collection and data integration. Final cell constants were determined by global refinement of reflections from the complete data set. Data were corrected for systematic errors using SADABS³⁶ based on the Laue symmetry using equivalent reflections. Structure solutions and refinement were carried out using the SHELXTL- PLUS software package.³⁷ The structures were refined with full matrix least-squares refinement by minimizing $\sum w(F_o^2 - F_c^2)^2$. All non-

hydrogen atoms were refined anisotropically to convergence. Typically, H atoms are added at the calculated positions in the final refinement cycles. The complete listings of x-ray diffraction parameters are included in Appendix B.

6.2.3 Deprotonation Comparison Studies

UV-Vis studies for deprotonation reaction. A 0.125 mM solution of **3** or **4** in tetrahydrofuran was placed into a quartz cuvette (1 cm pathlength) equipped with a septum-sealed cap and a magnetic stirring bar. The preliminary spectrum was then collected. To the cuvette 5 equivalents lithium bis(trimethylsilyl)amide was added and the spectrum was again collected. Lastly, 5 equivalents trifluoromethanesulfonic acid was added and the final spectrum was collected. The reactivity reaction was then monitored using a Varian Cary 50 Bio spectrophotometer.

EPR studies for deprotonation reaction. A 1.0 mM stock solution of **3** or **4** in 3:1 tetrahydrofuran-toluene was prepared. A 500 μ L aliquot of the stock solution was placed into a sealed EPR tube. Five equivalents lithium bis(trimethylsilyl)amide was added to the remaining stock solution. Another 500 μ L aliquot was placed in a second EPR tube. Lastly, five equivalents trifluoromethanesulfonic acid were added to the basified-stock solution. A final 500 μ L aliquot was placed in a third EPR tube. Additional toluene was added to each EPR tube to adjust the samples to a similar final concentration. All three samples were then frozen (77 K) and analyzed using a JEOL JES-FA X-band (9.2 GHz) EPR spectrometer.

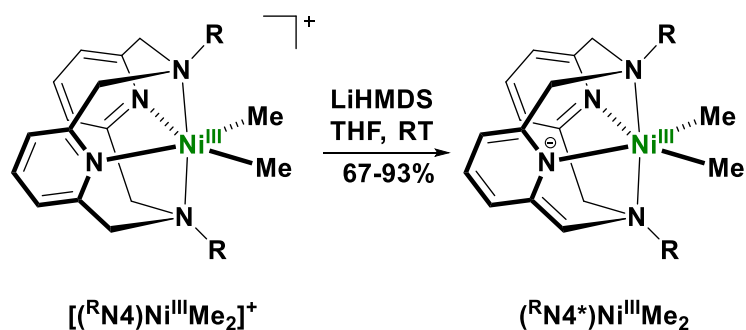
ESI-MS studies for deprotonation reaction. To start, 0.012 M solutions of ^tBuN4 and **6** in concentrated DCl/D₂O were prepared. Additionally, a 0.024 M solution of ^tBuN4 in the presence of 5 equivalents lithium bis(trimethylsilyl)amide was prepared in THF and diluted with an equal volume of concentrated DCl/D₂O. The three samples were then heated at 70°C for 1 hour, at which point each sample was diluted with 1 mL deuterated methanol. The diluted samples were further diluted to achieve a final concentration of approximately 2 μM. The final samples were injected into the instrument to determine the percentage of deuterium incorporated into the free ligand.

6.3 Results and Discussion

6.3.1 Synthesis and Structure of Deprotonated Ni^{III} Complex.

Complexes **3** and **4** were deprotonated with 1 equivalent lithium bis(trimethylsilyl)amide in THF at room temperature to yield [^{Me}N4*]Ni^{III}Me₂, **5**, and [^tBuN4*]Ni^{III}Me₂, **6**, as red solids in 67% and 93% yield, respectively (Scheme 6.1). To determine whether the deprotonated complexes were actually isolated, a deuterium quenching experiment was conducted using complex **6**. Complex **5** and the analogous controls all decomposed under the reaction conditions, therefore only the results for complex **6** are discussed. The experiment was conducted by exposing complex **6** and free ^tBuN4 ligand (with and without prior exposure to base) to concentrated DCl in D₂O, and determining the percentage of deuterium incorporation. The isolated complex showed approximately 70% deuterium adducts versus 6% for the free ligand. With these results we are confident our isolated complexes are in the deprotonated state.

Scheme 6.1 Synthesis of $(^R\text{N}4^*)\text{Ni}^{\text{III}}\text{Me}_2$ Complex ($R = \text{tBu}$ or Me).



Additionally, quality crystals of **5** for single crystal X-ray diffraction analysis were obtained from a slow evaporation of complex **1** in diethyl ether. This unexpected crystal allowed for a direct structural comparison between complexes **3** and **5** (Figure 6.1). Complex **5** adopts a distorted octahedral geometry in which the aromaticity of one pyridine ring has been disturbed resulting in an average axial Ni-N_{amine} bond length of 2.242 Å and an average equatorial Ni-N_{pyridyl} bond length of 1.960 Å. Compared to complex **3** the average Ni-N_{pyridyl} bond length of **5** is shortened due to one Ni-N_{pyridyl} bond length being significantly shorter, 1.945 Å, as a result of the anionic character now associated with that pyridine. Furthermore, the average Ni-C_{Me} bond length, 1.962 Å, was also shortened compared to complex **3**. Further attempts to obtain quality crystals of complex **5** from isolated samples failed due to the ease in which the complex is protonated, however continued effort in the regard is ongoing.

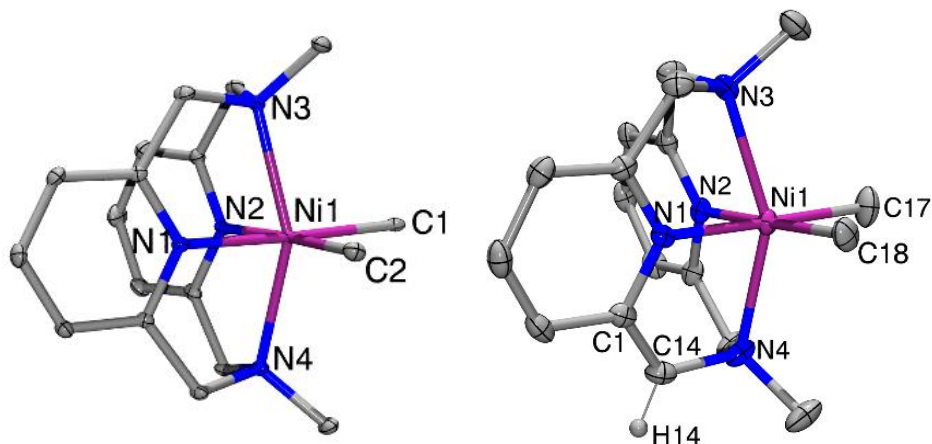


Figure 6.1 ORTEP³⁸ representation of the cations **3** (left) and **5** (right) with 50% probability thermal ellipsoids. Selected bond lengths (Å), **3**: Ni1-C1, 1.987; Ni1-C2, 1.978; Ni1-N1, 1.979; Ni1-N2, 1.996; Ni1-N3, 2.252; Ni1-N4, 2.240; **5**: Ni1-C18, 1.959; Ni1-C17, 1.965; Ni1-N1, 1.945; Ni1-N2, 1.974; Ni1-N3, 2.233; Ni1-N4, 2.251, N4-C14, 1.455; C1-C14, 1.358; C14-H14, 0.970. Selected bond angles, **5**: C1-C14-H14, 122.8°. A complete listings of structural parameters are included in Appendix B.

6.3.2 Comparison of Cationic and Deprotonated Ni^{III} Complexes.

The deprotonation of complexes **3** and **4** was monitored using EPR and UV-Vis spectroscopy. The EPR spectra of complexes **3** and **5** exhibited pseudo axial signals, whereas the EPR spectra of complexes **4** and **6** exhibited rhombic signals. Additionally, all complexes exhibit superhyperfine coupling in the g_z direction due to the two axial N donors ($I = 1$) coupling to the Ni^{III} metal center (Figure 6.2 and 6.3). These results are consistent with a distorted octahedral Ni^{III} metal center in a d_z^2 ground state.³⁹⁻⁴³ The deprotonation of both complexes **3** and **4** resulted in small yet significant shifts of the g_x and g_y values, therefore we could monitor the deprotonation reaction using via EPR spectroscopy.

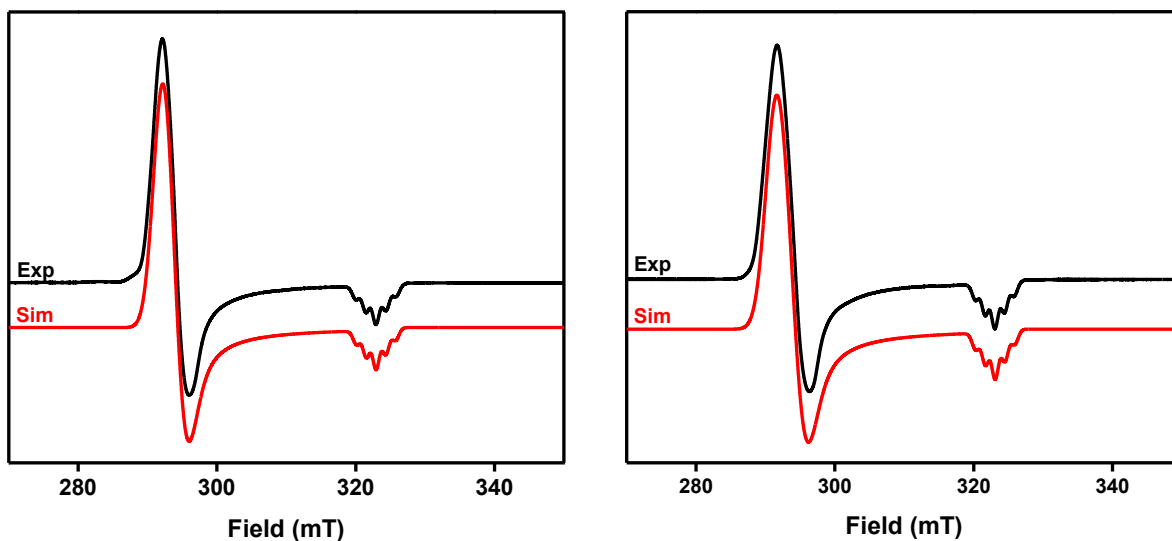


Figure 6.2 Comparison of EPR spectra of $[(^{\text{Me}}\text{N4})\text{Ni}^{\text{III}}\text{Me}_2]\text{PF}_6$ (right) and $(^{\text{Me}}\text{N4}^*)\text{Ni}^{\text{III}}\text{Me}_2$ (left) in 3:1 THF-Toluene at 77 K. The simulated EPR spectra (red lines) were obtained using the following parameters: $[(^{\text{Me}}\text{N4})\text{Ni}^{\text{III}}\text{Me}_2]\text{PF}_6$; $g_x=2.225$, $g_y=2.208$, $g_z=2.013$ ($A_{2\text{N}}=14.0$ G) and $(^{\text{Me}}\text{N4}^*)\text{Ni}^{\text{III}}\text{Me}_2$; $g_x=2.231$, $g_y=2.208$, $g_z=2.012$ ($A_{2\text{N}}=14.0$ G).

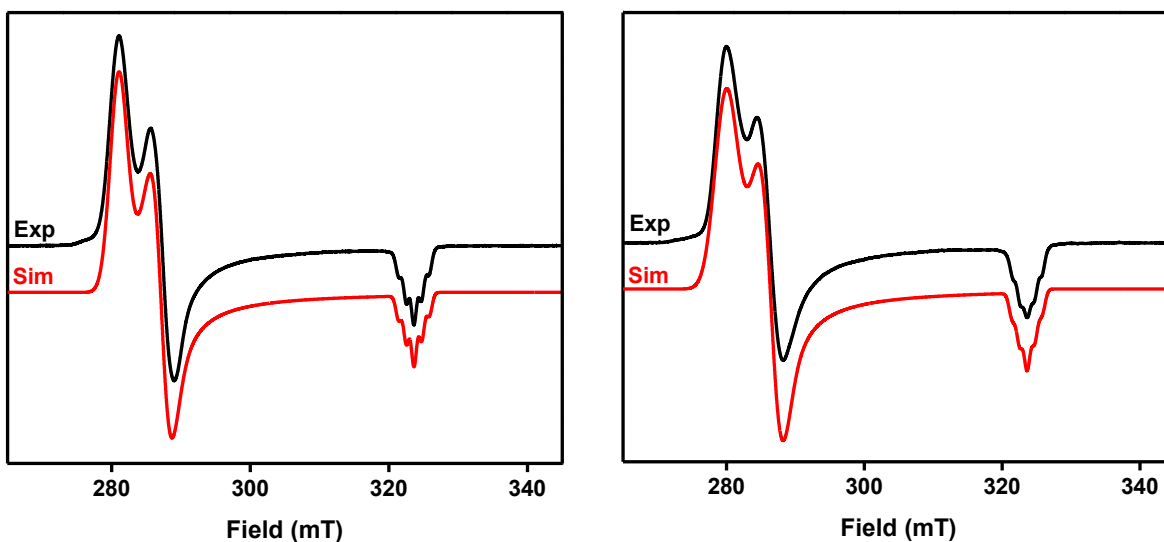


Figure 6.3 Comparison of EPR spectra of $[(^{\text{tBu}}\text{N4})\text{Ni}^{\text{III}}\text{Me}_2]\text{PF}_6$ (right) and $(^{\text{tBu}}\text{N4}^*)\text{Ni}^{\text{III}}\text{Me}_2$ (left) in 3:1 THF-Toluene at 77 K. The simulated EPR spectra (red lines) were obtained using the following parameters: $[(^{\text{tBu}}\text{N4})\text{Ni}^{\text{III}}\text{Me}_2]\text{PF}_6$; $g_x=2.314$, $g_y=2.264$, $g_z=2.009$ ($A_{2\text{N}}=11.0$ G) and $(^{\text{tBu}}\text{N4}^*)\text{Ni}^{\text{III}}\text{Me}_2$; $g_x=2.323$ ($A_{\text{N}}=8.0$), $g_y=2.269$ ($A_{\text{N}}=8.0$), $g_z=2.009$ ($A_{2\text{N}}=10.75$ G).

The UV-Vis spectra of complexes **3** and **5** exhibit similar features, however the extension coefficients for the cationic complex **3** are significantly reduced compared to the deprotonated complex **5** (Figure 6.4). Similarly, complexes **4** and **6** have similar peaks of interest, which follow a similar trend of increasing extension coefficients upon deprotonation (Figure 6.5). These resulting shifts in g-values and extension coefficients were further highlighted by performing a toggle experiment, by first reacting complexes **3** and **4** with lithium bis(trimethylsilyl)amide (LiHMDS) and monitoring the change in-situ of the EPR and UV-Vis spectra. The resulting complexes **5** and **6** were then reacted with trifluoromethanesulfonic acid (TfOH) to return the complex to the cationic starting complexes (Figure 6.6 and 6.7). As a whole, these results confirm that complexes **3** and **4** can undergo deprotonation to form stable neutral Ni^{III}Me₂ complexes.

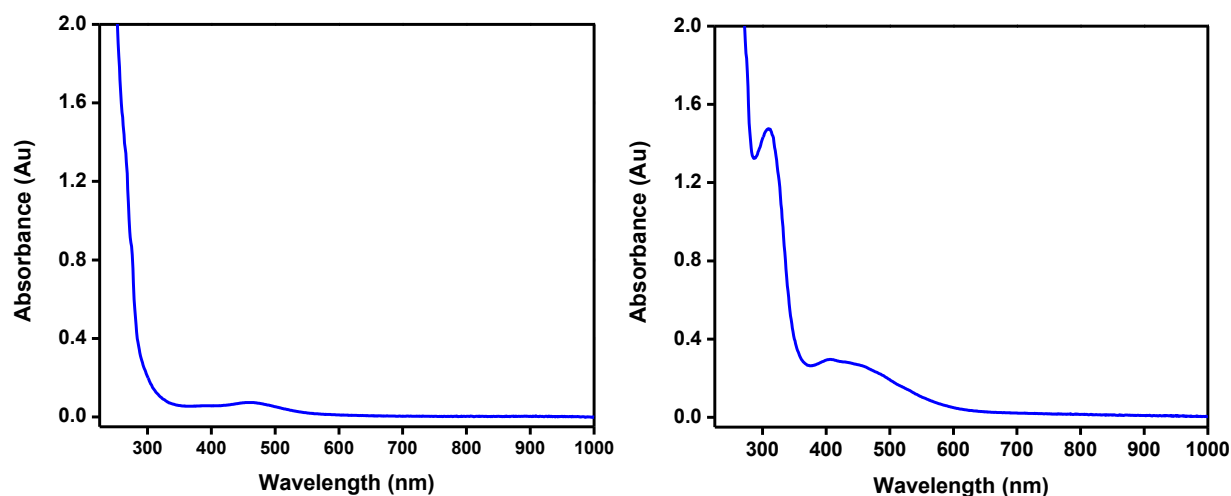


Figure 6.4 Comparison of UV-Vis spectra of $[(\text{Me}_4\text{N})\text{Ni}^{\text{III}}\text{Me}_2]\text{PF}_6$ (right) and $(\text{Me}_4\text{N}^+)\text{Ni}^{\text{III}}\text{Me}_2$ (left) in THF (1.25×10^{-4} M).

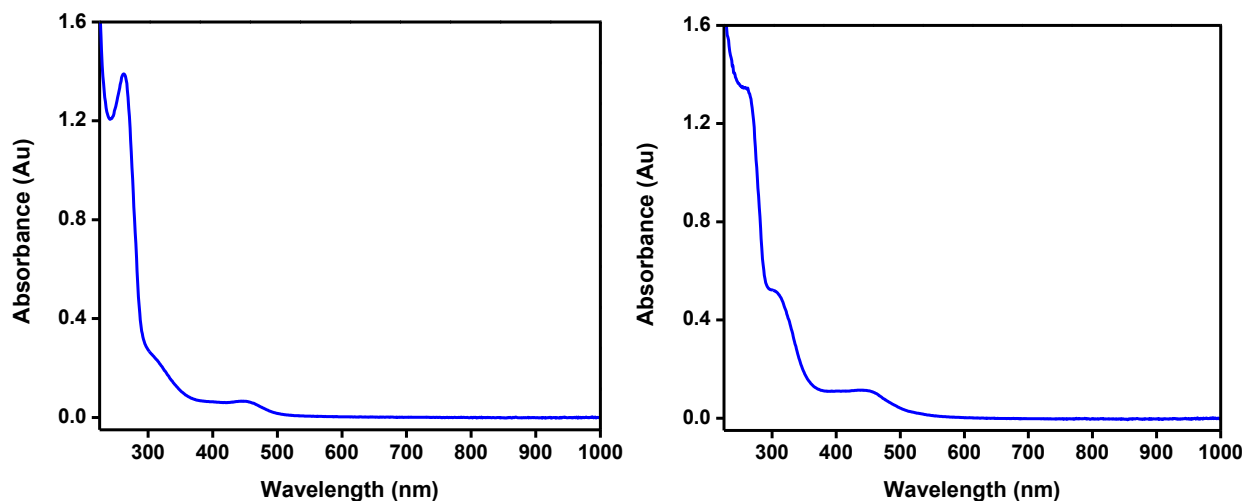


Figure 6.5 Comparison of UV-Vis spectra of $[(^t\text{BuN4})\text{Ni}^{\text{III}}\text{Me}_2]\text{PF}_6$ (right) and $(^t\text{BuN4}^*)\text{Ni}^{\text{III}}\text{Me}_2$ (left) in THF (1.25×10^{-4} M).

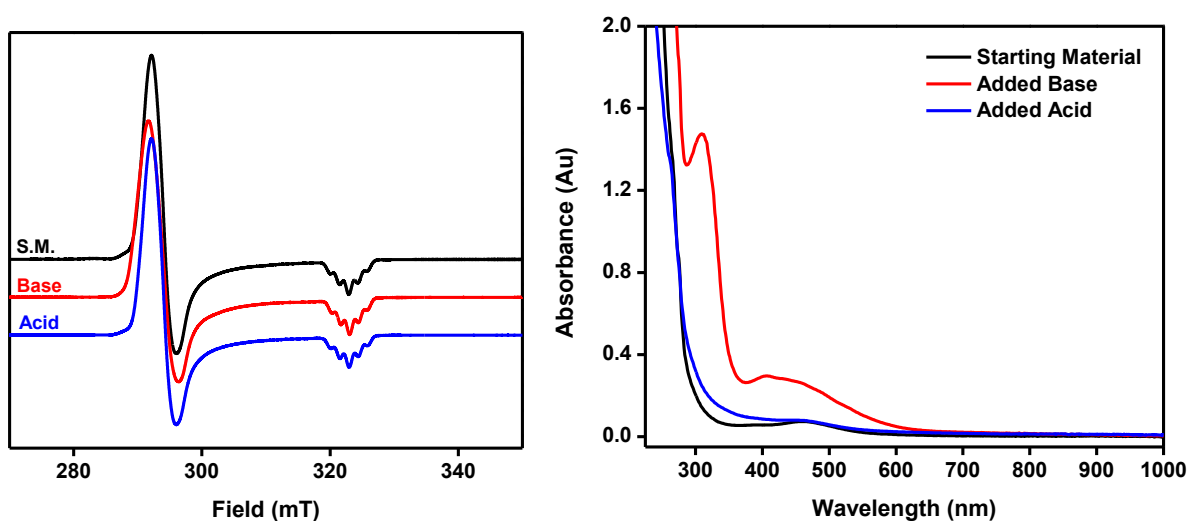


Figure 6.6 Interconversion between $[(^{\text{Me}}\text{N4})\text{Ni}^{\text{III}}\text{Me}_2]\text{PF}_6$ (black & blue lines) and $(^{\text{Me}}\text{N4}^*)\text{Ni}^{\text{III}}\text{Me}_2$ (red line) monitored by EPR (right) and UV-visible (left) spectroscopy. Lithium bis(trimethylsilyl)amide (base) and trifluoromethanesulfonic acid (acid) were added as stock solutions.

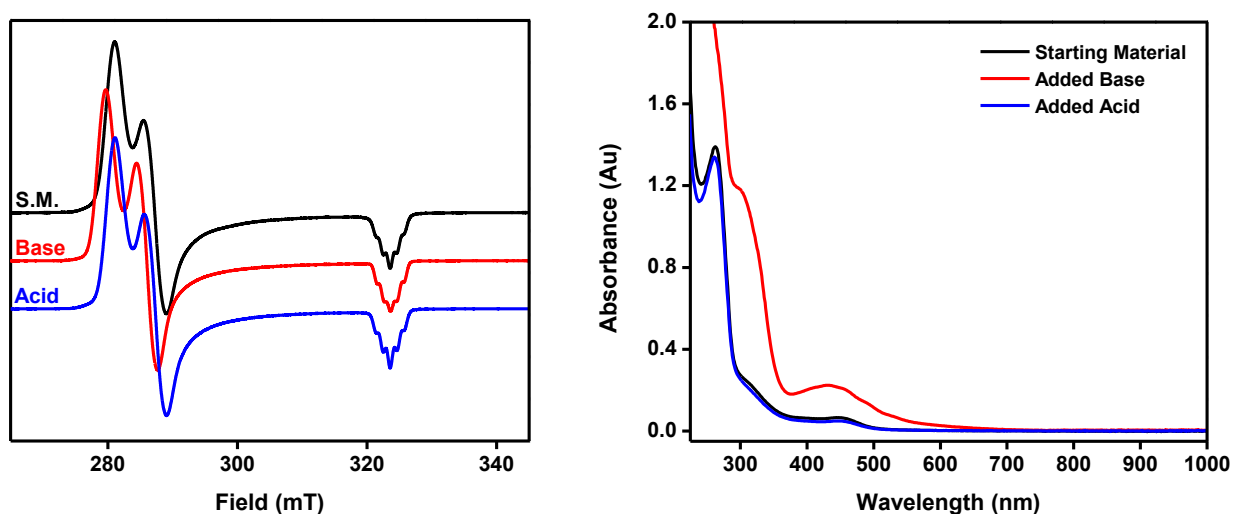
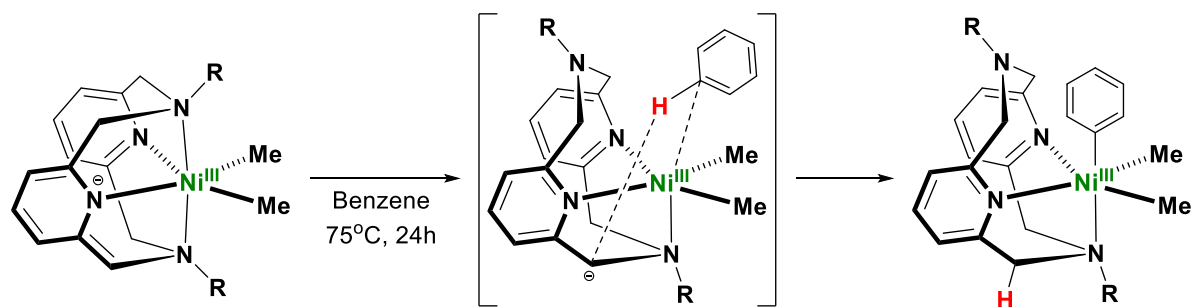


Figure 6.7 Interconversion between $[(^t\text{BuN4})\text{Ni}^{\text{III}}\text{Me}_2]\text{PF}_6$ (black & blue lines) and $(^t\text{BuN4}^*)\text{Ni}^{\text{III}}\text{Me}_2$ (red line) monitored by EPR (right) and UV-visible (left) spectroscopy. Lithium bis(trimethylsilyl)amide (base) and trifluoromethanesulfonic acid (acid) were added as stock solutions.

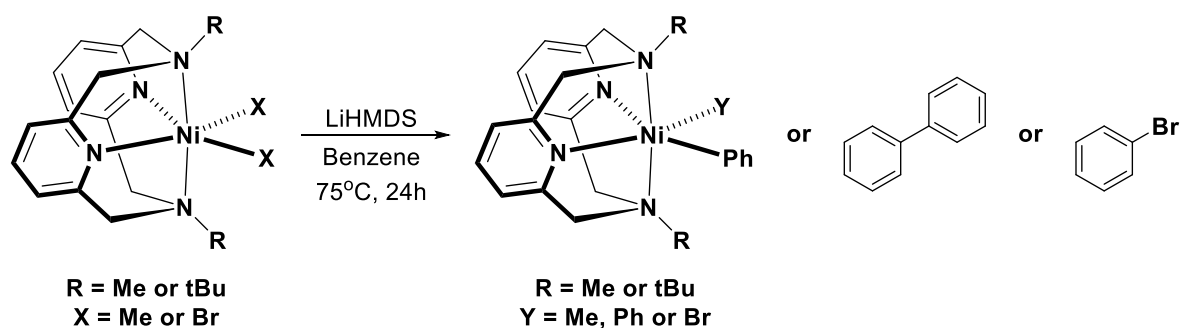
6.3.3 Preliminary C-H Activation Studies.

On account of the observed deprotonation of the above nickel complexes, as well as the previously observed reactivity of the $(\text{PNP}^*)\text{Ir}^{\text{I}}(\text{COE})$ complex with benzene, we proposed that these pyridinophane supported nickel complexes could similarly facilitate the C-H activation (Scheme 6.2). Therefore, solutions of complexes **1**, **2**, and $(^t\text{BuN4})\text{Ni}^{\text{II}}\text{Br}_2$ in benzene were exposed to LiHMDS and heat (75°C) for 24 hours. The reactions were monitored by NMR and gas chromatography (GC). However, no desired products were observed (Scheme 6.3). These were only preliminary studies and investigating different reaction conditions is needed to confidently ascertain whether these complexes are capable of C-H activation (i.e. varying the temperature, solvent and base used). Additionally, different types of C-H compounds with varying bond strengths should be investigated.

Scheme 6.2 Proposed mechanism for C-H activation by pyridinophane supported Ni complexes.



Scheme 6.3 C-H activation reactivity of pyridinophane supported nickel complexes.



6.4 Conclusion

In summary, the studies reported herein provide evidence for the deprotonation of the pyridinophane ligand system (N4) resulting in the formation of neutral Ni^{III} dimethyl complexes. The deprotonation reactions were monitored and confirmed in-situ by using UV-Vis and EPR spectroscopy. Additionally, a crystal structure of the ^{Me}N4 supported deprotonated complex, (^{Me}N4*)Ni^{III}Me₂, was independently ascertained serendipitously. Lastly, these complexes were unable to facilitate the C-H activation of benzene. Consequently, further investigation is needed to properly determine whether these complexes are capable of C-H activation.

6.5 Acknowledgements

I appreciate Professor Nigam P. Rath of the Department of Chemistry and Biochemistry at the University of Missouri-St. Louis for his help and advice in solving all the reported crystal structures. Additionally, I appreciate my colleagues Ying Zhang and Ming Cheng for their help and advice in performing the in situ ESI-MS experiments.

6.6 References

1. Grützmacher, H. *Angew. Chem. Int. Ed.* **2008**, *47*, 1814.
2. Noyori, R.; Ohkuma, T. *Angew. Chem. Int. Ed.* **2001**, *40*, 40.
3. Clapham, S. E.; Hadzovic, A.; Morris, R. H. *Coord. Chem. Rev.* **2004**, *248*, 2201.
4. Ikariya, T.; Blacker, A. J. *Acc. Chem. Res.* **2007**, *40*, 1300.
5. Maire, P.; Büttner, T.; Breher, F.; Le Floch, P.; Grützmacher, H. *Angew. Chem. Int. Ed.* **2005**, *44*, 6318.
6. Fryzuk, M. D.; MacNeil, P. A. *Organometallics* **1983**, *2*, 682.
7. Samec, J. S. M.; Backvall, J.-E.; Andersson, P. G.; Brandt, P. *Chem. Soc. Rev.* **2006**, *35*, 237.
8. Casey, C. P.; Beetner, S. E.; Johnson, J. B. *J. Am. Chem. Soc.* **2008**, *130*, 2285.
9. Shvo, Y.; Czarkie, D.; Rahamim, Y.; Chodosh, D. F. *J. Am. Chem. Soc.* **1986**, *108*, 7400.
10. Bullock, R. M. *Chemistry – A European Journal* **2004**, *10*, 2366.
11. Ben-Ari, E.; Leitun, G.; Shimon, L. J. W.; Milstein, D. *J. Am. Chem. Soc.* **2006**, *128*, 15390.
12. Schwartsburd, L.; Iron, M. A.; Konstantinovski, L.; Diskin-Posner, Y.; Leitun, G.; Shimon, L. J. W.; Milstein, D. *Organometallics* **2010**, *29*, 3817.
13. Schwartsburd, L.; Iron, M. A.; Konstantinovski, L.; Ben-Ari, E.; Milstein, D. *Organometallics* **2011**, *30*, 2721.

14. Musa, S.; Filippov, O. A.; Belkova, N. V.; Shubina, E. S.; Silantyev, G. A.; Ackermann, L.; Gelman, D. *Chemistry – A European Journal* **2013**, *19*, 16906.
15. Bichler, B.; Holzhaecker, C.; Stöger, B.; Puchberger, M.; Veiros, L. F.; Kirchner, K. *Organometallics* **2013**, *32*, 4114.
16. Prechtel, M. H. G.; Hölscher, M.; Ben-David, Y.; Theyssen, N.; Loschen, R.; Milstein, D.; Leitner, W. *Angew. Chem. Int. Ed.* **2007**, *46*, 2269.
17. Kloek, S. M.; Heinekey, D. M.; Goldberg, K. I. *Angew. Chem. Int. Ed.* **2007**, *46*, 4736.
18. de Boer, S. Y.; Gloaguen, Y.; Lutz, M.; van der Vlugt, J. I. *Inorg. Chim. Acta* **2012**, *380*, 336.
19. Hanson, S. K.; Heinekey, D. M.; Goldberg, K. I. *Organometallics* **2008**, *27*, 1454.
20. Kohl, S. W.; Weiner, L.; Schwartsburd, L.; Konstantinovski, L.; Shimon, L. J. W.; Ben-David, Y.; Iron, M. A.; Milstein, D. *Science* **2009**, *324*, 74.
21. Scharf, A.; Goldberg, I.; Vigalok, A. *Inorg. Chem.* **2014**, *53*, 12.
22. van der Vlugt, J. I.; Pidko, E. A.; Bauer, R. C.; Gloaguen, Y.; Rong, M. K.; Lutz, M. *Chemistry – A European Journal* **2011**, *17*, 3850.
23. van der Vlugt, J. I.; Lutz, M.; Pidko, E. A.; Vogt, D.; Spek, A. L. *Dalton Trans.* **2009**, 1016.
24. Feller, M.; Diskin-Posner, Y.; Shimon, L. J. W.; Ben-Ari, E.; Milstein, D. *Organometallics* **2012**, *31*, 4083.
25. Khaskin, E.; Iron, M. A.; Shimon, L. J. W.; Zhang, J.; Milstein, D. *J. Am. Chem. Soc.* **2010**, *132*, 8542.
26. Chang, Y.-H.; Nakajima, Y.; Tanaka, H.; Yoshizawa, K.; Ozawa, F. *Organometallics* **2014**, *33*, 715.
27. Chang, Y.-H.; Nakajima, Y.; Tanaka, H.; Yoshizawa, K.; Ozawa, F. *J. Am. Chem. Soc.* **2013**, *135*, 11791.
28. Myers, T. W.; Berben, L. A. *J. Am. Chem. Soc.* **2013**, *135*, 9988.
29. de Boer, S. Y.; Gloaguen, Y.; Reek, J. N. H.; Lutz, M.; van der Vlugt, J. I. *Dalton Trans.* **2012**, *41*, 11276.

30. Anaby, A.; Butschke, B.; Ben-David, Y.; Shimon, L. J. W.; Leitus, G.; Feller, M.; Milstein, D. *Organometallics* **2014**, *33*, 3716.
31. Feller, M.; Ben-Ari, E.; Diskin-Posner, Y.; Carmieli, R.; Weiner, L.; Milstein, D. *J. Am. Chem. Soc.* **2015**, *137*, 4634.
32. Gunanathan, C.; Milstein, D. *Chem. Rev.* **2014**, *114*, 12024.
33. Che, C. M.; Li, Z. Y.; Wong, K. Y.; Poon, C. K.; Mak, T. C. W.; Peng, S. M. *Polyhedron* **1994**, *13*, 771.
34. Bottino, F.; Di Grazia, M.; Finocchiaro, P.; Fronczek, F. R.; Mamo, A.; Pappalardo, S. *J. Org. Chem.* **1988**, *53*, 3521.
35. Fulmer, G. R.; Miller, A. J. M.; Sherden, N. H.; Gottlieb, H. E.; Nudelman, A.; Stoltz, B. M.; Bercaw, J. E.; Goldberg, K. I. *Organometallics* **2010**, *29*, 2176.
36. Bruker Analytical X-Ray, Madison, WI, 2008
37. Sheldrick, G. *Acta Crystallogr. Sect. A: Found. Crystallogr.* **2008**, *64*, 112.
38. Burnett, M. N.; Johnson, C. K. *ORTEP-III: Oak Ridge Thermal Ellipsoid Plot Program for Crystal Structure Illustrations, Oak Ridge National Laboratory Report ORNL-6895* **1996**.
39. Grove, D. M.; Vankoten, G.; Mul, W. P.; Vanderzeijden, A. A. H.; Terheijden, J.; Zoutberg, M. C.; Stam, C. H. *Organometallics* **1986**, *5*, 322.
40. van de Kuil, L. A.; Veldhuizen, Y. S. J.; Grove, D. M.; Zwikker, J. W.; Jenneskens, L. W.; Drenth, W.; Smeets, W. J. J.; Spek, A. L.; van Koten, G. *J. Organomet. Chem.* **1995**, *488*, 191.
41. Grove, D. M.; van Koten, G.; Zoet, R.; Murrall, N. W.; Welch, A. J. *J. Am. Chem. Soc.* **1983**, *105*, 1379.
42. Grove, D. M.; van Koten, G.; Mul, P.; Zoet, R.; van der Linden, J. G. M.; Legters, J.; Schmitz, J. E. J.; Murrall, N. W.; Welch, A. J. *Inorg. Chem.* **1988**, *27*, 2466.
43. Iluc, V. M.; Miller, A. J. M.; Anderson, J. S.; Monreal, M. J.; Mehn, M. P.; Hillhouse, G. L. *J. Am. Chem. Soc.* **2011**, *133*, 13055.

Chapter 7

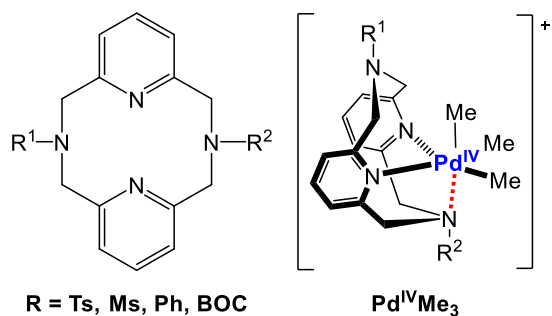
Future Directions

7.1 Reactivity of Organometallic Palladium Complexes

In chapter 2, we showed an organometallic $\text{Pd}^{\text{II}}\text{Me}_2$ complex supported by the newly synthesized “pseudo-tridentate” N4 ligand, $^{\text{TsMe}}\text{N}_4$, showed a slightly improved rate of C-C bond formation reactivity. The pseudo-tridentate nature of the $^{\text{TsMe}}\text{N}_4$ ligand was shown via spectroscopic methods to destabilize the high-valent Pd^{III} metal center, leading a more rapid C-C bond formation. However, upon further investigation, the improvement was found to be due to the reaction proceeding directly to the key $\text{Pd}^{\text{IV}}\text{Me}_3$ intermediate. Therefore, the subsequent reductive elimination was minimally affected by the destabilization of the Pd^{III} intermediate.

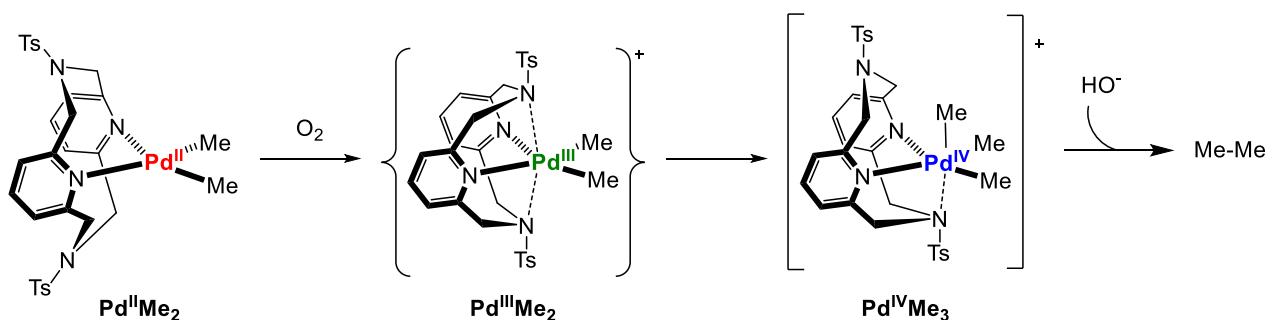
These studies showed the rate determining step controlling the aerobically induced C-C bond formation is the reductive elimination of ethane from the key $\text{Pd}^{\text{IV}}\text{Me}_3$ intermediate. To this point, we propose future experiments should be focused in two major areas. The continued destabilization of the $\text{Pd}^{\text{III}}\text{Me}_2$ intermediate, as well as the destabilization of the $\text{Pd}^{\text{IV}}\text{Me}_3$ intermediate via modifications to the N4 ligand system. By continuing to vary the substituents on the axial amines we can possibly further destabilize these key intermediates (Scheme 7.1).

Scheme 7.1 Possible modifications to the N4 ligand system.



The use of the symmetric TsN_4 ligand could accomplish both these objectives. The TsN_4 ligand would have a more limited donating ability than the TsMeN_4 ligand due to the two tosylated amines (Scheme 7.2). The resulting $\text{Pd}^{\text{III}}\text{Me}_2$ intermediate would be greatly destabilized, and hopefully result in a more rapid formation of the $\text{Pd}^{\text{IV}}\text{Me}_3$ intermediate. Similarly, the two tosylated amines would allow the $\text{Pd}^{\text{IV}}\text{Me}_3$ intermediate to more rapidly achieve the 5-coordinate geometry necessary to undergo reductive elimination.¹⁻³ Overall, we propose these experiments will improve the rate of reactivity, giving us a greater insight into the scope of high-valent palladium catalysis.

Scheme 7.2 Proposed aerobically induced C-C bond formation reactivity of the $(\text{TsN}_4)\text{Pd}^{\text{II}}\text{Me}_2$ complex.



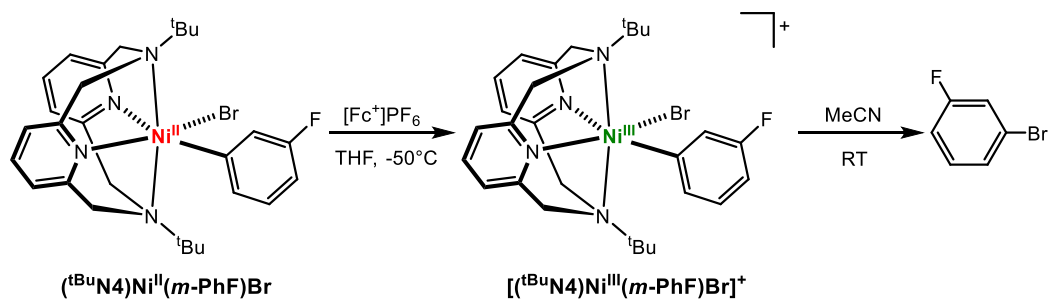
7.2 Characterization of Arene-Substituted Nickel Complexes

The synthesis of a series of *ortho*-substituted organometallic Ni^{III} complexes reported in Chapter 3 allowed for a direct comparison to the previously synthesized *para*-substituted counterparts. To study the impact of altering the ligand's electronic and steric effects, the *ortho*- and *para*-substituted complexes were characterized and their reactivity investigated. Interestingly, the *ortho*-substituents were found to destabilize the resulting Ni^{III} intermediates. The decreased stability had varying effects ranging from greatly improving the rate of reactivity to preventing the

formation of the desired product. Overall, these studies have confirmed the importance ligand electronics and sterics play in controlling the stability of high-valent nickel intermediates.

To further our understanding of these effects, we propose additional reactivity studies to be conducted on the *ortho*-substituted complexes. By using different reaction conditions, oxidants, and characterization methods we may be able to improve our analysis of these destabilized high-valent nickel complexes. Additionally, the *meta*-substituted complexes should be investigated and similarly compared to the *ortho*- and *para*-substituted complexes (Scheme 7.3). Overall, these studies are valuable for the developing more efficient and selective catalysts for various catalytic transformations.

Scheme 7.3 Proposed synthesis and reactivity of *meta*-substituted nickel complex.

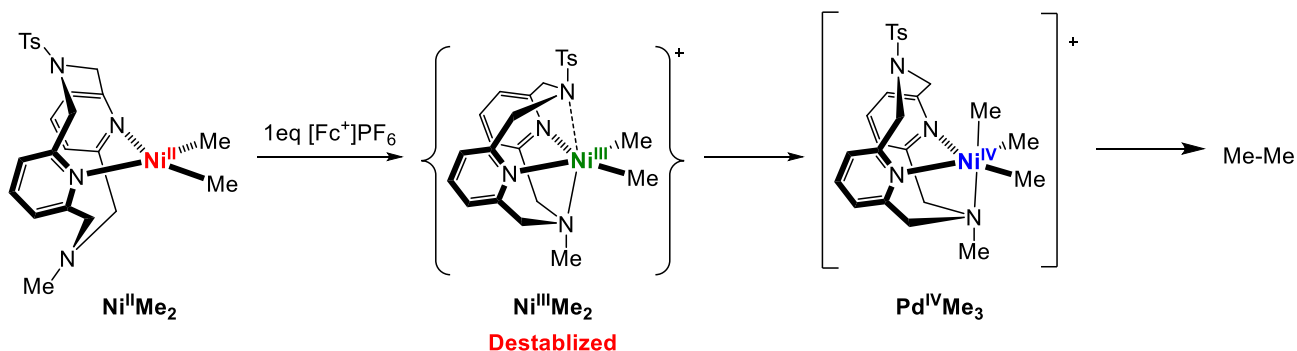


7.3 Reactivity of Dialkyl and Diaryl Nickel Complexes

The studies in chapter 4 provided the first reported stable Ni^{III} dialkyl complexes stabilized using the unique tetradentate pyridonophane ligand. Additionally, the oxidative reactivity was shown to proceed through two distinctive high-valent pathways. The ability to isolate and characterize these high-valent nickel complexes has provided strong support for Ni^{III} and Ni^{IV} complexes playing critical roles in various catalytic transformations.

Surprisingly, these studies showed the $\text{Ni}^{\text{III}}\text{Me}_2$ complex exhibited limited reactivity without further oxidation. The $\text{Ni}^{\text{III}}\text{Me}_2$ complex would undergo a very slow non-radical methyl group transfer between two $\text{Ni}^{\text{III}}\text{Me}_2$ intermediates, resulting in the formation of a reactive $\text{Ni}^{\text{IV}}\text{Me}_3$ intermediate. Only after the reactive $\text{Ni}^{\text{IV}}\text{Me}_3$ intermediate was formed would the complex undergo reductive elimination. To improve the sluggish rate of reactivity of the $\text{Ni}^{\text{III}}\text{Me}_2$ complex we propose using the $^{\text{TsMe}}\text{N}4$ and $^{\text{Ts}}\text{N}4$ ligands to destabilize the $\text{Ni}^{\text{III}}\text{Me}_2$ intermediate. Our previous work with palladium has shown the $^{\text{TsMe}}\text{N}4$ ligand does destabilize the $\text{Pd}^{\text{III}}\text{Me}_2$ complex resulting in rapid formation of the $\text{Pd}^{\text{IV}}\text{Me}_3$ intermediate (Chapter 2). We propose similar results may be observed for our nickel counterparts (Scheme 7.4). All told, these studies will provide a rare opportunity to directly investigate high-valent Ni intermediates pivotal to various C-C bond formation reactions.

Scheme 7.4 Proposed reactivity of the $[(^{\text{TsMe}}\text{N}4)\text{Ni}^{\text{III}}\text{Me}_2]^+$ complex.

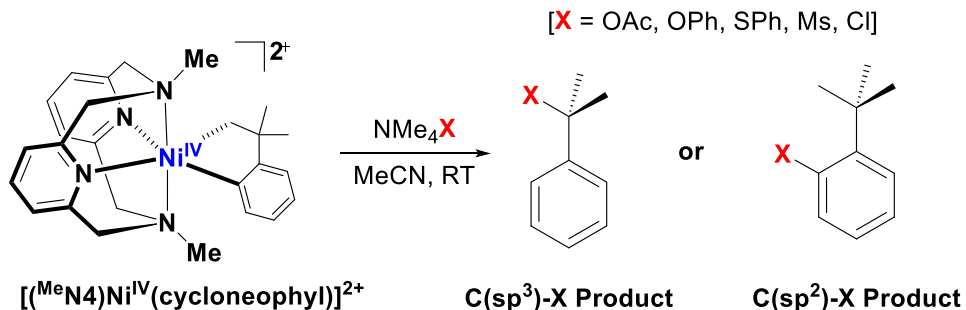


7.4 Reactivity of Cycloneophyl Supported Ni^{IV} Complexes

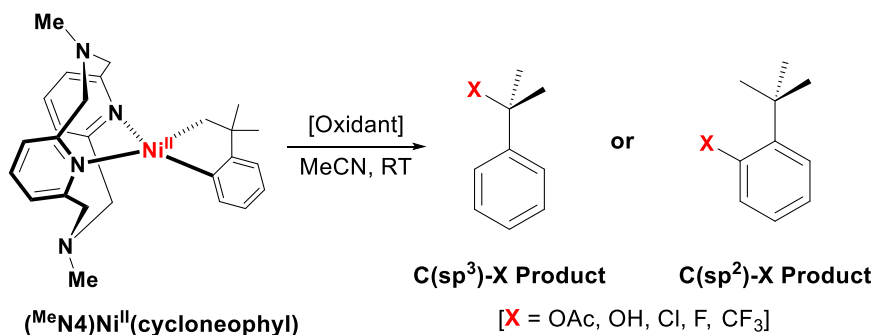
The synthesis and characterization of the stable Ni^{IV} complex reported in Chapter 5 was possible due to the use of the cycloneophyl group and the $^{\text{Me}}\text{N}4$ ligand system. This stable Ni^{IV} complex confirmed the $^{\text{Me}}\text{N}4$ ligand system is capable of supporting the Ni^{IV} oxidation state,

providing valuable evidence for our previously proposed reactivity pathways involving a Ni^{IV} intermediate (Chapter 4). Overall, these studies did provide a rare opportunity to directly investigate high-valent Ni complexes, however, the reactivity of the Ni^{IV} complex was not fully investigated. We propose additional reactivity studies should be conducted to determine the affinity of the Ni^{III} and Ni^{IV} complexes to undergo nucleophilic attack similar to other reported high-valent nickel and palladium complexes (Scheme 7.5).⁴⁻⁷ Additionally, the reactivity of the Ni^{II} precursor with various oxidants should be conducted in the hope of observing a variety of different C-X bond formation products (Scheme 7.6).⁸⁻¹¹ These studies will give us a better insight into the reactivity of these high-valent Ni^{IV} intermediates and what roles they play in various C-C and C-heteroatom bond formation reactions.

Scheme 7.5 Proposed reactivity of Ni^{IV} complex via nucleophilic attack.



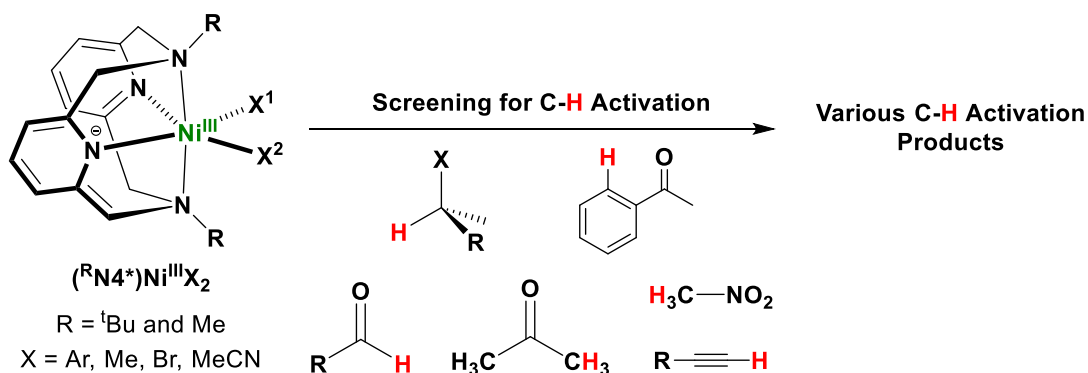
Scheme 7.6 Proposed reactivity of Ni^{II} complexes with various oxidants.



7.5 Deprotonation of Organometallic Nickel Complexes

In Chapter 6, the deprotonation of the pyridinophane ligand system (N4) was shown to form neutral Ni^{III} complexes. The deprotonation reactions were monitored and confirmed in-situ by using UV-Vis and EPR spectroscopy, however these complexes were unable to facilitate the C-H activation of benzene in preliminary reactivity studies. Further reactivity studies are needed to properly determine whether these complexes are capable of C-H activation. We propose investigating different reaction conditions and different compounds with varying C-H bond strengths (Scheme 7.7). Additionally, other N4-supported nickel complexes should be investigated to determine if their deprotonation results in the formation of new high-valent nickel complexes and/or C-H activation. Overall, these studies are critical to confidently ascertain whether these complexes are capable of C-H activation and deserve further focus.

Scheme 7.7 Proposed C-H activation studies on deprotonated (N4)Ni complexes.



7.6 References

1. Luedtke, A. T.; Goldberg, K. I. *Inorg. Chem.* **2007**, *46*, 8496.
2. Puddephatt, R. J. *Angew. Chem. Int. Ed.* **2002**, *41*, 261.
3. Brown, M. P.; Puddephatt, R. J.; Upton, C. E. E. *J. Chem. Soc., Dalton Trans.* **1974**, 2457.
4. Camasso, N. M.; Sanford, M. S. *Science* **2015**, *347*, 1218.
5. Dimitrov, V.; Linden, A. *Angew. Chem. Int. Ed.* **2003**, *42*, 2631.
6. Sehnal, P.; Taylor, R. J. K.; Fairlamb, I. J. S. *Chem. Rev.* **2010**, *110*, 824.
7. Canty, A., J. *J. Chem. Soc., Dalton Trans.* **2009**, 10409.
8. Klein, H. F.; Bickelhaupt, A.; Jung, T.; Cordier, G. *Organometallics* **1994**, *13*, 2557.
9. Hickman, A. J.; Sanford, M. S. *Nature* **2012**, *484*, 177.
10. Lyons, T. W.; Sanford, M. S. *Chem. Rev.* **2010**, *110*, 1147.
11. Muniz, K. *Angew. Chem. Int. Ed.* **2009**, *48*, 9412.

Appendix A

Select NMR Spectra of Ligands and Metal Complexes

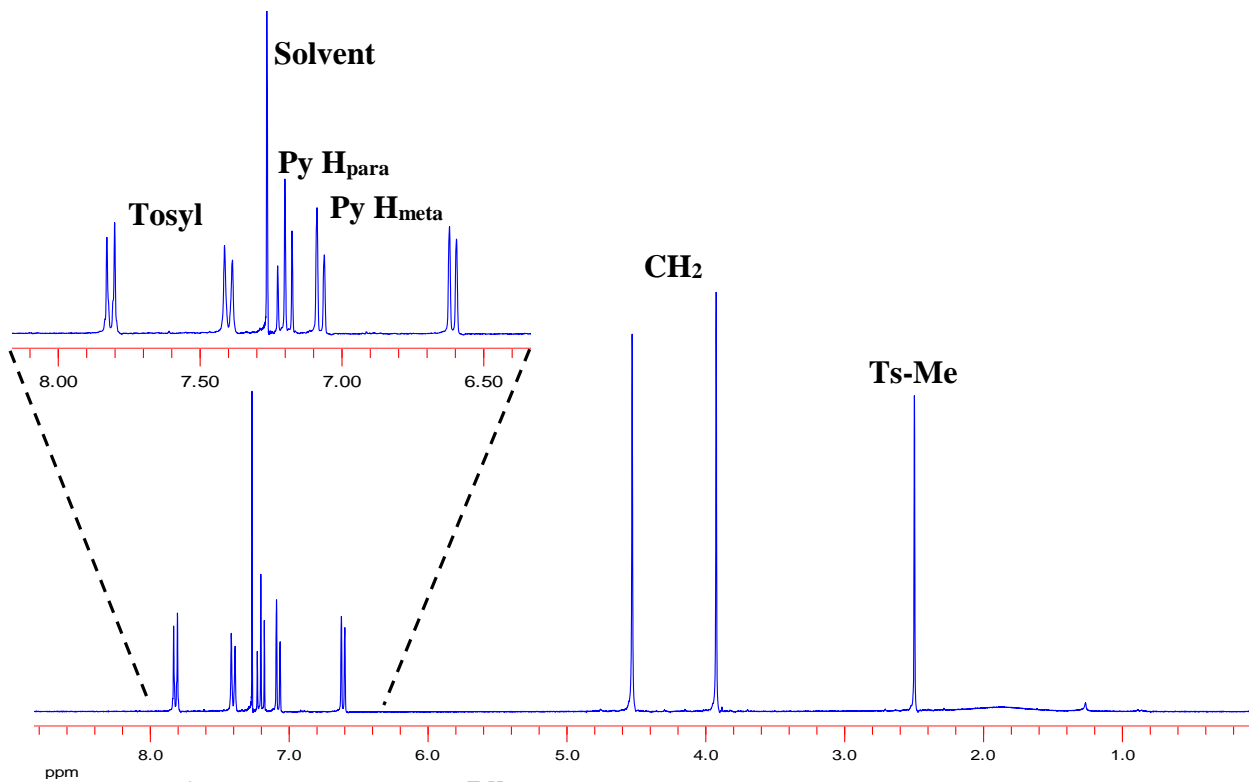


Figure A1: ^1H NMR spectrum of $\text{Ts}^{\text{H}}\text{N}4$ in CDCl_3 .

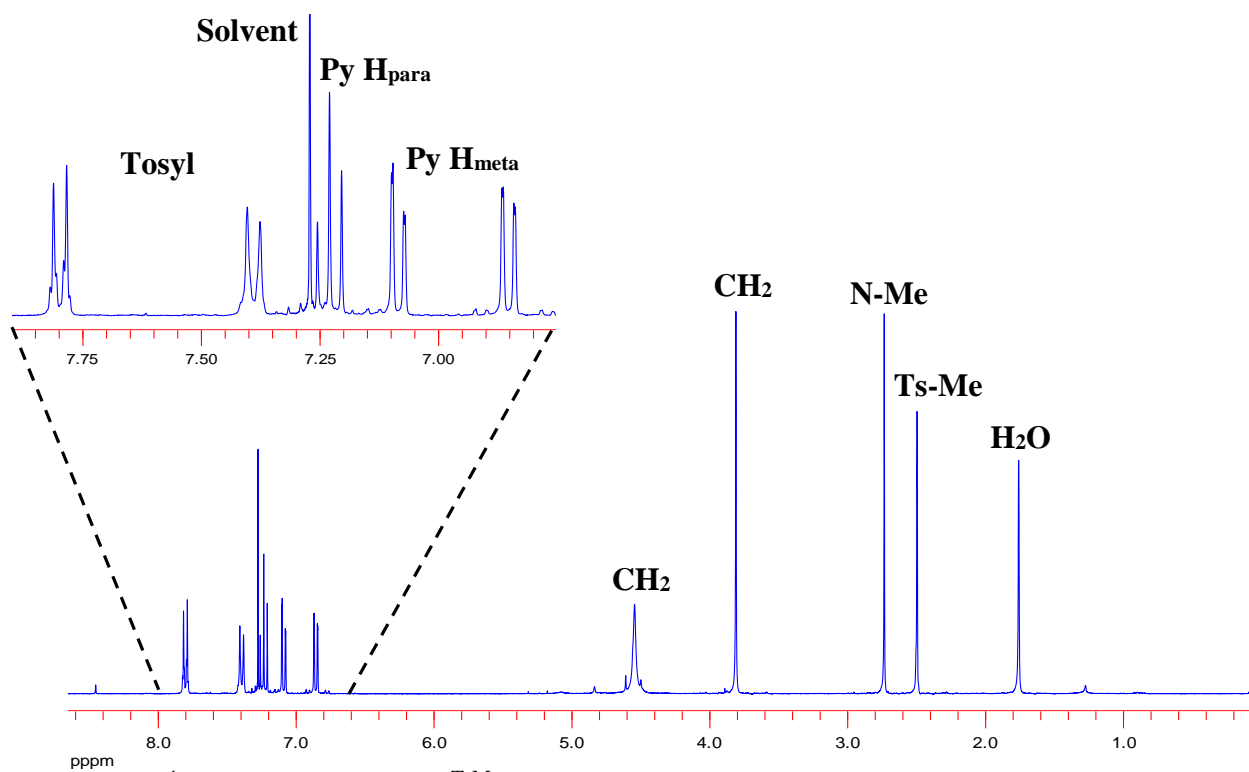


Figure A2: ^1H NMR spectrum of $\text{Ts}^{\text{Me}}\text{N}4$ in CDCl_3 .

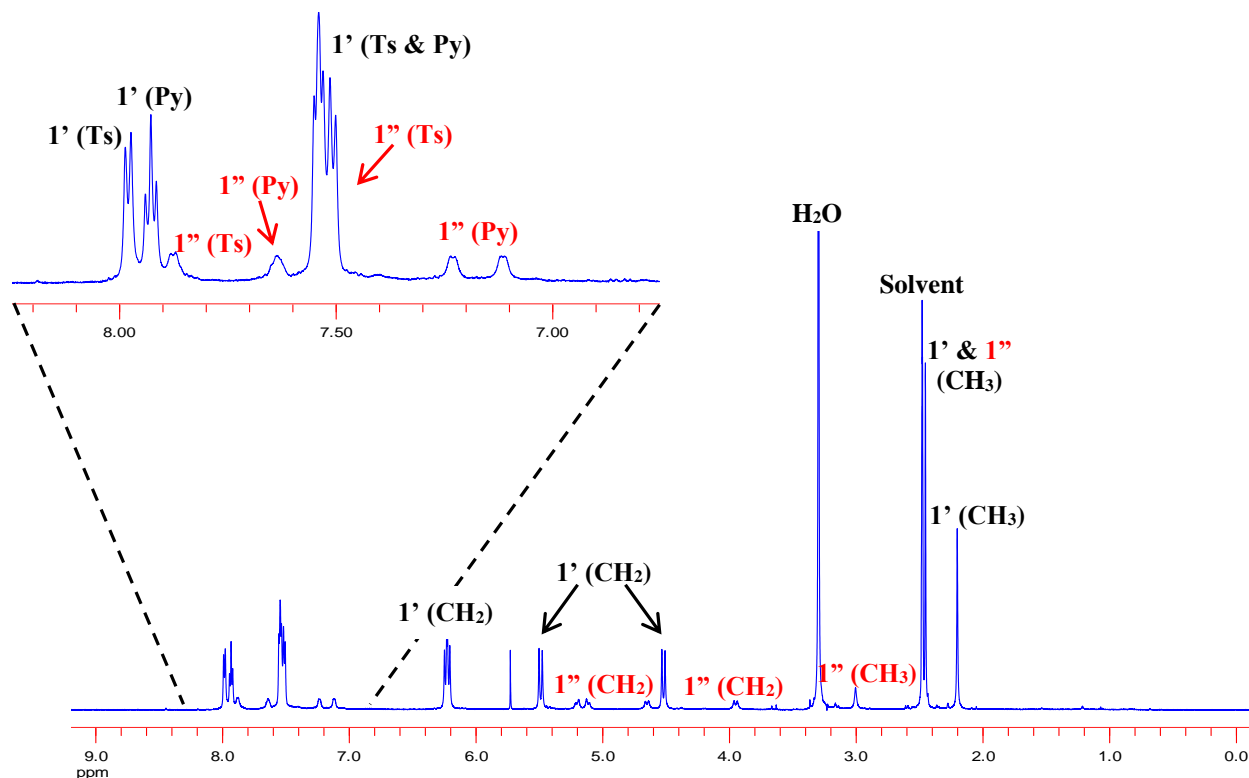


Figure A3: ¹H NMR spectrum of (TsMeN₄)Pd^{II}Cl₂ in DMSO.

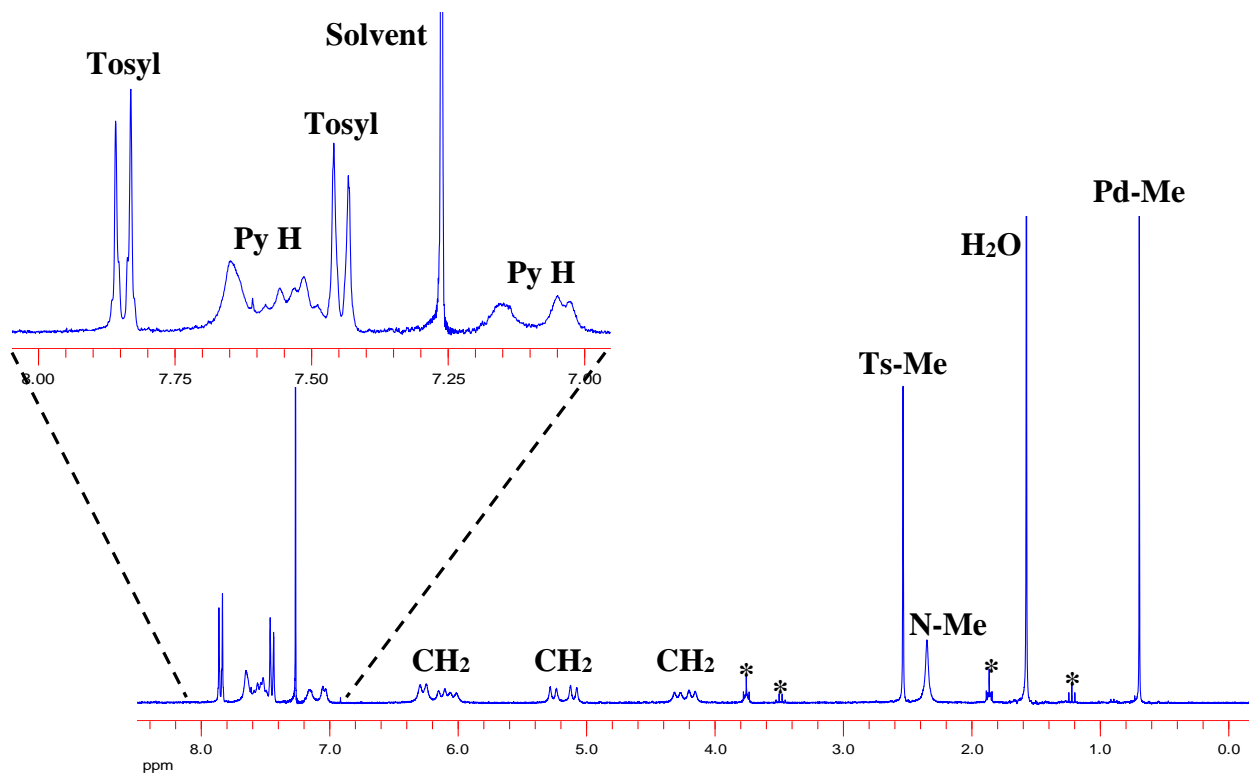


Figure A4: ¹H NMR spectrum of (TsMeN₄)Pd^{II}MeCl in CDCl₃. Peaks marked with an asterisk correspond to a trace amount of solvent (ether and pentane) in the sample.

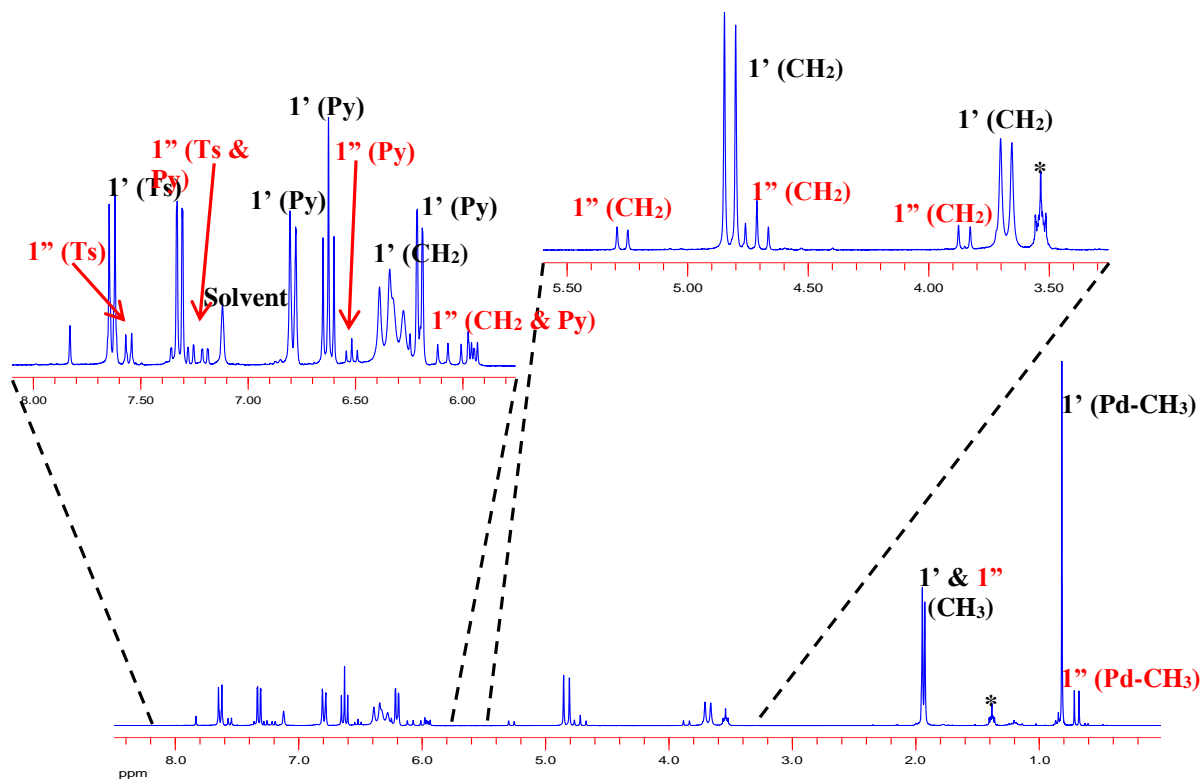


Figure A5: ^1H NMR spectrum of $(^{\text{TsMe}}\text{N}_4)\text{Pd}^{\text{II}}\text{Me}_2$ in Benzene. Peaks marked with an asterisk correspond to a trace amount of solvent (tetrahydrofuran) in the sample.

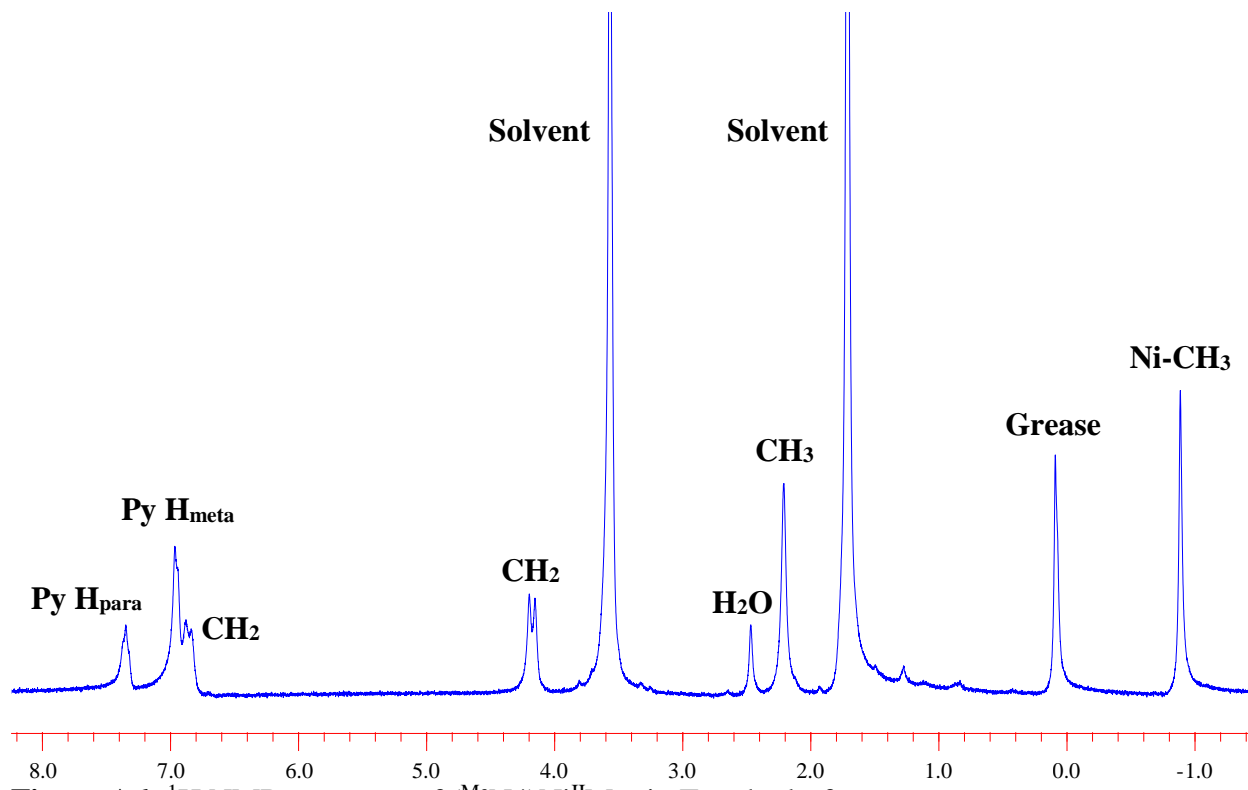


Figure A6: ^1H NMR spectrum of $(^{\text{Me}}\text{N}_4)\text{Ni}^{\text{II}}\text{Me}_2$ in Tetrahydrofuran.

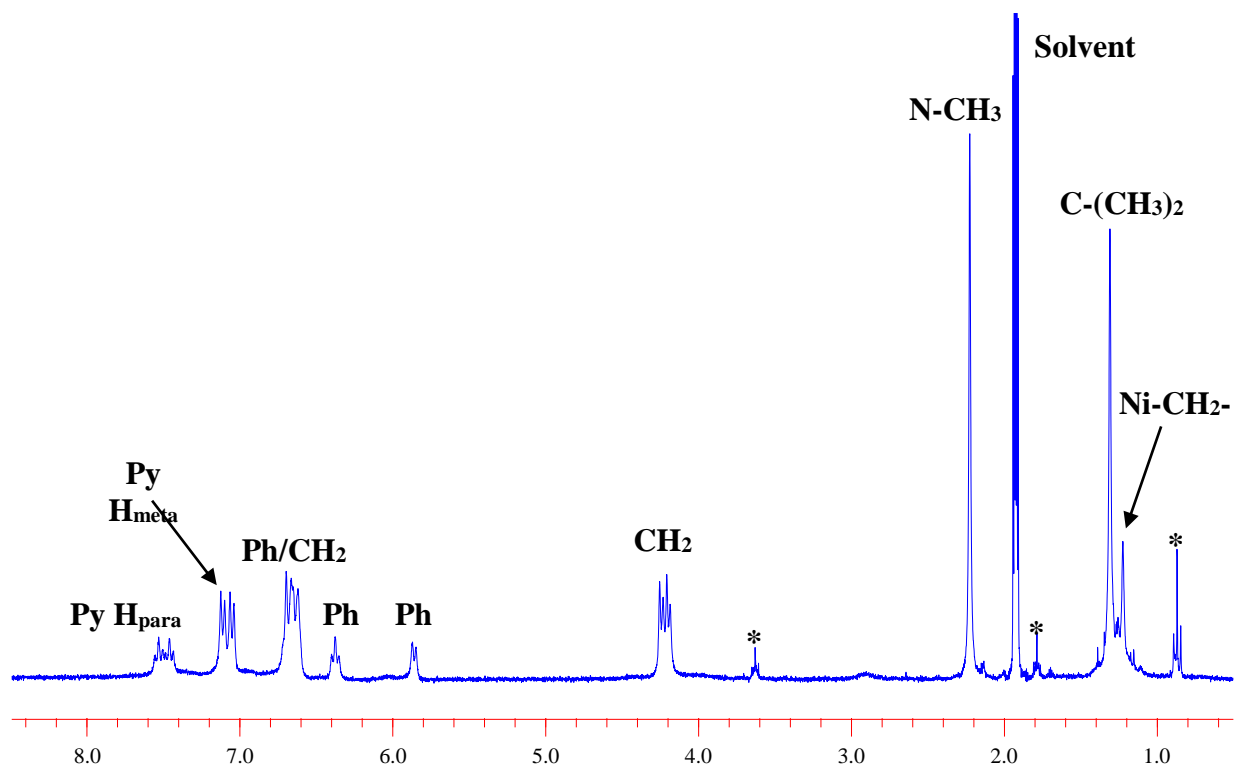


Figure A7: ^1H NMR spectrum of $(^{\text{Me}}\text{N}_4)\text{Ni}^{\text{II}}(\text{cycloneophyl})$ in MeCN. Peaks marked with an asterisk correspond to a trace amount of solvent (tetrahydrofuran and pentane) in the sample.

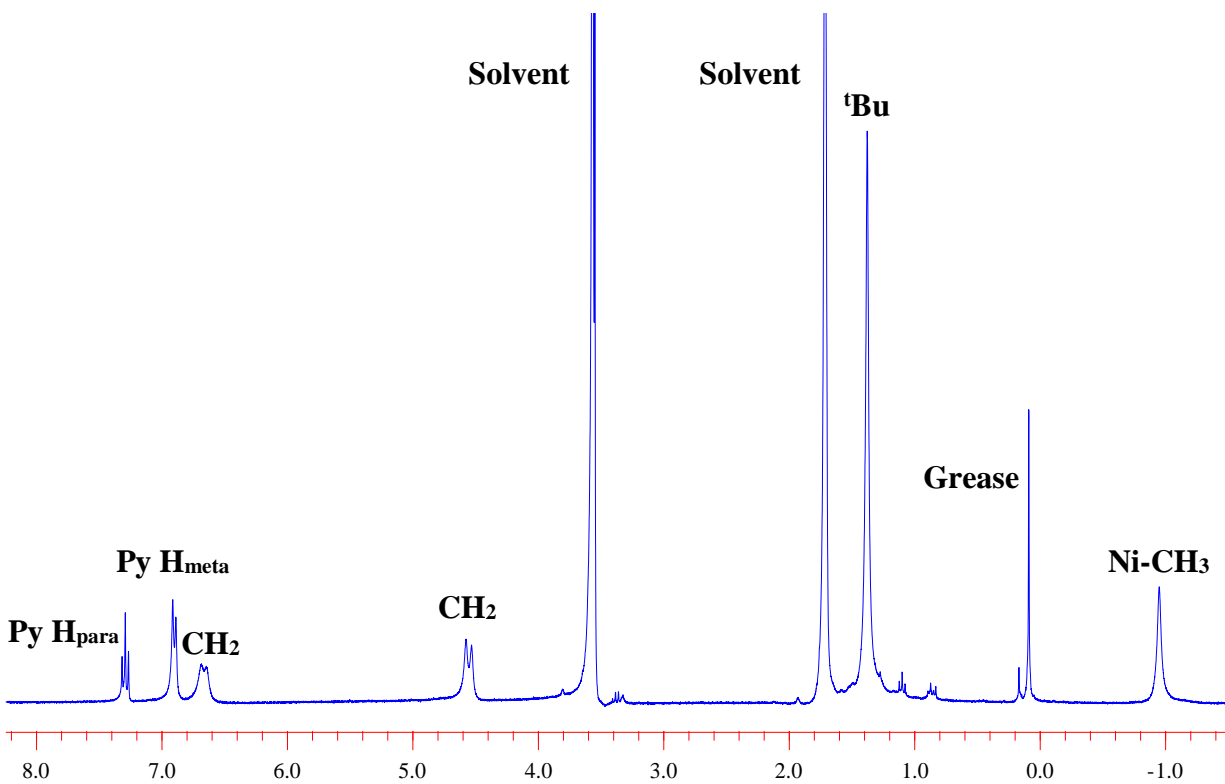


Figure A8: ^1H NMR spectrum of $(^{\text{tBu}}\text{N}_4)\text{Ni}^{\text{II}}\text{Me}_2$ in Tetrahydrofuran.

NMR Spectra of Ni^{IV} Complex [(^{Me}N4)Ni^{IV}(cycloneophyl)](PF₆)₂

¹H-NMR (300 MHz, CDCl₃), δ (ppm): 8.05 (t, 1H, **F**), 7.97 (t, 1H, **G**), 7.51 (d, 2H, **I**), 7.41 (d, 2H, **H**), 7.25 (t, 1H, **L**), 7.19 (d, 1H, **K**), 6.92 (t, 1H, **M**), 6.55 (d, 1H, **N**), 5.33 (s, 2H, **O**), 5.01 (d, 2H, **E**), 4.56 (d, 2H, **B**), 4.22 (d, 2H, **D**), 4.08 (d, 2H, **C**), 2.38 (s, 6H, **A**), 1.67 (s, 6H, **J**).

¹³C-NMR (600 MHz, CDCl₃), δ (ppm): 159.42 (**p**, **k**), 158.44 (**i**), 156.25 (**g**), 154.50 (**c**), 144.89 (**e**), 133.85 (**o**), 132.31 (**n**), 131.31 (**l**), 131.15 (**m**), 125.82 (**d**), 125.07 (**f**), 79.77 (**h**), 77.38 (**b**), 57.31 (**a**), 36.00 (**j**).

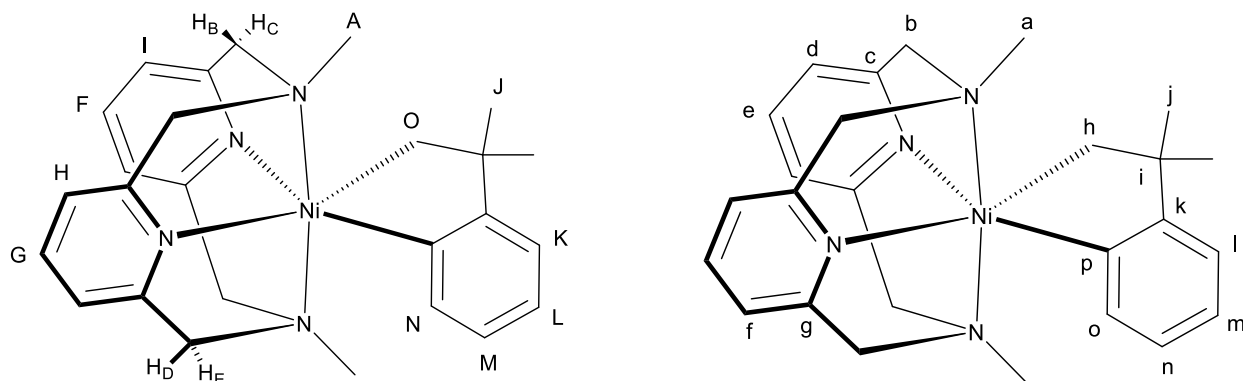


Figure A9. Proton (left) and carbon (right) structural assignments from NMR experiments.

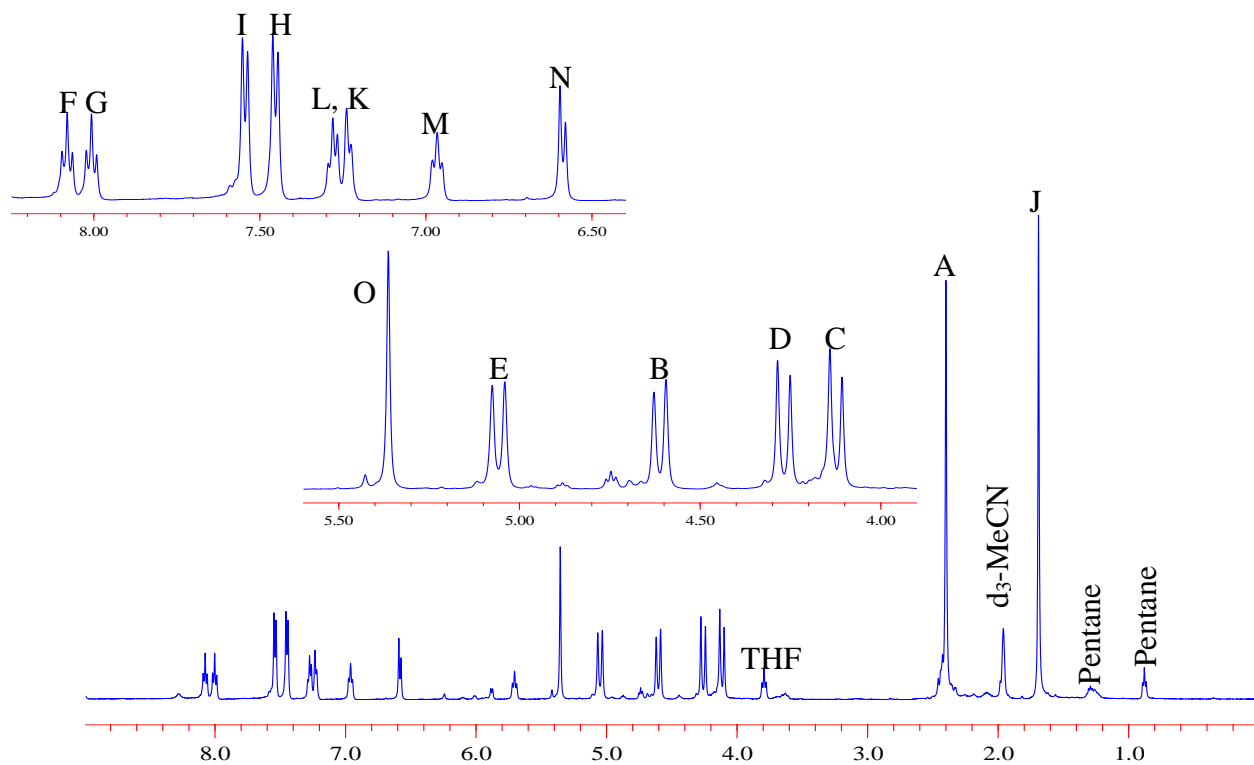


Figure A10. ^1H NMR spectrum of $[(^{\text{Me}}\text{N}_4)\text{Ni}^{\text{IV}}(\text{cycloneophyl})](\text{PF}_6)_2$ in MeCN at -15°C .

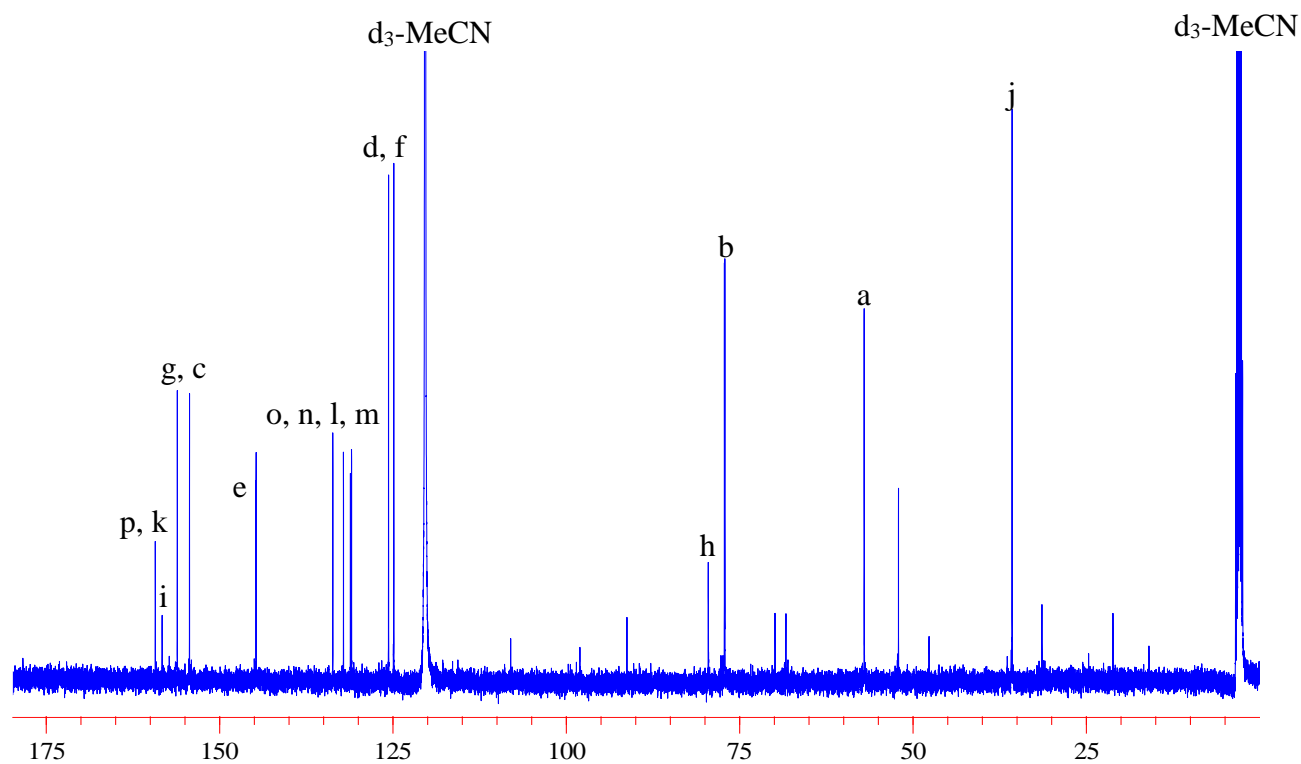


Figure A11. ^{13}C NMR spectrum of $[(^{\text{Me}}\text{N}_4)\text{Ni}^{\text{IV}}(\text{cycloneophyl})](\text{PF}_6)_2$ in MeCN at -15°C .

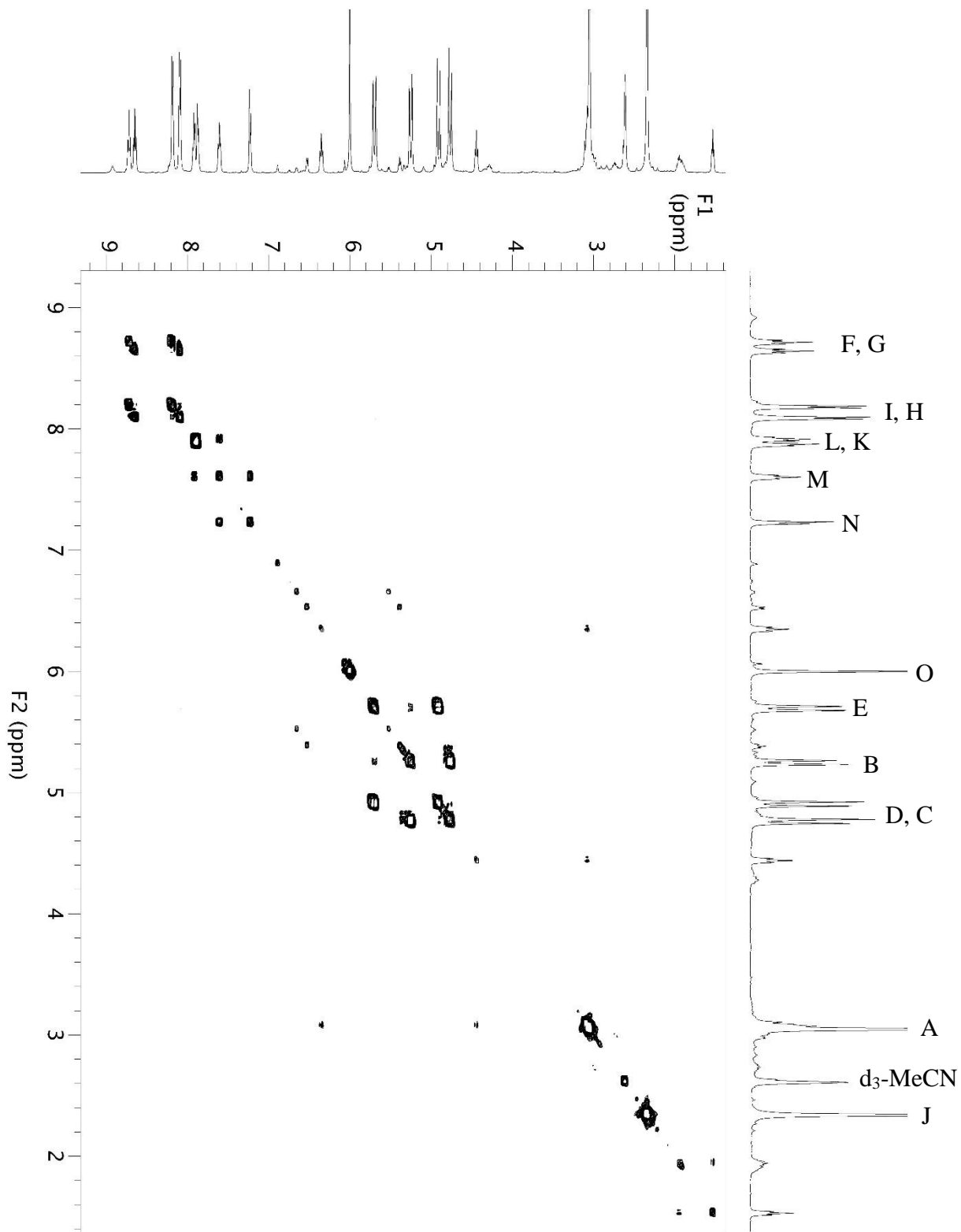


Figure A12. ^1H - ^1H COSY spectrum of $[(^{\text{Me}}\text{N}4)\text{Ni}^{\text{IV}}(\text{cycloneophyl})](\text{PF}_6)_2$ in MeCN at -15°C .

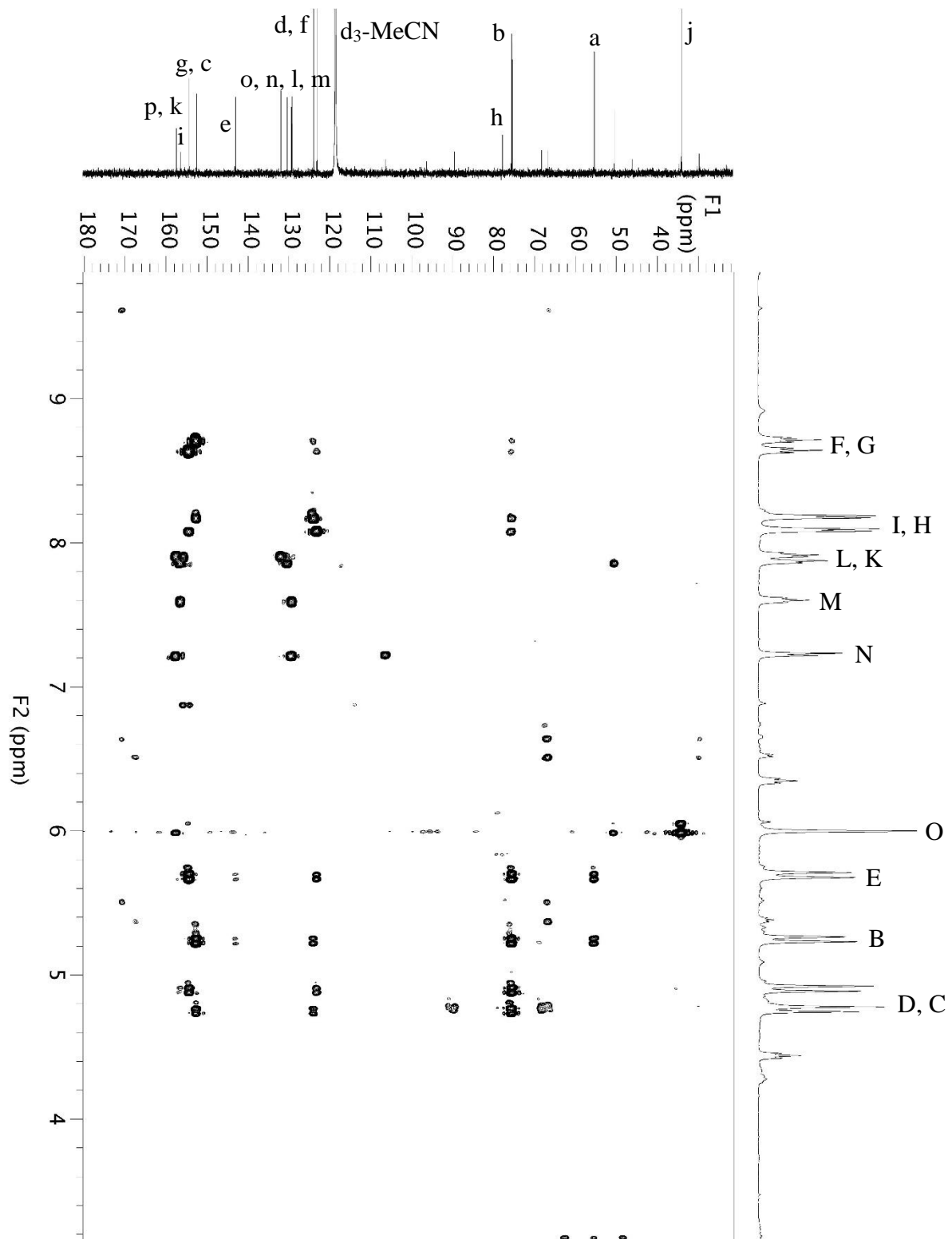


Figure A13. ^1H - ^{13}C HMBC spectrum of $[(^{\text{Me}}\text{N}_4)\text{Ni}^{\text{IV}}(\text{cycloneophyl})](\text{PF}_6)_2$ in MeCN at -15°C .

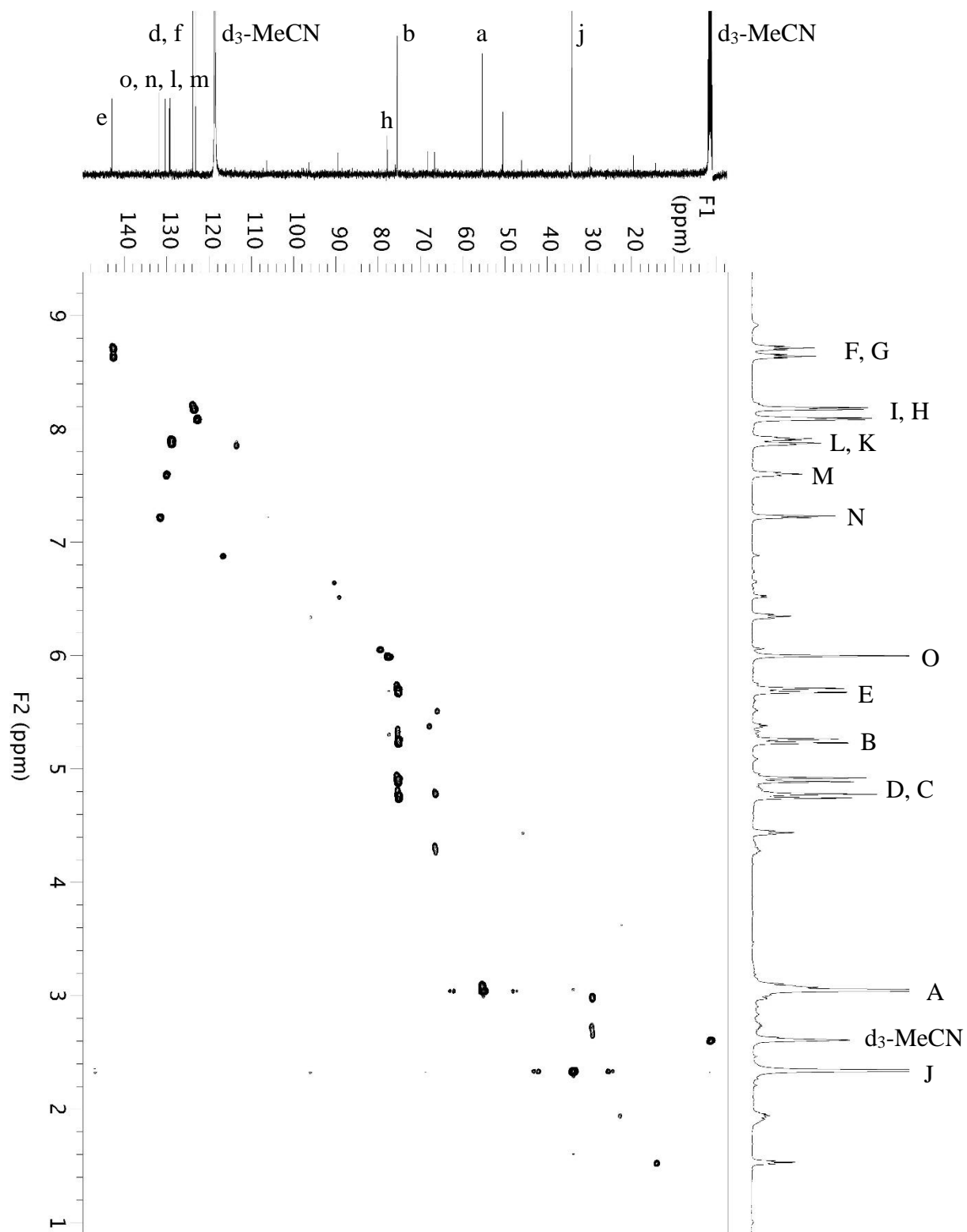


Figure A14. ^1H - ^{13}C HSQC spectrum of $[(^{\text{Me}}\text{N}_4)\text{Ni}^{\text{IV}}(\text{cycloneophyl})](\text{PF}_6)_2$ in MeCN at -15°C .

Appendix B

X-ray Crystal Structure Data of Metal Complexes

Table B1. Crystal data and structure refinement for $(\text{TsMe}_4\text{N})\text{Pd}^{\text{II}}\text{Cl}_2$.

Identification code	16912	
Empirical formula	$\text{C}_{22} \text{H}_{24} \text{Cl}_2 \text{N}_4 \text{O}_2 \text{Pd S}$	
Formula weight	585.81	
Temperature	100(2) K	
Wavelength	0.71073 Å	
Crystal system	Monoclinic	
Space group	$P2_1/c$	
Unit cell dimensions	$a = 13.8080(13) \text{ Å}$ $b = 13.9729(12) \text{ Å}$ $c = 12.1642(11) \text{ Å}$	$\alpha = 90^\circ$. $\beta = 101.523(5)^\circ$. $\gamma = 90^\circ$.
Volume	$2299.6(4) \text{ Å}^3$	
Z	4	
Density (calculated)	1.692 Mg/m^3	
Absorption coefficient	1.158 mm^{-1}	
F(000)	1184	
Crystal size	$0.25 \times 0.19 \times 0.08 \text{ mm}^3$	
Theta range for data collection	2.10 to 27.55° .	
Index ranges	$-17 \leq h \leq 17$, $-18 \leq k \leq 18$, $-15 \leq l \leq 15$	
Reflections collected	31868	
Independent reflections	5287 [R(int) = 0.0550]	
Completeness to $\theta = 27.55^\circ$	99.7 %	
Absorption correction	Semi-empirical from equivalents	
Max. and min. transmission	0.9110 and 0.7613	
Refinement method	Full-matrix least-squares on F^2	
Data / restraints / parameters	5287 / 0 / 298	
Goodness-of-fit on F^2	1.018	
Final R indices [I > 2sigma(I)]	R1 = 0.0344, wR2 = 0.0687	
R indices (all data)	R1 = 0.0580, wR2 = 0.0773	
Largest diff. peak and hole	0.664 and -0.713 e.Å^{-3}	

Table B2. Bond lengths [\AA]and angles [$^\circ$] for $(^{\text{Tsmc}}\text{N}_4)\text{Pd}^{\text{II}}\text{Cl}_2$.

Pd(1)-N(2)	2.057(2)	C(6)-H(6B)	0.9900	N(2)-Pd(1)-Cl(2)	96.41(8)
Pd(1)-N(3)	2.062(3)	C(7)-C(8)	1.499(4)	N(3)-Pd(1)-Cl(2)	174.72(7)
Pd(1)-Cl(1)	2.2792(9)	C(7)-H(7A)	0.9900	Cl(1)-Pd(1)-Cl(2)	88.67(3)
Pd(1)-Cl(2)	2.3065(8)	C(7)-H(7B)	0.9900	N(2)-Pd(1')-N(3)	82.4(5)
Pd(1')-N(2)	2.027(13)	C(8)-C(9)	1.377(4)	N(2)-Pd(1')-Cl(1')	159.1(17)
Pd(1')-N(3)	2.063(14)	C(9)-C(10)	1.371(5)	N(3)-Pd(1')-Cl(1')	84.0(14)
Pd(1')-Cl(1')	2.17(5)	C(9)-H(9)	0.9500	N(2)-Pd(1')-N(1)	76.7(5)
Pd(1')-N(1)	2.550(19)	C(10)-C(11)	1.379(5)	N(3)-Pd(1')-N(1)	86.8(5)
Pd(1')-Cl(2)	2.569(15)	C(10)-H(10)	0.9500	Cl(1')-Pd(1')-N(1)	118.3(16)
Pd(1')-C(6)	2.610(15)	C(11)-C(12)	1.383(4)	N(2)-Pd(1')-Cl(2)	89.5(5)
S(1)-O(2)	1.430(2)	C(11)-H(11)	0.9500	N(3)-Pd(1')-Cl(2)	140.6(9)
S(1)-O(1)	1.432(2)	C(12)-C(14)	1.520(4)	Cl(1')-Pd(1')-Cl(2)	91.0(14)
S(1)-N(4)	1.629(3)	C(13)-H(13A)	0.9900	N(1)-Pd(1')-Cl(2)	128.7(6)
S(1)-C(16)	1.759(3)	C(13)-H(13B)	0.9900	N(2)-Pd(1')-C(6)	91.9(5)
N(1)-C(1)	1.339(4)	C(14)-H(14A)	0.9900	N(3)-Pd(1')-C(6)	35.4(2)
N(1)-C(5)	1.341(4)	C(14)-H(14B)	0.9900	Cl(1')-Pd(1')-C(6)	86.1(14)
N(2)-C(12)	1.343(4)	C(15)-H(15A)	0.9800	N(1)-Pd(1')-C(6)	56.0(4)
N(2)-C(8)	1.352(4)	C(15)-H(15B)	0.9800	Cl(2)-Pd(1')-C(6)	175.3(8)
N(3)-C(15)	1.492(4)	C(15)-H(15C)	0.9800	O(2)-S(1)-O(1)	119.98(14)
N(3)-C(7)	1.493(4)	C(16)-C(17)	1.384(4)	O(2)-S(1)-N(4)	106.50(13)
N(3)-C(6)	1.513(4)	C(16)-C(21)	1.388(4)	O(1)-S(1)-N(4)	106.54(14)
N(4)-C(14)	1.475(4)	C(17)-C(18)	1.379(5)	O(2)-S(1)-C(16)	107.80(14)
N(4)-C(13)	1.480(4)	C(17)-H(17)	0.9500	O(1)-S(1)-C(16)	107.79(15)
C(1)-C(2)	1.389(5)	C(18)-C(19)	1.393(5)	N(4)-S(1)-C(16)	107.68(14)
C(1)-C(13)	1.506(4)	C(18)-H(18)	0.9500	C(1)-N(1)-C(5)	117.0(3)
C(2)-C(3)	1.371(5)	C(19)-C(20)	1.395(5)	C(1)-N(1)-Pd(1')	132.6(3)
C(2)-H(2)	0.9500	C(19)-C(22)	1.495(5)	C(5)-N(1)-Pd(1')	90.2(3)
C(3)-C(4)	1.378(5)	C(20)-C(21)	1.365(5)	C(12)-N(2)-C(8)	118.6(3)
C(3)-H(3)	0.9500	C(20)-H(20)	0.9500	C(12)-N(2)-Pd(1')	121.6(5)
C(4)-C(5)	1.374(5)	C(21)-H(21)	0.9500	C(8)-N(2)-Pd(1')	115.1(4)
C(4)-H(4)	0.9500	C(22)-H(22A)	0.9800	C(12)-N(2)-Pd(1)	130.7(2)
C(5)-C(6)	1.507(4)	C(22)-H(22B)	0.9800	C(8)-N(2)-Pd(1)	110.7(2)
C(6)-H(6A)	0.9900	C(22)-H(22C)	0.9800	C(15)-N(3)-C(7)	107.2(2)
		N(2)-Pd(1)-N(3)	81.72(10)	C(15)-N(3)-C(6)	105.1(2)
		N(2)-Pd(1)-Cl(1)	174.69(8)	C(7)-N(3)-C(6)	113.6(2)
		N(3)-Pd(1)-Cl(1)	93.09(7)	C(15)-N(3)-Pd(1)	116.0(2)

C(7)-N(3)-Pd(1)	103.37(18)	N(3)-C(7)-H(7B)	109.4	C(17)-C(16)-C(21)	119.9(3)
C(6)-N(3)-Pd(1)	111.81(19)	C(8)-C(7)-H(7B)	109.4	C(17)-C(16)-S(1)	119.9(3)
C(15)-N(3)-Pd(1')	127.0(4)	H(7A)-C(7)-H(7B)	108.0	C(21)-C(16)-S(1)	120.2(2)
C(7)-N(3)-Pd(1')	110.5(4)	N(2)-C(8)-C(9)	122.2(3)	C(18)-C(17)-C(16)	119.5(3)
C(6)-N(3)-Pd(1')	92.5(6)	N(2)-C(8)-C(7)	116.3(3)	C(18)-C(17)-H(17)	120.3
C(14)-N(4)-C(13)	114.6(2)	C(9)-C(8)-C(7)	121.4(3)	C(16)-C(17)-H(17)	120.3
C(14)-N(4)-S(1)	118.6(2)	C(10)-C(9)-C(8)	118.8(3)	C(17)-C(18)-C(19)	121.6(3)
C(13)-N(4)-S(1)	118.7(2)	C(10)-C(9)-H(9)	120.6	C(17)-C(18)-H(18)	119.2
N(1)-C(1)-C(2)	123.0(3)	C(8)-C(9)-H(9)	120.6	C(19)-C(18)-H(18)	119.2
N(1)-C(1)-C(13)	116.3(3)	C(9)-C(10)-C(11)	119.0(3)	C(18)-C(19)-C(20)	117.6(3)
C(2)-C(1)-C(13)	120.4(3)	C(9)-C(10)-H(10)	120.5	C(18)-C(19)-C(22)	120.8(3)
C(3)-C(2)-C(1)	118.6(3)	C(11)-C(10)-H(10)	120.5	C(20)-C(19)-C(22)	121.6(3)
C(3)-C(2)-H(2)	120.7	C(10)-C(11)-C(12)	119.9(3)	C(21)-C(20)-C(19)	121.5(3)
C(1)-C(2)-H(2)	120.7	C(10)-C(11)-H(11)	120.1	C(21)-C(20)-H(20)	119.3
C(2)-C(3)-C(4)	119.3(3)	C(12)-C(11)-H(11)	120.1	C(19)-C(20)-H(20)	119.3
C(2)-C(3)-H(3)	120.4	N(2)-C(12)-C(11)	120.8(3)	C(20)-C(21)-C(16)	120.0(3)
C(4)-C(3)-H(3)	120.4	N(2)-C(12)-C(14)	119.4(3)	C(20)-C(21)-H(21)	120.0
C(5)-C(4)-C(3)	118.5(3)	C(11)-C(12)-C(14)	119.5(3)	C(16)-C(21)-H(21)	120.0
C(5)-C(4)-H(4)	120.8	N(4)-C(13)-C(1)	108.1(3)	C(19)-C(22)-H(22A)	109.5
C(3)-C(4)-H(4)	120.8	N(4)-C(13)-H(13A)	110.1	C(19)-C(22)-H(22B)	109.5
N(1)-C(5)-C(4)	123.5(3)	C(1)-C(13)-H(13A)	110.1	H(22A)-C(22)-H(22B)	109.5
N(1)-C(5)-C(6)	116.6(3)	N(4)-C(13)-H(13B)	110.1	C(19)-C(22)-H(22C)	109.5
C(4)-C(5)-C(6)	119.9(3)	C(1)-C(13)-H(13B)	110.1	H(22A)-C(22)-H(22C)	109.5
C(5)-C(6)-N(3)	115.0(3)	H(13A)-C(13)-H(13B)	108.4	H(22B)-C(22)-H(22C)	109.5
C(5)-C(6)-Pd(1')	84.5(4)	N(4)-C(14)-C(12)	109.8(2)		
N(3)-C(6)-Pd(1')	52.1(4)	N(4)-C(14)-H(14A)	109.7		
C(5)-C(6)-H(6A)	108.5	C(12)-C(14)-H(14A)	109.7		
N(3)-C(6)-H(6A)	108.5	N(4)-C(14)-H(14B)	109.7		
Pd(1')-C(6)-H(6A)	80.7	C(12)-C(14)-H(14B)	109.7		
C(5)-C(6)-H(6B)	108.5	H(14A)-C(14)-H(14B)	108.2		
N(3)-C(6)-H(6B)	108.5	N(3)-C(15)-H(15A)	109.5		
Pd(1')-C(6)-H(6B)	160.6	N(3)-C(15)-H(15B)	109.5		
H(6A)-C(6)-H(6B)	107.5	H(15A)-C(15)-H(15B)	109.5		
N(3)-C(7)-C(8)	111.2(2)	N(3)-C(15)-H(15C)	109.5		
N(3)-C(7)-H(7A)	109.4	H(15A)-C(15)-H(15C)	109.5		
C(8)-C(7)-H(7A)	109.4	H(15B)-C(15)-H(15C)	109.5		

Table B3. Crystal data and structure refinement for (T^sMeN₄)Pd^{II}MeCl.

Identification code	16412/lt/JS-01-022812	
Empirical formula	C ₂₃ H ₂₇ Cl N ₄ O ₂ Pd S	
Formula weight	565.40	
Temperature	100(2) K	
Wavelength	0.71073 Å	
Crystal system	Monoclinic	
Space group	P2 ₁ /c	
Unit cell dimensions	a = 16.0105(7) Å	α = 90°.
	b = 9.8303(5) Å	β = 97.558(3)°.
	c = 14.9486(7) Å	γ = 90°.
Volume	2332.29(19) Å ³	
Z	4	
Density (calculated)	1.610 Mg/m ³	
Absorption coefficient	1.028 mm ⁻¹	
F(000)	1152	
Crystal size	0.22 x 0.18 x 0.18 mm ³	
Theta range for data collection	2.44 to 27.55°.	
Index ranges	-20 ≤ h ≤ 20, -12 ≤ k ≤ 12, -19 ≤ l ≤ 19	
Reflections collected	48475	
Independent reflections	5356 [R(int) = 0.0533]	
Completeness to theta = 27.55°	99.5 %	
Absorption correction	Semi-empirical from equivalents	
Max. and min. transmission	0.8374 and 0.8047	
Refinement method	Full-matrix least-squares on F ²	
Data / restraints / parameters	5356 / 0 / 292	
Goodness-of-fit on F ²	1.036	
Final R indices [I > 2σ(I)]	R1 = 0.0277, wR2 = 0.0591	
R indices (all data)	R1 = 0.0389, wR2 = 0.0636	
Largest diff. peak and hole	0.789 and -0.418 e.Å ⁻³	

Table B4. Bond lengths [\AA]and angles [$^\circ$] for $(^{\text{Tsm}}\text{MeN}_4)\text{Pd}^{\text{II}}\text{MeCl}$.

Pd(1)-C(1)	2.027(2)	C(8)-H(8B)	0.9900	O(2)-S(1)-O(1)	119.34(11)
Pd(1)-N(1)	2.044(2)	C(9)-C(10)	1.384(3)	O(2)-S(1)-N(4)	108.77(11)
Pd(1)-N(2)	2.1724(19)	C(10)-C(11)	1.382(4)	O(1)-S(1)-N(4)	106.50(11)
Pd(1)-Cl(1)	2.3073(6)	C(10)-H(10)	0.9500	O(2)-S(1)-C(17)	106.90(11)
S(1)-O(2)	1.4302(18)	C(11)-C(12)	1.380(3)	O(1)-S(1)-C(17)	109.06(11)
S(1)-O(1)	1.4307(19)	C(11)-H(11)	0.9500	N(4)-S(1)-C(17)	105.47(11)
S(1)-N(4)	1.628(2)	C(12)-C(13)	1.380(3)	C(6)-N(1)-C(2)	119.6(2)
S(1)-C(17)	1.756(2)	C(12)-H(12)	0.9500	C(6)-N(1)-Pd(1)	119.78(17)
N(1)-C(6)	1.350(3)	C(13)-C(14)	1.512(3)	C(2)-N(1)-Pd(1)	120.28(16)
N(1)-C(2)	1.351(3)	C(14)-H(14A)	0.9900	C(13)-N(2)-C(9)	119.08(19)
N(2)-C(13)	1.344(3)	C(14)-H(14B)	0.9900	C(13)-N(2)-Pd(1)	120.19(15)
N(2)-C(9)	1.352(3)	C(15)-H(15A)	0.9900	C(9)-N(2)-Pd(1)	120.38(15)
N(3)-C(16)	1.445(3)	C(15)-H(15B)	0.9900	C(16)-N(3)-C(7)	115.5(2)
N(3)-C(7)	1.456(3)	C(16)-H(16A)	0.9800	C(16)-N(3)-C(8)	115.4(2)
N(3)-C(8)	1.459(3)	C(16)-H(16B)	0.9800	C(7)-N(3)-C(8)	119.5(2)
N(4)-C(15)	1.465(3)	C(16)-H(16C)	0.9800	C(15)-N(4)-C(14)	121.24(19)
N(4)-C(14)	1.468(3)	C(17)-C(18)	1.379(3)	C(15)-N(4)-S(1)	120.60(16)
C(1)-H(1A)	0.9800	C(17)-C(22)	1.391(3)	C(14)-N(4)-S(1)	117.76(15)
C(1)-H(1B)	0.9800	C(18)-C(19)	1.380(3)	Pd(1)-C(1)-H(1A)	109.5
C(1)-H(1C)	0.9800	C(18)-H(18)	0.9500	Pd(1)-C(1)-H(1B)	109.5
C(2)-C(3)	1.376(4)	C(19)-C(20)	1.386(3)	H(1A)-C(1)-H(1B)	109.5
C(2)-C(15)	1.507(3)	C(19)-H(19)	0.9500	Pd(1)-C(1)-H(1C)	109.5
C(3)-C(4)	1.383(4)	C(20)-C(21)	1.389(4)	H(1A)-C(1)-H(1C)	109.5
C(3)-H(3)	0.9500	C(20)-C(23)	1.504(4)	H(1B)-C(1)-H(1C)	109.5
C(4)-C(5)	1.381(4)	C(21)-C(22)	1.379(3)	N(1)-C(2)-C(3)	121.7(2)
C(4)-H(4)	0.9500	C(21)-H(21)	0.9500	N(1)-C(2)-C(15)	117.4(2)
C(5)-C(6)	1.384(4)	C(22)-H(22)	0.9500	C(3)-C(2)-C(15)	120.8(2)
C(5)-H(5)	0.9500	C(23)-H(23A)	0.9800	C(2)-C(3)-C(4)	119.4(2)
C(6)-C(7)	1.514(4)	C(23)-H(23B)	0.9800	C(2)-C(3)-H(3)	120.3
C(7)-H(7A)	0.9900	C(23)-H(23C)	0.9800	C(4)-C(3)-H(3)	120.3
C(7)-H(7B)	0.9900	C(1)-Pd(1)-N(1)	91.11(9)	C(5)-C(4)-C(3)	118.6(3)
C(8)-C(9)	1.515(3)	C(1)-Pd(1)-N(2)	173.51(9)	C(5)-C(4)-H(4)	120.7
C(8)-H(8A)	0.9900	N(1)-Pd(1)-N(2)	82.96(7)	C(3)-C(4)-H(4)	120.7
		C(1)-Pd(1)-Cl(1)	89.59(8)	C(4)-C(5)-C(6)	120.3(2)
		N(1)-Pd(1)-Cl(1)	178.41(6)	C(4)-C(5)-H(5)	119.9
		N(2)-Pd(1)-Cl(1)	96.41(5)	C(6)-C(5)-H(5)	119.9

N(1)-C(6)-C(5)	120.4(2)	C(10)-C(11)-H(11)	120.7	C(18)-C(17)-S(1)	120.14(18)
N(1)-C(6)-C(7)	118.7(2)	C(11)-C(12)-C(13)	119.6(2)	C(22)-C(17)-S(1)	119.16(18)
C(5)-C(6)-C(7)	120.9(2)	C(11)-C(12)-H(12)	120.2	C(17)-C(18)-C(19)	119.3(2)
N(3)-C(7)-C(6)	117.7(2)	C(13)-C(12)-H(12)	120.2	C(17)-C(18)-H(18)	120.3
N(3)-C(7)-H(7A)	107.9	N(2)-C(13)-C(12)	121.7(2)	C(19)-C(18)-H(18)	120.3
C(6)-C(7)-H(7A)	107.9	N(2)-C(13)-C(14)	117.3(2)	C(18)-C(19)-C(20)	121.3(2)
N(3)-C(7)-H(7B)	107.9	C(12)-C(13)-C(14)	121.0(2)	C(18)-C(19)-H(19)	119.4
C(6)-C(7)-H(7B)	107.9	N(4)-C(14)-C(13)	114.82(19)	C(20)-C(19)-H(19)	119.4
H(7A)-C(7)-H(7B)	107.2	N(4)-C(14)-H(14A)	108.6	C(19)-C(20)-C(21)	118.5(2)
N(3)-C(8)-C(9)	116.2(2)	C(13)-C(14)-H(14A)	108.6	C(19)-C(20)-C(23)	120.6(2)
N(3)-C(8)-H(8A)	108.2	N(4)-C(14)-H(14B)	108.6	C(21)-C(20)-C(23)	120.8(2)
C(9)-C(8)-H(8A)	108.2	C(13)-C(14)-H(14B)	108.6	C(22)-C(21)-C(20)	121.1(2)
N(3)-C(8)-H(8B)	108.2	H(14A)-C(14)-H(14B)	107.5	C(22)-C(21)-H(21)	119.5
C(9)-C(8)-H(8B)	108.2	N(4)-C(15)-C(2)	112.24(19)	C(20)-C(21)-H(21)	119.5
H(8A)-C(8)-H(8B)	107.4	N(4)-C(15)-H(15A)	109.2	C(21)-C(22)-C(17)	119.2(2)
N(2)-C(9)-C(10)	121.2(2)	C(2)-C(15)-H(15A)	109.2	C(21)-C(22)-H(22)	120.4
N(2)-C(9)-C(8)	118.0(2)	N(4)-C(15)-H(15B)	109.2	C(17)-C(22)-H(22)	120.4
C(10)-C(9)-C(8)	120.8(2)	C(2)-C(15)-H(15B)	109.2	C(20)-C(23)-H(23A)	109.5
C(11)-C(10)-C(9)	119.7(2)	H(15A)-C(15)-H(15B)	107.9	C(20)-C(23)-H(23B)	109.5
C(11)-C(10)-H(10)	120.2	N(3)-C(16)-H(16A)	109.5	H(23A)-C(23)-H(23B)	109.5
C(9)-C(10)-H(10)	120.2	N(3)-C(16)-H(16B)	109.5	C(20)-C(23)-H(23C)	109.5
C(12)-C(11)-C(10)	118.6(2)	N(3)-C(16)-H(16C)	109.5	H(23A)-C(23)-H(23C)	109.5
C(12)-C(11)-H(11)	120.7	C(18)-C(17)-C(22)	120.6(2)	H(23B)-C(23)-H(23C)	109.5

Table B5. Crystal data and structure refinement for $(\text{TsMe}_4\text{N})\text{Pd}^{\text{II}}\text{Me}_2$.

Identification code	119712/lt/JS-01-092512	
Empirical formula	$\text{C}_{28} \text{H}_{38} \text{N}_4 \text{O}_3 \text{Pd S}$	
Formula weight	617.08	
Temperature	100(2) K	
Wavelength	0.71073 Å	
Crystal system	Monoclinic	
Space group	$\text{P2}_1/\text{m}$	
Unit cell dimensions	$a = 9.0624(12) \text{ Å}$	$\alpha = 90^\circ$.
	$b = 11.9786(15) \text{ Å}$	$\beta = 97.064(8)^\circ$.
	$c = 12.5671(15) \text{ Å}$	$\gamma = 90^\circ$.
Volume	$1353.9(3) \text{ Å}^3$	
Z	2	
Density (calculated)	1.514 Mg/m^3	
Absorption coefficient	0.800 mm^{-1}	
F(000)	640	
Crystal size	$0.31 \times 0.26 \times 0.09 \text{ mm}^3$	
Theta range for data collection	1.63 to 26.73° .	
Index ranges	$-11 \leq h \leq 11, -14 \leq k \leq 15, -15 \leq l \leq 15$	
Reflections collected	41945	
Independent reflections	3019 [R(int) = 0.0780]	
Completeness to $\theta = 26.73^\circ$	100.0 %	
Absorption correction	Semi-empirical from equivalents	
Max. and min. transmission	0.9308 and 0.7908	
Refinement method	Full-matrix least-squares on F^2	
Data / restraints / parameters	3019 / 54 / 168	
Goodness-of-fit on F^2	1.140	
Final R indices [I > 2σ(I)]	R1 = 0.0774, wR2 = 0.1711	
R indices (all data)	R1 = 0.0984, wR2 = 0.1880	
Extinction coefficient	0.0074(13)	
Largest diff. peak and hole	2.378 and -2.619 e.Å^{-3}	

Table B6. Bond lengths [\AA]and angles [$^\circ$] for $(^{\text{TsMe}}\text{N4})\text{Pd}^{\text{II}}\text{Me}_2$

Pd(1)-C(1)#1	2.053(7)	C(10)-C(11)	1.380(13)	O(1)-S(1)-O(1)#1	119.4(5)
Pd(1)-C(1)	2.053(7)	C(10)-H(10)	0.9500	O(1)-S(1)-N(2)	106.7(2)
Pd(1)-N(1)#1	2.151(6)	C(11)-C(10)#1	1.380(13)	O(1)#1-S(1)-N(2)	106.7(3)
Pd(1)-N(1)	2.151(6)	C(11)-C(12)	1.503(19)	O(1)-S(1)-C(8)	108.1(3)
S(1)-O(1)	1.425(5)	C(12)-H(12A)	0.9800	O(1)#1-S(1)-C(8)	108.1(3)
S(1)-O(1)#1	1.425(5)	C(12)-H(12B)	0.9800	N(2)-S(1)-C(8)	107.3(4)
S(1)-N(2)	1.627(7)	C(12)-H(12C)	0.9800	C(6)-N(1)-C(2)	119.4(6)
S(1)-C(8)	1.757(10)	C(13)-H(13A)	0.9900	C(6)-N(1)-Pd(1)	119.6(4)
N(1)-C(6)	1.345(10)	C(13)-H(13B)	0.9900	C(2)-N(1)-Pd(1)	120.8(5)
N(1)-C(2)	1.356(8)	C(14)-H(14A)	0.9800	C(7)-N(2)-C(7)#1	118.7(7)
N(2)-C(7)	1.476(8)	C(14)-H(14B)	0.9800	C(7)-N(2)-S(1)	118.5(4)
N(2)-C(7)#1	1.476(8)	C(14)-H(14C)	0.9800	C(7)#1-N(2)-S(1)	118.5(4)
N(3)-C(13)	1.455(9)	C(1S)-O(1S)	1.1533	C(13)-N(3)-C(13)#1	119.6(9)
N(3)-C(13)#1	1.455(9)	C(1S)-C(2S)	1.4259	C(13)-N(3)-C(14)	115.2(5)
N(3)-C(14)	1.462(17)	C(1S)-C(4S)	1.9046	C(13)#1-N(3)-C(14)	115.2(5)
C(1)-H(1A)	0.9800	C(1S)-H(1SA)	0.9601	Pd(1)-C(1)-H(1A)	109.5
C(1)-H(1B)	0.9800	C(1S)-H(1SB)	0.9605	Pd(1)-C(1)-H(1B)	109.5
C(1)-H(1C)	0.9800	C(2S)-C(3S)	1.6065	H(1A)-C(1)-H(1B)	109.5
C(2)-C(3)	1.381(10)	C(2S)-C(3S')	1.8306	Pd(1)-C(1)-H(1C)	109.5
C(2)-C(7)	1.511(11)	C(2S)-H(2SA)	0.9605	H(1A)-C(1)-H(1C)	109.5
C(3)-C(4)	1.390(12)	C(2S)-H(2SB)	0.9602	H(1B)-C(1)-H(1C)	109.5
C(3)-H(3)	0.9500	C(3S)-C(3S')	0.6027	N(1)-C(2)-C(3)	121.3(7)
C(4)-C(5)	1.388(11)	C(3S)-C(4S)	1.7546	N(1)-C(2)-C(7)	117.1(6)
C(4)-H(4)	0.9500	C(3S)-H(3SA)	0.9602	C(3)-C(2)-C(7)	121.6(6)
C(5)-C(6)	1.377(11)	C(3S)-H(3SB)	0.9606	C(2)-C(3)-C(4)	119.7(7)
C(5)-H(5)	0.9500	C(4S)-O(1S)	1.4088	C(2)-C(3)-H(3)	120.2
C(6)-C(13)	1.517(9)	C(4S)-H(4SA)	0.9606	C(4)-C(3)-H(3)	120.2
C(7)-H(7A)	0.9900	C(4S)-H(4SB)	0.9601	C(5)-C(4)-C(3)	118.1(8)
C(7)-H(7B)	0.9900	C(3S')-H(3SA)	0.6256	C(5)-C(4)-H(4)	121.0
C(8)-C(9)	1.385(10)	C(3S')-H(3SB)	1.0705	C(3)-C(4)-H(4)	121.0
C(8)-C(9)#1	1.385(10)	C(1)#1-Pd(1)-C(1)	87.9(4)	C(6)-C(5)-C(4)	120.1(8)
C(9)-C(10)	1.367(13)	C(1)#1-Pd(1)-N(1)#1	176.8(3)	C(6)-C(5)-H(5)	120.0
C(9)-H(9)	0.9500	C(1)-Pd(1)-N(1)#1	94.9(2)	C(4)-C(5)-H(5)	120.0
		C(1)#1-Pd(1)-N(1)	94.9(3)	N(1)-C(6)-C(5)	121.3(6)
		C(1)-Pd(1)-N(1)	176.8(3)	N(1)-C(6)-C(13)	118.2(6)
		N(1)#1-Pd(1)-N(1)	82.2(3)	C(5)-C(6)-C(13)	120.5(7)

N(2)-C(7)-C(2)	111.6(7)	N(3)-C(14)-H(14A)	109.5	C(3S')-C(3S)-C(4S)	152.8
N(2)-C(7)-H(7A)	109.3	N(3)-C(14)-H(14B)	109.5	C(2S)-C(3S)-C(4S)	91.3
C(2)-C(7)-H(7A)	109.3	H(14A)-C(14)-H(14B)	109.5	C(3S')-C(3S)-H(3SA)	39.4
N(2)-C(7)-H(7B)	109.3	N(3)-C(14)-H(14C)	109.5	C(2S)-C(3S)-H(3SA)	113.4
C(2)-C(7)-H(7B)	109.3	H(14A)-C(14)-H(14C)	109.5	C(4S)-C(3S)-H(3SA)	113.4
H(7A)-C(7)-H(7B)	108.0	H(14B)-C(14)-H(14C)	109.5	C(3S')-C(3S)-H(3SB)	83.1
C(9)-C(8)-C(9)#1	118.5(10)	O(1S)-C(1S)-C(2S)	130.9	C(2S)-C(3S)-H(3SB)	113.4
C(9)-C(8)-S(1)	120.7(5)	O(1S)-C(1S)-C(4S)	47.4	C(4S)-C(3S)-H(3SB)	113.4
C(9)#1-C(8)-S(1)	120.7(5)	C(2S)-C(1S)-C(4S)	91.3	H(3SA)-C(3S)-H(3SB)	110.8
C(10)-C(9)-C(8)	120.5(9)	O(1S)-C(1S)-H(1SA)	104.6	O(1S)-C(4S)-C(3S)	105.6
C(10)-C(9)-H(9)	119.7	C(2S)-C(1S)-H(1SA)	104.7	O(1S)-C(4S)-C(1S)	37.1
C(8)-C(9)-H(9)	119.7	C(4S)-C(1S)-H(1SA)	149.5	C(3S)-C(4S)-C(1S)	77.3
C(9)-C(10)-C(11)	121.0(10)	O(1S)-C(1S)-H(1SB)	104.4	O(1S)-C(4S)-H(4SA)	110.6
C(9)-C(10)-H(10)	119.5	C(2S)-C(1S)-H(1SB)	104.4	C(3S)-C(4S)-H(4SA)	110.6
C(11)-C(10)-H(10)	119.5	C(4S)-C(1S)-H(1SB)	94.9	C(1S)-C(4S)-H(4SA)	99.5
C(10)-C(11)-C(10)#1	118.4(12)	H(1SA)-C(1S)-H(1SB)	105.7	O(1S)-C(4S)-H(4SB)	110.6
C(10)-C(11)-C(12)	120.8(6)	C(1S)-C(2S)-C(3S)	97.8	C(3S)-C(4S)-H(4SB)	110.6
C(10)#1-C(11)-C(12)	120.8(6)	C(1S)-C(2S)-C(3S')	116.2	C(1S)-C(4S)-H(4SB)	144.6
C(11)-C(12)-H(12A)	109.5	C(3S)-C(2S)-C(3S')	18.8	H(4SA)-C(4S)-H(4SB)	108.8
C(11)-C(12)-H(12B)	109.5	C(1S)-C(2S)-H(2SA)	112.2	C(1S)-O(1S)-C(4S)	95.5
C(11)-C(12)-H(12C)	109.5	C(3S)-C(2S)-H(2SA)	112.2	C(3S)-C(3S')-C(2S)	59.1
N(3)-C(13)-C(6)	117.1(6)	C(3S')-C(2S)-H(2SA)	99.9	C(3S)-C(3S')-H(3SA)	102.8
N(3)-C(13)-H(13A)	108.0	C(1S)-C(2S)-H(2SB)	112.2	C(2S)-C(3S')-H(3SA)	115.5
C(6)-C(13)-H(13A)	108.0	C(3S)-C(2S)-H(2SB)	112.2	C(3S)-C(3S')-H(3SB)	63.0
N(3)-C(13)-H(13B)	108.0	C(3S')-C(2S)-H(2SB)	105.6	C(2S)-C(3S')-H(3SB)	93.4
C(6)-C(13)-H(13B)	108.0	H(2SA)-C(2S)-H(2SB)	109.8	H(3SA)-C(3S')-H(3SB)	135.9
H(13A)-C(13)-H(13B)	107.3	C(3S')-C(3S)-C(2S)	102.1		

Table B7. Crystal data and structure refinement for [(^tBuN₄)Ni^{III}(*o*-PhF)Br]PF₆.

Identification code	115413/lt/JS-01-091313
Empirical formula	C ₃₂ H ₄₄ Br F ₇ N ₄ Ni O P
Formula weight	803.30
Temperature	100(2) K
Wavelength	0.71073 Å
Crystal system	Monoclinic
Space group	C _{2/c}
Unit cell dimensions	a = 35.9614(13) Å α = 90°. b = 13.0696(5) Å β = 90.599(2)°. c = 15.4316(5) Å γ = 90°.
Volume	7252.5(4) Å ³
Z	8
Density (calculated)	1.471 Mg/m ³
Absorption coefficient	1.748 mm ⁻¹
F(000)	3304
Crystal size	0.508 x 0.504 x 0.055 mm ³
Theta range for data collection	1.658 to 25.472°.
Index ranges	-43 ≤ h ≤ 43, -15 ≤ k ≤ 15, -18 ≤ l ≤ 18
Reflections collected	48245
Independent reflections	6705 [R(int) = 0.0907]
Completeness to theta = 25.242°	100.0 %
Absorption correction	Semi-empirical from equivalents
Max. and min. transmission	4901 and 0.3796
Refinement method	Full-matrix least-squares on F ²
Data / restraints / parameters	6705 / 942 / 471
Goodness-of-fit on F ²	1.110
Final R indices [I > 2σ(I)]	R1 = 0.0896, wR2 = 0.2245
R indices (all data)	R1 = 0.1352, wR2 = 0.2515
Extinction coefficient	n/a
Largest diff. peak and hole	0.977 and -1.076 e.Å ⁻³

Table B8. Bond lengths [\AA]and angles [$^\circ$] for[(^tBuN₄)Ni^{III}(*o*-PhF)Br]PF₆.

Br(1)-Ni(1)	2.4404(18)	C(9)-C(10)	1.377(11)	C(23)-C(28)	1.43(2)
Br(1')-Ni(1)	2.400(5)	C(9)-H(9)	0.9500	C(24)-C(25)	1.39(2)
Ni(1)-N(2)	1.956(6)	C(10)-C(11)	1.374(10)	C(24)-F(1)	1.419(18)
Ni(1)-N(1)	1.981(6)	C(10)-H(10)	0.9500	C(25)-C(26)	1.39(3)
Ni(1)-C(23')	1.982(10)	C(11)-C(12)	1.396(10)	C(25)-H(25)	0.9500
Ni(1)-C(23)	1.993(18)	C(11)-H(11)	0.9500	C(26)-C(27)	1.31(3)
Ni(1)-N(3)	2.342(7)	C(12)-C(13)	1.510(9)	C(26)-H(26)	0.9500
Ni(1)-N(4)	2.345(7)	C(13)-H(13A)	0.9900	C(27)-C(28)	1.40(3)
N(1)-C(1)	1.329(11)	C(13)-H(13B)	0.9900	C(27)-H(27)	0.9500
N(1)-C(5)	1.339(9)	C(14)-H(14A)	0.9900	C(28)-H(28)	0.9500
N(2)-C(12)	1.324(9)	C(14)-H(14B)	0.9900	C(23')-C(24')	1.276(18)
N(2)-C(8)	1.343(9)	C(15)-C(17)	1.503(16)	C(23')-C(28')	1.428(17)
N(3)-C(6)	1.479(11)	C(15)-C(18)	1.546(15)	C(24')-C(25')	1.383(18)
N(3)-C(7)	1.491(10)	C(15)-C(16)	1.567(15)	C(24')-F(1')	1.416(16)
N(3)-C(15)	1.534(12)	C(16)-H(16A)	0.9800	C(25')-C(26')	1.38(2)
N(4)-C(13)	1.482(10)	C(16)-H(16B)	0.9800	C(25')-H(25')	0.9500
N(4)-C(14)	1.503(9)	C(16)-H(16C)	0.9800	C(26')-C(27')	1.31(2)
N(4)-C(19)	1.534(9)	C(17)-H(17A)	0.9800	C(26')-H(26')	0.9500
C(1)-C(2)	1.386(11)	C(17)-H(17B)	0.9800	C(27')-C(28')	1.392(19)
C(1)-C(14)	1.476(10)	C(17)-H(17C)	0.9800	C(27')-H(27')	0.9500
C(2)-C(3)	1.399(11)	C(18)-H(18A)	0.9800	C(28')-H(28')	0.9500
C(2)-H(2)	0.9500	C(18)-H(18B)	0.9800	P(1)-F(2)	1.588(5)
C(3)-C(4)	1.351(12)	C(18)-H(18C)	0.9800	P(1)-F(3)	1.590(6)
C(3)-H(3)	0.9500	C(19)-C(21)	1.507(12)	P(1)-F(4)	1.589(6)
C(4)-C(5)	1.383(11)	C(19)-C(22)	1.532(14)	P(1)-F(7)	1.592(5)
C(4)-H(4)	0.9500	C(19)-C(20)	1.535(13)	P(1)-F(6)	1.602(5)
C(5)-C(6)	1.484(12)	C(20)-H(20A)	0.9800	P(1)-F(5)	1.604(6)
C(6)-H(6A)	0.9900	C(20)-H(20B)	0.9800	O(2S)-C(5S)	1.4130
C(6)-H(6B)	0.9900	C(20)-H(20C)	0.9800	O(2S)-C(8S)	1.4134
C(7)-C(8)	1.478(11)	C(21)-H(21A)	0.9800	C(5S)-C(6S)	1.3930
C(7)-H(7A)	0.9900	C(21)-H(21B)	0.9800	C(5S)-H(5S1)	0.9900
C(7)-H(7B)	0.9900	C(21)-H(21C)	0.9800	C(5S)-H(5S2)	0.9900
C(8)-C(9)	1.382(10)	C(22)-H(22A)	0.9800	C(6S)-C(7S)	1.3923
		C(22)-H(22B)	0.9800	C(6S)-H(6S1)	0.9900
		C(22)-H(22C)	0.9800	C(6S)-H(6S2)	0.9900
		C(23)-C(24)	1.27(2)	C(7S)-C(8S)	1.3950

C(7S)-H(7S1)	0.9900	N(1)-Ni(1)-Br(1)	164.5(2)	C(4)-C(5)-C(6)	122.5(7)
C(7S)-H(7S2)	0.9900	C(23)-Ni(1)-Br(1)	97.9(13)	N(3)-C(6)-C(5)	116.9(7)
C(8S)-H(8S1)	0.9900	N(3)-Ni(1)-Br(1)	93.85(19)	N(3)-C(6)-H(6A)	108.1
C(8S)-H(8S2)	0.9900	N(4)-Ni(1)-Br(1)	100.22(16)	C(5)-C(6)-H(6A)	108.1
O(1S)-C(4S)	1.4140	C(1)-N(1)-C(5)	121.3(7)	N(3)-C(6)-H(6B)	108.1
O(1S)-C(1S)	1.4149	C(1)-N(1)-Ni(1)	118.0(5)	C(5)-C(6)-H(6B)	108.1
C(1S)-C(2S)	1.3947	C(5)-N(1)-Ni(1)	117.6(5)	H(6A)-C(6)-H(6B)	107.3
C(1S)-H(2S1)	0.9900	C(12)-N(2)-C(8)	121.2(6)	C(8)-C(7)-N(3)	113.2(6)
C(1S)-H(2S2)	0.9900	C(12)-N(2)-Ni(1)	119.4(4)	C(8)-C(7)-H(7A)	108.9
C(2S)-C(3S)	1.3947	C(8)-N(2)-Ni(1)	118.2(5)	N(3)-C(7)-H(7A)	108.9
C(2S)-H(3S1)	0.9900	C(6)-N(3)-C(7)	109.5(6)	C(8)-C(7)-H(7B)	108.9
C(2S)-H(3S2)	0.9900	C(6)-N(3)-C(15)	109.7(7)	N(3)-C(7)-H(7B)	108.9
C(3S)-C(4S)	1.3940	C(7)-N(3)-C(15)	110.2(7)	H(7A)-C(7)-H(7B)	107.8
C(3S)-H(4S1)	0.9900	C(6)-N(3)-Ni(1)	102.0(5)	N(2)-C(8)-C(9)	120.5(7)
C(3S)-H(4S2)	0.9900	C(7)-N(3)-Ni(1)	98.8(5)	N(2)-C(8)-C(7)	116.1(6)
C(4S)-H(1S1)	0.9900	C(15)-N(3)-Ni(1)	125.5(5)	C(9)-C(8)-C(7)	123.4(6)
C(4S)-H(1S2)	0.9900	C(13)-N(4)-C(14)	108.0(6)	C(10)-C(9)-C(8)	118.8(6)
N(2)-Ni(1)-N(1)	80.6(2)	C(13)-N(4)-C(19)	109.1(6)	C(10)-C(9)-H(9)	120.6
N(2)-Ni(1)-C(23')	178.3(5)	C(14)-N(4)-C(19)	109.9(5)	C(8)-C(9)-H(9)	120.6
N(1)-Ni(1)-C(23')	97.7(5)	C(13)-N(4)-Ni(1)	103.4(4)	C(11)-C(10)-C(9)	120.4(7)
N(2)-Ni(1)-C(23)	176.5(17)	C(14)-N(4)-Ni(1)	99.0(5)	C(11)-C(10)-H(10)	119.8
N(1)-Ni(1)-C(23)	97.5(14)	C(19)-N(4)-Ni(1)	126.0(6)	C(9)-C(10)-H(10)	119.8
N(2)-Ni(1)-N(3)	80.3(2)	N(1)-C(1)-C(2)	120.8(7)	C(10)-C(11)-C(12)	118.2(7)
N(1)-Ni(1)-N(3)	81.3(3)	N(1)-C(1)-C(14)	116.0(7)	C(10)-C(11)-H(11)	120.9
C(23')-Ni(1)-N(3)	100.0(6)	C(2)-C(1)-C(14)	123.2(8)	C(12)-C(11)-H(11)	120.9
C(23)-Ni(1)-N(3)	102(2)	C(1)-C(2)-C(3)	117.9(8)	N(2)-C(12)-C(11)	120.9(6)
N(2)-Ni(1)-N(4)	81.0(2)	C(1)-C(2)-H(2)	121.1	N(2)-C(12)-C(13)	118.6(6)
N(1)-Ni(1)-N(4)	79.7(2)	C(3)-C(2)-H(2)	121.1	C(11)-C(12)-C(13)	120.4(7)
C(23')-Ni(1)-N(4)	98.2(5)	C(4)-C(3)-C(2)	120.1(8)	N(4)-C(13)-C(12)	115.2(7)
C(23)-Ni(1)-N(4)	95.7(19)	C(4)-C(3)-H(3)	119.9	N(4)-C(13)-H(13A)	108.5
N(3)-Ni(1)-N(4)	155.2(2)	C(2)-C(3)-H(3)	119.9	C(12)-C(13)-H(13A)	108.5
N(2)-Ni(1)-Br(1')	99.6(5)	C(3)-C(4)-C(5)	119.6(7)	N(4)-C(13)-H(13B)	108.5
N(1)-Ni(1)-Br(1')	174.7(4)	C(3)-C(4)-H(4)	120.2	C(12)-C(13)-H(13B)	108.5
N(3)-Ni(1)-Br(1')	103.9(4)	C(5)-C(4)-H(4)	120.2	H(13A)-C(13)-H(13B)	107.5
N(4)-Ni(1)-Br(1')	95.1(3)	N(1)-C(5)-C(4)	120.2(8)	C(1)-C(14)-N(4)	111.7(6)
N(2)-Ni(1)-Br(1)	84.10(18)	N(1)-C(5)-C(6)	117.2(7)	C(1)-C(14)-H(14A)	109.3

N(4)-C(14)-H(14A)	109.3	H(20A)-C(20)-H(20B)	109.5	C(28')-C(23')-Ni(1)	116.4(10)
C(1)-C(14)-H(14B)	109.3	C(19)-C(20)-H(20C)	109.5	C(23')-C(24')-C(25')	127.1(14)
N(4)-C(14)-H(14B)	109.3	H(20A)-C(20)-H(20C)	109.5	C(23')-C(24')-F(1')	121.4(11)
H(14A)-C(14)-H(14B)	107.9	H(20B)-C(20)-H(20C)	109.5	C(25')-C(24')-F(1')	110.0(12)
C(17)-C(15)-N(3)	110.2(9)	C(19)-C(21)-H(21A)	109.5	C(24')-C(25')-C(26')	116.3(15)
C(17)-C(15)-C(18)	109.2(9)	C(19)-C(21)-H(21B)	109.5	C(24')-C(25')-H(25')	121.9
N(3)-C(15)-C(18)	110.5(8)	H(21A)-C(21)-H(21B)	109.5	C(26')-C(25')-H(25')	121.9
C(17)-C(15)-C(16)	108.8(10)	C(19)-C(21)-H(21C)	109.5	C(27')-C(26')-C(25')	120.0(14)
N(3)-C(15)-C(16)	110.0(8)	H(21A)-C(21)-H(21C)	109.5	C(27')-C(26')-H(26')	120.0
C(18)-C(15)-C(16)	108.1(10)	H(21B)-C(21)-H(21C)	109.5	C(25')-C(26')-H(26')	120.0
C(15)-C(16)-H(16A)	109.5	C(19)-C(22)-H(22A)	109.5	C(26')-C(27')-C(28')	121.5(15)
C(15)-C(16)-H(16B)	109.5	C(19)-C(22)-H(22B)	109.5	C(26')-C(27')-H(27')	119.3
H(16A)-C(16)-H(16B)	109.5	H(22A)-C(22)-H(22B)	109.5	C(28')-C(27')-H(27')	119.3
C(15)-C(16)-H(16C)	109.5	C(19)-C(22)-H(22C)	109.5	C(27')-C(28')-C(23')	118.9(14)
H(16A)-C(16)-H(16C)	109.5	H(22A)-C(22)-H(22C)	109.5	C(27')-C(28')-H(28')	120.6
H(16B)-C(16)-H(16C)	109.5	H(22B)-C(22)-H(22C)	109.5	C(23')-C(28')-H(28')	120.6
C(15)-C(17)-H(17A)	109.5	C(24)-C(23)-C(28)	115(2)	F(2)-P(1)-F(3)	90.8(3)
C(15)-C(17)-H(17B)	109.5	C(24)-C(23)-Ni(1)	107(3)	F(2)-P(1)-F(4)	90.2(3)
H(17A)-C(17)-H(17B)	109.5	C(28)-C(23)-Ni(1)	129(3)	F(3)-P(1)-F(4)	91.6(3)
C(15)-C(17)-H(17C)	109.5	C(23)-C(24)-C(25)	123(3)	F(2)-P(1)-F(7)	178.6(4)
H(17A)-C(17)-H(17C)	109.5	C(23)-C(24)-F(1)	126(3)	F(3)-P(1)-F(7)	90.5(3)
H(17B)-C(17)-H(17C)	109.5	C(25)-C(24)-F(1)	104(2)	F(4)-P(1)-F(7)	90.4(3)
C(15)-C(18)-H(18A)	109.5	C(24)-C(25)-C(26)	121(3)	F(2)-P(1)-F(6)	90.0(3)
C(15)-C(18)-H(18B)	109.5	C(24)-C(25)-H(25)	119.6	F(3)-P(1)-F(6)	89.8(3)
H(18A)-C(18)-H(18B)	109.5	C(26)-C(25)-H(25)	119.6	F(4)-P(1)-F(6)	178.6(3)
C(15)-C(18)-H(18C)	109.5	C(27)-C(26)-C(25)	119(3)	F(7)-P(1)-F(6)	89.3(3)
H(18A)-C(18)-H(18C)	109.5	C(27)-C(26)-H(26)	120.5	F(2)-P(1)-F(5)	89.4(3)
H(18B)-C(18)-H(18C)	109.5	C(25)-C(26)-H(26)	120.5	F(3)-P(1)-F(5)	179.3(3)
C(21)-C(19)-C(22)	110.0(9)	C(26)-C(27)-C(28)	119(3)	F(4)-P(1)-F(5)	89.1(3)
C(21)-C(19)-C(20)	108.3(9)	C(26)-C(27)-H(27)	120.7	F(7)-P(1)-F(5)	89.3(3)
C(22)-C(19)-C(20)	107.7(7)	C(28)-C(27)-H(27)	120.7	F(6)-P(1)-F(5)	89.5(3)
C(21)-C(19)-N(4)	109.7(6)	C(27)-C(28)-C(23)	123(3)	C(5S)-O(2S)-C(8S)	103.5
C(22)-C(19)-N(4)	110.8(7)	C(27)-C(28)-H(28)	118.5	C(6S)-C(5S)-O(2S)	109.3
C(20)-C(19)-N(4)	110.2(7)	C(23)-C(28)-H(28)	118.5	C(6S)-C(5S)-H(5S1)	109.8
C(19)-C(20)-H(20A)	109.5	C(24')-C(23')-C(28')	115.7(11)	O(2S)-C(5S)-H(5S1)	109.8
C(19)-C(20)-H(20B)	109.5	C(24')-C(23')-Ni(1)	127.8(11)	C(6S)-C(5S)-H(5S2)	109.8

O(2S)-C(5S)-H(5S2)	109.8	C(7S)-C(8S)-H(8S1)	111.1	C(3S)-C(2S)-H(3S2)	111.4
H(5S1)-C(5S)-H(5S2)	108.3	O(2S)-C(8S)-H(8S1)	111.1	C(1S)-C(2S)-H(3S2)	111.4
C(7S)-C(6S)-C(5S)	100.3	C(7S)-C(8S)-H(8S2)	111.1	H(3S1)-C(2S)-H(3S2)	109.2
C(7S)-C(6S)-H(6S1)	111.7	O(2S)-C(8S)-H(8S2)	111.1	C(4S)-C(3S)-C(2S)	102.8
C(5S)-C(6S)-H(6S1)	111.7	H(8S1)-C(8S)-H(8S2)	109.0	C(4S)-C(3S)-H(4S1)	111.2
C(7S)-C(6S)-H(6S2)	111.7	C(4S)-O(1S)-C(1S)	101.8	C(2S)-C(3S)-H(4S1)	111.2
C(5S)-C(6S)-H(6S2)	111.7	C(2S)-C(1S)-O(1S)	108.6	C(4S)-C(3S)-H(4S2)	111.2
H(6S1)-C(6S)-H(6S2)	109.5	C(2S)-C(1S)-H(2S1)	110.0	C(2S)-C(3S)-H(4S2)	111.2
C(6S)-C(7S)-C(8S)	104.6	O(1S)-C(1S)-H(2S1)	110.0	H(4S1)-C(3S)-H(4S2)	109.1
C(6S)-C(7S)-H(7S1)	110.8	C(2S)-C(1S)-H(2S2)	110.0	C(3S)-C(4S)-O(1S)	100.9
C(8S)-C(7S)-H(7S1)	110.8	O(1S)-C(1S)-H(2S2)	110.0	C(3S)-C(4S)-H(1S1)	111.6
C(6S)-C(7S)-H(7S2)	110.8	H(2S1)-C(1S)-H(2S2)	108.4	O(1S)-C(4S)-H(1S1)	111.6
C(8S)-C(7S)-H(7S2)	110.8	C(3S)-C(2S)-C(1S)	102.0	C(3S)-C(4S)-H(1S2)	111.6
H(7S1)-C(7S)-H(7S2)	108.9	C(3S)-C(2S)-H(3S1)	111.4	O(1S)-C(4S)-H(1S2)	111.6
C(7S)-C(8S)-O(2S)	103.5	C(1S)-C(2S)-H(3S1)	111.4	H(1S1)-C(4S)-H(1S2)	109.4

Table B9. Crystal data and structure refinement for (^{Me}N₄)Ni^{II}Me₂.

Identification code	113514/lt/x8/JS-091514-01	
Empirical formula	C ₁₈ H ₂₆ N ₄ Ni	
Formula weight	357.14	
Temperature	100(2) K	
Wavelength	0.71073 Å	
Crystal system	Monoclinic	
Space group	C2/c	
Unit cell dimensions	a = 14.2510(7) Å	α = 90°.
	b = 13.1814(5) Å	β = 98.280(3)°.
	c = 9.2333(4) Å	γ = 90°.
Volume	1716.38(13) Å ³	
Z	4	
Density (calculated)	1.382 Mg/m ³	
Absorption coefficient	1.135 mm ⁻¹	
F(000)	760	
Crystal size	0.289 x 0.204 x 0.078 mm ³	
Theta range for data collection	2.115 to 28.316°.	
Index ranges	-18 ≤ h ≤ 18, -17 ≤ k ≤ 17, -12 ≤ l ≤ 11	
Reflections collected	10169	
Independent reflections	2135 [R(int) = 0.0360]	
Completeness to theta = 25.242°	100.0 %	
Absorption correction	Semi-empirical from equivalents	
Max. and min. transmission	0.8621 and 0.7705	
Refinement method	Full-matrix least-squares on F ²	
Data / restraints / parameters	2135 / 0 / 215	
Goodness-of-fit on F ²	1.016	
Final R indices [I > 2σ(I)]	R1 = 0.0263, wR2 = 0.0544	
R indices (all data)	R1 = 0.0358, wR2 = 0.0591	
Extinction coefficient	n/a	
Largest diff. peak and hole	0.241 and -0.162 e.Å ⁻³	

Table B10. Bond lengths [Å]

and angles [°] for

 $(\text{Me}_4\text{N})\text{Ni}^{\text{II}}\text{Me}_2$.

Ni(1)-C(1)	1.913(7)	N(1')-C(6')	1.341(4)	C(9)-N(2)-C(7)	114.4(3)
Ni(1)-C(1)#1	1.913(7)	N(1')-C(2')	1.353(6)	Ni(1)-C(1)-H(1A)	109.5
Ni(1)-N(1)	1.973(6)	N(2')-C(8')#1	1.441(6)	Ni(1)-C(1)-H(1B)	109.5
Ni(1)-N(1)#1	1.973(6)	N(2')-C(9')	1.460(5)	H(1A)-C(1)-H(1B)	109.5
N(1)-C(6)	1.342(6)	N(2')-C(7')	1.470(4)	Ni(1)-C(1)-H(1C)	109.5
N(1)-C(2)	1.351(5)	C(1')-H(1'1)	0.9800	H(1A)-C(1)-H(1C)	109.5
N(2)-C(8)#1	1.447(4)	C(1')-H(1'2)	0.9800	H(1B)-C(1)-H(1C)	109.5
N(2)-C(9)	1.457(4)	C(1')-H(1'3)	0.9800	N(1)-C(2)-C(3)	121.4(4)
N(2)-C(7)	1.461(4)	C(2')-C(3')	1.371(5)	N(1)-C(2)-C(8)	118.6(4)
C(1)-H(1A)	0.9800	C(2')-C(8')	1.519(5)	C(3)-C(2)-C(8)	120.0(4)
C(1)-H(1B)	0.9800	C(3')-C(4')	1.389(6)	C(2)-C(3)-C(4)	119.6(3)
C(1)-H(1C)	0.9800	C(3')-H(3')	0.9500	C(2)-C(3)-H(3)	120.2
C(2)-C(3)	1.381(4)	C(4')-C(5')	1.348(9)	C(4)-C(3)-H(3)	120.2
C(2)-C(8)	1.520(5)	C(4')-H(4')	0.9500	C(3)-C(4)-C(5)	118.7(4)
C(3)-C(4)	1.395(4)	C(5')-C(6')	1.414(5)	C(3)-C(4)-H(4)	120.6
C(3)-H(3)	0.9500	C(5')-H(5')	0.9500	C(5)-C(4)-H(4)	120.6
C(4)-C(5)	1.402(5)	C(6')-C(7')	1.509(4)	C(6)-C(5)-C(4)	118.2(5)
C(4)-H(4)	0.9500	C(7')-H(7'A)	0.9900	C(6)-C(5)-H(5)	120.9
C(5)-C(6)	1.389(6)	C(7')-H(7'B)	0.9900	C(4)-C(5)-H(5)	120.9
C(5)-H(5)	0.9500	C(8')-N(2')#1	1.441(6)	N(1)-C(6)-C(5)	122.6(4)
C(6)-C(7)	1.493(4)	C(8')-H(8'A)	0.9900	N(1)-C(6)-C(7)	118.5(3)
C(7)-H(7A)	0.9900	C(8')-H(8'B)	0.9900	C(5)-C(6)-C(7)	118.9(4)
C(7)-H(7B)	0.9900	C(9')-H(9'A)	0.9800	N(2)-C(7)-C(6)	117.7(2)
C(8)-N(2)#1	1.447(4)	C(9')-H(9'B)	0.9800	N(2)-C(7)-H(7A)	107.9
C(8)-H(8A)	0.9900	C(9')-H(9'C)	0.9800	C(6)-C(7)-H(7A)	107.9
C(8)-H(8B)	0.9900	C(1)-Ni(1)-C(1)#1	91.1(7)	N(2)-C(7)-H(7B)	107.9
C(9)-H(9A)	0.9800	C(1)-Ni(1)-N(1)	91.6(3)	C(6)-C(7)-H(7B)	107.9
C(9)-H(9B)	0.9800	C(1)#1-Ni(1)-N(1)	173.5(7)	H(7A)-C(7)-H(7B)	107.2
C(9)-H(9C)	0.9800	C(1)-Ni(1)-N(1)#1	173.5(7)	N(2)#1-C(8)-C(2)	118.0(4)
Ni(1')-C(1')#1	1.915(7)	C(1)#1-Ni(1)-N(1)#1	91.6(3)	N(2)#1-C(8)-H(8A)	107.8
Ni(1')-C(1')	1.915(7)	N(1)-Ni(1)-N(1)#1	86.5(3)	C(2)-C(8)-H(8A)	107.8
Ni(1')-N(1')	1.950(7)	C(6)-N(1)-C(2)	119.4(4)	N(2)#1-C(8)-H(8B)	107.8
Ni(1')-N(1')#1	1.950(7)	C(6)-N(1)-Ni(1)	120.2(3)	C(2)-C(8)-H(8B)	107.8
		C(2)-N(1)-Ni(1)	120.5(4)	H(8A)-C(8)-H(8B)	107.1
		C(8)#1-N(2)-C(9)	112.8(3)	N(2)-C(9)-H(9A)	109.5
		C(8)#1-N(2)-C(7)	119.1(3)	N(2)-C(9)-H(9B)	109.5

H(9A)-C(9)-H(9B)	109.5	Ni(1')-C(1')-H(1'3)	109.5	N(2')-C(7')-H(7'A)	107.9
N(2)-C(9)-H(9C)	109.5	H(1'1)-C(1')-H(1'3)	109.5	C(6')-C(7')-H(7'A)	107.9
H(9A)-C(9)-H(9C)	109.5	H(1'2)-C(1')-H(1'3)	109.5	N(2')-C(7')-H(7'B)	107.9
H(9B)-C(9)-H(9C)	109.5	N(1')-C(2')-C(3')	122.3(5)	C(6')-C(7')-H(7'B)	107.9
C(1')#1-Ni(1')-C(1')	89.2(3)	N(1')-C(2')-C(8')	117.2(4)	H(7'A)-C(7')-H(7'B)	107.2
C(1')#1-Ni(1')-N(1')	177.1(3)	C(3')-C(2')-C(8')	120.5(3)	N(2')#1-C(8')-C(2')	117.8(3)
C(1')-Ni(1')-N(1')	92.1(2)	C(2')-C(3')-C(4')	118.7(4)	N(2')#1-C(8')-H(8'A)	107.9
C(1')#1-Ni(1')-N(1')#1	92.1(2)	C(2')-C(3')-H(3')	120.7	C(2')-C(8')-H(8'A)	107.9
C(1')-Ni(1')-N(1')#1	177.1(3)	C(4')-C(3')-H(3')	120.7	N(2')#1-C(8')-H(8'B)	107.9
N(1')-Ni(1')-N(1')#1	86.8(3)	C(5')-C(4')-C(3')	120.5(5)	C(2')-C(8')-H(8'B)	107.9
C(6')-N(1')-C(2')	118.3(5)	C(5')-C(4')-H(4')	119.8	H(8'A)-C(8')-H(8'B)	107.2
C(6')-N(1')-Ni(1')	119.7(4)	C(3')-C(4')-H(4')	119.8	N(2')-C(9')-H(9'A)	109.5
C(2')-N(1')-Ni(1')	121.9(4)	C(4')-C(5')-C(6')	118.3(4)	N(2')-C(9')-H(9'B)	109.5
C(8')#1-N(2')-C(9')	115.1(3)	C(4')-C(5')-H(5')	120.9	H(9'A)-C(9')-H(9'B)	109.5
C(8')#1-N(2')-C(7')	118.5(3)	C(6')-C(5')-H(5')	120.9	N(2')-C(9')-H(9'C)	109.5
C(9')-N(2')-C(7')	112.1(3)	N(1')-C(6')-C(5')	121.9(4)	H(9'A)-C(9')-H(9'C)	109.5
Ni(1')-C(1')-H(1'1)	109.5	N(1')-C(6')-C(7')	118.5(4)	H(9'B)-C(9')-H(9'C)	109.5
Ni(1')-C(1')-H(1'2)	109.5	C(5')-C(6')-C(7')	119.6(4)		
H(1'1)-C(1')-H(1'2)	109.5	N(2')-C(7')-C(6')	117.6(3)		

Table B11. Crystal data and structure refinement for [(^{Me}N₄)Ni^{III}Me₂]BPh₄.

Identification code	18714_sq/lt/x8/JS-061614-01	
Empirical formula	C ₄₆ H ₅₄ B N ₄ Ni O	
Formula weight	748.45	
Temperature	100(2) K	
Wavelength	0.71073 Å	
Crystal system	Triclinic	
Space group	P $\bar{1}$	
Unit cell dimensions	a = 8.9600(7) Å	$\alpha = 88.779(4)^\circ$.
	b = 14.2611(10) Å	$\beta = 75.985(4)^\circ$.
	c = 16.7826(12) Å	$\gamma = 73.867(4)^\circ$.
Volume	1996.3(3) Å ³	
Z	2	
Density (calculated)	1.245 Mg/m ³	
Absorption coefficient	0.526 mm ⁻¹	
F(000)	798	
Crystal size	0.323 x 0.224 x 0.149 mm ³	
Theta range for data collection	1.252 to 27.608°.	
Index ranges	-11 ≤ h ≤ 11, -18 ≤ k ≤ 18, -21 ≤ l ≤ 21	
Reflections collected	40240	
Independent reflections	9164 [R(int) = 0.0406]	
Completeness to theta = 25.242°	99.7 %	
Absorption correction	Semi-empirical from equivalents	
Max. and min. transmission	0.8621 and 0.7941	
Refinement method	Full-matrix least-squares on F ²	
Data / restraints / parameters	9164 / 1 / 487	
Goodness-of-fit on F ²	1.031	
Final R indices [I > 2σ(I)]	R1 = 0.0389, wR2 = 0.0904	
R indices (all data)	R1 = 0.0518, wR2 = 0.0966	
Extinction coefficient	n/a	
Largest diff. peak and hole	0.532 and -0.437 e.Å ⁻³	

Table B12. Bond lengths [Å]

and angles [°] for

[(^{Me}N₄)Ni^{III}Me₂]BPh₄.

Ni(1)-C(2)	1.9782(19)	C(6)-H(6)	0.9500	C(4S)-H(4SA)	0.9900
Ni(1)-N(1)	1.9792(14)	C(7)-C(8)	1.506(2)	C(4S)-H(4SB)	0.9900
Ni(1)-C(1)	1.987(2)	C(8)-H(8A)	0.9900	C(19)-C(24)	1.396(3)
Ni(1)-C(1')	1.994(9)	C(8)-H(8B)	0.9900	C(19)-C(20)	1.402(3)
Ni(1)-N(2)	1.9958(15)	C(9)-C(10)	1.500(2)	C(19)-B(1)	1.645(2)
Ni(1)-N(4)	2.2399(14)	C(9)-H(9A)	0.9900	C(20)-C(21)	1.394(3)
Ni(1)-N(3)	2.2519(14)	C(9)-H(9B)	0.9900	C(20)-H(20)	0.9500
N(1)-C(7)	1.340(2)	C(10)-C(11)	1.381(3)	C(21)-C(22)	1.380(3)
N(1)-C(3)	1.342(2)	C(11)-C(12)	1.384(3)	C(21)-H(21)	0.9500
N(2)-C(10)	1.343(2)	C(11)-H(11)	0.9500	C(22)-C(23)	1.380(3)
N(2)-C(14)	1.343(2)	C(12)-C(13)	1.388(3)	C(22)-H(22)	0.9500
N(3)-C(17)	1.471(2)	C(12)-H(12)	0.9500	C(23)-C(24)	1.396(3)
N(3)-C(8)	1.478(2)	C(13)-C(14)	1.378(3)	C(23)-H(23)	0.9500
N(3)-C(9)	1.485(2)	C(13)-H(13)	0.9500	C(24)-H(24)	0.9500
N(4)-C(18)	1.479(2)	C(14)-C(15)	1.506(3)	C(25)-C(30)	1.400(2)
N(4)-C(15)	1.480(2)	C(15)-H(15A)	0.9900	C(25)-C(26)	1.403(2)
N(4)-C(16)	1.484(2)	C(15)-H(15B)	0.9900	C(25)-B(1)	1.642(2)
C(1)-H(1A)	0.9800	C(16)-H(16A)	0.9900	C(26)-C(27)	1.389(3)
C(1)-H(1B)	0.9800	C(16)-H(16B)	0.9900	C(26)-H(26)	0.9500
C(1)-H(1C)	0.9800	C(17)-H(17A)	0.9800	C(27)-C(28)	1.385(3)
C(1')-H(1'1)	0.9800	C(17)-H(17B)	0.9800	C(27)-H(27)	0.9500
C(1')-H(1'2)	0.9800	C(17)-H(17C)	0.9800	C(28)-C(29)	1.383(3)
C(1')-H(1'3)	0.9800	C(18)-H(18A)	0.9800	C(28)-H(28)	0.9500
C(2)-H(2A)	0.9800	C(18)-H(18B)	0.9800	C(29)-C(30)	1.387(3)
C(2)-H(2B)	0.9800	C(18)-H(18C)	0.9800	C(29)-H(29)	0.9500
C(2)-H(2C)	0.9800	O(1S)-C(1S)	1.417(3)	C(30)-H(30)	0.9500
C(3)-C(4)	1.381(2)	O(1S)-C(4S)	1.432(3)	C(31)-C(36)	1.400(3)
C(3)-C(16)	1.506(2)	C(1S)-C(2S)	1.497(3)	C(31)-C(32)	1.404(3)
C(4)-C(5)	1.390(3)	C(1S)-H(1SA)	0.9900	C(31)-B(1)	1.644(3)
C(4)-H(4)	0.9500	C(1S)-H(1SB)	0.9900	C(32)-C(33)	1.396(3)
C(5)-C(6)	1.382(3)	C(2S)-C(3S)	1.507(3)	C(32)-H(32)	0.9500
C(5)-H(5)	0.9500	C(2S)-H(2SA)	0.9900	C(33)-C(34)	1.382(3)
C(6)-C(7)	1.383(3)	C(2S)-H(2SB)	0.9900	C(33)-H(33)	0.9500
		C(3S)-C(4S)	1.506(4)	C(34)-C(35)	1.382(3)
		C(3S)-H(3SA)	0.9900	C(34)-H(34)	0.9500
		C(3S)-H(3SB)	0.9900	C(35)-C(36)	1.397(3)

C(35)-H(35)	0.9500	C(3)-N(1)-Ni(1)	118.96(11)	C(4)-C(3)-C(16)	123.69(15)
C(36)-H(36)	0.9500	C(10)-N(2)-C(14)	120.20(16)	C(3)-C(4)-C(5)	118.80(16)
C(37)-C(42)	1.400(2)	C(10)-N(2)-Ni(1)	119.06(12)	C(3)-C(4)-H(4)	120.6
C(37)-C(38)	1.401(2)	C(14)-N(2)-Ni(1)	119.18(12)	C(5)-C(4)-H(4)	120.6
C(37)-B(1)	1.638(2)	C(17)-N(3)-C(8)	109.27(14)	C(6)-C(5)-C(4)	119.61(17)
C(38)-C(39)	1.390(3)	C(17)-N(3)-C(9)	108.37(13)	C(6)-C(5)-H(5)	120.2
C(38)-H(38)	0.9500	C(8)-N(3)-C(9)	112.00(14)	C(4)-C(5)-H(5)	120.2
C(39)-C(40)	1.385(3)	C(17)-N(3)-Ni(1)	116.59(11)	C(5)-C(6)-C(7)	118.94(16)
C(39)-H(39)	0.9500	C(8)-N(3)-Ni(1)	106.15(10)	C(5)-C(6)-H(6)	120.5
C(40)-C(41)	1.385(3)	C(9)-N(3)-Ni(1)	104.45(10)	C(7)-C(6)-H(6)	120.5
C(40)-H(40)	0.9500	C(18)-N(4)-C(15)	108.70(14)	N(1)-C(7)-C(6)	120.86(16)
C(41)-C(42)	1.391(3)	C(18)-N(4)-C(16)	108.27(14)	N(1)-C(7)-C(8)	116.22(15)
C(41)-H(41)	0.9500	C(15)-N(4)-C(16)	112.40(14)	C(6)-C(7)-C(8)	122.84(16)
C(42)-H(42)	0.9500	C(18)-N(4)-Ni(1)	116.36(11)	N(3)-C(8)-C(7)	114.13(14)
C(2)-Ni(1)-N(1)	93.26(7)	C(15)-N(4)-Ni(1)	106.94(10)	N(3)-C(8)-H(8A)	108.7
C(2)-Ni(1)-C(1)	84.68(17)	C(16)-N(4)-Ni(1)	104.21(10)	C(7)-C(8)-H(8A)	108.7
N(1)-Ni(1)-C(1)	176.34(10)	Ni(1)-C(1)-H(1A)	109.5	N(3)-C(8)-H(8B)	108.7
C(2)-Ni(1)-C(1')	71.9(8)	Ni(1)-C(1)-H(1B)	109.5	C(7)-C(8)-H(8B)	108.7
N(1)-Ni(1)-C(1')	165.1(8)	H(1A)-C(1)-H(1B)	109.5	H(8A)-C(8)-H(8B)	107.6
C(2)-Ni(1)-N(2)	176.88(7)	Ni(1)-C(1)-H(1C)	109.5	N(3)-C(9)-C(10)	111.81(14)
N(1)-Ni(1)-N(2)	84.19(6)	H(1A)-C(1)-H(1C)	109.5	N(3)-C(9)-H(9A)	109.3
C(1)-Ni(1)-N(2)	97.96(16)	H(1B)-C(1)-H(1C)	109.5	C(10)-C(9)-H(9A)	109.3
C(1')-Ni(1)-N(2)	110.7(8)	Ni(1)-C(1')-H(1'1)	109.5	N(3)-C(9)-H(9B)	109.3
C(2)-Ni(1)-N(4)	97.74(7)	Ni(1)-C(1')-H(1'2)	109.5	C(10)-C(9)-H(9B)	109.3
N(1)-Ni(1)-N(4)	80.22(6)	H(1'1)-C(1')-H(1'2)	109.5	H(9A)-C(9)-H(9B)	107.9
C(1)-Ni(1)-N(4)	103.03(9)	Ni(1)-C(1')-H(1'3)	109.5	N(2)-C(10)-C(11)	121.49(17)
C(1')-Ni(1)-N(4)	101.5(6)	H(1'1)-C(1')-H(1'3)	109.5	N(2)-C(10)-C(9)	114.91(15)
N(2)-Ni(1)-N(4)	80.07(6)	H(1'2)-C(1')-H(1'3)	109.5	C(11)-C(10)-C(9)	123.56(16)
C(2)-Ni(1)-N(3)	101.88(7)	Ni(1)-C(2)-H(2A)	109.5	C(10)-C(11)-C(12)	118.48(18)
N(1)-Ni(1)-N(3)	80.42(6)	Ni(1)-C(2)-H(2B)	109.5	C(10)-C(11)-H(11)	120.8
C(1)-Ni(1)-N(3)	97.02(10)	H(2A)-C(2)-H(2B)	109.5	C(12)-C(11)-H(11)	120.8
C(1')-Ni(1)-N(3)	102.0(6)	Ni(1)-C(2)-H(2C)	109.5	C(11)-C(12)-C(13)	119.78(19)
N(2)-Ni(1)-N(3)	79.51(6)	H(2A)-C(2)-H(2C)	109.5	C(11)-C(12)-H(12)	120.1
N(4)-Ni(1)-N(3)	153.07(6)	H(2B)-C(2)-H(2C)	109.5	C(13)-C(12)-H(12)	120.1
C(7)-N(1)-C(3)	120.86(15)	N(1)-C(3)-C(4)	120.85(16)	C(14)-C(13)-C(12)	118.82(18)
C(7)-N(1)-Ni(1)	119.74(12)	N(1)-C(3)-C(16)	115.40(15)	C(14)-C(13)-H(13)	120.6

C(12)-C(13)-H(13)	120.6	C(1S)-C(2S)-H(2SA)	111.6	C(30)-C(25)-B(1)	121.90(15)
N(2)-C(14)-C(13)	121.15(17)	C(3S)-C(2S)-H(2SA)	111.6	C(26)-C(25)-B(1)	122.61(15)
N(2)-C(14)-C(15)	115.85(16)	C(1S)-C(2S)-H(2SB)	111.6	C(27)-C(26)-C(25)	122.76(17)
C(13)-C(14)-C(15)	122.91(17)	C(3S)-C(2S)-H(2SB)	111.6	C(27)-C(26)-H(26)	118.6
N(4)-C(15)-C(14)	112.96(14)	H(2SA)-C(2S)-H(2SB)	109.4	C(25)-C(26)-H(26)	118.6
N(4)-C(15)-H(15A)	109.0	C(4S)-C(3S)-C(2S)	102.12(19)	C(28)-C(27)-C(26)	120.27(17)
C(14)-C(15)-H(15A)	109.0	C(4S)-C(3S)-H(3SA)	111.3	C(28)-C(27)-H(27)	119.9
N(4)-C(15)-H(15B)	109.0	C(2S)-C(3S)-H(3SA)	111.3	C(26)-C(27)-H(27)	119.9
C(14)-C(15)-H(15B)	109.0	C(4S)-C(3S)-H(3SB)	111.3	C(29)-C(28)-C(27)	118.67(17)
H(15A)-C(15)-H(15B)	107.8	C(2S)-C(3S)-H(3SB)	111.3	C(29)-C(28)-H(28)	120.7
N(4)-C(16)-C(3)	112.52(14)	H(3SA)-C(3S)-H(3SB)	109.2	C(27)-C(28)-H(28)	120.7
N(4)-C(16)-H(16A)	109.1	O(1S)-C(4S)-C(3S)	105.58(19)	C(28)-C(29)-C(30)	120.36(17)
C(3)-C(16)-H(16A)	109.1	O(1S)-C(4S)-H(4SA)	110.6	C(28)-C(29)-H(29)	119.8
N(4)-C(16)-H(16B)	109.1	C(3S)-C(4S)-H(4SA)	110.6	C(30)-C(29)-H(29)	119.8
C(3)-C(16)-H(16B)	109.1	O(1S)-C(4S)-H(4SB)	110.6	C(29)-C(30)-C(25)	122.85(17)
H(16A)-C(16)-H(16B)	107.8	C(3S)-C(4S)-H(4SB)	110.6	C(29)-C(30)-H(30)	118.6
N(3)-C(17)-H(17A)	109.5	H(4SA)-C(4S)-H(4SB)	108.8	C(25)-C(30)-H(30)	118.6
N(3)-C(17)-H(17B)	109.5	C(24)-C(19)-C(20)	115.28(16)	C(36)-C(31)-C(32)	115.30(16)
H(17A)-C(17)-H(17B)	109.5	C(24)-C(19)-B(1)	123.96(16)	C(36)-C(31)-B(1)	122.82(16)
N(3)-C(17)-H(17C)	109.5	C(20)-C(19)-B(1)	120.40(16)	C(32)-C(31)-B(1)	121.59(16)
H(17A)-C(17)-H(17C)	109.5	C(21)-C(20)-C(19)	122.63(19)	C(33)-C(32)-C(31)	122.94(18)
H(17B)-C(17)-H(17C)	109.5	C(21)-C(20)-H(20)	118.7	C(33)-C(32)-H(32)	118.5
N(4)-C(18)-H(18A)	109.5	C(19)-C(20)-H(20)	118.7	C(31)-C(32)-H(32)	118.5
N(4)-C(18)-H(18B)	109.5	C(22)-C(21)-C(20)	120.08(19)	C(34)-C(33)-C(32)	119.62(18)
H(18A)-C(18)-H(18B)	109.5	C(22)-C(21)-H(21)	120.0	C(34)-C(33)-H(33)	120.2
N(4)-C(18)-H(18C)	109.5	C(20)-C(21)-H(21)	120.0	C(32)-C(33)-H(33)	120.2
H(18A)-C(18)-H(18C)	109.5	C(21)-C(22)-C(23)	119.20(17)	C(35)-C(34)-C(33)	119.47(18)
H(18B)-C(18)-H(18C)	109.5	C(21)-C(22)-H(22)	120.4	C(35)-C(34)-H(34)	120.3
C(1S)-O(1S)-C(4S)	108.59(17)	C(23)-C(22)-H(22)	120.4	C(33)-C(34)-H(34)	120.3
O(1S)-C(1S)-C(2S)	107.74(19)	C(22)-C(23)-C(24)	120.03(19)	C(34)-C(35)-C(36)	120.13(19)
O(1S)-C(1S)-H(1SA)	110.2	C(22)-C(23)-H(23)	120.0	C(34)-C(35)-H(35)	119.9
C(2S)-C(1S)-H(1SA)	110.2	C(24)-C(23)-H(23)	120.0	C(36)-C(35)-H(35)	119.9
O(1S)-C(1S)-H(1SB)	110.2	C(23)-C(24)-C(19)	122.72(19)	C(35)-C(36)-C(31)	122.46(18)
C(2S)-C(1S)-H(1SB)	110.2	C(23)-C(24)-H(24)	118.6	C(35)-C(36)-H(36)	118.8
H(1SA)-C(1S)-H(1SB)	108.5	C(19)-C(24)-H(24)	118.6	C(31)-C(36)-H(36)	118.8
C(1S)-C(2S)-C(3S)	101.1(2)	C(30)-C(25)-C(26)	115.08(16)	C(42)-C(37)-C(38)	115.69(16)

C(42)-C(37)-B(1)	122.14(15)	C(41)-C(40)-C(39)	119.19(17)	C(37)-C(42)-H(42)	118.7
C(38)-C(37)-B(1)	121.88(16)	C(41)-C(40)-H(40)	120.4	C(37)-B(1)-C(25)	112.17(14)
C(39)-C(38)-C(37)	122.36(18)	C(39)-C(40)-H(40)	120.4	C(37)-B(1)-C(31)	104.59(13)
C(39)-C(38)-H(38)	118.8	C(40)-C(41)-C(42)	119.88(18)	C(25)-B(1)-C(31)	112.04(14)
C(37)-C(38)-H(38)	118.8	C(40)-C(41)-H(41)	120.1	C(37)-B(1)-C(19)	111.37(14)
C(40)-C(39)-C(38)	120.19(18)	C(42)-C(41)-H(41)	120.1	C(25)-B(1)-C(19)	103.18(13)
C(40)-C(39)-H(39)	119.9	C(41)-C(42)-C(37)	122.67(18)	C(31)-B(1)-C(19)	113.74(14)
C(38)-C(39)-H(39)	119.9	C(41)-C(42)-H(42)	118.7		

Table B13. Crystal data and structure refinement for (^{Me}N₄)Ni^{II}(cycloneophyl).

Identification code	119415t5/lt/JS-092815-01	
Empirical formula	C ₃₀ H ₄₀ N ₄ Ni O	
Formula weight	531.37	
Temperature	100(2) K	
Wavelength	0.71073 Å	
Crystal system	Monoclinic	
Space group	Pn	
Unit cell dimensions	a = 11.5021(9) Å	α = 90°.
	b = 17.8327(13) Å	β = 90.026(5)°.
	c = 12.9451(11) Å	γ = 90°.
Volume	2655.2(4) Å ³	
Z	4	
Density (calculated)	1.329 Mg/m ³	
Absorption coefficient	0.761 mm ⁻¹	
F(000)	1136	
Crystal size	0.589 x 0.566 x 0.232 mm ³	
Theta range for data collection	1.142 to 30.624°.	
Index ranges	-16 ≤ h ≤ 16, -25 ≤ k ≤ 25, -18 ≤ l ≤ 18	
Reflections collected	29108	
Independent reflections	29108 [R(int) = 0.042]	
Completeness to theta = 25.242°	99.5 %	
Absorption correction	Semi-empirical from equivalents	
Max. and min. transmission	0.746070 and 0.621766	
Refinement method	Full-matrix least-squares on F ²	
Data / restraints / parameters	29108 / 2 / 658	
Goodness-of-fit on F ²	1.041	
Final R indices [I > 2σ(I)]	R1 = 0.0508, wR2 = 0.1253	
R indices (all data)	R1 = 0.0587, wR2 = 0.1316	
Absolute structure parameter	-0.010(16)	
Largest diff. peak and hole	1.273 and -1.586 e.Å ⁻³	

Table B14. Bond lengths [Å]

and angles [°]for

^{(MeN4)Ni^{II}(cycloneophyl).}

Ni(1)-C(1)	1.879(9)	C(10)-H(10A)	0.9800	Ni(1A)-C(1A)	1.905(9)
Ni(1)-N(1)	1.936(7)	C(10)-H(10B)	0.9800	Ni(1A)-N(2A)	1.944(7)
Ni(1)-C(8)	1.954(9)	C(10)-H(10C)	0.9800	Ni(1A)-N(1A)	1.973(7)
Ni(1)-N(2)	1.997(7)	C(11)-C(12)	1.366(13)	N(1A)-C(15A)	1.350(11)
N(1)-C(15)	1.339(10)	C(11)-C(24)	1.479(12)	N(1A)-C(11A)	1.362(12)
N(1)-C(11)	1.371(11)	C(12)-C(13)	1.373(13)	N(2A)-C(22A)	1.343(12)
N(2)-C(18)	1.343(11)	C(12)-H(12)	0.9500	N(2A)-C(18A)	1.350(11)
N(2)-C(22)	1.367(12)	C(13)-C(14)	1.383(14)	N(3A)-C(16A)	1.453(10)
N(3)-C(17)	1.442(12)	C(13)-H(13)	0.9500	N(3A)-C(25A)	1.454(11)
N(3)-C(25)	1.454(11)	C(14)-C(15)	1.374(12)	N(3A)-C(17A)	1.465(11)
N(3)-C(16)	1.473(11)	C(14)-H(14)	0.9500	N(4A)-C(24A)	1.431(12)
N(4)-C(23)	1.448(12)	C(15)-C(16)	1.511(13)	N(4A)-C(26A)	1.451(11)
N(4)-C(26)	1.462(12)	C(16)-H(16A)	0.9900	N(4A)-C(23A)	1.465(11)
N(4)-C(24)	1.476(11)	C(16)-H(16B)	0.9900	C(1A)-C(2A)	1.383(12)
C(1)-C(6)	1.411(12)	C(17)-C(18)	1.524(12)	C(1A)-C(6A)	1.409(11)
C(1)-C(2)	1.421(12)	C(17)-H(17A)	0.9900	C(2A)-C(3A)	1.400(12)
C(2)-C(3)	1.379(12)	C(17)-H(17B)	0.9900	C(2A)-H(2A)	0.9500
C(2)-H(2)	0.9500	C(18)-C(19)	1.393(12)	C(3A)-C(4A)	1.377(13)
C(3)-C(4)	1.391(13)	C(19)-C(20)	1.395(13)	C(3A)-H(3AA)	0.9500
C(3)-H(3)	0.9500	C(19)-H(19)	0.9500	C(4A)-C(5A)	1.378(13)
C(4)-C(5)	1.391(13)	C(20)-C(21)	1.389(13)	C(4A)-H(4AA)	0.9500
C(4)-H(4A)	0.9500	C(20)-H(20)	0.9500	C(5A)-C(6A)	1.402(12)
C(5)-C(6)	1.375(12)	C(21)-C(22)	1.389(13)	C(5A)-H(5A)	0.9500
C(5)-H(5)	0.9500	C(21)-H(21)	0.9500	C(6A)-C(7A)	1.490(12)
C(6)-C(7)	1.521(13)	C(22)-C(23)	1.515(13)	C(7A)-C(9A)	1.508(12)
C(7)-C(8)	1.506(12)	C(23)-H(23A)	0.9900	C(7A)-C(8A)	1.554(13)
C(7)-C(9)	1.537(12)	C(23)-H(23B)	0.9900	C(7A)-C(10A)	1.569(14)
C(7)-C(10)	1.546(13)	C(24)-H(24A)	0.9900	C(8A)-H(8AA)	0.9900
C(8)-H(8A)	0.9900	C(24)-H(24B)	0.9900	C(8A)-H(8AB)	0.9900
C(8)-H(8B)	0.9900	C(25)-H(25A)	0.9800	C(9A)-H(9AA)	0.9800
C(9)-H(9A)	0.9800	C(25)-H(25B)	0.9800	C(9A)-H(9AB)	0.9800
C(9)-H(9B)	0.9800	C(25)-H(25C)	0.9800	C(9A)-H(9AC)	0.9800
C(9)-H(9C)	0.9800	C(26)-H(26A)	0.9800	C(10A)-H(10D)	0.9800
		C(26)-H(26B)	0.9800	C(10A)-H(10E)	0.9800
		C(26)-H(26C)	0.9800	C(10A)-H(10F)	0.9800
		Ni(1A)-C(8A)	1.903(8)	C(11A)-C(12A)	1.405(13)

C(11A)-C(24A)	1.529(12)	C(2S)-C(3S)	1.500(16)	C(23)-N(4)-C(26)	113.8(9)
C(12A)-C(13A)	1.386(13)	C(2S)-H(2SA)	0.9900	C(23)-N(4)-C(24)	117.7(7)
C(12A)-H(12A)	0.9500	C(2S)-H(2SB)	0.9900	C(26)-N(4)-C(24)	113.3(8)
C(13A)-C(14A)	1.396(14)	C(3S)-C(4S)	1.516(16)	C(6)-C(1)-C(2)	117.8(8)
C(13A)-H(13A)	0.9500	C(3S)-H(3SA)	0.9900	C(6)-C(1)-Ni(1)	116.6(7)
C(14A)-C(15A)	1.401(13)	C(3S)-H(3SB)	0.9900	C(2)-C(1)-Ni(1)	125.6(6)
C(14A)-H(14A)	0.9500	C(4S)-H(4SA)	0.9900	C(3)-C(2)-C(1)	120.8(9)
C(15A)-C(16A)	1.519(13)	C(4S)-H(4SB)	0.9900	C(3)-C(2)-H(2)	119.6
C(16A)-H(16C)	0.9900	O(2S)-C(8S)	1.403(12)	C(1)-C(2)-H(2)	119.6
C(16A)-H(16D)	0.9900	O(2S)-C(5S)	1.426(14)	C(2)-C(3)-C(4)	120.0(9)
C(17A)-C(18A)	1.515(13)	C(5S)-C(6S)	1.490(17)	C(2)-C(3)-H(3)	120.0
C(17A)-H(17C)	0.9900	C(5S)-H(5SA)	0.9900	C(4)-C(3)-H(3)	120.0
C(17A)-H(17D)	0.9900	C(5S)-H(5SB)	0.9900	C(3)-C(4)-C(5)	120.1(9)
C(18A)-C(19A)	1.370(11)	C(6S)-C(7S)	1.514(19)	C(3)-C(4)-H(4A)	120.0
C(19A)-C(20A)	1.387(13)	C(6S)-H(6SA)	0.9900	C(5)-C(4)-H(4A)	120.0
C(19A)-H(19A)	0.9500	C(6S)-H(6SB)	0.9900	C(6)-C(5)-C(4)	120.5(9)
C(20A)-C(21A)	1.374(13)	C(7S)-C(8S)	1.493(17)	C(6)-C(5)-H(5)	119.7
C(20A)-H(20A)	0.9500	C(7S)-H(7SA)	0.9900	C(4)-C(5)-H(5)	119.7
C(21A)-C(22A)	1.369(12)	C(7S)-H(7SB)	0.9900	C(5)-C(6)-C(1)	120.7(8)
C(21A)-H(21A)	0.9500	C(8S)-H(8S1)	0.9900	C(5)-C(6)-C(7)	124.2(8)
C(22A)-C(23A)	1.533(13)	C(8S)-H(8S2)	0.9900	C(1)-C(6)-C(7)	114.9(8)
C(23A)-H(23C)	0.9900	C(1)-Ni(1)-N(1)	176.0(3)	C(8)-C(7)-C(6)	105.3(7)
C(23A)-H(23D)	0.9900	C(1)-Ni(1)-C(8)	83.5(3)	C(8)-C(7)-C(9)	109.6(8)
C(24A)-H(24C)	0.9900	N(1)-Ni(1)-C(8)	93.6(3)	C(6)-C(7)-C(9)	109.5(7)
C(24A)-H(24D)	0.9900	C(1)-Ni(1)-N(2)	98.7(3)	C(8)-C(7)-C(10)	111.4(8)
C(25A)-H(25D)	0.9800	N(1)-Ni(1)-N(2)	84.4(3)	C(6)-C(7)-C(10)	112.5(8)
C(25A)-H(25E)	0.9800	C(8)-Ni(1)-N(2)	175.3(4)	C(9)-C(7)-C(10)	108.4(8)
C(25A)-H(25F)	0.9800	C(15)-N(1)-C(11)	118.5(7)	C(7)-C(8)-Ni(1)	113.8(6)
C(26A)-H(26D)	0.9800	C(15)-N(1)-Ni(1)	120.2(6)	C(7)-C(8)-H(8A)	108.8
C(26A)-H(26E)	0.9800	C(11)-N(1)-Ni(1)	120.8(6)	Ni(1)-C(8)-H(8A)	108.8
C(26A)-H(26F)	0.9800	C(18)-N(2)-C(22)	117.0(8)	C(7)-C(8)-H(8B)	108.8
O(1S)-C(1S)	1.409(13)	C(18)-N(2)-Ni(1)	121.9(6)	Ni(1)-C(8)-H(8B)	108.8
O(1S)-C(4S)	1.450(12)	C(22)-N(2)-Ni(1)	120.1(6)	H(8A)-C(8)-H(8B)	107.7
C(1S)-C(2S)	1.517(14)	C(17)-N(3)-C(25)	113.4(7)	C(7)-C(9)-H(9A)	109.5
C(1S)-H(1SA)	0.9900	C(17)-N(3)-C(16)	118.1(6)	C(7)-C(9)-H(9B)	109.5
C(1S)-H(1SB)	0.9900	C(25)-N(3)-C(16)	115.0(7)	H(9A)-C(9)-H(9B)	109.5

C(7)-C(9)-H(9C)	109.5	N(2)-C(18)-C(19)	123.4(8)	N(4)-C(26)-H(26C)	109.5
H(9A)-C(9)-H(9C)	109.5	N(2)-C(18)-C(17)	114.6(8)	H(26A)-C(26)-H(26C)	109.5
H(9B)-C(9)-H(9C)	109.5	C(19)-C(18)-C(17)	121.9(8)	H(26B)-C(26)-H(26C)	109.5
C(7)-C(10)-H(10A)	109.5	C(18)-C(19)-C(20)	119.6(8)	C(8A)-Ni(1A)-C(1A)	83.9(4)
C(7)-C(10)-H(10B)	109.5	C(18)-C(19)-H(19)	120.2	C(8A)-Ni(1A)-N(2A)	175.8(4)
H(10A)-C(10)-H(10B)	109.5	C(20)-C(19)-H(19)	120.2	C(1A)-Ni(1A)-N(2A)	98.3(3)
C(7)-C(10)-H(10C)	109.5	C(21)-C(20)-C(19)	117.3(8)	C(8A)-Ni(1A)-N(1A)	94.3(3)
H(10A)-C(10)-H(10C)	109.5	C(21)-C(20)-H(20)	121.3	C(1A)-Ni(1A)-N(1A)	176.1(3)
H(10B)-C(10)-H(10C)	109.5	C(19)-C(20)-H(20)	121.3	N(2A)-Ni(1A)-N(1A)	83.7(3)
C(12)-C(11)-N(1)	121.8(8)	C(22)-C(21)-C(20)	120.3(9)	C(15A)-N(1A)-C(11A)	119.7(8)
C(12)-C(11)-C(24)	120.8(9)	C(22)-C(21)-H(21)	119.8	C(15A)-N(1A)-Ni(1A)	118.9(6)
N(1)-C(11)-C(24)	117.3(8)	C(20)-C(21)-H(21)	119.8	C(11A)-N(1A)-Ni(1A)	120.8(6)
C(11)-C(12)-C(13)	119.6(9)	N(2)-C(22)-C(21)	122.4(8)	C(22A)-N(2A)-C(18A)	119.2(7)
C(11)-C(12)-H(12)	120.2	N(2)-C(22)-C(23)	116.5(8)	C(22A)-N(2A)-Ni(1A)	118.8(6)
C(13)-C(12)-H(12)	120.2	C(21)-C(22)-C(23)	121.1(8)	C(18A)-N(2A)-Ni(1A)	121.3(6)
C(12)-C(13)-C(14)	118.5(9)	N(4)-C(23)-C(22)	119.8(8)	C(16A)-N(3A)-C(25A)	113.5(7)
C(12)-C(13)-H(13)	120.8	N(4)-C(23)-H(23A)	107.4	C(16A)-N(3A)-C(17A)	116.8(7)
C(14)-C(13)-H(13)	120.8	C(22)-C(23)-H(23A)	107.4	C(25A)-N(3A)-C(17A)	115.6(7)
C(15)-C(14)-C(13)	120.3(9)	N(4)-C(23)-H(23B)	107.4	C(24A)-N(4A)-C(26A)	113.2(7)
C(15)-C(14)-H(14)	119.9	C(22)-C(23)-H(23B)	107.4	C(24A)-N(4A)-C(23A)	118.3(7)
C(13)-C(14)-H(14)	119.9	H(23A)-C(23)-H(23B)	106.9	C(26A)-N(4A)-C(23A)	115.0(8)
N(1)-C(15)-C(14)	121.3(9)	N(4)-C(24)-C(11)	117.9(7)	C(2A)-C(1A)-C(6A)	115.6(8)
N(1)-C(15)-C(16)	116.2(7)	N(4)-C(24)-H(24A)	107.8	C(2A)-C(1A)-Ni(1A)	127.6(6)
C(14)-C(15)-C(16)	122.5(8)	C(11)-C(24)-H(24A)	107.8	C(6A)-C(1A)-Ni(1A)	116.7(6)
N(3)-C(16)-C(15)	117.9(7)	N(4)-C(24)-H(24B)	107.8	C(1A)-C(2A)-C(3A)	122.5(8)
N(3)-C(16)-H(16A)	107.8	C(11)-C(24)-H(24B)	107.8	C(1A)-C(2A)-H(2A)	118.7
C(15)-C(16)-H(16A)	107.8	H(24A)-C(24)-H(24B)	107.2	C(3A)-C(2A)-H(2A)	118.7
N(3)-C(16)-H(16B)	107.8	N(3)-C(25)-H(25A)	109.5	C(4A)-C(3A)-C(2A)	120.9(8)
C(15)-C(16)-H(16B)	107.8	N(3)-C(25)-H(25B)	109.5	C(4A)-C(3A)-H(3AA)	119.5
H(16A)-C(16)-H(16B)	107.2	H(25A)-C(25)-H(25B)	109.5	C(2A)-C(3A)-H(3AA)	119.5
N(3)-C(17)-C(18)	117.9(7)	N(3)-C(25)-H(25C)	109.5	C(3A)-C(4A)-C(5A)	118.2(9)
N(3)-C(17)-H(17A)	107.8	H(25A)-C(25)-H(25C)	109.5	C(3A)-C(4A)-H(4AA)	120.9
C(18)-C(17)-H(17A)	107.8	H(25B)-C(25)-H(25C)	109.5	C(5A)-C(4A)-H(4AA)	120.9
N(3)-C(17)-H(17B)	107.8	N(4)-C(26)-H(26A)	109.5	C(4A)-C(5A)-C(6A)	120.8(8)
C(18)-C(17)-H(17B)	107.8	N(4)-C(26)-H(26B)	109.5	C(4A)-C(5A)-H(5A)	119.6
H(17A)-C(17)-H(17B)	107.2	H(26A)-C(26)-H(26B)	109.5	C(6A)-C(5A)-H(5A)	119.6

C(5A)-C(6A)-C(1A)	121.9(8)	C(14A)	117.5(8)	C(20A)	119.8(9)
C(5A)-C(6A)-C(7A)	123.7(8)	C(12A)-C(13A)-H(13A)	121.3	C(22A)-C(21A)-H(21A)	120.1
C(1A)-C(6A)-C(7A)	114.3(8)	C(14A)-C(13A)-H(13A)	121.3	C(20A)-C(21A)-H(21A)	120.1
C(6A)-C(7A)-C(9A)	112.4(8)	C(13A)-C(14A)-		N(2A)-C(22A)-C(21A)	121.2(9)
C(6A)-C(7A)-C(8A)	106.4(7)	C(15A)	119.8(8)	N(2A)-C(22A)-C(23A)	118.0(8)
C(9A)-C(7A)-C(8A)	112.6(8)	C(13A)-C(14A)-H(14A)	120.1	C(21A)-C(22A)-	
C(6A)-C(7A)-C(10A)	108.0(7)	C(15A)-C(14A)-H(14A)	120.1	C(23A)	120.6(8)
C(9A)-C(7A)-C(10A)	109.3(8)	N(1A)-C(15A)-C(14A)	121.7(9)	N(4A)-C(23A)-C(22A)	117.2(8)
C(8A)-C(7A)-C(10A)	107.9(8)	N(1A)-C(15A)-C(16A)	118.1(8)	N(4A)-C(23A)-H(23C)	108.0
C(7A)-C(8A)-Ni(1A)	113.7(6)	C(14A)-C(15A)-		C(22A)-C(23A)-H(23C)	108.0
C(7A)-C(8A)-H(8AA)	108.8	C(16A)	120.2(8)	N(4A)-C(23A)-H(23D)	108.0
Ni(1A)-C(8A)-H(8AA)	108.8	N(3A)-C(16A)-C(15A)	118.5(7)	C(22A)-C(23A)-H(23D)	108.0
C(7A)-C(8A)-H(8AB)	108.8	N(3A)-C(16A)-H(16C)	107.7	H(23C)-C(23A)-H(23D)	107.2
Ni(1A)-C(8A)-H(8AB)	108.8	C(15A)-C(16A)-H(16C)	107.7	N(4A)-C(24A)-C(11A)	118.4(7)
H(8AA)-C(8A)-H(8AB)	107.7	N(3A)-C(16A)-H(16D)	107.7	N(4A)-C(24A)-H(24C)	107.7
C(7A)-C(9A)-H(9AA)	109.5	C(15A)-C(16A)-H(16D)	107.7	C(11A)-C(24A)-H(24C)	107.7
C(7A)-C(9A)-H(9AB)	109.5	H(16C)-C(16A)-H(16D)	107.1	N(4A)-C(24A)-H(24D)	107.7
H(9AA)-C(9A)-H(9AB)	109.5	N(3A)-C(17A)-C(18A)	117.7(8)	C(11A)-C(24A)-H(24D)	107.7
C(7A)-C(9A)-H(9AC)	109.5	N(3A)-C(17A)-H(17C)	107.9	H(24C)-C(24A)-H(24D)	107.1
H(9AA)-C(9A)-H(9AC)	109.5	C(18A)-C(17A)-H(17C)	107.9	N(3A)-C(25A)-H(25D)	109.5
H(9AB)-C(9A)-H(9AC)	109.5	N(3A)-C(17A)-H(17D)	107.9	N(3A)-C(25A)-H(25E)	109.5
C(7A)-C(10A)-H(10D)	109.5	C(18A)-C(17A)-H(17D)	107.9	H(25D)-C(25A)-H(25E)	109.5
C(7A)-C(10A)-H(10E)	109.5	H(17C)-C(17A)-H(17D)	107.2	N(3A)-C(25A)-H(25F)	109.5
H(10D)-C(10A)-H(10E)	109.5	N(2A)-C(18A)-C(19A)	121.9(8)	H(25D)-C(25A)-H(25F)	109.5
C(7A)-C(10A)-H(10F)	109.5	N(2A)-C(18A)-C(17A)	117.2(7)	H(25E)-C(25A)-H(25F)	109.5
H(10D)-C(10A)-H(10F)	109.5	C(19A)-C(18A)-		N(4A)-C(26A)-H(26D)	109.5
H(10E)-C(10A)-H(10F)	109.5	C(17A)	120.8(8)	N(4A)-C(26A)-H(26E)	109.5
N(1A)-C(11A)-C(12A)	119.9(8)	C(18A)-C(19A)-		H(26D)-C(26A)-H(26E)	109.5
N(1A)-C(11A)-C(24A)	117.6(8)	C(20A)	118.6(8)	N(4A)-C(26A)-H(26F)	109.5
C(12A)-C(11A)-		C(18A)-C(19A)-H(19A)	120.7	H(26D)-C(26A)-H(26F)	109.5
C(24A)	122.5(8)	C(20A)-C(19A)-H(19A)	120.7	H(26E)-C(26A)-H(26F)	109.5
C(13A)-C(12A)-		C(21A)-C(20A)-		C(1S)-O(1S)-C(4S)	108.4(9)
C(11A)	121.4(9)	C(19A)	119.1(8)	O(1S)-C(1S)-C(2S)	108.0(8)
C(13A)-C(12A)-H(12A)	119.3	C(21A)-C(20A)-H(20A)	120.5	O(1S)-C(1S)-H(1SA)	110.1
C(11A)-C(12A)-H(12A)	119.3	C(19A)-C(20A)-H(20A)	120.5	C(2S)-C(1S)-H(1SA)	110.1
C(12A)-C(13A)-		C(22A)-C(21A)-		O(1S)-C(1S)-H(1SB)	110.1

C(2S)-C(1S)-H(1SB)	110.1	O(1S)-C(4S)-H(4SA)	110.4	C(5S)-C(6S)-H(6SB)	111.0
H(1SA)-C(1S)-H(1SB)	108.4	C(3S)-C(4S)-H(4SA)	110.4	C(7S)-C(6S)-H(6SB)	111.0
C(3S)-C(2S)-C(1S)	102.6(9)	O(1S)-C(4S)-H(4SB)	110.4	H(6SA)-C(6S)-H(6SB)	109.0
C(3S)-C(2S)-H(2SA)	111.3	C(3S)-C(4S)-H(4SB)	110.4	C(8S)-C(7S)-C(6S)	102.8(10)
C(1S)-C(2S)-H(2SA)	111.3	H(4SA)-C(4S)-H(4SB)	108.6	C(8S)-C(7S)-H(7SA)	111.2
C(3S)-C(2S)-H(2SB)	111.3	C(8S)-O(2S)-C(5S)	108.0(8)	C(6S)-C(7S)-H(7SA)	111.2
C(1S)-C(2S)-H(2SB)	111.3	O(2S)-C(5S)-C(6S)	107.9(9)	C(8S)-C(7S)-H(7SB)	111.2
H(2SA)-C(2S)-H(2SB)	109.2	O(2S)-C(5S)-H(5SA)	110.1	C(6S)-C(7S)-H(7SB)	111.2
C(2S)-C(3S)-C(4S)	102.0(9)	C(6S)-C(5S)-H(5SA)	110.1	H(7SA)-C(7S)-H(7SB)	109.1
C(2S)-C(3S)-H(3SA)	111.4	O(2S)-C(5S)-H(5SB)	110.1	O(2S)-C(8S)-C(7S)	105.1(10)
C(4S)-C(3S)-H(3SA)	111.4	C(6S)-C(5S)-H(5SB)	110.1	O(2S)-C(8S)-H(8S1)	110.7
C(2S)-C(3S)-H(3SB)	111.4	H(5SA)-C(5S)-H(5SB)	108.4	C(7S)-C(8S)-H(8S1)	110.7
C(4S)-C(3S)-H(3SB)	111.4	C(5S)-C(6S)-C(7S)	103.9(10)	O(2S)-C(8S)-H(8S2)	110.7
H(3SA)-C(3S)-H(3SB)	109.2	C(5S)-C(6S)-H(6SA)	111.0	C(7S)-C(8S)-H(8S2)	110.7
O(1S)-C(4S)-C(3S)	106.4(9)	C(7S)-C(6S)-H(6SA)	111.0	H(8S1)-C(8S)-H(8S2)	108.8

Table B15. Crystal data and structure refinement for [(^{Me}N₄)Ni^{III}(cycloneophyl)]BPh₄.

Identification code	19315/lt/smart/JS-050415-01	
Empirical formula	C ₆₂ H ₇₆ B N ₄ Ni O ₃	
Formula weight	994.78	
Temperature	100(2) K	
Wavelength	0.71073 Å	
Crystal system	Monoclinic	
Space group	P2 ₁ /c	
Unit cell dimensions	a = 18.0244(6) Å	α = 90°.
	b = 12.6029(4) Å	β = 98.4100(16)°.
	c = 23.9084(8) Å	γ = 90°.
Volume	5372.6(3) Å ³	
Z	4	
Density (calculated)	1.230 Mg/m ³	
Absorption coefficient	0.410 mm ⁻¹	
F(000)	2132	
Crystal size	0.572 x 0.194 x 0.072 mm ³	
Theta range for data collection	1.722 to 27.512°.	
Index ranges	-23 ≤ h ≤ 23, -8 ≤ k ≤ 16, -31 ≤ l ≤ 30	
Reflections collected	84276	
Independent reflections	12338 [R(int) = 0.0678]	
Completeness to theta = 25.242°	100.0 %	
Absorption correction	Semi-empirical from equivalents	
Max. and min. transmission	0.8621 and 0.7578	
Refinement method	Full-matrix least-squares on F ²	
Data / restraints / parameters	12338 / 114 / 645	
Goodness-of-fit on F ²	1.031	
Final R indices [I > 2σ(I)]	R1 = 0.0613, wR2 = 0.1446	
R indices (all data)	R1 = 0.0970, wR2 = 0.1660	
Extinction coefficient	n/a	
Largest diff. peak and hole	0.858 and -0.570 e.Å ⁻³	

Table B16. Bond lengths [Å]
and angles [°] for
[(^{Me}N4)Ni^{III}(cycloneophyl)]BPh₄
.

Ni(1)-C(18)	1.920(3)	C(9)-H(9)	0.9500	C(26)-H(26B)	0.9800
Ni(1)-C(17)	1.973(3)	C(10)-C(11)	1.374(5)	C(26)-H(26C)	0.9800
Ni(1)-N(2)	1.997(2)	C(10)-H(10)	0.9500	C(27)-C(32)	1.405(4)
Ni(1)-N(1)	2.001(2)	C(11)-C(12)	1.398(4)	C(27)-C(28)	1.408(4)
Ni(1)-N(3)	2.241(2)	C(11)-H(11)	0.9500	C(27)-B(1)	1.648(4)
Ni(1)-N(4)	2.266(3)	C(12)-C(13)	1.489(5)	C(28)-C(29)	1.388(4)
N(1)-C(5)	1.340(3)	C(13)-H(13A)	0.9900	C(28)-H(28)	0.9500
N(1)-C(1)	1.345(4)	C(13)-H(13B)	0.9900	C(29)-C(30)	1.386(4)
N(2)-C(8)	1.338(4)	C(14)-H(14A)	0.9900	C(29)-H(29)	0.9500
N(2)-C(12)	1.346(4)	C(14)-H(14B)	0.9900	C(30)-C(31)	1.383(4)
N(3)-C(15)	1.478(3)	C(15)-H(15A)	0.9800	C(30)-H(30)	0.9500
N(3)-C(7)	1.484(4)	C(15)-H(15B)	0.9800	C(31)-C(32)	1.394(4)
N(3)-C(6)	1.485(4)	C(15)-H(15C)	0.9800	C(31)-H(31)	0.9500
N(4)-C(16)	1.474(4)	C(16)-H(16A)	0.9800	C(32)-H(32)	0.9500
N(4)-C(13)	1.488(4)	C(16)-H(16B)	0.9800	C(33)-C(38)	1.401(4)
N(4)-C(14)	1.490(4)	C(16)-H(16C)	0.9800	C(33)-C(34)	1.412(4)
C(1)-C(2)	1.386(4)	C(17)-C(24)	1.551(4)	C(33)-B(1)	1.654(4)
C(1)-C(14)	1.507(4)	C(17)-H(17A)	0.9900	C(34)-C(35)	1.396(4)
C(2)-C(3)	1.380(4)	C(17)-H(17B)	0.9900	C(34)-H(34)	0.9500
C(2)-H(2)	0.9500	C(18)-C(19)	1.393(4)	C(35)-C(36)	1.383(5)
C(3)-C(4)	1.388(4)	C(18)-C(23)	1.403(4)	C(35)-H(35)	0.9500
C(3)-H(3)	0.9500	C(19)-C(20)	1.393(5)	C(36)-C(37)	1.381(5)
C(4)-C(5)	1.383(4)	C(19)-H(19)	0.9500	C(36)-H(36)	0.9500
C(4)-H(4)	0.9500	C(20)-C(21)	1.381(5)	C(37)-C(38)	1.386(4)
C(5)-C(6)	1.502(4)	C(20)-H(20)	0.9500	C(37)-H(37)	0.9500
C(6)-H(6A)	0.9900	C(21)-C(22)	1.384(5)	C(38)-H(38)	0.9500
C(6)-H(6B)	0.9900	C(21)-H(21)	0.9500	C(39)-C(44)	1.400(4)
C(7)-C(8)	1.494(4)	C(22)-C(23)	1.401(4)	C(39)-C(40)	1.406(4)
C(7)-H(7A)	0.9900	C(22)-H(22)	0.9500	C(39)-B(1)	1.638(4)
C(7)-H(7B)	0.9900	C(23)-C(24)	1.509(4)	C(40)-C(41)	1.392(4)
C(8)-C(9)	1.395(4)	C(24)-C(25)	1.539(4)	C(40)-H(40)	0.9500
C(9)-C(10)	1.369(5)	C(24)-C(26)	1.539(4)	C(41)-C(42)	1.382(5)
		C(25)-H(25A)	0.9800	C(41)-H(41)	0.9500
		C(25)-H(25B)	0.9800	C(42)-C(43)	1.381(5)
		C(25)-H(25C)	0.9800	C(42)-H(42)	0.9500
		C(26)-H(26A)	0.9800	C(43)-C(44)	1.396(4)

C(43)-H(43)	0.9500	C(6S)-H(6SA)	0.9900	C(5)-N(1)-C(1)	120.0(2)
C(44)-H(44)	0.9500	C(6S)-H(6SB)	0.9900	C(5)-N(1)-Ni(1)	118.05(18)
C(45)-C(50)	1.399(4)	C(7S)-C(8S)	1.502(8)	C(1)-N(1)-Ni(1)	119.31(19)
C(45)-C(46)	1.406(4)	C(7S)-H(7SA)	0.9900	C(8)-N(2)-C(12)	119.9(3)
C(45)-B(1)	1.655(4)	C(7S)-H(7SB)	0.9900	C(8)-N(2)-Ni(1)	119.0(2)
C(46)-C(47)	1.391(4)	C(8S)-O(2S')	1.666(16)	C(12)-N(2)-Ni(1)	118.8(2)
C(46)-H(46)	0.9500	C(8S)-H(8S1)	0.9900	C(15)-N(3)-C(7)	109.8(2)
C(47)-C(48)	1.382(5)	C(8S)-H(8S2)	0.9900	C(15)-N(3)-C(6)	108.6(2)
C(47)-H(47)	0.9500	O(3S)-C(12S)	1.395(6)	C(7)-N(3)-C(6)	111.3(2)
C(48)-C(49)	1.391(5)	O(3S)-C(9S)	1.399(6)	C(15)-N(3)-Ni(1)	116.63(17)
C(48)-H(48)	0.9500	C(9S)-C(10S)	1.490(6)	C(7)-N(3)-Ni(1)	107.22(17)
C(49)-C(50)	1.395(4)	C(9S)-H(9SA)	0.9900	C(6)-N(3)-Ni(1)	103.21(16)
C(49)-H(49)	0.9500	C(9S)-H(9SB)	0.9900	C(16)-N(4)-C(13)	109.7(3)
C(50)-H(50)	0.9500	C(10S)-C(11S)	1.504(6)	C(16)-N(4)-C(14)	108.9(3)
O(1S)-C(1S)	1.388(7)	C(10S)-H(10A)	0.9900	C(13)-N(4)-C(14)	112.2(3)
O(1S)-C(4S)	1.495(8)	C(10S)-H(10B)	0.9900	C(16)-N(4)-Ni(1)	116.6(2)
C(1S)-O(1S')	1.429(16)	C(11S)-C(12S)	1.489(7)	C(13)-N(4)-Ni(1)	103.31(18)
C(1S)-C(2S)	1.472(7)	C(11S)-H(11A)	0.9900	C(14)-N(4)-Ni(1)	106.08(18)
C(1S)-H(1SA)	0.9900	C(11S)-H(11B)	0.9900	N(1)-C(1)-C(2)	121.0(3)
C(1S)-H(1SB)	0.9900	C(12S)-H(12A)	0.9900	N(1)-C(1)-C(14)	115.2(3)
C(2S)-C(3S)	1.510(7)	C(12S)-H(12B)	0.9900	C(2)-C(1)-C(14)	123.7(3)
C(2S)-H(2SA)	0.9900	C(18)-Ni(1)-C(17)	82.88(12)	C(3)-C(2)-C(1)	119.0(3)
C(2S)-H(2SB)	0.9900	C(18)-Ni(1)-N(2)	177.67(11)	C(3)-C(2)-H(2)	120.5
C(3S)-C(4S)	1.414(7)	C(17)-Ni(1)-N(2)	95.35(10)	C(1)-C(2)-H(2)	120.5
C(3S)-H(3SA)	0.9900	C(18)-Ni(1)-N(1)	99.00(11)	C(2)-C(3)-C(4)	119.8(3)
C(3S)-H(3SB)	0.9900	C(17)-Ni(1)-N(1)	178.08(11)	C(2)-C(3)-H(3)	120.1
C(4S)-O(1S')	1.233(15)	N(2)-Ni(1)-N(1)	82.78(9)	C(4)-C(3)-H(3)	120.1
C(4S)-H(4SA)	0.9900	C(18)-Ni(1)-N(3)	102.09(11)	C(5)-C(4)-C(3)	118.4(3)
C(4S)-H(4SB)	0.9900	C(17)-Ni(1)-N(3)	99.39(10)	C(5)-C(4)-H(4)	120.8
O(2S)-C(8S)	1.378(7)	N(2)-Ni(1)-N(3)	79.68(9)	C(3)-C(4)-H(4)	120.8
O(2S)-C(5S)	1.468(8)	N(1)-Ni(1)-N(3)	79.84(9)	N(1)-C(5)-C(4)	121.8(3)
C(5S)-C(6S)	1.416(10)	C(18)-Ni(1)-N(4)	99.36(11)	N(1)-C(5)-C(6)	114.3(2)
C(5S)-O(2S')	1.501(15)	C(17)-Ni(1)-N(4)	100.34(11)	C(4)-C(5)-C(6)	124.0(3)
C(5S)-H(5S1)	0.9900	N(2)-Ni(1)-N(4)	79.42(10)	N(3)-C(6)-C(5)	111.1(2)
C(5S)-H(5S2)	0.9900	N(1)-Ni(1)-N(4)	79.82(9)	N(3)-C(6)-H(6A)	109.4
C(6S)-C(7S)	1.468(9)	N(3)-Ni(1)-N(4)	152.39(9)	C(5)-C(6)-H(6A)	109.4

N(3)-C(6)-H(6B)	109.4	N(3)-C(15)-H(15A)	109.5	C(23)-C(24)-C(25)	110.3(2)
C(5)-C(6)-H(6B)	109.4	N(3)-C(15)-H(15B)	109.5	C(23)-C(24)-C(26)	111.1(3)
H(6A)-C(6)-H(6B)	108.0	H(15A)-C(15)-H(15B)	109.5	C(25)-C(24)-C(26)	107.9(2)
N(3)-C(7)-C(8)	112.5(2)	N(3)-C(15)-H(15C)	109.5	C(23)-C(24)-C(17)	106.2(2)
N(3)-C(7)-H(7A)	109.1	H(15A)-C(15)-H(15C)	109.5	C(25)-C(24)-C(17)	110.2(2)
C(8)-C(7)-H(7A)	109.1	H(15B)-C(15)-H(15C)	109.5	C(26)-C(24)-C(17)	111.2(2)
N(3)-C(7)-H(7B)	109.1	N(4)-C(16)-H(16A)	109.5	C(24)-C(25)-H(25A)	109.5
C(8)-C(7)-H(7B)	109.1	N(4)-C(16)-H(16B)	109.5	C(24)-C(25)-H(25B)	109.5
H(7A)-C(7)-H(7B)	107.8	H(16A)-C(16)-H(16B)	109.5	H(25A)-C(25)-H(25B)	109.5
N(2)-C(8)-C(9)	121.6(3)	N(4)-C(16)-H(16C)	109.5	C(24)-C(25)-H(25C)	109.5
N(2)-C(8)-C(7)	116.0(3)	H(16A)-C(16)-H(16C)	109.5	H(25A)-C(25)-H(25C)	109.5
C(9)-C(8)-C(7)	122.3(3)	H(16B)-C(16)-H(16C)	109.5	H(25B)-C(25)-H(25C)	109.5
C(10)-C(9)-C(8)	118.6(3)	C(24)-C(17)-Ni(1)	116.21(19)	C(24)-C(26)-H(26A)	109.5
C(10)-C(9)-H(9)	120.7	C(24)-C(17)-H(17A)	108.2	C(24)-C(26)-H(26B)	109.5
C(8)-C(9)-H(9)	120.7	Ni(1)-C(17)-H(17A)	108.2	H(26A)-C(26)-H(26B)	109.5
C(9)-C(10)-C(11)	120.1(3)	C(24)-C(17)-H(17B)	108.2	C(24)-C(26)-H(26C)	109.5
C(9)-C(10)-H(10)	119.9	Ni(1)-C(17)-H(17B)	108.2	H(26A)-C(26)-H(26C)	109.5
C(11)-C(10)-H(10)	119.9	H(17A)-C(17)-H(17B)	107.4	H(26B)-C(26)-H(26C)	109.5
C(10)-C(11)-C(12)	119.0(3)	C(19)-C(18)-C(23)	118.5(3)	C(32)-C(27)-C(28)	114.8(3)
C(10)-C(11)-H(11)	120.5	C(19)-C(18)-Ni(1)	123.2(2)	C(32)-C(27)-B(1)	124.7(2)
C(12)-C(11)-H(11)	120.5	C(23)-C(18)-Ni(1)	118.2(2)	C(28)-C(27)-B(1)	120.3(2)
N(2)-C(12)-C(11)	120.7(3)	C(20)-C(19)-C(18)	121.3(3)	C(29)-C(28)-C(27)	122.9(3)
N(2)-C(12)-C(13)	114.8(3)	C(20)-C(19)-H(19)	119.4	C(29)-C(28)-H(28)	118.6
C(11)-C(12)-C(13)	124.5(3)	C(18)-C(19)-H(19)	119.4	C(27)-C(28)-H(28)	118.6
N(4)-C(13)-C(12)	112.0(3)	C(21)-C(20)-C(19)	119.8(3)	C(30)-C(29)-C(28)	120.2(3)
N(4)-C(13)-H(13A)	109.2	C(21)-C(20)-H(20)	120.1	C(30)-C(29)-H(29)	119.9
C(12)-C(13)-H(13A)	109.2	C(19)-C(20)-H(20)	120.1	C(28)-C(29)-H(29)	119.9
N(4)-C(13)-H(13B)	109.2	C(20)-C(21)-C(22)	120.0(3)	C(31)-C(30)-C(29)	118.9(3)
C(12)-C(13)-H(13B)	109.2	C(20)-C(21)-H(21)	120.0	C(31)-C(30)-H(30)	120.5
H(13A)-C(13)-H(13B)	107.9	C(22)-C(21)-H(21)	120.0	C(29)-C(30)-H(30)	120.5
N(4)-C(14)-C(1)	112.9(2)	C(21)-C(22)-C(23)	120.5(3)	C(30)-C(31)-C(32)	120.2(3)
N(4)-C(14)-H(14A)	109.0	C(21)-C(22)-H(22)	119.7	C(30)-C(31)-H(31)	119.9
C(1)-C(14)-H(14A)	109.0	C(23)-C(22)-H(22)	119.7	C(32)-C(31)-H(31)	119.9
N(4)-C(14)-H(14B)	109.0	C(22)-C(23)-C(18)	119.8(3)	C(31)-C(32)-C(27)	122.8(3)
C(1)-C(14)-H(14B)	109.0	C(22)-C(23)-C(24)	123.7(3)	C(31)-C(32)-H(32)	118.6
H(14A)-C(14)-H(14B)	107.8	C(18)-C(23)-C(24)	116.4(3)	C(27)-C(32)-H(32)	118.6

C(38)-C(33)-C(34)	114.6(3)	C(50)-C(45)-C(46)	114.8(3)	C(3S)-C(2S)-H(2SB)	111.3
C(38)-C(33)-B(1)	124.1(3)	C(50)-C(45)-B(1)	123.5(2)	H(2SA)-C(2S)-H(2SB)	109.2
C(34)-C(33)-B(1)	121.3(3)	C(46)-C(45)-B(1)	121.5(3)	C(4S)-C(3S)-C(2S)	103.1(4)
C(35)-C(34)-C(33)	122.7(3)	C(47)-C(46)-C(45)	123.2(3)	C(4S)-C(3S)-H(3SA)	111.2
C(35)-C(34)-H(34)	118.6	C(47)-C(46)-H(46)	118.4	C(2S)-C(3S)-H(3SA)	111.2
C(33)-C(34)-H(34)	118.6	C(45)-C(46)-H(46)	118.4	C(4S)-C(3S)-H(3SB)	111.2
C(36)-C(35)-C(34)	120.1(3)	C(48)-C(47)-C(46)	120.1(3)	C(2S)-C(3S)-H(3SB)	111.2
C(36)-C(35)-H(35)	120.0	C(48)-C(47)-H(47)	119.9	H(3SA)-C(3S)-H(3SB)	109.1
C(34)-C(35)-H(35)	120.0	C(46)-C(47)-H(47)	119.9	O(1S)-C(4S)-C(3S)	103.8(8)
C(37)-C(36)-C(35)	118.9(3)	C(47)-C(48)-C(49)	118.8(3)	C(3S)-C(4S)-O(1S)	110.8(4)
C(37)-C(36)-H(36)	120.5	C(47)-C(48)-H(48)	120.6	C(3S)-C(4S)-H(4SA)	109.5
C(35)-C(36)-H(36)	120.5	C(49)-C(48)-H(48)	120.6	O(1S)-C(4S)-H(4SA)	109.5
C(36)-C(37)-C(38)	120.4(3)	C(48)-C(49)-C(50)	120.0(3)	C(3S)-C(4S)-H(4SB)	109.5
C(36)-C(37)-H(37)	119.8	C(48)-C(49)-H(49)	120.0	O(1S)-C(4S)-H(4SB)	109.5
C(38)-C(37)-H(37)	119.8	C(50)-C(49)-H(49)	120.0	H(4SA)-C(4S)-H(4SB)	108.1
C(37)-C(38)-C(33)	123.2(3)	C(49)-C(50)-C(45)	123.1(3)	C(8S)-O(2S)-C(5S)	102.3(5)
C(37)-C(38)-H(38)	118.4	C(49)-C(50)-H(50)	118.5	C(6S)-C(5S)-O(2S)	105.4(7)
C(33)-C(38)-H(38)	118.4	C(45)-C(50)-H(50)	118.5	C(6S)-C(5S)-O(2S')	113.4(8)
C(44)-C(39)-C(40)	115.0(3)	C(39)-B(1)-C(27)	109.7(2)	C(6S)-C(5S)-H(5S1)	110.7
C(44)-C(39)-B(1)	123.6(3)	C(39)-B(1)-C(33)	110.6(2)	O(2S)-C(5S)-H(5S1)	110.7
C(40)-C(39)-B(1)	121.4(3)	C(27)-B(1)-C(33)	108.9(2)	C(6S)-C(5S)-H(5S2)	110.7
C(41)-C(40)-C(39)	122.6(3)	C(39)-B(1)-C(45)	107.9(2)	O(2S)-C(5S)-H(5S2)	110.7
C(41)-C(40)-H(40)	118.7	C(27)-B(1)-C(45)	109.5(2)	H(5S1)-C(5S)-H(5S2)	108.8
C(39)-C(40)-H(40)	118.7	C(33)-B(1)-C(45)	110.2(2)	C(5S)-C(6S)-C(7S)	105.1(6)
C(42)-C(41)-C(40)	120.1(3)	C(1S)-O(1S)-C(4S)	101.6(4)	C(5S)-C(6S)-H(6SA)	110.7
C(42)-C(41)-H(41)	120.0	O(1S)-C(1S)-C(2S)	106.4(4)	C(7S)-C(6S)-H(6SA)	110.7
C(40)-C(41)-H(41)	120.0	O(1S)-C(1S)-C(2S)	101.6(7)	C(5S)-C(6S)-H(6SB)	110.7
C(43)-C(42)-C(41)	119.5(3)	O(1S)-C(1S)-H(1SA)	110.5	C(7S)-C(6S)-H(6SB)	110.7
C(43)-C(42)-H(42)	120.2	C(2S)-C(1S)-H(1SA)	110.5	H(6SA)-C(6S)-H(6SB)	108.8
C(41)-C(42)-H(42)	120.2	O(1S)-C(1S)-H(1SB)	110.5	C(6S)-C(7S)-C(8S)	104.6(5)
C(42)-C(43)-C(44)	119.5(3)	C(2S)-C(1S)-H(1SB)	110.5	C(6S)-C(7S)-H(7SA)	110.8
C(42)-C(43)-H(43)	120.2	H(1SA)-C(1S)-H(1SB)	108.6	C(8S)-C(7S)-H(7SA)	110.8
C(44)-C(43)-H(43)	120.2	C(1S)-C(2S)-C(3S)	102.2(4)	C(6S)-C(7S)-H(7SB)	110.8
C(43)-C(44)-C(39)	123.2(3)	C(1S)-C(2S)-H(2SA)	111.3	C(8S)-C(7S)-H(7SB)	110.8
C(43)-C(44)-H(44)	118.4	C(3S)-C(2S)-H(2SA)	111.3	H(7SA)-C(7S)-H(7SB)	108.9
C(39)-C(44)-H(44)	118.4	C(1S)-C(2S)-H(2SB)	111.3	O(2S)-C(8S)-C(7S)	103.5(5)

C(7S)-C(8S)-O(2S')	106.1(6)	C(10S)-C(9S)-H(9SB)	110.3	C(12S)-C(11S)-H(11B)	111.6
O(2S)-C(8S)-H(8S1)	111.1	H(9SA)-C(9S)-H(9SB)	108.5	C(10S)-C(11S)-H(11B)	111.6
C(7S)-C(8S)-H(8S1)	111.1	C(9S)-C(10S)-C(11S)	102.0(4)	H(11A)-C(11S)-H(11B)	109.4
O(2S)-C(8S)-H(8S2)	111.1	C(9S)-C(10S)-H(10A)	111.4	O(3S)-C(12S)-C(11S)	106.8(4)
C(7S)-C(8S)-H(8S2)	111.1	C(11S)-C(10S)-H(10A)	111.4	O(3S)-C(12S)-H(12A)	110.4
H(8S1)-C(8S)-H(8S2)	109.0	C(9S)-C(10S)-H(10B)	111.4	C(11S)-C(12S)-H(12A)	110.4
C(12S)-O(3S)-C(9S)	109.2(4)	C(11S)-C(10S)-H(10B)	111.4	O(3S)-C(12S)-H(12B)	110.4
O(3S)-C(9S)-C(10S)	107.2(4)	H(10A)-C(10S)-H(10B)	109.2	C(11S)-C(12S)-H(12B)	110.4
O(3S)-C(9S)-H(9SA)	110.3	C(12S)-C(11S)-C(10S)	100.7(4)	H(12A)-C(12S)-H(12B)	108.6
C(10S)-C(9S)-H(9SA)	110.3	C(12S)-C(11S)-H(11A)	111.6	C(4S)-O(1S')-C(1S)	114.1(12)
O(3S)-C(9S)-H(9SB)	110.3	C(10S)-C(11S)-H(11A)	111.6	C(5S)-O(2S')-C(8S)	88.7(9)

Table B17. Crystal data and structure refinement for (^tBu₄N)⁺Ni^{II}Me₂.

Identification code	118812/lt/BZ-12	
Empirical formula	C ₂₄ H ₃₈ N ₄ Ni	
Formula weight	441.29	
Temperature	100(2) K	
Wavelength	0.71073 Å	
Crystal system	Monoclinic	
Space group	C2/c	
Unit cell dimensions	a = 13.739(5) Å	α = 90°.
	b = 13.549(5) Å	β = 117.78(3)°.
	c = 14.404(5) Å	γ = 90°.
Volume	2372.2(14) Å ³	
Z	4	
Density (calculated)	1.236 Mg/m ³	
Absorption coefficient	0.834 mm ⁻¹	
F(000)	952	
Crystal size	0.15 x 0.14 x 0.05 mm ³	
Theta range for data collection	2.25 to 25.33°.	
Index ranges	-16 ≤ h ≤ 16, -16 ≤ k ≤ 16, -17 ≤ l ≤ 17	
Reflections collected	20583	
Independent reflections	2139 [R(int) = 0.2373]	
Completeness to theta = 25.33°	98.2 %	
Absorption correction	Numerical	
Max. and min. transmission	0.9579 and 0.8844	
Refinement method	Full-matrix least-squares on F ²	
Data / restraints / parameters	2139 / 0 / 136	
Goodness-of-fit on F ²	1.156	
Final R indices [I > 2σ(I)]	R1 = 0.1261, wR2 = 0.2893	
R indices (all data)	R1 = 0.1571, wR2 = 0.3047	
Largest diff. peak and hole	1.115 and -1.466 e.Å ⁻³	

Table B18. Bond lengths [Å]

and angles [°] for

^tBuN4Ni^{II}Me₂.

Ni(1)-C(1)#1	1.930(9)	C(11)-H(11B)	0.9800	C(5)-C(6)-C(7)	120.4(9)
Ni(1)-C(1)	1.930(9)	C(11)-H(11C)	0.9800	N(3)#1-C(7)-C(6)	113.0(8)
Ni(1)-N(1)#1	2.005(8)	C(12)-H(12A)	0.9800	N(3)#1-C(7)-H(7A)	109.0
Ni(1)-N(1)	2.005(8)	C(12)-H(12B)	0.9800	C(6)-C(7)-H(7A)	109.0
N(1)-C(2)	1.348(12)	C(12)-H(12C)	0.9800	N(3)#1-C(7)-H(7B)	109.0
N(1)-C(6)	1.365(12)	C(1)#1-Ni(1)-C(1)	89.7(7)	C(6)-C(7)-H(7B)	109.0
N(3)-C(7)#1	1.467(12)	C(1)#1-Ni(1)-N(1)#1	94.2(4)	H(7A)-C(7)-H(7B)	107.8
N(3)-C(8)	1.478(12)	C(1)-Ni(1)-N(1)#1	175.1(4)	N(3)-C(8)-C(2)	112.9(8)
N(3)-C(9)	1.506(12)	C(1)#1-Ni(1)-N(1)	175.1(4)	N(3)-C(8)-H(8A)	109.0
C(1)-H(1A)	0.9800	C(1)-Ni(1)-N(1)	94.2(4)	C(2)-C(8)-H(8A)	109.0
C(1)-H(1B)	0.9800	N(1)#1-Ni(1)-N(1)	82.0(4)	N(3)-C(8)-H(8B)	109.0
C(1)-H(1C)	0.9800	C(2)-N(1)-C(6)	119.7(8)	C(2)-C(8)-H(8B)	109.0
C(2)-C(3)	1.398(13)	C(2)-N(1)-Ni(1)	119.9(6)	H(8A)-C(8)-H(8B)	107.8
C(2)-C(8)	1.488(13)	C(6)-N(1)-Ni(1)	118.4(6)	N(3)-C(9)-C(12)	108.6(9)
C(3)-C(4)	1.386(15)	C(7)#1-N(3)-C(8)	109.6(7)	N(3)-C(9)-C(11)	108.0(8)
C(3)-H(3)	0.9500	C(7)#1-N(3)-C(9)	113.6(7)	C(12)-C(9)-C(11)	107.0(9)
C(4)-C(5)	1.377(15)	C(8)-N(3)-C(9)	114.8(8)	N(3)-C(9)-C(10)	111.8(8)
C(4)-H(4)	0.9500	Ni(1)-C(1)-H(1A)	109.5	C(12)-C(9)-C(10)	111.3(10)
C(5)-C(6)	1.382(14)	Ni(1)-C(1)-H(1B)	109.5	C(11)-C(9)-C(10)	110.0(9)
C(5)-H(5)	0.9500	H(1A)-C(1)-H(1B)	109.5	C(9)-C(10)-H(10A)	109.5
C(6)-C(7)	1.512(14)	Ni(1)-C(1)-H(1C)	109.5	C(9)-C(10)-H(10B)	109.5
C(7)-N(3)#1	1.467(12)	H(1A)-C(1)-H(1C)	109.5	H(10A)-C(10)-H(10B)	109.5
C(7)-H(7A)	0.9900	H(1B)-C(1)-H(1C)	109.5	C(9)-C(10)-H(10C)	109.5
C(7)-H(7B)	0.9900	N(1)-C(2)-C(3)	120.4(9)	H(10A)-C(10)-H(10C)	109.5
C(8)-H(8A)	0.9900	N(1)-C(2)-C(8)	118.7(8)	H(10B)-C(10)-H(10C)	109.5
C(8)-H(8B)	0.9900	C(3)-C(2)-C(8)	120.8(9)	C(9)-C(11)-H(11A)	109.5
C(9)-C(12)	1.519(15)	C(4)-C(3)-C(2)	119.6(9)	C(9)-C(11)-H(11B)	109.5
C(9)-C(11)	1.524(14)	C(4)-C(3)-H(3)	120.2	H(11A)-C(11)-H(11B)	109.5
C(9)-C(10)	1.539(16)	C(2)-C(3)-H(3)	120.2	C(9)-C(11)-H(11C)	109.5
C(10)-H(10A)	0.9800	C(5)-C(4)-C(3)	119.6(9)	H(11A)-C(11)-H(11C)	109.5
C(10)-H(10B)	0.9800	C(5)-C(4)-H(4)	120.2	H(11B)-C(11)-H(11C)	109.5
C(10)-H(10C)	0.9800	C(3)-C(4)-H(4)	120.2	C(9)-C(12)-H(12A)	109.5
C(11)-H(11A)	0.9800	C(4)-C(5)-C(6)	119.0(10)	C(9)-C(12)-H(12B)	109.5
		C(4)-C(5)-H(5)	120.5	H(12A)-C(12)-H(12B)	109.5
		C(6)-C(5)-H(5)	120.5	C(9)-C(12)-H(12C)	109.5
		N(1)-C(6)-C(5)	121.6(9)	H(12A)-C(12)-H(12C)	109.5
		N(1)-C(6)-C(7)	118.0(8)	H(12B)-C(12)-H(12C)	109.5

Table B19. Crystal data and structure refinement for [(^tBuN₄)Ni^{III}Me₂](BPh₄).

Identification code	18214/lt/smart/JS-530-01	
Empirical formula	C ₅₂ H ₆₆ B N ₄ Ni O	
Formula weight	832.60	
Temperature	100(2) K	
Wavelength	0.71073 Å	
Crystal system	Monoclinic	
Space group	P 2 ₁	
Unit cell dimensions	a = 12.5441(5) Å	α = 90°.
	b = 12.5846(6) Å	β = 108.530(3)°.
	c = 16.0244(7) Å	γ = 90°.
Volume	2398.51(19) Å ³	
Z	2	
Density (calculated)	1.153 Mg/m ³	
Absorption coefficient	0.444 mm ⁻¹	
F(000)	894	
Crystal size	0.279 x 0.104 x 0.075 mm ³	
Theta range for data collection	2.101 to 25.038°.	
Index ranges	-14 ≤ h ≤ 14, -14 ≤ k ≤ 14, -19 ≤ l ≤ 19	
Reflections collected	37699	
Independent reflections	8270 [R(int) = 0.0889]	
Completeness to theta = 25.000°	98.6 %	
Absorption correction	Semi-empirical from equivalents	
Max. and min. transmission	0.9281 and 0.8565	
Refinement method	Full-matrix least-squares on F ²	
Data / restraints / parameters	8270 / 957 / 501	
Goodness-of-fit on F ²	1.031	
Final R indices [I > 2σ(I)]	R1 = 0.0610, wR2 = 0.1393	
R indices (all data)	R1 = 0.0926, wR2 = 0.1587	
Absolute structure parameter	0.011(10)	
Extinction coefficient	n/a	
Largest diff. peak and hole	0.660 and -0.398 e.Å ⁻³	

Table B20. Bond lengths [Å]

and angles [°] for

[(^tBuN₄)Ni^{III}Me₂](BPh₄).

Ni(1)-N(2)	1.956(6)	C(16)-H(16A)	0.9800	C(35)-H(35)	0.9500
Ni(1)-C(24)	1.957(7)	C(16)-H(16B)	0.9800	C(36)-H(36)	0.9500
Ni(1)-N(1)	1.966(6)	C(16)-H(16C)	0.9800	C(37)-C(38)	1.388(10)
Ni(1)-C(23)	1.968(7)	C(17)-H(17A)	0.9800	C(37)-C(42)	1.414(10)
Ni(1)-N(4)	2.372(6)	C(17)-H(17B)	0.9800	C(37)-B(1)	1.658(12)
Ni(1)-N(3)	2.400(6)	C(17)-H(17C)	0.9800	C(38)-C(39)	1.413(11)
N(1)-C(5)	1.358(9)	C(18)-H(18A)	0.9800	C(38)-H(38)	0.9500
N(1)-C(1)	1.367(9)	C(18)-H(18B)	0.9800	C(39)-C(40)	1.383(11)
N(2)-C(12)	1.343(8)	C(18)-H(18C)	0.9800	C(39)-H(39)	0.9500
N(2)-C(8)	1.359(8)	C(19)-C(21)	1.518(10)	C(40)-C(41)	1.390(11)
N(3)-C(6)	1.487(10)	C(19)-C(22)	1.527(11)	C(40)-H(40)	0.9500
N(3)-C(7)	1.503(9)	C(19)-C(20)	1.538(12)	C(41)-C(42)	1.414(10)
N(3)-C(15)	1.526(9)	C(20)-H(20A)	0.9800	C(41)-H(41)	0.9500
N(4)-C(13)	1.487(10)	C(20)-H(20B)	0.9800	C(42)-H(42)	0.9500
N(4)-C(14)	1.495(9)	C(20)-H(20C)	0.9800	C(43)-C(48)	1.398(10)
N(4)-C(19)	1.524(9)	C(21)-H(21A)	0.9800	C(43)-C(44)	1.400(10)
C(1)-C(2)	1.403(10)	C(21)-H(21B)	0.9800	C(43)-B(1)	1.655(12)
C(1)-C(14)	1.492(10)	C(21)-H(21C)	0.9800	C(44)-C(45)	1.381(10)
C(2)-C(3)	1.372(11)	C(22)-H(22A)	0.9800	C(44)-H(44)	0.9500
C(2)-H(2)	0.9500	C(22)-H(22B)	0.9800	C(45)-C(46)	1.385(10)
C(3)-C(4)	1.409(11)	C(22)-H(22C)	0.9800	C(45)-H(45)	0.9500
C(3)-H(3)	0.9500	C(23)-H(23A)	0.9800	C(46)-C(47)	1.368(10)
C(4)-C(5)	1.364(11)	C(23)-H(23B)	0.9800	C(46)-H(46)	0.9500
C(4)-H(4)	0.9500	C(23)-H(23C)	0.9800	C(47)-C(48)	1.391(10)
C(5)-C(6)	1.500(10)	C(24)-H(24A)	0.9800	C(47)-H(47)	0.9500
C(6)-H(6A)	0.9900	C(24)-H(24B)	0.9800	C(48)-H(48)	0.9500
C(6)-H(6B)	0.9900	C(24)-H(24C)	0.9800	O(2S)-C(8S)	1.37(2)
C(7)-C(8)	1.500(11)	C(25)-C(26)	1.403(11)	O(2S)-C(5S)	1.41(2)
C(7)-H(7A)	0.9900	C(25)-C(30)	1.416(11)	C(5S)-C(6S)	1.33(3)
C(7)-H(7B)	0.9900	C(25)-B(1)	1.657(9)	C(5S)-H(5SA)	0.9900
C(8)-C(9)	1.393(9)	C(26)-C(27)	1.383(10)	C(5S)-H(5SB)	0.9900
C(9)-C(10)	1.385(10)	C(26)-H(26)	0.9500	C(6S)-C(7S)	1.49(3)
C(9)-H(9)	0.9500	C(27)-C(28)	1.390(12)	C(6S)-H(6SA)	0.9900
C(10)-C(11)	1.395(10)	C(27)-H(27)	0.9500	C(6S)-H(6SB)	0.9900
C(10)-H(10)	0.9500	C(28)-C(29)	1.386(11)	C(7S)-C(8S)	1.40(3)
C(11)-C(12)	1.383(10)	C(28)-H(28)	0.9500	C(7S)-H(7SA)	0.9900
C(11)-H(11)	0.9500	C(29)-C(30)	1.391(10)	C(7S)-H(7SB)	0.9900
C(12)-C(13)	1.500(10)	C(29)-H(29)	0.9500	C(8S)-H(8SA)	0.9900
C(13)-H(13A)	0.9900	C(30)-H(30)	0.9500	C(8S)-H(8SB)	0.9900
C(13)-H(13B)	0.9900	C(31)-C(36)	1.394(9)	O(1S)-C(4S)	1.39(2)
C(14)-H(14A)	0.9900	C(31)-C(32)	1.413(9)	O(1S)-C(1S)	1.44(2)
C(14)-H(14B)	0.9900	C(31)-B(1)	1.651(9)	C(1S)-C(2S)	1.27(3)
C(15)-C(18)	1.531(13)	C(32)-C(33)	1.405(9)	C(1S)-H(1SA)	0.9900
C(15)-C(17)	1.539(10)	C(32)-H(32)	0.9500	C(1S)-H(1SB)	0.9900
C(15)-C(16)	1.542(11)	C(33)-C(34)	1.398(11)	C(2S)-C(3S)	1.50(3)
		C(33)-H(33)	0.9500	C(2S)-H(2SA)	0.9900
		C(34)-C(35)	1.378(11)	C(2S)-H(2SB)	0.9900
		C(34)-H(34)	0.9500	C(3S)-C(4S)	1.37(3)
		C(35)-C(36)	1.393(10)	C(3S)-H(3SA)	0.9900

C(3S)-H(3SB)	0.9900	N(1)-C(5)-C(6)	115.0(6)	H(16A)-C(16)-H(16B)	109.5
C(4S)-H(4SA)	0.9900	C(4)-C(5)-C(6)	122.9(7)	C(15)-C(16)-H(16C)	109.5
C(4S)-H(4SB)	0.9900	N(3)-C(6)-C(5)	111.2(6)	H(16A)-C(16)-H(16C)	109.5
N(2)-Ni(1)-C(24)	93.0(3)	N(3)-C(6)-H(6A)	109.4	H(16B)-C(16)-H(16C)	109.5
N(2)-Ni(1)-N(1)	88.4(2)	C(5)-C(6)-H(6A)	109.4	C(15)-C(17)-H(17A)	109.5
C(24)-Ni(1)-N(1)	178.4(3)	N(3)-C(6)-H(6B)	109.4	C(15)-C(17)-H(17B)	109.5
N(2)-Ni(1)-C(23)	177.6(3)	C(5)-C(6)-H(6B)	109.4	H(17A)-C(17)-H(17B)	109.5
C(24)-Ni(1)-C(23)	85.2(3)	H(6A)-C(6)-H(6B)	108.0	C(15)-C(17)-H(17C)	109.5
N(1)-Ni(1)-C(23)	93.5(3)	C(8)-C(7)-N(3)	113.7(6)	H(17A)-C(17)-H(17C)	109.5
N(2)-Ni(1)-N(4)	75.8(2)	C(8)-C(7)-H(7A)	108.8	H(17B)-C(17)-H(17C)	109.5
C(24)-Ni(1)-N(4)	99.7(3)	N(3)-C(7)-H(7A)	108.8	C(15)-C(18)-H(18A)	109.5
N(1)-Ni(1)-N(4)	79.8(2)	C(8)-C(7)-H(7B)	108.8	C(15)-C(18)-H(18B)	109.5
C(23)-Ni(1)-N(4)	105.9(3)	N(3)-C(7)-H(7B)	108.8	H(18A)-C(18)-H(18B)	109.5
N(2)-Ni(1)-N(3)	79.5(2)	H(7A)-C(7)-H(7B)	107.7	C(15)-C(18)-H(18C)	109.5
C(24)-Ni(1)-N(3)	105.4(3)	N(2)-C(8)-C(9)	120.9(7)	H(18A)-C(18)-H(18C)	109.5
N(1)-Ni(1)-N(3)	75.6(2)	N(2)-C(8)-C(7)	115.8(6)	H(18B)-C(18)-H(18C)	109.5
C(23)-Ni(1)-N(3)	99.5(3)	C(9)-C(8)-C(7)	122.9(6)	C(21)-C(19)-N(4)	109.8(6)
N(4)-Ni(1)-N(3)	145.4(2)	C(10)-C(9)-C(8)	118.7(7)	C(21)-C(19)-C(22)	110.1(7)
C(5)-N(1)-C(1)	120.0(6)	C(10)-C(9)-H(9)	120.7	N(4)-C(19)-C(22)	112.0(6)
C(5)-N(1)-Ni(1)	120.1(5)	C(8)-C(9)-H(9)	120.7	C(21)-C(19)-C(20)	108.2(6)
C(1)-N(1)-Ni(1)	119.9(5)	C(9)-C(10)-C(11)	120.0(7)	N(4)-C(19)-C(20)	107.4(6)
C(12)-N(2)-C(8)	119.7(6)	C(9)-C(10)-H(10)	120.0	C(22)-C(19)-C(20)	109.1(6)
C(12)-N(2)-Ni(1)	119.3(5)	C(11)-C(10)-H(10)	120.0	C(19)-C(20)-H(20A)	109.5
C(8)-N(2)-Ni(1)	120.7(4)	C(12)-C(11)-C(10)	118.2(7)	C(19)-C(20)-H(20B)	109.5
C(6)-N(3)-C(7)	109.7(5)	C(12)-C(11)-H(11)	120.9	H(20A)-C(20)-H(20B)	109.5
C(6)-N(3)-C(15)	112.9(6)	C(10)-C(11)-H(11)	120.9	C(19)-C(20)-H(20C)	109.5
C(7)-N(3)-C(15)	109.6(5)	N(2)-C(12)-C(11)	122.0(7)	H(20A)-C(20)-H(20C)	109.5
C(6)-N(3)-Ni(1)	98.5(4)	N(2)-C(12)-C(13)	114.9(6)	H(20B)-C(20)-H(20C)	109.5
C(7)-N(3)-Ni(1)	101.4(4)	C(11)-C(12)-C(13)	123.1(7)	C(19)-C(21)-H(21A)	109.5
C(15)-N(3)-Ni(1)	123.6(4)	N(4)-C(13)-C(12)	111.6(6)	C(19)-C(21)-H(21B)	109.5
C(13)-N(4)-C(14)	108.3(5)	N(4)-C(13)-H(13A)	109.3	H(21A)-C(21)-H(21B)	109.5
C(13)-N(4)-C(19)	110.9(6)	C(12)-C(13)-H(13A)	109.3	C(19)-C(21)-H(21C)	109.5
C(14)-N(4)-C(19)	111.9(5)	N(4)-C(13)-H(13B)	109.3	H(21A)-C(21)-H(21C)	109.5
C(13)-N(4)-Ni(1)	98.2(4)	C(12)-C(13)-H(13B)	109.3	H(21B)-C(21)-H(21C)	109.5
C(14)-N(4)-Ni(1)	101.5(4)	H(13A)-C(13)-H(13B)	108.0	C(19)-C(22)-H(22A)	109.5
C(19)-N(4)-Ni(1)	124.5(4)	C(1)-C(14)-N(4)	114.2(6)	C(19)-C(22)-H(22B)	109.5
N(1)-C(1)-C(2)	119.8(7)	C(1)-C(14)-H(14A)	108.7	H(22A)-C(22)-H(22B)	109.5
N(1)-C(1)-C(14)	115.9(6)	N(4)-C(14)-H(14A)	108.7	C(19)-C(22)-H(22C)	109.5
C(2)-C(1)-C(14)	123.5(6)	C(1)-C(14)-H(14B)	108.7	H(22A)-C(22)-H(22C)	109.5
C(3)-C(2)-C(1)	119.2(7)	N(4)-C(14)-H(14B)	108.7	H(22B)-C(22)-H(22C)	109.5
C(3)-C(2)-H(2)	120.4	H(14A)-C(14)-H(14B)	107.6	Ni(1)-C(23)-H(23A)	109.5
C(1)-C(2)-H(2)	120.4	N(3)-C(15)-C(18)	109.0(6)	Ni(1)-C(23)-H(23B)	109.5
C(2)-C(3)-C(4)	120.3(7)	N(3)-C(15)-C(17)	108.8(6)	H(23A)-C(23)-H(23B)	109.5
C(2)-C(3)-H(3)	119.8	C(18)-C(15)-C(17)	108.6(7)	Ni(1)-C(23)-H(23C)	109.5
C(4)-C(3)-H(3)	119.8	N(3)-C(15)-C(16)	111.1(6)	H(23A)-C(23)-H(23C)	109.5
C(5)-C(4)-C(3)	118.2(7)	C(18)-C(15)-C(16)	110.8(7)	H(23B)-C(23)-H(23C)	109.5
C(5)-C(4)-H(4)	120.9	C(17)-C(15)-C(16)	108.4(6)	Ni(1)-C(24)-H(24A)	109.5
C(3)-C(4)-H(4)	120.9	C(15)-C(16)-H(16A)	109.5	Ni(1)-C(24)-H(24B)	109.5
N(1)-C(5)-C(4)	122.1(7)	C(15)-C(16)-H(16B)	109.5	H(24A)-C(24)-H(24B)	109.5

Ni(1)-C(24)-H(24C)	109.5	C(39)-C(38)-H(38)	118.8	C(5S)-C(6S)-C(7S)	105(2)
H(24A)-C(24)-H(24C)	109.5	C(40)-C(39)-C(38)	120.6(7)	C(5S)-C(6S)-H(6SA)	110.7
H(24B)-C(24)-H(24C)	109.5	C(40)-C(39)-H(39)	119.7	C(7S)-C(6S)-H(6SA)	110.7
C(26)-C(25)-C(30)	114.8(5)	C(38)-C(39)-H(39)	119.7	C(5S)-C(6S)-H(6SB)	110.7
C(26)-C(25)-B(1)	121.7(8)	C(39)-C(40)-C(41)	119.2(7)	C(7S)-C(6S)-H(6SB)	110.7
C(30)-C(25)-B(1)	123.5(8)	C(39)-C(40)-H(40)	120.4	H(6SA)-C(6S)-H(6SB)	108.8
C(27)-C(26)-C(25)	124.1(7)	C(41)-C(40)-H(40)	120.4	C(8S)-C(7S)-C(6S)	104(2)
C(27)-C(26)-H(26)	118.0	C(40)-C(41)-C(42)	119.4(7)	C(8S)-C(7S)-H(7SA)	111.0
C(25)-C(26)-H(26)	118.0	C(40)-C(41)-H(41)	120.3	C(6S)-C(7S)-H(7SA)	111.0
C(26)-C(27)-C(28)	119.5(7)	C(42)-C(41)-H(41)	120.3	C(8S)-C(7S)-H(7SB)	111.0
C(26)-C(27)-H(27)	120.3	C(41)-C(42)-C(37)	122.7(7)	C(6S)-C(7S)-H(7SB)	111.0
C(28)-C(27)-H(27)	120.3	C(41)-C(42)-H(42)	118.7	H(7SA)-C(7S)-H(7SB)	109.0
C(29)-C(28)-C(27)	118.7(6)	C(37)-C(42)-H(42)	118.7	O(2S)-C(8S)-C(7S)	104.2(19)
C(29)-C(28)-H(28)	120.7	C(48)-C(43)-C(44)	114.8(7)	O(2S)-C(8S)-H(8SA)	110.9
C(27)-C(28)-H(28)	120.7	C(48)-C(43)-B(1)	124.0(6)	C(7S)-C(8S)-H(8SA)	110.9
C(28)-C(29)-C(30)	121.3(7)	C(44)-C(43)-B(1)	121.2(6)	O(2S)-C(8S)-H(8SB)	110.9
C(28)-C(29)-H(29)	119.4	C(45)-C(44)-C(43)	123.1(7)	C(7S)-C(8S)-H(8SB)	110.9
C(30)-C(29)-H(29)	119.4	C(45)-C(44)-H(44)	118.5	H(8SA)-C(8S)-H(8SB)	108.9
C(29)-C(30)-C(25)	121.6(7)	C(43)-C(44)-H(44)	118.5	C(4S)-O(1S)-C(1S)	103.7(16)
C(29)-C(30)-H(30)	119.2	C(44)-C(45)-C(46)	120.3(7)	C(2S)-C(1S)-O(1S)	109.5(19)
C(25)-C(30)-H(30)	119.2	C(44)-C(45)-H(45)	119.9	C(2S)-C(1S)-H(1SA)	109.8
C(36)-C(31)-C(32)	114.8(6)	C(46)-C(45)-H(45)	119.9	O(1S)-C(1S)-H(1SA)	109.8
C(36)-C(31)-B(1)	124.8(6)	C(47)-C(46)-C(45)	118.5(7)	C(2S)-C(1S)-H(1SB)	109.8
C(32)-C(31)-B(1)	120.4(6)	C(47)-C(46)-H(46)	120.7	O(1S)-C(1S)-H(1SB)	109.8
C(33)-C(32)-C(31)	122.7(7)	C(45)-C(46)-H(46)	120.7	H(1SA)-C(1S)-H(1SB)	108.2
C(33)-C(32)-H(32)	118.7	C(46)-C(47)-C(48)	120.7(7)	C(1S)-C(2S)-C(3S)	106(2)
C(31)-C(32)-H(32)	118.7	C(46)-C(47)-H(47)	119.6	C(1S)-C(2S)-H(2SA)	110.6
C(34)-C(33)-C(32)	119.8(7)	C(48)-C(47)-H(47)	119.6	C(3S)-C(2S)-H(2SA)	110.6
C(34)-C(33)-H(33)	120.1	C(47)-C(48)-C(43)	122.6(7)	C(1S)-C(2S)-H(2SB)	110.6
C(32)-C(33)-H(33)	120.1	C(47)-C(48)-H(48)	118.7	C(3S)-C(2S)-H(2SB)	110.6
C(35)-C(34)-C(33)	118.6(7)	C(43)-C(48)-H(48)	118.7	H(2SA)-C(2S)-H(2SB)	108.7
C(35)-C(34)-H(34)	120.7	C(31)-B(1)-C(43)	109.6(6)	C(4S)-C(3S)-C(2S)	99.6(19)
C(33)-C(34)-H(34)	120.7	C(31)-B(1)-C(25)	109.7(5)	C(4S)-C(3S)-H(3SA)	111.8
C(34)-C(35)-C(36)	120.7(7)	C(43)-B(1)-C(25)	109.8(6)	C(2S)-C(3S)-H(3SA)	111.8
C(34)-C(35)-H(35)	119.6	C(31)-B(1)-C(37)	108.9(6)	C(4S)-C(3S)-H(3SB)	111.8
C(36)-C(35)-H(35)	119.6	C(43)-B(1)-C(37)	109.6(5)	C(2S)-C(3S)-H(3SB)	111.8
C(35)-C(36)-C(31)	123.4(7)	C(25)-B(1)-C(37)	109.3(7)	H(3SA)-C(3S)-H(3SB)	109.6
C(35)-C(36)-H(36)	118.3	C(8S)-O(2S)-C(5S)	109.0(19)	C(3S)-C(4S)-O(1S)	106.0(19)
C(31)-C(36)-H(36)	118.3	C(6S)-C(5S)-O(2S)	108(2)	C(3S)-C(4S)-H(4SA)	110.5
C(38)-C(37)-C(42)	115.8(7)	C(6S)-C(5S)-H(5SA)	110.1	O(1S)-C(4S)-H(4SA)	110.5
C(38)-C(37)-B(1)	123.8(7)	O(2S)-C(5S)-H(5SA)	110.1	C(3S)-C(4S)-H(4SB)	110.5
C(42)-C(37)-B(1)	120.4(6)	C(6S)-C(5S)-H(5SB)	110.1	O(1S)-C(4S)-H(4SB)	110.5
C(37)-C(38)-C(39)	122.3(7)	O(2S)-C(5S)-H(5SB)	110.1	H(4SA)-C(4S)-H(4SB)	108.7
C(37)-C(38)-H(38)	118.8	H(5SA)-C(5S)-H(5SB)	108.4		

Table B21. Crystal data and structure refinement for (^{Mc}N4*)Ni^{III}Me₂.

Identification code	111014/lt/JS-072114-01	
Empirical formula	C ₁₈ H ₂₅ N ₄ Ni	
Formula weight	356.13	
Temperature	100(2) K	
Wavelength	0.71073 Å	
Crystal system	Orthorhombic	
Space group	P b c a	
Unit cell dimensions	a = 14.2465(19) Å	α = 90°.
	b = 12.9539(17) Å	β = 90°.
	c = 18.915(3) Å	γ = 90°.
Volume	3490.7(8) Å ³	
Z	8	
Density (calculated)	1.355 Mg/m ³	
Absorption coefficient	1.116 mm ⁻¹	
F(000)	1512	
Crystal size	0.284 x 0.231 x 0.129 mm ³	
Theta range for data collection	2.153 to 27.985°.	
Index ranges	-17 ≤ h ≤ 18, -17 ≤ k ≤ 17, -24 ≤ l ≤ 24	
Reflections collected	45796	
Independent reflections	4197 [R(int) = 0.0607]	
Completeness to theta = 25.242°	100.0 %	
Absorption correction	Semi-empirical from equivalents	
Max. and min. transmission	0.8621 and 0.7776	
Refinement method	Full-matrix least-squares on F ²	
Data / restraints / parameters	4197 / 15 / 240	
Goodness-of-fit on F ²	1.027	
Final R indices [I > 2σ(I)]	R1 = 0.0314, wR2 = 0.0702	
R indices (all data)	R1 = 0.0464, wR2 = 0.0772	
Extinction coefficient	n/a	
Largest diff. peak and hole	0.445 and -0.346 e.Å ⁻³	

Table B22. Bond lengths [Å]

and angles [°] for

 $(^{Me}N_4^*)Ni^{III}Me_2$.

Ni(1)-N(1)	1.9453(15)	C(10)-C(11)	1.379(3)	C(5)-N(1)-Ni(1)	121.02(12)
Ni(1)-C(18)	1.9593(18)	C(10)-H(10)	0.9500	C(1)-N(1)-Ni(1)	116.62(12)
Ni(1)-C(17)	1.965(2)	C(11)-C(12)	1.386(2)	C(8)-N(2)-C(12)	120.75(15)
Ni(1)-N(2)	1.9736(15)	C(11)-H(11)	0.9500	C(8)-N(2)-Ni(1)	120.31(12)
Ni(1)-N(4)	2.2329(16)	C(12)-C(13)	1.501(3)	C(12)-N(2)-Ni(1)	118.94(12)
Ni(1)-N(3)	2.2507(15)	C(13)-H(13A)	0.984(11)	C(15)-N(3)-C(6)	110.03(15)
N(1)-C(5)	1.340(2)	C(13)-H(13B)	0.982(11)	C(15)-N(3)-C(7)	110.68(14)
N(1)-C(1)	1.386(2)	C(14)-H(14)	0.97(2)	C(6)-N(3)-C(7)	111.54(15)
N(2)-C(8)	1.335(2)	C(15)-H(15A)	0.9800	C(15)-N(3)-Ni(1)	114.67(12)
N(2)-C(12)	1.343(2)	C(15)-H(15B)	0.9800	C(6)-N(3)-Ni(1)	102.25(10)
N(3)-C(15)	1.472(2)	C(15)-H(15C)	0.9800	C(7)-N(3)-Ni(1)	107.42(11)
N(3)-C(6)	1.475(2)	C(16)-H(16A)	0.9800	C(14)-N(4)-C(16)	111.00(16)
N(3)-C(7)	1.481(2)	C(16)-H(16B)	0.9800	C(14)-N(4)-C(13)	111.78(15)
N(4)-C(14)	1.455(3)	C(16)-H(16C)	0.9800	C(16)-N(4)-C(13)	110.21(15)
N(4)-C(16)	1.473(2)	C(17)-H(17A)	0.9800	C(14)-N(4)-Ni(1)	104.19(11)
N(4)-C(13)	1.476(2)	C(17)-H(17B)	0.9800	C(16)-N(4)-Ni(1)	115.89(13)
C(1)-C(14)	1.358(3)	C(17)-H(17C)	0.9800	C(13)-N(4)-Ni(1)	103.47(12)
C(1)-C(2)	1.449(3)	C(18)-H(18A)	0.9800	C(14)-C(1)-N(1)	118.17(17)
C(2)-C(3)	1.351(3)	C(18)-H(18B)	0.9800	C(14)-C(1)-C(2)	125.68(17)
C(2)-H(2)	0.9500	C(18)-H(18C)	0.9800	N(1)-C(1)-C(2)	116.15(16)
C(3)-C(4)	1.419(3)	N(1)-Ni(1)-C(18)	94.03(7)	C(3)-C(2)-C(1)	120.35(17)
C(3)-H(3)	0.9500	N(1)-Ni(1)-C(17)	178.75(8)	C(3)-C(2)-H(2)	119.8
C(4)-C(5)	1.376(3)	C(18)-Ni(1)-C(17)	85.49(9)	C(1)-C(2)-H(2)	119.8
C(4)-H(4)	0.9500	N(1)-Ni(1)-N(2)	88.39(6)	C(2)-C(3)-C(4)	121.47(17)
C(5)-C(6)	1.506(3)	C(18)-Ni(1)-N(2)	177.58(7)	C(2)-C(3)-H(3)	119.3
C(6)-H(6A)	0.984(11)	C(17)-Ni(1)-N(2)	92.08(8)	C(4)-C(3)-H(3)	119.3
C(6)-H(6B)	0.988(11)	N(1)-Ni(1)-N(4)	81.31(6)	C(5)-C(4)-C(3)	116.52(17)
C(7)-C(8)	1.508(3)	C(18)-Ni(1)-N(4)	101.97(7)	C(5)-C(4)-H(4)	121.7
C(7)-H(7A)	0.975(11)	C(17)-Ni(1)-N(4)	99.92(8)	C(3)-C(4)-H(4)	121.7
C(7)-H(7B)	0.980(11)	N(2)-Ni(1)-N(4)	78.39(6)	N(1)-C(5)-C(4)	123.14(17)
C(8)-C(9)	1.389(2)	N(1)-Ni(1)-N(3)	78.27(6)	N(1)-C(5)-C(6)	112.72(15)
C(9)-C(10)	1.386(3)	C(18)-Ni(1)-N(3)	100.04(7)	C(4)-C(5)-C(6)	124.10(16)
C(9)-H(9)	0.9500	C(17)-Ni(1)-N(3)	100.67(8)	N(3)-C(6)-C(5)	110.74(15)
		N(2)-Ni(1)-N(3)	80.43(6)	N(3)-C(6)-H(6A)	110.8(13)
		N(4)-Ni(1)-N(3)	150.83(6)	C(5)-C(6)-H(6A)	110.6(13)
		C(5)-N(1)-C(1)	121.76(15)	N(3)-C(6)-H(6B)	105.5(12)

C(5)-C(6)-H(6B)	109.0(12)	H(15A)-C(15)-H(15C)	109.5
H(6A)-C(6)-H(6B)	110.1(17)	H(15B)-C(15)-H(15C)	109.5
N(3)-C(7)-C(8)	114.34(15)	N(4)-C(16)-H(16A)	109.5
N(3)-C(7)-H(7A)	108.2(13)	N(4)-C(16)-H(16B)	109.5
C(8)-C(7)-H(7A)	108.7(13)	H(16A)-C(16)-H(16B)	109.5
N(3)-C(7)-H(7B)	110.3(14)	N(4)-C(16)-H(16C)	109.5
C(8)-C(7)-H(7B)	107.4(13)	H(16A)-C(16)-H(16C)	109.5
H(7A)-C(7)-H(7B)	107.8(19)	H(16B)-C(16)-H(16C)	109.5
N(2)-C(8)-C(9)	120.73(17)	Ni(1)-C(17)-H(17A)	109.5
N(2)-C(8)-C(7)	117.04(15)	Ni(1)-C(17)-H(17B)	109.5
C(9)-C(8)-C(7)	122.17(16)	H(17A)-C(17)-H(17B)	109.5
C(10)-C(9)-C(8)	118.99(17)	Ni(1)-C(17)-H(17C)	109.5
C(10)-C(9)-H(9)	120.5	H(17A)-C(17)-H(17C)	109.5
C(8)-C(9)-H(9)	120.5	H(17B)-C(17)-H(17C)	109.5
C(11)-C(10)-C(9)	119.55(17)	Ni(1)-C(18)-H(18A)	109.5
C(11)-C(10)-H(10)	120.2	Ni(1)-C(18)-H(18B)	109.5
C(9)-C(10)-H(10)	120.2	H(18A)-C(18)-H(18B)	109.5
C(10)-C(11)-C(12)	118.88(18)	Ni(1)-C(18)-H(18C)	109.5
C(10)-C(11)-H(11)	120.6	H(18A)-C(18)-H(18C)	109.5
C(12)-C(11)-H(11)	120.6	H(18B)-C(18)-H(18C)	109.5
N(2)-C(12)-C(11)	120.99(17)		
N(2)-C(12)-C(13)	114.78(16)		
C(11)-C(12)-C(13)	124.19(17)		
N(4)-C(13)-C(12)	110.82(15)		
N(4)-C(13)-H(13A)	112.0(13)		
C(12)-C(13)-H(13A)	110.8(14)		
N(4)-C(13)-H(13B)	107.0(13)		
C(12)-C(13)-H(13B)	108.7(13)		
H(13A)-C(13)-H(13B)	107.4(19)		
C(1)-C(14)-N(4)	119.55(17)		
C(1)-C(14)-H(14)	122.8(14)		
N(4)-C(14)-H(14)	117.3(14)		
N(3)-C(15)-H(15A)	109.5		
N(3)-C(15)-H(15B)	109.5		
H(15A)-C(15)-H(15B)	109.5		
N(3)-C(15)-H(15C)	109.5		

Appendix C

Supplemental Reactivity Data

Table C1. Yields of the products of elimination from (^{TsMe}N4)Pd^{II}Me₂ in saturated CD₃OD with O₂ at 20°C (average of 2 runs).

Time, h	Me-Me, %	CH ₄ , %	CH ₃ D, %	(^{TsMe} N4)Pd ^{II} Me(OH)
1	37±7	0.0	0.0	76±4
2	42±1	0.0	0.0	81±1
4	49±1	0.0	0.0	83±2

Table C2. Yields of the products of elimination from (^{TsMe}N4)Pd^{II}Me₂ in saturated CD₃OD with O₂ in the presence of TEMPO at 20°C.

Time, h	Me-Me, %	Me-H/D, %	(^{TsMe} N4)Pd ^{II} Me(OH)	Me-TEMPO, %
1	40	0	84	0
2	50	0	88	0
4	51	1	85	0

Table C3. Yields of the products of elimination from (^{TsMe}N4)Pd^{II}Me₂ in d₆-actone with 1 equivalent of MeI at 20°C (average of 2 runs).

Time, h	Me-Me, %	CH ₄ , %	CH ₃ D, %	(^{TsMe} N4)Pd ^{II} MeI
0.5	32±1	0	0	33±1
1	49±2	0	0	50±4
3	68±1	0	0	68±4
5	79±8	0	0	73±10
7	82±1	0	0	81±3
9	84±2	0	0	83±3
12	85±2	0	0	85±2
15	87±2	0	0	89±2
22	88±2	0	0	92±2
24	89±2	0	0	93±3

Table C4. Yields of the products of elimination from (^{TsMe}N4)Pd^{II}Me₂ in d₆-actone with 20 equivalents MeI at 20°C.

Time, h	Me-Me, %	CH ₄ , %	CH ₃ D, %	(^{TsMe} N4)Pd ^{II} MeI
1	92	0	0	96
2	99	0	0	98

Table C5. Yields of the products of elimination from (^{TsMe}N4)Pd^{II}Me₂ in d₆-actone with CD₃I at 20°C (average of 2 runs).

Time, h	CH ₃ -CH ₃ , %	CH ₃ -CD ₃ , %	Me-H/D, %	(^{TsMe} N4)Pd ^{II} MeI
1	17 ± 4	19 ± 5	0	34 ± 9
2	24 ± 4	27 ± 12	0	50 ± 12
4	29 ± 5	45 ± 11	0	59 ± 13
7	32 ± 2	50 ± 5	0	63 ± 7
10	34 ± 4	57 ± 11	0	67 ± 12
24	35 ± 4	63 ± 7	0	69 ± 10

Table C6. Yields of the products from the reaction of (^{tBu}N4)Ni^{II}(*o*-PhF)Br with 1 equivalent of FcPF₆ in d₃-MeCN at RT.

	¹ H NMR	¹⁹ F NMR	GC-FID
Time, h	<i>o</i> -FPhBr, %	<i>o</i> -FPhBr, %	<i>o</i> -FPhBr, %
1	96		
2	97		
3		90	
20	97		92

Table C7. Yields of the products from the reaction of [(^{tBu}N4)Ni^{III}(*o*-PhF)Br]PF₆ in MeCN at RT.

	GC-FID
Time, h	<i>o</i> -FPhBr, %
20	86

Table C8. Yields of the products of elimination from (^{Me}N4)NiMe₂ in d₃-MeCN at RT.

Time, h	Me-Me, %	Me-H/D, %
1	3	0
2	5	2
4	8	3
8	11	5
24	15	18

Table C9. Yields of the products from the reaction of (^{Me}N₄)NiMe₂ with 1 equivalent of FcPF₆ in d₃-MeCN at RT.

Time, h	Me-Me, %	Me-H/D, %
1	31 ± 3	5 ± 4
2	36 ± 3	6 ± 6
4	44 ± 4	10 ± 4
8	56 ± 5	15 ± 4
24	64 ± 1	31 ± 9

Table C10. Yields of the products from the reaction of (^{Me}N₄)NiMe₂ with 1 equivalent of ^{Ac}FcBF₄ in d₃-MeCN at RT.

Time, h	Me-Me, %	Me-H/D, %
0.5	35 ± 1	5 ± 1
1	37 ± 2	5 ± 1
2	43 ± 1	6 ± 1
4	55 ± 1	8 ± 1
8	67 ± 1	11 ± 2
24	77 ± 3	20 ± 3

Table C11. Yields of the products from the reaction of (^{Me}N₄)NiMe₂ with 1 equivalent of ^{Ac}FcBF₄ and 2 equivalents of TEMPO in d₃-MeCN at RT.

Time, h	Me-Me, %	Me-H/D, %
0.5	34	1
1	35	1
2	41	1
4	50	1
8	65	2
24	76	13

Table C12. Yields of the products from the crossover of (^{Me}N₄)NiMe₂ and (^{Me}N₄)Ni(CD₃)₂ with 1 equivalent of ^{Ac}FcBF₄ in d₃-MeCN at RT.

Time, h	Me-Me, %	CD ₃ -CH ₃ , %	[CD ₃ -CD ₃], %	Me-H/D, %
0.5	14 ± 1	5 ± 1	16	1 ± 1
1	15 ± 1	6 ± 1	16	1 ± 1
2	17 ± 1	8 ± 3	18	2 ± 3
4	20 ± 1	15 ± 4	20	4 ± 5
8	25 ± 2	25 ± 2	17	11 ± 9
24	26 ± 4	30 ± 11	21	18 ± 6

Table C13. Yields of the products from the crossover of (^{Me}N₄)NiMe₂ and (^{Me}N₄)Ni(CD₃)₂ with 1 equivalent of ^{Ac}FcBF₄ and 2 equivalents of TEMPO in d₃-MeCN at RT.

Time, h	Me-Me, %	CD ₃ -CH ₃ , %	[CD ₃ -CD ₃], %	Me-H/D, %
0.5	14	5	16	0
1	14	5	18	0
2	17	6	20	0
4	21	13	21	1
8	27	26	14	5
24	29	38	10	15

Table C14. Yields of the products from the reaction of (^{Me}N₄)NiMe₂ with 2 equivalents of ^{Ac}FcBF₄ in d₃-MeCN at RT.

Time, h	Me-Me, %	Me-H/D, %
0.5	88 ± 1	1 ± 1
1	89 ± 1	1 ± 1
2	89 ± 1	1 ± 1
4	89 ± 1	1 ± 1
8	89 ± 1	1 ± 1
24	90 ± 1	1 ± 1

Table C15. Yields of the products from the reaction of (^{Me}N₄)NiMe₂ with 2 equivalents of ^{Ac}FcBF₄ and 2 equivalents of TEMPO in d₃-MeCN at RT.

Time, h	Me-Me, %	Me-H/D, %
0.5	66	1
1	68	1
2	69	1
4	73	1
8	78	1
24	80	1

Table C16. Yields of the products from the crossover of (^{Me}N₄)NiMe₂ and (^{Me}N₄)Ni(CD₃)₂ with 2 equivalents of ^{Ac}FcBF₄ in d₃-MeCN at RT.

Time, h	Me-Me, %	CD ₃ -CH ₃ , %	[CD ₃ -CD ₃], %	Me-H/D, %
0.5	34 ± 10	6 ± 1	48	0 ± 1
1	35 ± 10	4 ± 3	50	0 ± 1
2	36 ± 9	6 ± 2	47	0 ± 1
4	37 ± 7	6 ± 2	46	0 ± 1
8	38 ± 4	9 ± 4	43	0 ± 1
24	41 ± 3	10 ± 5	39	0 ± 1

Table C17. Yields of the products from the crossover of (^{Me}N4)NiMe₂ and (^{Me}N4)Ni(CD₃)₂ with 2 equivalents of ^{Ac}FcBF₄ and 2 equivalents of TEMPO in d₃-MeCN at RT.

Time, h	Me-Me, %	CD ₃ -CH ₃ , %	[CD ₃ -CD ₃], %	Me-H/D, %
0.5	27	6	56	0
1	28	6	55	0
2	30	8	51	0
4	32	8	49	0
8	35	11	44	0
24	39	13	38	0

Table C18. Yields of the products from the reaction of (^{Me}N4)NiMe₂ with 1 equivalent of CD₃I in d₃-MeCN at RT.

Time, h	Me-Me, %	CD ₃ -CH ₃ , %	Me-H/D, %
0.75	9	8	2
1	10	8	2
2	17	10	2
4	32	12	2
8	48	12	2
24	67	20	2

Table C19. Yields of the products from the reaction of (^{Me}N4)NiMe₂ with 1 equivalent of CD₃I and 2 equivalents of TEMPO in d₃-MeCN at RT.

Time, h	Me-Me, %	CD ₃ -CH ₃ , %	Me-H/D, %	TEMPO-CD ₃ , %
0.75	11	3	0	31
1	15	8	2	32
2	23	7	2	38
4	37	10	3	54
8	54	11	2	74
24	70	8	3	85

Table C20. Yields of the products from the reaction of (^{Me}N4)NiMe₂ with 2 equivalents CD₃I in d₃-MeCN at RT.

Time, h	Me-Me, %	CD ₃ -CH ₃ , %	Me-H/D, %
4	25	13	2
8	51	22	2
24	66	27	1

Table C21. Yields of the products from the reaction of (^{Me}N₄)NiMe₂ with 1 equivalent of FcPF₆ and 1 equivalent of CD₃I in d₃-MeCN at RT.

Time, h	Me-Me, %	CD ₃ -CH ₃ , %	Me-H/D, %
4	37	7	1
8	52	16	1
24	67	21	0

Table C22. Yields of the products from the reaction of (^{Me}N₄)NiMe₂ with 1 equivalents of CD₃I and 2 equivalents of TEMPO in d₃-MeCN at RT.

Product	Structure	Yield
TEMPO-H		7
TEMPO-CD ₃		84

Table C23. Yields of the products from the reaction of [(^{Me}N₄)Ni^{III}Me₂]BPh₄ in d₃-MeCN at RT.

Time, h	Me-Me, %	Me-H/D, %
0.5	11 ± 4	6 ± 1
1	14 ± 4	9 ± 2
2	19 ± 3	10 ± 3
4	31 ± 3	16 ± 6
8	43 ± 4	21 ± 5
24	54 ± 2	30 ± 1

Table C24. Yields of the products from the reaction of [(^{Me}N₄)Ni^{III}Me₂]BPh₄ with 1 equivalent of ^{Ac}FcBF₄ in d₃-MeCN at RT.

Time, h	Me-Me, %	Me-H/D, %
0.5	22 ± 3	1 ± 1
1	25 ± 2	1 ± 1
2	30 ± 3	1 ± 1
4	38 ± 6	1 ± 1
8	59 ± 1	1 ± 1
24	84 ± 1	1 ± 2

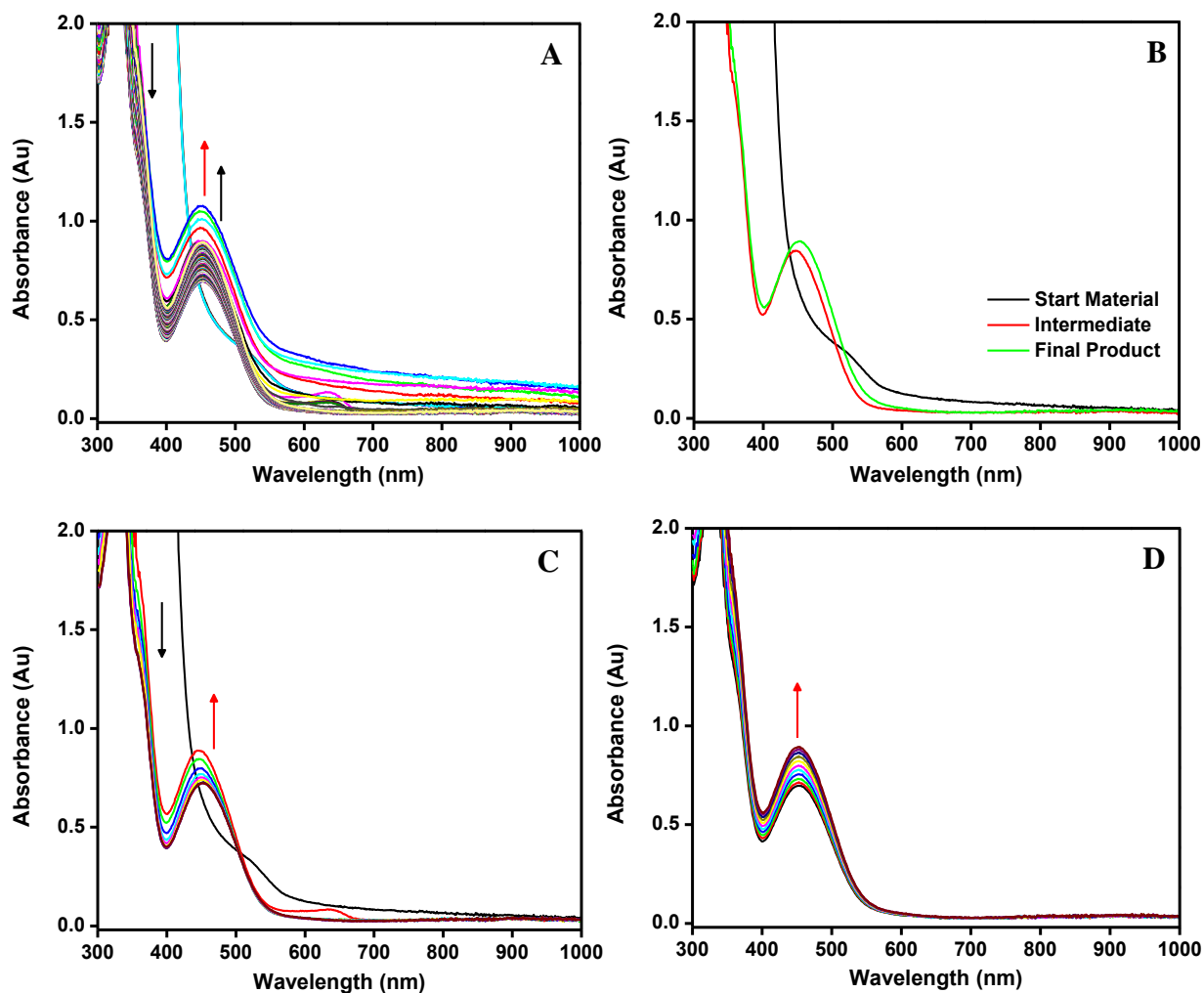


Figure C1. UV-Vis spectra of 0.50 mM solution of $\text{Me}_4\text{N}_4\text{Ni}(\text{II})\text{Me}_2$ in MeCN reacted with 2 equivalents of AcFcBF_4 at -35°C . The spectra are shown at different time points: **A)** Full reaction, **B)** Individual species, **C)** Oxidation Reaction, and **D)** Warming to RT.

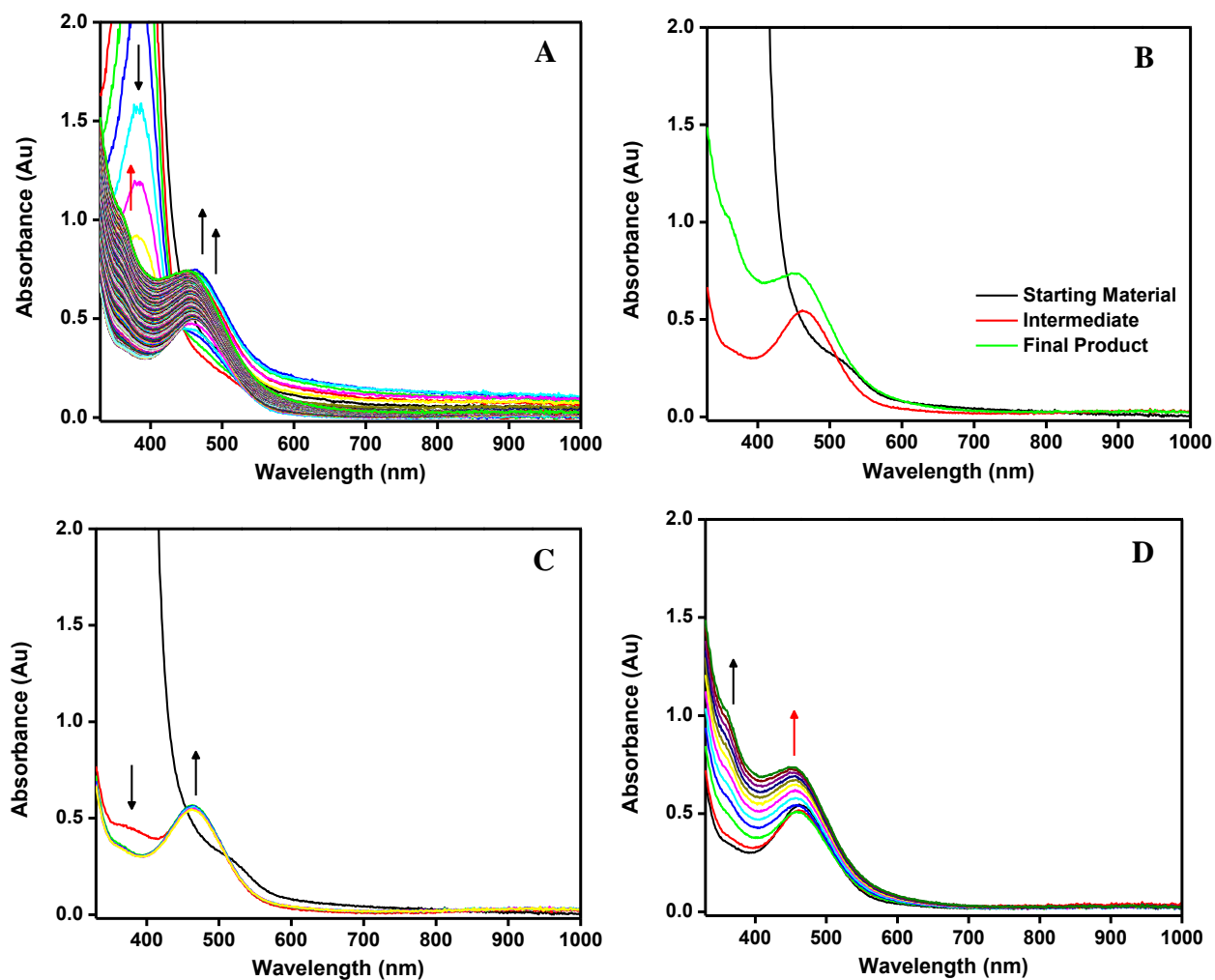


Figure C2. UV-Vis spectra of 0.50 mM solution of $\text{Me}_4\text{N}_4\text{Ni}(\text{II})\text{Me}_2$ in MeCN reacted with 2 equivalents of H_2O_2 at -35°C . The spectra are shown at different time points: **A)** Full reaction, **B)** Individual species, **C)** Oxidation Reaction, and **D)** Warming to RT.

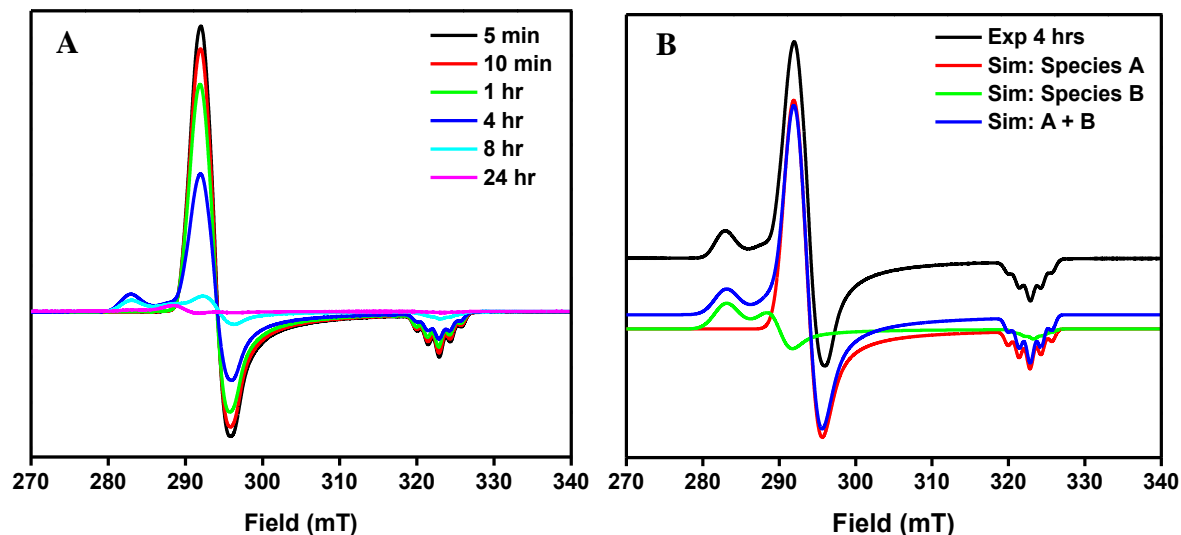


Figure C3. A) EPR monitoring of ($^{Me}N_4$)NiMe₂ reacting with 1 equivalent of CD₃I at RT over 24 hours. B) EPR spectrum and simulation of reaction species at the 4 hour time point. The ratio of species A to species B at 4 hours is 9:1. Simulation used the following parameters: Species A) $g_x=2.2283$, $g_y=2.2100$, $g_z=2.0137$ ($A_N = 14.30$ G), Species B) $g_x=2.2960$, $g_y=2.2398$, $g_z=2.0100$ ($A_N = 12.00$ G).

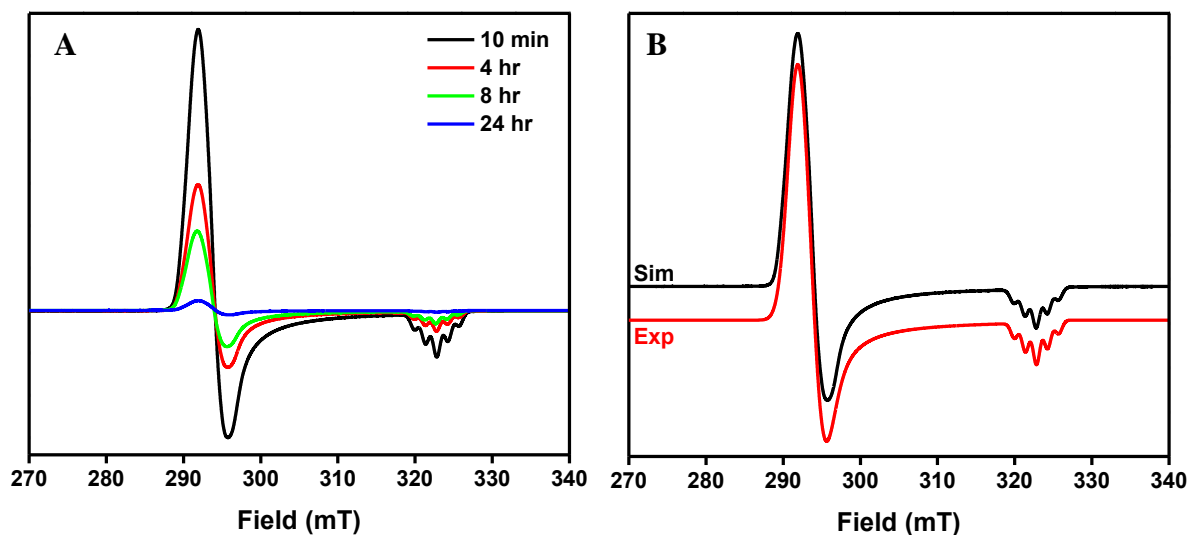
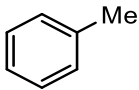
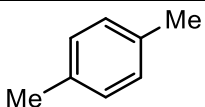
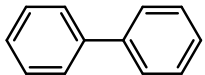
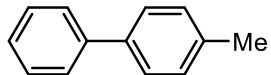
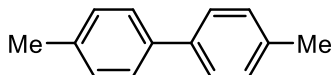


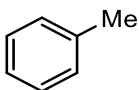
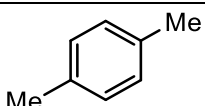
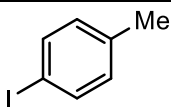
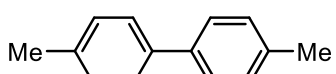
Figure C4. A) EPR monitoring of ($^{Me}N_4$)NiMe₂ reacting with 1 equivalent of Iodotoluene at RT over 24 hours. B) EPR spectrum and simulation of reactions species at 4 hour time point. Simulation used the following parameters: $g_x=2.2283$, $g_y=2.2100$, $g_z=2.0137$ ($A_N = 14.30$ G).

Table C25. Products and yields from the Kumada cross-coupling reactions of Iodotoluene and PhMgBr catalyzed by 5 mol % (^{Me}N4)NiMe₂ or [(^{Me}N4)Ni^{III}Me₂]BPh₄.

Product	Structure	Ni ^{II} Yield	Ni ^{III} Yield
Toluene		23	18
p-Xylene		0	0
Biphenyl		27	24
4-methyl-1,1'-biphenyl		52	51
4,4'-dimethylbiphenyl		5	5

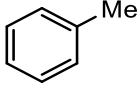
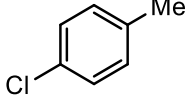
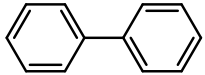
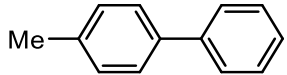
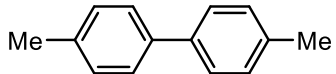
*Hexamethylbenzene was used as an internal standard. Reaction Time: 1 hour.

Table C26. Products and yields from the Kumada cross-coupling reactions of Iodotoluene and MeMgCl catalyzed by 5 mol % (^{Me}N4)NiMe₂ or [(^{Me}N4)Ni^{III}Me₂]BPh₄.

Product	Structure	Ni ^{II} Yield	Ni ^{III} Yield
Toluene		8	7
p-Xylene		43	44
Iodotoluene		11	0
4,4'-dimethylbiphenyl		4	4

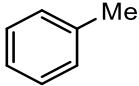
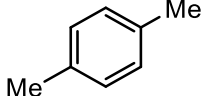
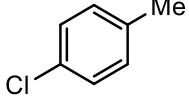
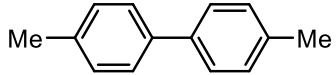
*Hexamethylbenzene was used as an internal standard. Reaction Time: (^{Me}N4)NiMe₂, 1hour; and [(^{Me}N4)Ni^{III}Me₂]BPh₄, 4 hours.

Table C27 Products and yields from the Kumada cross-coupling reactions of Chlorotoluene and PhMgBr catalyzed by 5 mol % (^{Me}N₄)NiMe₂ or [(^{Me}N₄)Ni^{III}Me₂]BPh₄.

Product	Structure	Ni ^{II} Yield	Ni ^{III} Yield
Toluene		11	5
Chlorotoluene		14	5
Biphenyl		22	23
4-methyl-1,1'-Biphenyl		42	71
4,4'-Dimethylbiphenyl		7	13

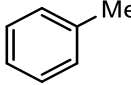
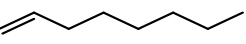
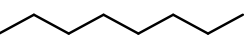
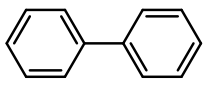
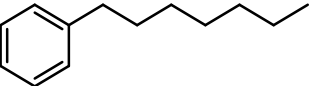
*Hexamethylbenzene was used as an internal standard. Reaction Time: 24 hours.

Table C28. Products and yields from the Kumada cross-coupling reactions of Chlorotoluene and MeMgCl catalyzed by 5 mol % (^{Me}N₄)NiMe₂ or [(^{Me}N₄)Ni^{III}Me₂]BPh₄.

Product	Structure	Ni ^{II} Yield	Ni ^{III} Yield
Toluene		2	2
p-Xylene		6	5
Chlorotoluene		46	48
4,4'-Dimethylbiphenyl		1	1

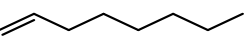
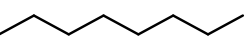
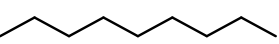
*Hexamethylbenzene was used as an internal standard. Reaction Time: 24 hours.

Table C29. Products and yields from the Kumada cross-coupling reactions of Iodoctane and PhMgBr catalyzed by 5 mol % $(^{\text{Me}}\text{N4})\text{NiMe}_2$ or $[(^{\text{Me}}\text{N4})\text{Ni}^{\text{III}}\text{Me}_2]\text{BPh}_4$.

Product	Structure	Ni ^{II} Yield	Ni ^{III} Yield
Toluene		1	1
Octene		11	6
Octane		28	23
Biphenyl		40	37
Octylbenzene		4	5
Hexadecane	$\text{C}_{16}\text{H}_{34}$	12	13

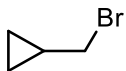
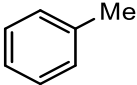
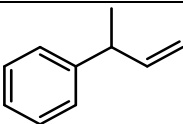
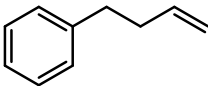
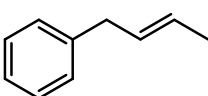
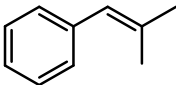
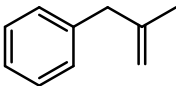
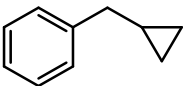
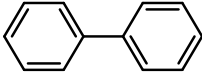
*Dodecane was used as an internal standard. Reaction Time: 1 hour.

Table C30. Products and yields from the Kumada cross-coupling reactions of Iodoctane and MeMgCl catalyzed by 5 mol % $(^{\text{Me}}\text{N4})\text{NiMe}_2$ or $[(^{\text{Me}}\text{N4})\text{Ni}^{\text{III}}\text{Me}_2]\text{BPh}_4$.

Product	Structure	Ni ^{II} Yield	Ni ^{III} Yield
Octene		8	6
Octane		40	27
Nonane		7	6
Hexadecane	$\text{C}_{16}\text{H}_{34}$	2	1

*Dodecane was used as an internal standard. Reaction Time: 1 hour.

Table C31. Products and yields from the Kumada cross-coupling reactions of PhMgBr and (Bromomethyl)cyclopropane catalyzed by 5 mol % (^{Me}N4)NiMe₂.

Product	Structure	Yield
(Bromomethyl)cyclopropane		15
Toluene		5
3-phenyl-but-1-ene		2
4-phenyl-1-butene		1
1-phenyl-2-butene		1
2-methyl-1-phenylpropene		2
2-Methyl-3-phenyl-1-propene		1
Cyclopropylphenylmethane		2
Biphenyl		37

*Hexamethylbenzene was used as an internal standard. Reaction Time: 3 hours.

Table C32. Yields of the products from the reaction of (^{tBu}N4)NiMe₂PF₆ in d₃-MeCN at 50°C.

Time, h	Me-Me, %	Me-H/D, %
2	23 ± 1	0 ± 1
4	30 ± 1	0 ± 1
6	35 ± 1	0 ± 1
8	38 ± 1	1 ± 1
24	46 ± 1	1 ± 1

Table C33. Yields of the products from the reaction of (^tBuN4)NiMe₂PF₆ and (^tBuN4)Ni(CD₃)₂PF₆ in d₃-MeCN at 50°C.

Time, h	Me-Me, %	CD ₃ -CH ₃ , %	Me-H/D, %
2	12 ± 1	0 ± 1	0 ± 1
4	16 ± 1	0 ± 1	0 ± 1
8	20 ± 1	0 ± 1	0 ± 1
24	25 ± 1	0 ± 1	1 ± 1

Table C34. Yields of the products from the reaction of (^tBuN4)NiMe₂PF₆ with 2 eq TEMPO in d₃-MeCN at 50°C.

Time, h	Me-Me, %	Me-H/D, %
4	34	2
8	42	2
24	47	2

Table C35. Yields of the products from the reaction of (^tBuN4)NiMe₂ with O₂ in d₃-MeCN at 50°C.

Time, h	Me-Me, %	Me-H/D, %
2	36 ± 4	0 ± 1
4	46 ± 4	1 ± 1
8	48 ± 3	5 ± 7
24	48 ± 4	5 ± 7

Table C36. Yields of the products from the reaction of (^tBuN4)NiMe₂PF₆ with 1 eq ThBF₄ d₃-MeCN at 50°C.

Time, h	Me-Me, %	Me-H/D, %
1	50	0
2	57	0
4	62	0
8	68	0
24	81	0
48	86	0

Table C37. Yields of the products from the reaction of (^tBuN₄)NiMe₂ with 1 eq FcPF₆ d₃-MeCN at 50°C.

Time, h	Me-Me, %	Me-H/D, %
1	34	0
2	39	0
4	51	0
8	62	0
24	68	0
48	71	0

Table C38. Yields of the products from the reaction of (^tBuN₄)NiMe₂ and (^tBuN₄)Ni(CD₃)₂ with 1 eq FcPF₆ in d₃-MeCN at 50°C.

Time, h	Me-Me, %	CD ₃ -CH ₃ , %	Me-H/D, %
2	31	0	10
4	31	0	9
7	30	0	8
24	31	0	6